Study on RAFT polymerization and nano-structured hybrid system of POSS macromers

Yuanming Deng

N° d'ordre 2012-ISAL-0050 Année 2012

Thèse

présentée devant

l'Institut National des Sciences Appliquées de Lyon

pour obtenir

le grade de Docteur

École Doctorale : Matériaux de Lyon
Spécialité : Matériaux Polymères et Composites

par

Yuanming DENG

Study on RAFT Polymerization and Nano-structured Hybrid System of POSS Macromers

---

Soutenue 8 Juin 2012 devant la Commission d'Examen :

JURY

Prof. LU	Canzhong	Fujian Institute of Structure of Matter, CAS	–Rapporteur
Prof. CHEN	Xudong	Sun Yat-sen University	–Rapporteur
Prof.GERARD	Jean-François	INSA Lyon	–Directrice de thèse
Prof DAI	Lizong	Xiamen University	–Directrice de thèse
Prof. Wu	Huihuang	Xiamen University	–Examinateur
Dr. XU	Yiting	Xiamen University	–Examinateur

INSA Direction de la Recherche - Ecoles Doctorales – Quinquennal 2011-2015

SIGLE	ECOLE DOCTORALE	NOM ET COORDONNEES DU RESPONSABLE
CHIMIE	**CHIMIE DE LYON** http://www.edchimie-lyon.fr M. Jean Marc LANCELIN Insa : R. GOURDON	M. Jean Marc LANCELIN Université Claude Bernard Lyon 1 Bât CPE 43 bd du 11 novembre 1918 69622 VILLEURBANNE Cedex Tél : 04.72.43 13 95 Fax : lancelin@hikari.cpe.fr
E.E.A.	**ELECTRONIQUE, ELECTROTECHNIQUE, AUTOMATIQUE** http://edeea.ec-lyon.fr Secrétariat : M.C. HAVGOUDOUKIAN eea@ec-lyon.fr	M. Gérard SCORLETTI Ecole Centrale de Lyon 36 avenue Guy de Collongue 69134 ECULLY Tél : 04.72.18 60 97 Fax : 04 78 43 37 17 Gerard.scorletti@ec-lyon.fr
E2M2	**EVOLUTION, ECOSYSTEME, MICROBIOLOGIE, MODELISATION** http://e2m2.universite-lyon.fr **Insa : H. CHARLES**	Mme Gudrun BORNETTE CNRS UMR 5023 LEHNA Université Claude Bernard Lyon 1 Bât Forel 43 bd du 11 novembre 1918 69622 VILLEURBANNE Cédex Tél : 04.72.43.12.94 e2m2@biomserv.univ-lyon1.fr
EDISS	**INTERDISCIPLINAIRE SCIENCES-SANTE** Sec : Safia Boudjema M. Didier REVEL Insa : M. LAGARDE	M. Didier REVEL Hôpital Cardiologique de Lyon Bâtiment Central 28 Avenue Doyen Lépine 69500 BRON Tél : 04.72.68 49 09 Fax :04 72 35 49 16 Didier.revel@creatis.uni-lyon1.fr
INFOMATHS	**INFORMATIQUE ET MATHEMATIQUES** http://infomaths.univ-lyon1.fr	M. Johannes KELLENDONK Université Claude Bernard Lyon 1 INFOMATHS Bâtiment Braconnier 43 bd du 11 novembre 1918 69622 VILLEURBANNE Cedex Tél : 04.72. 44.82.94 Fax 04 72 43 16 87 infomaths@univ-lyon1.fr
Matériaux	**MATERIAUX DE LYON** Secrétariat : M. LABOUNE PM : 71.70 –Fax : 87.12 Bat. Saint Exupéry Ed.materiaux@insa-lyon.fr	M. Jean Yves BUFFIERE INSA de Lyon MATEIS Bâtiment Saint Exupéry 7 avenue Jean Capelle 69621 VILLEURBANNE Cédex Tél : 04.72.43 83 18 Fax 04 72 43 85 28 Jean-yves.buffiere@insa-lyon.fr
MEGA	**MECANIQUE, ENERGETIQUE, GENIE CIVIL, ACOUSTIQUE** M. Jean Louis GUYADER Secrétariat : M. LABOUNE PM : 71.70 –Fax : 87.12	M. Jean Louis GUYADER INSA de Lyon Laboratoire de Vibrations et Acoustique Bâtiment Antoine de Saint Exupéry 25 bis avenue Jean Capelle 69621 VILLEURBANNE Cedex Tél :04.72.18.71.70 Fax : 04 72 43 72 37 mega@lva.insa-lyon.fr
ScSo	**ScSo*** M. OBADIA Lionel Insa : J.Y. TOUSSAINT	M. OBADIA Lionel Université Lyon 2 86 rue Pasteur 69365 LYON Cedex 07 Tél : 04.78.69.72.76 Fax : 04.37.28.04.48 Lionel.Obadia@univ-lyon2.fr

*ScSo : Histoire, Geographie, Aménagement, Urbanisme, Archéologie, Science politique, Sociologie, Anthropologie

Acknowlegements

How time flies! It is my 11th year in XMU, and also the 7th year in Prof. Dai's group. My graduate career became the end when I typed these words. I'm growing up with the growth of the College of Materials, with painful, enjoyable and grateful feeling, and there so many people who deserved my deep thanks.

First and foremost, I would like to express my deep and sincere gratitude to my supervisor, Prof. DAI. He brought us to the frontline of science and industry from the very beginning with his wide knowledge and great patience. Thereafter, he pinned great hopes on me. Sometimes even I felt that I have let him down, but he always trust me with endless positive energy and kind comments. He also offered me an opportunity to go aboard to pursuit my work. I should say, this dissertation would not have been possible without his expert guidance. I also want to thank him for his toleration and apologize for my unintentional offense in debate.

Special thanks are given to Prof. GERARD, who invited me to pursuit my research in INSA Lyon as a co-supervised doctoral student for one year. I'd like to thank him for the hospitality, constructive comments, and important support throughout this work. I deeply appreciate Dr. Julien BERNARD not only was he readily available for me, as he so generously is for all of his students, but he always read and responded to the drafts of my work. Without his stimulating enthusiasm, constructive comments, and inspiring suggestions, the project would never have been in the same shape as it is right now. I also want to give my great thanks to the faculty, staff, and administration of IMP/LMM, especially Jocelyne Galy, Pierre Alcouff and Isabelle POLO et al.

I am very grateful for all the supports I have constantly received from Dr. XU Yiting in these years. She is a person easy to get along with and her wide knowledge helped me a lot. I also want to thank Dr ZENG Birong and Dr. LUO Weiang for their help. Many people on the faculty and staff of the College of Materials and the Center of Analysis assisted and encouraged me in various ways during these years. I am grateful to all of them for all that they have taught and offered me.

My special thanks go to CHEN Jiangfeng & YUAN Conghui, the ones whom I always turn to with every possible kinds of problem. Not only the great contribution on ideas for the project that they provided, but also their patience and stimulating motivation that brought me

to where I am now and still enthusiastic to step forward. I am particularly thankful to my friends for their kind hearted help and nice memory. We not only studied, relaxed, and traveled well together, but they were even willing to read some portions of this dissertation and thus provided some very useful input.

I'm very grateful for my parents. Their selfless love and support made this happened. Their kind-hearted personality affected me to be steadfast. Their understanding and love encouraged me to continue pursuing a PhD project. I also want to thank my relatives for their generous help in need.

The financial support of the CSC and NSF of Chinese government is gratefully acknowledged.

Étude sur la polymérisation RAFT et nanostructurés système hybride de macromères POSS

Résumé

Ce travail est généralement destiné à synthétiser BCPs à base d'POSS par polymérisation RAFT, à étudier leurs comportements d'auto-assemblage, à la recherche sur l'effet de POSS auto-assemblage structure sur les propriétés en vrac et à préparer nanostructuré époxy hybride par auto-assemblage de la copolymère base d'POSS.

Dans le Chapitre1, Nous avons étudié la polymérisation RAFT de macromères POSS et capables de synthétiser bien définis BCPs à base d'POSS avec la fraction POSS élevé et une topologie différente tels que AB, BAB et (BA)3. Le groupe de vertex et l'effet sur la morphologie propriétés thermo-mécaniques de BCPs à base d'POSS et la relation structure-propriété ont été investigated.

Polymérisation RAFT dispersion dans solvant apolaire a été appliquée pour obtenir divers agrégats ayant une morphologie différente dans Chapitre2. Refroidissement de transition induite morphologie réversible a été trouvé et la sélection dans la formation des vésicules voie a été étudiée.

Nano-construction de matériaux O/I époxy hybrides à base de copolymères à base d'POSS a été étudiée dans Chapitre 4. L'effet de la teneur en groupe fonctionnel sur la miscibilité de copolymère statistique base d'POSS et de l'époxy a été étudiée. Une nouvelle méthode à la technologie hybride époxy nanostructure impliquant l'auto-assemblage de BCPs à base d'POSS en résine époxy a été présenté. Homogénéité élevée et bien la taille/morphologie de contrôle de coeur-corona structure contenant coeur POSS rigide et soluble dans les réseaux corona PMMA ont été obtenus.

Mots clés: nanocomposites; POSS; O / I hybrides; copolymère à bloc; auto-assemblage;

Study on RAFT Polymerization and Nanostructured Hybrid System of POSS macromers

Abstract

This work is generally aimed to synthesize POSS based BCPs via RAFT polymerization, to study their self-assembly behaviors, to research on the effect of POSS self-assembly structure on the bulk properties and to prepare nanostructured hybrid epoxy via self-assembly of POSS based copolymer.

In Chapter1, We studied the RAFT polymerization of POSS macromers and capable to synthesize well defined POSS based BCPs with high POSS fraction and different topology such as AB， BAB and $(BA)_3$. The vertex group and the morphology effect on thermo-mechanical properties of POSS based BCPs as well as the structure-property relationship was investigated.

Dispersion RAFT polymerization in apolar solvent was applied and various aggregates with different morphology in Chapter2. Cooling induced reversible micelle formation and transition was found and the pathway selection in vesicle formation was investigated.

Nano-construction of O/I hybrid epoxy materials based on POSS based copolymers was investigated in Chapter4. The effect of functional group content on miscibility of POSS based statistic copolymer and epoxy was investigated. A novel method to nanostructure epoxy hybrid involving self-assembly of POSS based BCPs in epoxy was presented. High homogeneity and well size/morphology control of core-corona structure containing rigid POSS core and soluble PMMA corona in networks were obtained.

Key words: nanocomposites; POSS; O/I hybrids; block copolymer; self-assembly

Abréviations et symboles

AIBN: 2,2-Azobis-(isobutyronitrile)

ATRP: Atom Transfer Radical Polymerization

BCP : Block Copolymer

BuA: Butyl Arylate

CDB: Cumyl dithiobenzoate

CPAD: 4-Cyano-4-(phenylcarbonothioylthio) pentanoic acid

CTA: Chain Transfer agent

CTE: Chain Transfer Efficiency

CRP: Living/Controlled free Radical Polymerization

C_{tr}: Chain Transfer Constant

Cy: Cyclohexyl

DP_n: Number-average Degree of Polymerization

GMA: Glycidyl Methacrylate

iBu: Isobutyl

LCP: Living/Controlled Polymerization

LAP: Living Anonic Polymerization

MMA : Methyl Methacrylatre

MAiBuPOSS : 3-(3, 5, 7, 9, 11, 13, 15-heptaisobutyl-pentacyclo [9.5.1.13, 9.15, 15.17, 13] -octasiloxane-1-yl)propyl methacrylate

MACyPOSS : 3-(3, 5, 7, 9, 11, 13, 15-heptacyclohexyl-pentacyclo [9.5.1.13, 9.15, 15.17, 13] -octasiloxane-1-yl)propyl methacrylate

MAPhPOSS: 3-(3, 5, 7, 9, 11, 13, 15-heptacyphenyl-pentacyclo [9.5.1.13, 9.15, 15.17, 13] -octasiloxane-1-yl) propyl methacrylate

MW: Molecular Weight

O/I: Organic/Inoranic

PDI: Polydispersity Index

POSS: Polyhedral Oligmeric Silsesquioxane

Ph: Phenyl

RAFT: Reversible Addition-Fragmentation Chain Transfer

ROMP: Ring-Opening Metathesis Polymerization

St: Styrene

$\boldsymbol{T_g}$**:** Glass Transition Temperature

Table of Contents

Chapter1 Review on POSS Based Polymers and Their Self-assembly

1.1. General introduction of POSS based polymer preparation

1.1.1 A brief introduction of NCs

Materials have accompanied mankind virtually from the very beginning of its existence. For thousands of years, materials were as a scale to civilization and have been considered of such importance that historians and other scholars have named certain ancient periods after the material which was predominantly utilized at that respective time. Examples are the Stone Age, the Copper–Stone Age, the Bronze Age, and the Iron Age etc. Even for a long time natural polymeric materials have came into human's life, and modified natural polymer and synthetic polymer have been used since 19 century, they played an increasingly important role till the development of polymer science since 50's 20th century.

Relative to metals and ceramics, polymeric materials generally have low density, good processibilty and flexibility along with lower module and strength. Therefore, the reinforcement of polymeric materials with second phase particles to generate the so-called "composite" became one of the most important issues in polymer science. NPs (having at least one dimension in the range 1~100 nm) prove to effectively improve the mechanical properties of polymers even at relatively low filler content, generating "NCs". Using this approach, the polymer properties can be efficiently improved while maintaining its inherently low density and high ductility. Conventional routes to introduce inorganic NPs included the dispersion of pre-formed nano-scaled inorganic materials, i.e. silica, metal or metal oxides, into a polymer matrix[1, 2], or by a conventional sol-gel process involving hydrolysis and condensation reactions from metal alkoxides, commonly alkoxysilane[3]. Tailor-made inorganic clusters such as carbon nano-materials, layer silicates and POSS provided a third promising way to reinforce polymer matrices with inorganic-rich domains.

1.1.2 Synthesis of POSS

POSS was a type of inner O/I hybrid nanofiller originated from the development of silicon chemistry. Typical molecular structure of POSS is $(RSiO_{3/2})_n$, which was between silica（SiO_2）and silicon rubber(R_2SiO), composed of a inorganic Si-O cubic core and organic substituent R connected to Si vertex, in which R could be hydrogen, alkyl, alkenyl, aryl or their derivates[4,5]. With a size between 1～3nm，which was in the same order of gyration radius of polymer chain, POSS was considered as the smallest silica particle[6].

In 1946, Scott et al[7] have obtained compounds formulated $(RSi_{1.5}O)_2$, namely methyl silsesquioxane occasionally in the investigation of the thermal rearrangement of branched chain methylpolysiloxane synthesized from dimethyldichlorosilane and methyltrichlorosi1ane. Brown et al[8] successfully synthesized after a few days gave the dimer, Cy-$T_2(OH)_4$ in 84 % yield. By increase the proportion of acetone in the solvent, as shown in scheme, mixture product precipitate, $[Cy_7Si_7O_9(OH)_3]$, $[Cy_6Si_6O_9]$ $[Cy_8Si_8O_{11}(OH)_2]$ were obtained via hydrolysis of $CySiCl_3$ in water/acetone mixture for 2~36monthes.

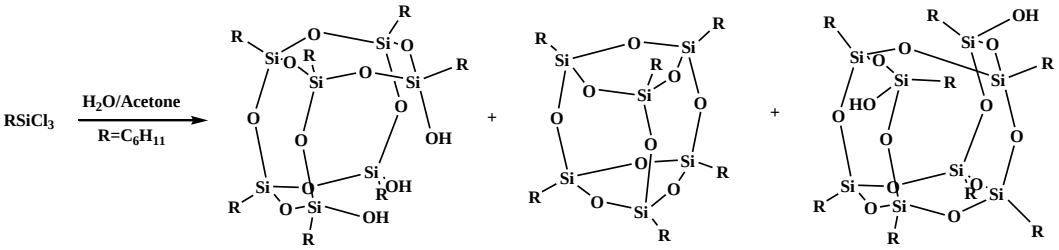

Fig 1.1 preparation of POSS by hydrolysis of trichlorosilane

Till 1980s', POSS gained increasing interest in catalysis area and has been extensively studied by Frank Feher and co-workers[9, 10]. The field of silsesquioxane chemistry has grown dramatically in the past two decades and scientists paid more attention in catalyst support area till in 1990s'. Since Edwards Air Force Base (U. S. A.) has devoted to the study on POSSs in the application of aerospace materials, POSS became a tailored "nano-filler" to reinforce polymer materials. It is funded the Air Force Office of Scientific Research which is an excellent model to transitioned the collaboration of government-academic to the commercial

sector. The major POSS manufactory marked the start-up of Hybrid Plastics in Fountain Valley, CA, was set up in the fall of 1998, and monopolized the main production and market of commercial POSSs.

The synthesis of POSSs mainly includes, the control hydrolysis and condensation of reactive silane as mentioned above [11, 12], corner-capping of incompletely closed POSSs[13, 14] (Fig1.2) , control cleavage of preformed POSSs [9, 14-20] (Fig1.3), and converse of functional POSS vertex groups (Fig1.4) which was well reviewed in a recent publication by Cordes et al[21].

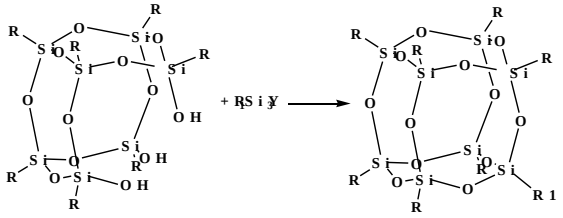

Fig 1.2 Synthesis of POSS via corner-capping reaction

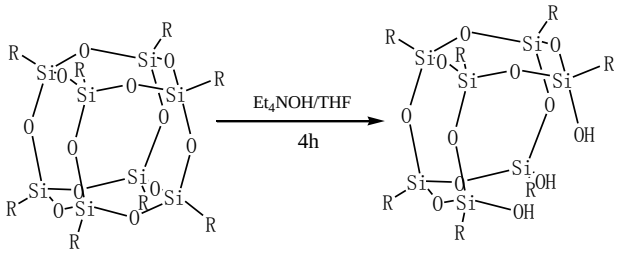

Fig 1.3 Synthesis of POSS silanol via cleavage of POSS cage

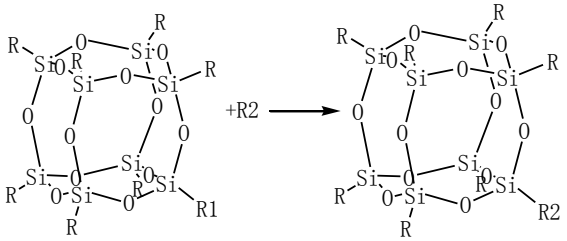

Fig 1.4 Synthesis of POSS via converse of functional group

1.1.3 Synthesis of POSS /polymer nano hybrids

Among the various applications of POSS, a very important field was the preparation of polymer NCs (O/I nano-hybrids), with the aim to obtain multifunctional materials with intermediate properties between those of organic polymers and of ceramics. POSS can be incorporated in through directly blend or chemically bonded to polymer chain, obtaining blending, tethered, main chain or cross-linked composites (Fig 1.5).

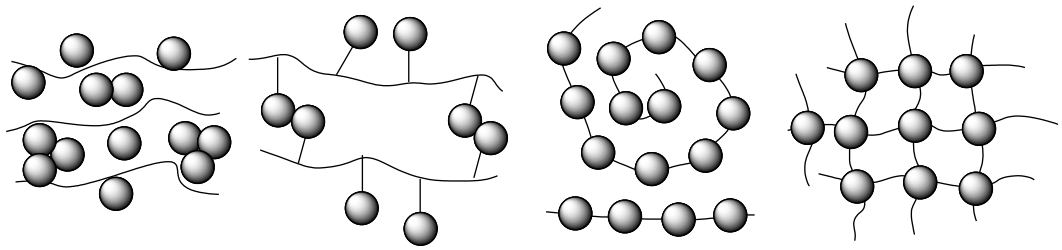

Fig 1.5 The structure of POSS based polymer

Practically speaking, physical mixing was the easiest way to prepare POSS NCs and, naturally, has been adopted by many research groups. POSS moieties can be dispersed in the polymer matrix at a level mediated by weak (van der Waals) or strong (hydrogen-bonding) interactions. POSS moieties physically blended into a polymer matrix tended to aggregate and crystallize as NPs and only molecularly dispersed at very low loadings and with favorable POSS-matrix interactions, if without specific interaction. This simple, feasible and promising route to mass production of POSS/thermoplastics were extensively investigated in the past decades and well reviewed by Alberto Fina et al[22] and Kuo et al[23]. Thanks to the versatility of POSS vertex groups, various thermoplastics such as HDPE[24], PE/PP[25], PP[26], polysiloxane[27], PVC[28, 29], PC[30, 31], PMMA[32, 33], PS[34, 35], PA[36, 37] etc. were potential to be matrices. The crucial factor on properties of such kind of blending was the dispersion state of POSS in the matrices, which was obviously depend on the balance between polymer–POSS interactions and POSS-POSS self-interactions. It was worth noting that physical blending may lead to macroscopic phase separation between POSS and the polymeric host at higher loadings, if driven to do so thermodynamically. Special processing or interaction was required to achieve better miscibility[38-43].

A prevailing methodology to prepare POSS tethering polymers was to (co)polymerize the POSS macromer bearing one polymerizable group and the remaining inert vertex groups, with a suitable host comonomer to obtain the desired O/I hybrid polymer NCs. There several polymerization method to achieve such target, depending on the type of polymerizable group. POSS bearing reactive double bond was one of the most popular macromer for POSS tethering polymers. The synthesis of reactive double bond POSS macromers brought about a new period of POSS based nano-hybrid [44-53]. Their homopolymer and copolymer with various well-known monomers have been widely synthesized and studied. Step growth polymerization also could be applied for the synthesis of POSS tethering polymers if bearing proper functional groups[54-58]. Grafting mono-functionalized POSS onto a polymer chain modified with reactive groups was an alternative way to side chain tethering POSS based polymers. Various chemical reactions could be applied for grafting POSS onto reactive polymer chain[59-66].

POSS based polymer network could be formed via copolymerization of multifunctional monomers with POSS monomer[67-75]. As one of the most successful commercial thermosetting precursors, epoxy set a representative example for polymer network. Reinforcement by inorganic NPs has been proved to be a promising method to conquer the poor toughness and flame retardancy. For the past two decades, there were amounts of work involved the introduction of POSS into epoxy. Both mono-[76-84] and multi-[70, 85-99] functionalized POSS were employed to reinforce the epoxy matrix. It was found that the POSS dispersion and system homogeneity increased with the increasing POSS functionality. However, competition between aggregation and dispersion still existed due to the low reactivity of functional group and steric hindrance, particularly for mono-functionalized POSS. Enhanced extent of reaction between POSS and precursors of matrices is required for well miscible system. Pre-reaction between POSS and precursors has been proved to be an efficient route to enhance the extent of reaction [100-103].

1.2. Effect of POSS on the properties of polymer

Incorporation of the POSS into a polymer matrix can result in significant improvements

in a variety of physical properties due to the reinforcement at the molecular level and the inorganic framework's ceramic-like properties. Recent work showed that the physical cross-links formed by the POSS can significantly retard chain motion, while at the same time the individual POSS cages can act as flow-aids at elevated temperatures. The addition of POSS to organic polymers was found to drastically modify the polymer's properties supplying improved thermal stability as well as modifying the polymer T_g, stiffness and resilience. In addition, POSS was composed of Si-O framework, covered by organic vertex groups, which shows inner-hybrid character. The silicon oxide core can react with atomic oxygen in simulated low Earth orbit environments and rapidly form a protective SiO_2 layer, which can self-heal just as quickly due to the uniform dispersion of POSS throughout the organic matrix. Moreover, incorporation of POSS molecules was responsible for reductions in the rate of combustion in the event of fire, improved dielectrical properties as well as for bringing other functional properties, accordingly with the high versatility of POSS synthesis. Such multi-functional behavior allowed their implementation in a variety of applications.

1.2.1 Morphology, rheology and glass transition of POSS based polymers

From the microscopic viewpoint, the characteristic nano-size of the POSS molecule (1~3nm) was comparable to the dimensions of polymeric segments or "blobs" in the condensed phase (molten or solid), yet nearly double typical intermolecular spacing. Undoubtedly, the incorporation of POSS moieties into linear polymer chains and/or polymer networks will modify the local molecular interactions, local molecular topology, and the resulting polymer chain and segment mobility. It was well-known that the effectiveness of POSS in enhancing the properties of polymer in NCs or in creating new properties primarily depends on the degree of dispersion and distribution of the POSS cages in the polymer matrix and on type of organic substituent of the silicon atoms of the POSS cage[104]. This behavior depended on the thermodynamic interaction between POSS and the polymer matrix, particularly the constituent polymer segments. If the interaction was favorable or mutually unfavorable relative to POSS-POSS interactions, POSS moieties were well-dispersed; otherwise POSS aggregated. Unlike a filled system or blend, however, POSS aggregation could be limited due to covalent attachment to the polymer backbone that prevented

aggregation beyond a scale of about one radius of gyration.

Rheology behavior of system in which non-chemical bonding POSS molecular dispersed in polymer matrices has been well investigated. Joshi et al[105] have investigated the rheological and viscoelastic behavior of HDPE-octamethyl-POSS NCs prepared by the melt mixing route. The results showed that, at lower filler concentration (0.25-0.5 wt %), fine dispersion with some level of PE chain-POSS interaction, i.e., weak van der Waals forces, POSS particles acted as lubricant, decreasing chain entanglements and more prociding free volume in the melt, thus resulting in lower complex viscosity (η^*). In other publication by Kopesky et al[39], two liquid POSS: octamethacryl-propyl (MA-POSS) and hydrogenated octamethacryl propyl-POSS (hMAPOSS) loaded in PMMA lowered the viscosity monotonically with POSS loading. Time-Temperature-Superposition (TTS) was successfully employed for all blends and, surprisingly, the Williams-Landel-Ferry (WLF) analysis indicated that the decrease in T_g and viscosity observed could not be ascribed to an increase in free volume with increasing POSS content.

Higher loading of POSS above molecular dispersion level caused aggregation (nanocrystal) of POSS if the interaction favored. POSS aggregates dramatically change the rheology behavior of neat matrix. Literature[105] reported that introduction of POSS increased the complex viscosity of the NCs at higher POSS loading when nanocrystal formed. Fu et al[25] demonstrated that the addition of POSS molecules changed the rheological behavior above melting temperature from melt-like in the neat resin to solid-like in the NCs, physically cross-linking the molten of ethylene-propylene copolymers. WAXD results showed formation of POSS crystal aggregates, suggesting that the particle-to-particle interactions between POSS molecules contributed to the unusual rheological behaviors of the EP/POSS NCs. PMMA modified with untethered iBuPOSS and CyPOSS showed similar rheology behavior[39].

While the particle-to-particle interactions dominated the rheological behavior of physically mixed polymer-POSS NCs, the particle-to-matrix interactions may be more important in the chemically grafted POSS/PNCs, in which the POSS molecules were easily dispersed at the molecular level, Unless the aggregation occurs when the density of strong interact POSS in the polymer chain was high enough. Work on rheology studies by Wu et al[106] showed that TTS worked well for entangled PS tethered with iBuPOSS up to 50wt%,

revealing a single phase, which was also evidenced by XRD and TEM. Within the terminal zone, no secondary rubbery plateau was observed, indicating that the interaction between iBuPOSS groups within PS segments was not sufficient to yield "sticky reputation"-like behavior. It was argued that within the framework of the reputation tube theory, the presence of a POSS moiety significantly changed the microscopic topology of the random copolymer chains and led to an increase in the effective tube diameter, which could be the origin of POSS-based dilution of entanglement density. Uribe et al[107] have found rubbery plateau in a largely unentangled poly(4-methylstyrene) copolymers tethered by CpPOSS and CyPOSS moieties. While poly(4-methylstyrene) copolymer with 27wt% of CyPOSS showed terminal ($G' \propto \omega^2$) and Rouse zones ($G' \propto \omega^{1/2}$) without an intervening rubbery plateau. The rubbery plateau spanned 4decades in frequency as the CyPOSS loading increased to 64wt%. This observation was attributed to the formation of the limited POSS aggregation evidenced by WAXS. Similar results were achieved by Lee et al[108] on the PS grafting Al-containing PhPOSS cages, and attributed to the strong POSS-POSS interaction. The difference of rheology behavior on POSS content was explained by the average length between successive POSS cages: when the average length between successive POSS cages is comparable to the size of a POSS cage, the intrachain POSS-POSS interaction will gradually dominate the dynamics of POSS copolymer. The linear viscoelastic response of the POSS-grafted copolymers then changed from a viscoelastic liquid-like response to a viscoelastic gel-like behavior. Rheology study of a miscible system composed of low *MW* POSS-PS copolymer and high *MW* polystyrene also demonstrated that PS-POSS acts as a lubricating agent, decreasing the zero-shear viscosity η_0 and rubbery moduli G_N^0 [109]. Later work by Wu et al[110] has demonstrated the vertex group effect on the rheology behavior of PS POSS copolymers, further confirming the POSS-POSS interaction on morphology and rheology behavior.

In reactive blending, or co-cure reactions with reactive POSS, the extension of chemical reaction depended on the reactivity of functional group and process, and both tethered and un-tethered POSS moieties existed. The tethered POSS could act as compatiblizer on the interface of matrices and un-tethered POSS. Galy et al[111] have found that the chemical bonding between multi-functional POSS and polymer matrix led to very well dispersed clusters at the molecular scale, whereas the mono-functionalized POSS showed a high

tendency to phase separate and to form crystalline domains during network formation. This effect was clearly more pronounced with CyPOSS as compared to iBuPOSS, due to the stronger POSS-POSS interactions in the first case. Moreover it was also demonstrated that most of the mono-functionalized POSS were not covalently bonded to the network. Solid-state NMR spectroscopy with recently developed re-coupling techniques clearly confirmed that the resulting networks structure and morphology, containing either chemical or physical POSS aggregates, led to remarkable motional heterogeneities[112].

By carefully control of the extension of reaction, size and distribution control POSS domain for well-tuned unique properties of resulted hybrids became possible. DiLuca et al[82] have explored the possibility of producing a dispersion of POSS crystalline platelets in situ during polymerization, starting from homogeneous solutions. The in-situ generation of POSS crystalline platelets can impart similar characteristics to those observed in clay-modified polymers (except for the nano-size), with the advantage of a much easier processing.

POSS cages were undoubtedly rigid and their significant volume could induce a steric barrier that would increase T_g. However, POSS moiety incorporated into the hybrid copolymer or polymer did not always increase T_g as expected. The large volume of POSS compared to a typical polymer chain segment implies that the POSS moiety may dominate the local chain motion of the polymer. Moreover, the inert vertex groups which contributed 80% of the POSS volume determined the interaction between POSS group and non-POSS polymeric segments. The computation of the volume-temperature (V-T) diagram using molecular dynamics allowed the prediction of the T_g, in spite of the time scale considered[113]. Herein, we discussed the individual effect of incorporated POSS on T_g of matrices.

Firstly, we considered the polymer containing non-functionalized POSS, in which POSS act as additives. As discussed above on the aggregation behavior of such kind of hybrids, Molecular dispersion of POSS could only be observed at very low loading level, and similarity of polymer chemical structure and POSS vertex group was required. In this case, well dispersed POSS always acted as plasticizer to decrease T_g due to the dilute effect and additional free volume caused by flexible vertex group[114]. When POSS with strong interaction was incorporated, nano-crystallization or aggregation occured, leading to hard second phase which might reinforce the matrices, causing a T_g increase. Strong specific

intermolecular interactions such as hydrogen bonding, ion-ion interactions, acid-base interactions, among others, can restrict polymer chain motion and result in enhancement of T_g.

In the case of polymer containing tethering POSS, the main influence of POSS on T_g was the POSS interaction which was determined by POSS vertex group. It was reported that the incorporation of CyPOSS into the PMMA backbone increased the T_g, while the incorporation of iBuPOSS decreased the T_g [113]. This result was an additional proof of the accuracy of the force field and protocols used. The authors have also found that in these semi-crystalline copolymers, the increase of T_g was attributed one part to the CyPOSS homogeneously dispersed on the material and another part to the presence of the crystalline lamellas, which restricted the molecular motions of the surrounding chains. The well-fitted WLF equation revealed that the fractional free volume at T_g, f_g increased with the iBuPOSS loading; however, the corresponding temperature coefficient of free volume was seen to decrease with increasing iBuPOSS content. Wu et al[110] proposed that the iBuPOSS groups played a plasticizer-like role in determining the T_g, increasing the glassy free volume fraction to enhance the PS segmental mobility.

Wu et al[110] have investigated the thermal and linear rheological behavior of polystyrene (PS)-based random copolymers incorporating POSS with three kinds of vertex groups: iBu, Cp, and Cy. As shown in Fig1.6, the weak iBuPOSS-PS segment interaction resulted in a T_g that monotonically decreased with increasing iBuPOSS content. Conversely, the strong CpPOSS/CyPOSS-PS segment interaction resulted in glass transition enhancement, though with complex dependence in the CyPOSS case. They asserted that the vertex group dependence of the glass transition of the copolymers results from competing effects of free volume addition and intermolecular interactions. In total, the variation of T_g in the random copolymers was the net result of several effects: free volume fraction, steric barrier, and POSS-polymeric segment interactions.

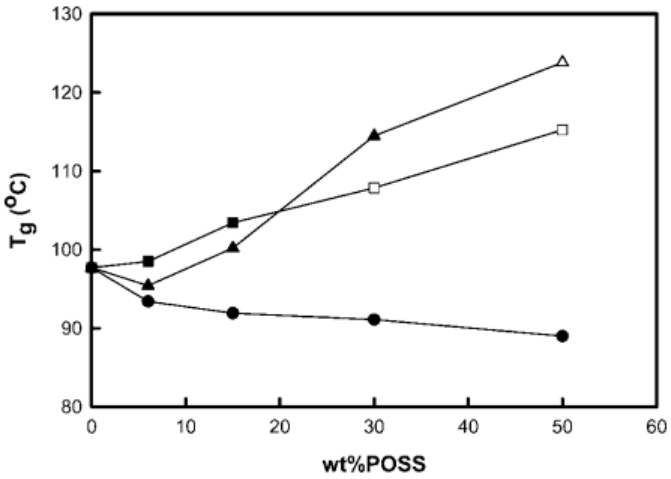

Fig 1.6 Variation of T_g for as-cast PS-based copolymers films as the function of POSS content. POSS vertex group varies with ● iBuPOSS, ■ CpPOSS, and ▲ CyPOSS. Open symbols: samples insoluble

Xu et al[115] have investigated the POSS effect on T_g by FTIR in PAS-POSS hybrids obtained from common free-radical polymerization, finding that the T_g improvement was associated with the aggregation of POSS particles and the dipole-dipole interaction between POSS and PAS molecules. The T_g decreased at lower POSS contents came from the inert diluent effect of POSS macromers, which reduced the dipole-dipole interaction of the homogeneous PAS molecules. With the increase of POSS contents, the enhancement of the dipole-dipole interactions of POSS-POSS and POSS-PAS surpassed the decrease of the dipole-dipole interaction of PAS-PAS to result in the increase of the T_g. Higher T_g and better thermal stability were observed in the star PAS-POSS hybrids than in the linear PAS-POSS hybrids at the same POSS content.

The influence of POSS on T_g of cross-linking polymer included the vertex effect, the reactivity of functional group, cross-linking density and nano-reinforcement effect. In fact, due to the lower reactivity of functional group on POSS, the competence between aggregation and dispersion made the effect on T_g much more complex than the other two systems mentioned above. The effect of POSS on cross-linking density was also complicated. On one hand, T_g was increased by multi-functionalized POSS and decreased by mono-functionalized POSS which increase chain ends, on the other hand, strong interaction between POSS and matrices provide additional physical cross-linking density.

1.2.2 Mechanical properties

New opportunities have emerged for reinforcing polymers using NPs without sacrificing strength, rigidity and T_g, as in the case with conventional elastomeric tougher. Such systems have attracted enormous interest from the materials community because they theoretically promised substantial improvement of mechanical properties at very low filler loadings. Consequently, this lower loading confered nano-filled matrices enormous advantages when compared to microfilled ones. Many characteristic properties of unmodified polymers such as light weight, transparency, ductility and good processability preserved after modification[116].

As a nano building block, thanks to the variation of POSS type, POSS could form NPs range from 1~3nm (molecular dispersion) to micrometers in various shape through aggregation or self-assembly. The introduction of small amounts of POSS cages gave rise to a certain increase in module, hardness, strength as well as toughness, named "nano-reinforcement effect"[117, 118]. Modulus enhancement depended on intrinsic properties of matrix and filler as well as interactions between matrix and filler; ultimate properties, on the other hand, were more sensitive to defects; while surface hardness mainly depended on the surface aggregation of POSS.

It was found that the POSS-POSS interaction was crucial for mechanical properties of POSS-containing networks while the POSS-network chain interactions were of minor importance[119]. Efficient reinforcement was observed mainly in the case of networks involving pendant POSS with a high propensity to crystallization which could form physical cross-links, thus increasing cross-linking density and rubbery modulus. Whereas POSS skeleton with "soft" flexible substituent, such as octyl, shows formation of weak aggregates only, which didn't contribute to reinforcement. The rubbery modulus of the networks with POSS in a junction grew with increasing POSS functionality due to enhanced network cross-link density. Liu et al[120] have reported POSS-reinforced OPBI NCs established by initiating the polymerization of DCDPE and DABz in the presence of octa PhPOSS. It was found that upon the addition of only 2wt%POSS, the Young's modulus, tensile strength, and toughness were all improved by 31, 76, and 138.2%, respectively. More importantly, the ductility for the composites was not reduced but improved, which overcomes the brittleness

brought by the addition of inorganic reinforced agent, a traditional shortcoming.

Fu et al[121] have studied morphology development of POSS aggregates under deformation by simultaneous in-situ WAXD and SAXS techniques. The tensile test showed that the incorporation of POSS molecules greatly enhanced the tensile modulus and the strength. The WAXD data shown in Fig1.7a indicated that nanoscale crystals of POSS molecules in the hard segment domains were destructed under stretching. The SAXS data shown in Fig1.7b showed that at strains larger than 100%, the microphase structure of POSS-PU was oriented along the stretching direction. The decrease in the scattering intensity indicates that hard segment domains were partially destroyed, which was consistent with the WAXD observation. At strains above 200%, the SAXS pattern showed an intense streak along the equatorial direction, which was attributed to the micro-fibrillar structure of the strain-induced crystallization of the soft segments, which was also evidenced by WAXD. TEM observations on a stretched and relaxed POSS-PU-34 sample indicated that tensile stretching broke the large hard segment domains into disk-like domains with plane normal almost parallel to the stretching direction.

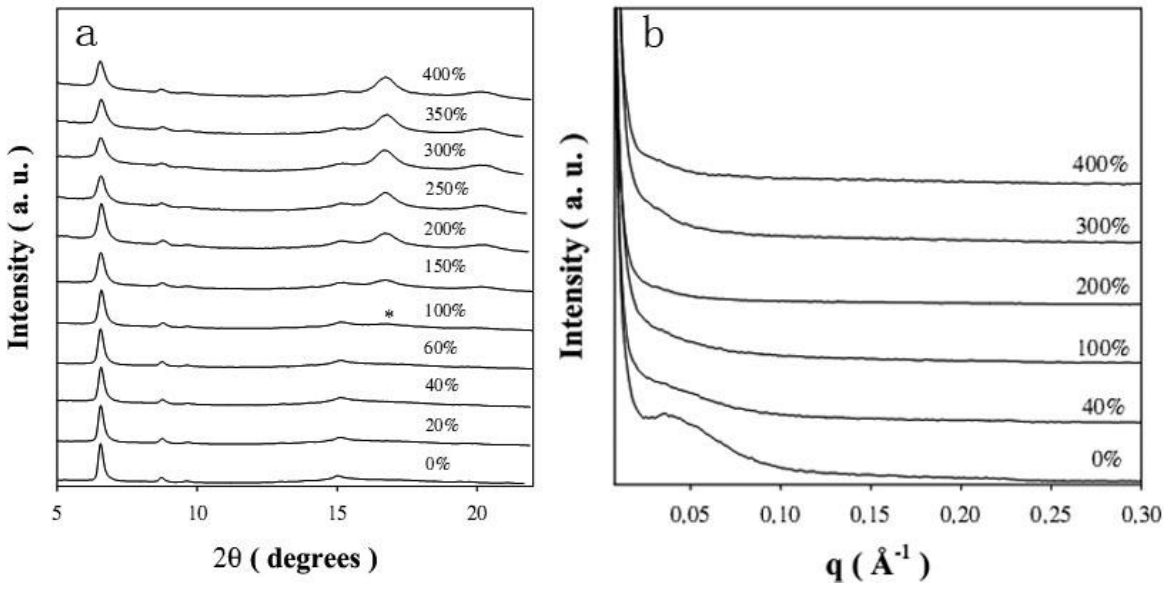

Fig 1.7 (a) WAXD profiles of POSS-PU-34 along the equatorial direction at different strains and (b) SAXS profiles of POSS-PU-34 along the meridional direction at different strains

To describe the mechanism of POSS nano-reinforcement in microscale, Kim et al[122] have observed TEM images of the near-crack, showing well-developed plastic deformation zones at the crack tips when POSS modified epoxy. A three-stage mechanism as shown in Fig1.8 was raised up to explain the results: In the first step, stress concentrated around the POSS aggregates in the matrix. Second, because of the high cross-linking density and strong anchoring of POSS aggregates to the cured system, the network structure couldn't maintain continuity under an external load. The highly concentrated stress could only be released by the formation of voids surrounding the POSS aggregates in the matrix. In the third stage, with the growth of voids orthogonal to the principal tensile stress direction, the shear yielding of the matrix was induced in the form of shear bands. Although the growth of the voids themselves might dissipate only a small portion of the energy, it enabled shear yielding of the matrix to be activated. The main contribution to the fracture energy increase in the POSS-reinforced thermosets studied was thus argued to be the shear yielding mechanism in the matrix triggered by void formation templated by POSS nano-aggregates.

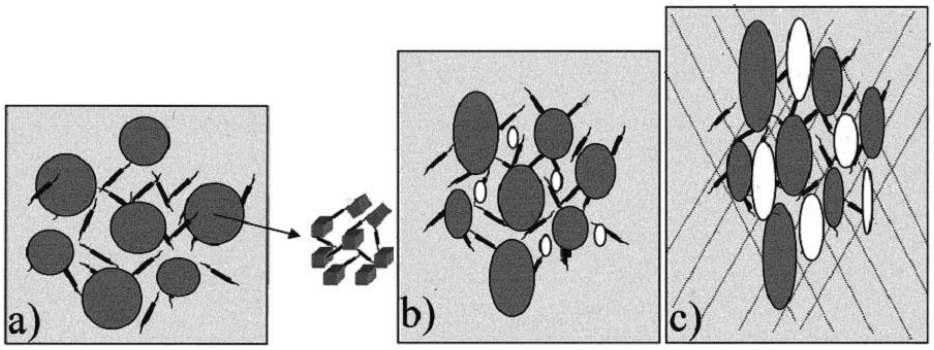

Fig 1.8 Schematic deformation process: (a) undeformed stage, (b) earlier stage of plastic deformation under a tensile load, and (c) advanced stage of plastic deformation. In parts b and c, the light regions represent nucleated voids

Jones et al[123] have found that introduction of octa-epoxycyclohexyl POSS could improve the tensile strength and modulus in ~20% as compared to the neat SC-15 epoxy systems. The authors set a linear equation to describe the contribution of POSS to mechanical performance: $E = E_0 + m_1 w_p$, $\sigma_s = \sigma_{s0} + m_2 w_p$. A nonlinear constitutive equation

$\ln(\frac{\varepsilon}{\sigma}-\frac{1}{E})=\ln\beta+m\ln\varepsilon$ was also established to predict the stress-strain tensile behavior of the POSS/epoxy NC. Fig1.9 show the results obtained by linear fitting.

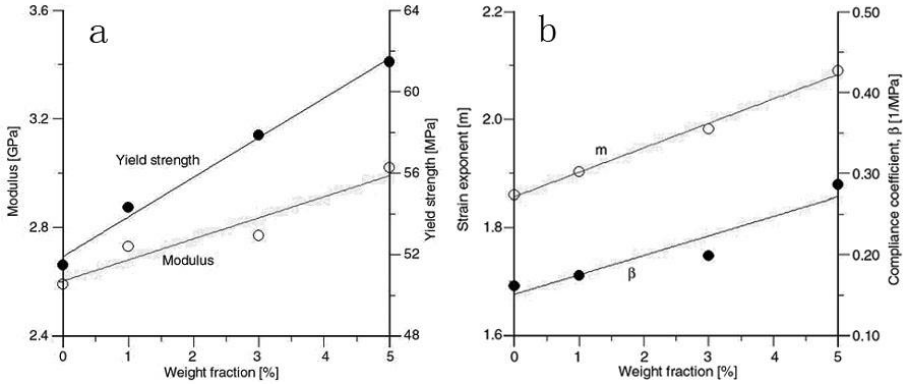

Fig 1.9 Effect of POSS weight fraction on (a) modulus and yield strength and (b) compliance factor β and strain exponent m

Kopesky et al[124] have investigated the toughen of poly(methyl methacrylate) (PMMA) using three distinct POSS species: a crystallizable type that did not disperse on a molecular scale within the PMMA matrix (CyPOSS), and two types of POSS that formed homogeneous mixtures over the loadings we have investigated (MAPOSS and trisilanol-PhPOSS) at loadings between 0 and 15 wt%. The results were shown in Fig1.10. However, all of these binary blends were highly flaw sensitive and thus the reproducibility of the toughening was poor. It was found that the combined addition of the crystallizable CyPOSS and the molecularly-dispersed MAPOSS led to not only the highest toughness values (an increase by a factor of 4 over PMMA) but also excellent reproducibility of the toughening, while not sacrificing the modulus. The authors attributed the toughening to the large amount of plastic deformation required to form the distinct crack structure in these ternary blends, which led to reduced flaw sensitivity. A weak interfacial bond was necessary to observe toughening. Strengthening of the interfacial bond (compatiblized by POSS random copolymer) led to embrittlement of the samples. Inclusions of approximately 100 nm that had a weak affinity for the matrix tend to toughen it in the absence of supercritical flaws; a third component, such as MAPOSS could be added to make the samples less flaw-sensitive.

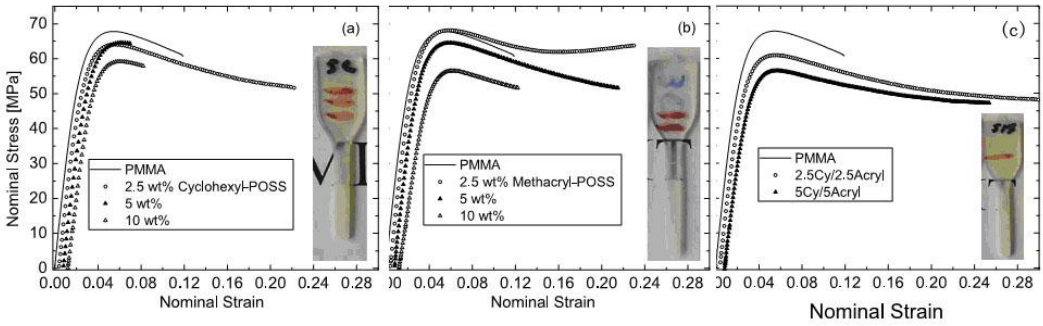

Fig1.10 Tensile properties of PMMA filled with: (a) CyPOSS; (b) MAPOSS; (c) both CyPOSS and MAPOSS

1.2.3 Thermal stability, and resistance

1.2.3.1. Thermal stability

There have been numerous studies on the thermal stability and decomposition pathways for T_8R_8 compounds (R=H, Me, i-Bu, i-Oct, Ph) and other POSS species (silanol) by TGA. Such studies could be complicated by the ready sublimation of many simple POSS compounds under nitrogen and the potential for some to be stable enough to sublime, at least partially, in air. Mantz et al[125] have investigated the thermolysis behavior of both fully and incompletely condensed POSS macromers as well as POSS containing polymers. Sublimation occurred and no cross-linking reactions readily underwent for both all the POSS moiety. Once incorporated into a polymeric form, POSS macromers do not sublime; rather they decompose primarily through partial loss of their organic substituents followed by subsequent cross-linking reactions which incorporates the remaining composition into a SiOxCy network (char). Bolln[126] et al have studied the thermal properties of alkyl (from C2 to C10) substituted cubic cage POSS. Thermogravimetric analysis showed that the weight loss onset shifted to higher temperatures when increasing the alkyl chain length. Further studies by Fina et al[127] showed that the thermal and thermo-oxidation behaviors were depend on POSS type of substitution.

As the POSS in polymer evidenced to low sublimate and in turn the rigid Si rich char prevent further decomposition of polymer matrices, POSS was widely studied as thermal

stability enhancer for polymer materials. Even the effect of POSS was complicate and the mechanism has remained controversy, so far as we know, for al most all the case, thermal stability of matrices is improved in different extension. Investigation of the thermal decomposition processes for polymeric systems can provide insight into the structure, composition, thermal stability, and thermo-chemistry of new macromolecular materials. The development of graftable and polymerizable POSS macromers based on structurally well-defined silsesquioxane precursors were examples of new polymer building blocks which promised the preparation of a wide variety of novel polymeric compositions. As there so many reports were related on this tropic, herein, we focused our concern on the process of decomposition and mechanism study on thermal stability improvement.

The effects of trisilanol iBuPOSS on the thermal staility of methylsilicone resin have been investigated and discussed[128, 129]. It was proposed that the terminal hydroxyl groups of polymer matrix and POSS silanol were crucial to improvement in thermal stabilities of POSS-containing NCs, which reduced the effect of reactive Si-OH end groups on the thermolysis. Moreover, the nanoscaled dispersion of POSS cages in methylsilicone matrixes was also an important factor to contribute to the enhanced thermal stability. It was plausible to propose that mass loss from segmental decomposition via gaseous fragments would be suppressed by well-dispersed POSS cubes at the molecular level. On the other hand, TGA, ^{29}Si NMR and XPS measurements showed that the degradation process at higher temperatures observed in trisilanol iBuPOSS reinforced methylsilicone was predominantly due to the retardation of chain motions by POSS molecules and the selective removal of iBu group followed by the resulting inorganic SiO2 layer to rigidize the polymer materials and prevent further degradation of the virgin polymer. The promising results combined with the numerous property enhancements previously reported for POSS incorporation into traditional polymer systems made their use as an attractive alternative to filler or coating systems when applied to space-based material applications.

NCs consisting of hybrid copolymers of MACyPOSS and MMA with up to 92 wt % (51 mol %) MACyPOSS and with superior thermal properties were synthesized using solution polymerization[130]. The addition of POSS-1 enhanced the thermal stability, increasing the degradation temperature, reducing the mass loss, and preventing PMMA-like degradation

from propagating along the chain. The initial stages of degradation involved mass loss from MMA alone, around 40% of the MMA units in Stages A+B and the remainder in Stage C. The degradation and sublimation mass loss from POSS-1 was around 58% in Stage D for the MACyPOSS monomer and for the copolymers with relatively low MACyPOSS contents. The Stage D mass loss from the copolymer with a relatively high POSS-1 content was limited to around 30% since the polymerization of POSS-1 with itself reduced sublimation. Exposure to 450^{o}C produced CyPOSS-like remnants in the MACyPOSS monomer and in all the copolymers. The degradation of these remnants, for the copolymers and for the MACyPOSS monomer, yielded 75% SiO_2 and an oxidized carbonaceous residue.

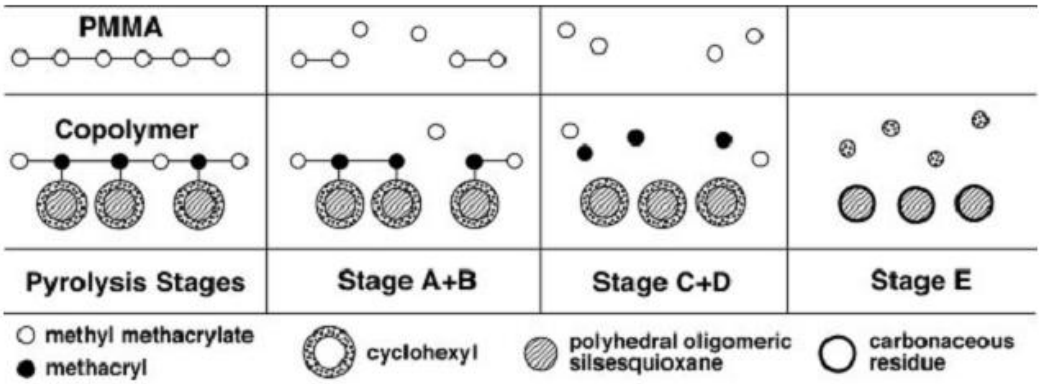

Fig1.11 Thermal pyrolysis process of MACyPOSS-MMA statistic copolymer

1.2.3.2. Flame retardancy

Regardless the advantages of polymers in contrast to traditional material, their flammability were one of the fatal drawbacks, which represented a major limitation to their extension application. New fire retardant strategies shifting from flame extinguishment to flame prevention by creation of flame starvation conditions during polymer combustion have been developed aiming at materials with low fire risk and hazard. In particular, a breakthrough could come from surface ceramisation and charring taking place in the combustion of polymer NCs. As a preceramic, POSS has been proved to enhance the thermo-oxidation resistance, attributed to the formation of the inert silica-like layer on the surface which can prevent the further oxidation of the inner part of the matrix. Camino et al[131]

briefly reviewed the development on POSS as fire retardant in recent decade.

In PC and trisilanol PhPOSS (TPOSS) blend[132], the addition of TPOSS significantly decreased the peak heat release rate (PHRR) of the hybrids, although the presence of POSS shortened the ignition time at all levels tested. The incorporation of TPOSS also retarded the oxidation of char residue and enhanced the intensity and thermal oxidative stability of the char layer which built up on the surface of the burning polymer. As the following result from Wu[133], the incorporation of POSS into the epoxy was beneficial for improving the flame retardancy of epoxy. The morphology influences the heat release rate (HRR), because of POSS as a non-halogen fire retardant, the homo-dispersion improved its efficiency. The addition of POSS in epoxy/POSS would accelerate the char formation, resulting in the reduction of the HRR. Franchini et al[134] have also reported that lower HRR was observed for 3.7 wt% pre-reacted glycidyl-PhPOSS incorporated into DGEBA as compared with that of non reactive Octa-PhPOSS.

However, single POSS component not always showed positive effect in flame retardancy as expected[135]. The most important role of POSS in flame retardancy has been proved to be the synergetic effect with other flame retardant[89, 136-140]. The possibility to subtract part of the organic polymer from combustion through carbonization was one of the main goals in polymer fire retardancy; in this sense metal-POSS compounds were promising fire retardants and synergic formulation with other flame retardant additives should be studied. Fina et al[141] have found that Al iBu POSS appeared to be an effective fire retardant for PP, resulting in lower HRR and Effective Heat of Combustion (EHC), whereas the addition of octa-iBuPOSS and PP/Zn-POSS not show any fire retardancy improvements. They attributed the PP/Al-POSS behavior probably to the catalytic effect of the Al moieties, promoting secondary reactions during polymer degradation and leading to partial PP charring, instead of complete volatilization.

Wang et al[143] have investigated the thermal stability of the phosphorus-containing epoxy resin PCEP/OVPOSS hybrids containing 0, 1, 2, and 3 wt % content of OVPOSS by TGA. The comparison between experimental TGA curves and the calculated ones indicated that the synergistic effect of phosphorus–silicon on flame retardancy: phosphorus promoted the char formation, and silicon protected the char from thermal degradation. The results from RT-FTIR

and Py-GC/MS showed that the thermal oxidative degradation process of PCEP/OVPOSS hybrid was very complicated which included the oxidation, condensation, and cross-linking reactions. The flame retardant properties evaluated by microscale combustion calorimetry experiments showed that the incorporation of OVPOSS into epoxy resins obviously decreased the peak heat release rate and total heat release of the hybrids. SEM and XPS study of char residues indicated that the addition of OVPOSS retarded the oxidation of char residue and enhanced the flame resistance of epoxy resins.

Gérard et al[143] have studied synergistic effect on flame retardance of OMPOSS and conventional flame retardant ammonium polyphosphate (APP) in an epoxy resin (Fig1.12). The morphology of the residues after burning as shown in Fig1.13 indicated that the addition of OMPOSS in combination with APP drastically increased the resistance of the final char residue due to less cracks and more homogeneous bubble distribution with smaller size even the intumescing ratio was slightly reduced. Furthermore, the char residual of epoxy modified with combined flame retardant was composed of two layers: the lower area was black whereas the upper one was filled with bubbles and has a metallic appearance.

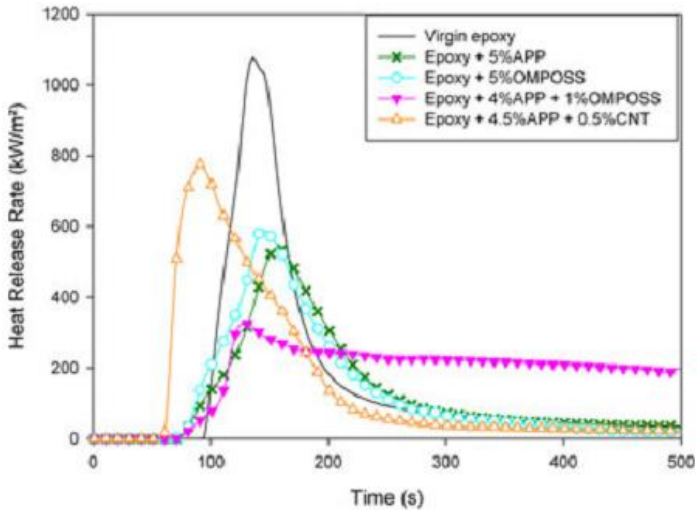

Fig1.12 Mass−loss calorimeter curves for epoxy formulations (heat flux: 35 kW/m^2)

The smoke was fatal when got fire, so the reduction of smoke release was meaningful to evaluate the fire retardant. The lower smoke production was related to the more aromatic specimen left in the carbonaceous layer, which led to higher char yield. Wu et al[144] have

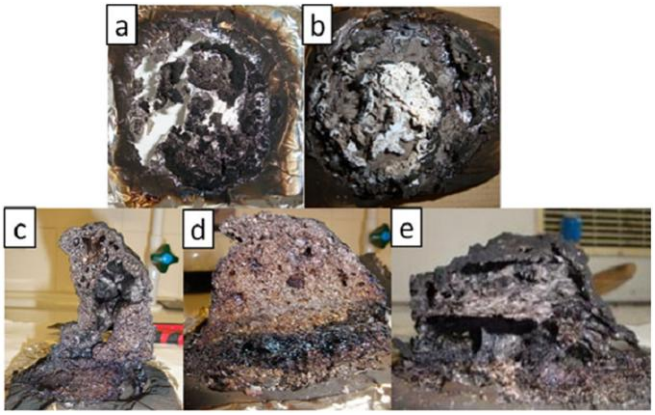

Fig 1.13 Chars obtained after mass-loss calorimeter test, top view: (a) virgin, (b) 5% OMPOSS, and cross-section: (c) 5% APP, (d) 4% APP-1% OMPOSS, and (e) 4.5% APP-0.5% CNT

investigated flame retardancy of the NCs of epoxy and POSS-triol prepared in the presence of metal complex latent catalyst, aluminum triacetylacetonate ([Al]) for the reaction between POSS-triol and DGEBA. The presence of [Al] latent catalyst resulted in smaller particle size of POSS dispersed in epoxy led to a decrease in combustion rate with respect to epoxy and epoxy/POSS composites as well as reduction in smoke, CO and CO_2 production rate as well as higher efficiency in forming insulating char on the surface of composites during combustion. The carbonaceous char obtained at the end of combustion showed compact structure, giving the positive evidence.

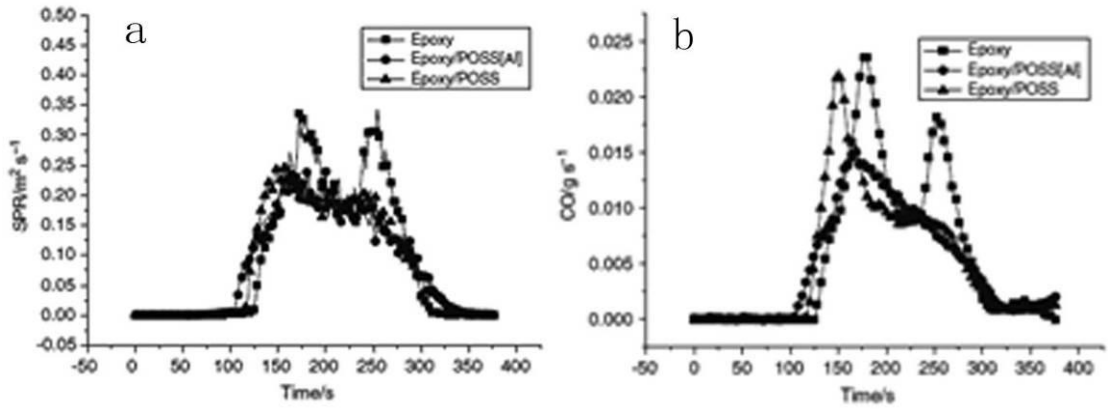

Fig 1.14 (a) Smoke production and (b) CO concentration during combustion of epoxy and epoxy/POSS

1.2.3.3. Photo-Oxidative Resistance

Si-O bond was much stronger than other covalent bond from energetically concern. Due to the Si-O skeleton, POSS could survive from not only in thermal degradation and combustion, but also in high-energy ion beams, vacuum ultraviolet and oxygen plasma in terms of SiO_2. Moreover, the pre-formed SiO2-like surface layer on the POSS materials prevented further etching and consumption. Such excellent oxidation resistance made it possible in the application in photo-oxidative resistance materials, aerospace materials and lithography technology.

Eon et al[145] have found that the etch rate decreased as the increase of POSS content of poly(tert-butyl methacrylate) (PtBMA)-based ethyl POSS random copolymers in oxygen. In situ XPS measurements showed that a silicon oxide layer was formed on top of the ethyl-POSS copolymers during oxygen plasma processing. Tegou et al[146] have reported the ethyl-POSS containing copolymers applied as resist components for nano-fabrication. Minton et al[147] included AO exposure of samples with protected and unprotected areas followed by depth profilometry erosion studies. As shown in Fig1.15, 10 wt% POSS-polyimide exhibited an order of magnitude decrease in erosion step height after exposure to AO relative to space-certified Kapton H. Lin et al[148] have prepared a series of negative-type photo-resists with various MI-POSS methacrylate contents via blending. This blending type photoresists with mono-methacrylate group POSS had similar photoresist characteristics as the copolymer type with slightly less efficiency but better processability.

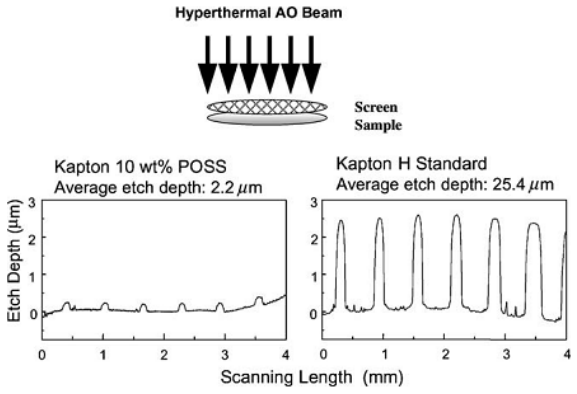

Fig 1.15 Profilometry measurements after AO fluence of 8.47×10^{20} atoms/cm^2

In recent, Moon et al[148] have fabricated 2D and 3D structured organosilcates from epoxy functionalized POSS cage materials using holographic lithography, which can be conveniently converted to silica structures by thermal removal of the organic moieties (Fig1.16). Ro et al[150] have precisely quantified the performance of octameric organosilicate materials with tunable chemical and mechanical properties as replication materials to create low-cost, high-resolution secondary nanoimprint lithography molds. Selective etching of well-patterned BCPs, PS-*b*-PMAPOSS and PMMA-*b*-PMAPOSS formed nanomaterials with precisely size control[151]. The control over domain orientation by solvent annealing on unmodified substrates, combined with the high etch selectivity between the blocks, and the ability to access very small domain sizes (<10 nm) makes these BCPs a unique and exciting material platform to create etch-resistant masks.

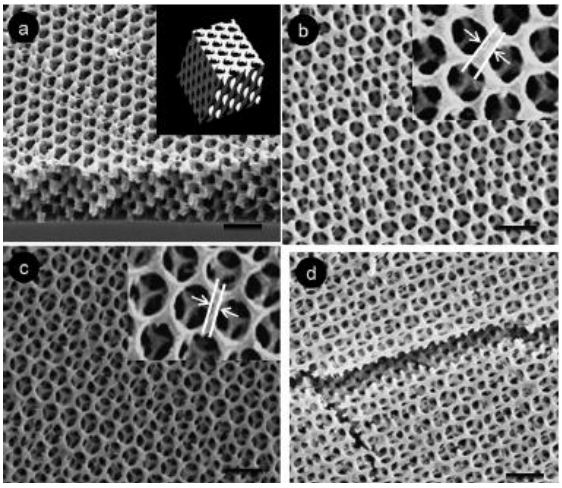

Fig 1.16 3-d Silicate layer obtained by holographic lithography

1.2.4 Surface properties

With a well-defined size of approximately 1.5 nm, POSS moieties were also good candidates to be utilized as a stabilizer to polymer thin films. POSS segregation at the film surface reduced the surface free energy and spreading coefficient, and its segregation at the film-substrate pinned the contact line polymer film and substrate, leading to the inhibition of dewetting. Concentration in-depth of copolymers with POSS mixed with t-BMA analyzed by ARXPS showed non-uniform distribution[152]. Thus surfaces wee almost identical for all

copolymers studied with silicon mass percentages from 3% to 19%. Below this surface, the bulk material seemed from the point of view of the XPS to be organized in a random way without particular structure.

Hosaka et al[153, 154] have found that the incorporation of CpPOSS could lead to a dewetting inhibition of PS thin film on silicon wafers. Accordingly, CpPOSS moieties were rich in two regions: one was at the surface of the film, where the Si concentration was 6 times as high as the theoretical value of the mixture. The other was at the film-substrate interface (the rim of the hole). Meanwhile, they realized that the POSS segregation and dispersion state were a function of vertex (R) groups surrounding the Si-O cage, which determined the interaction between POSS moieties and the polymer matrix. POSS-terminated polystyrene (PS-POSS) prepared by Nitroxide radical Mediated Polymerization (NMP) can actually stabilize PS thin films against dewetting[155]. Neutron reflectivity measurement of deuterated PS-POSS thin film revealed that the POSS moieties of PS-POSS formed enrichment layer at the interfaces of the film.

POSS cage decorated by aliphatic or fluorinated group had very low surface energy and tended to immigrated to surface, lowering the surface energy and improving the processbility of polymer. Wanke et al[156] have exposed polypropylene (PP) to plasma treatment and then reactively coated with POSS-isothiocyanate in order to modify both of its surface characteristics: chemical composition and roughness. The results showed that the POSS-coating promoted the reduction of surface roughness and induced a substantial increase in the water contact angle. Random incorporation of fluorinated POSS into PMMA chain have been reported to decrease the surface energy at very low POSS content (i.e. 3wt%)[157]. In these copolymers, microphase separation was observed, i.e., F-POSS units tend to form a nanostructured dispersed phase in the bulk of films prepared from solvent casting of copolymer solutions. Water and oil repellent terpolymers containing POSS and fluoropolyether segments have also been prepared and characterized[158]. With the increasing of the POSS content, better thermal stability and hydrophobicity of the terpolymer were obtained. The hydrophobicity and oleophobicity of the terpolymer could be adjusted by controlling the feed ratio of Ov-POSS. The cotton fabrics coated with the terpolymers could achieve super-hydrophobicity and high oleophobicity. MAiBuPOSS addition in

poly(isobornyl methacrylate) (IBoMA) has been reported to reduce the surface energy, which opened the way to obtain hydrophobic methacrylic coatings without the use of fluorinated monomers[67]. The effect was particularly important for cross-linked polymers where the addition of 30 wt% POSS decreased the surface energy from about 29 mN $m^{-1}$to 16 mN m^{-1}, a very low value for hydrocarbon materials.

1.3. Assembly behavior of POSS based polymer

POSS with inert vertex groups (linear- or cyclo-aliphatic) on the silicon-oxygen cage rendered it quite hydrophobic in nature and further provides the potential to create (quaisi) amphiphilic molecules when combined covalently with polymer chains. As for any other amphiphilic system, self-assembled nanostructures can be expected in both the bulk and solvent, especially if a solvent selective for one of the components is utilized. Moreover, the perfect asymmetric of cubic POSSs allowed them well packed to form crystal like aggregates. The strong ability of POSS to aggregate in non-solvents made it interesting to study the self-assembly behaviors of polymer-POSS hybrids. In such a selective solvent, amphiphilic molecules can display supermolecular aggregates ranging from spheres, to rods, to lamellae.

1.3.1 Assembly of POSS directed by other well defined structures

In some case, less defined POSS hybrid could form well patterned structure, if directed by well defined structure with specific interaction (strong dipole, hydrogen bonding or covalent bonding) between POSS and unique block. Novel single-molecular hybrid nano-cylinders by covalently attaching a monothiol-functionalized POSS (POSS-SH) to PGMA cylindrical brushes (Fig1.17)[159]. Then monothiol-functional POSS was covalently attached to the PGMA brushes by reaction with the epoxy groups. Due to the steric hindrance, only 20% of the epoxy groups reacted with POSS-SH, according to SLS before and after functionalization. Both the length and the diameter of the brushes increase due to functionalization, as indicated by AFM and non-stained TEM measurements. The residual SiO_2 obtained from the pyrolysis of PGMA-POSS in TGA measurement showed interesting connected cylindrical structures.

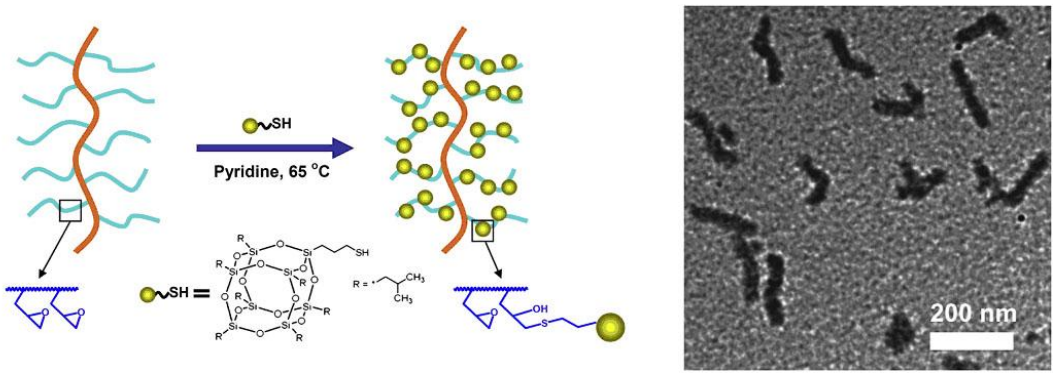

Fig 1.17 POSS grafting reaction and TEM image of silica nanofiber after pyrolysis

Lu et al[160] have reported PCL-*b*-P4VP directed blending octa-phenol POSS self-assembly mediated by hydrogen-bonding interactions. POSS interact with PVP and PCL gradually with the increase of its content and the morphology of BCP gradually changed from lamellar to cylindrical and spherical, finally to a miscible system as the pridyl to OH molar ratio increased from 1:0 to 1:2 as schematically illustrated in Fig1.18.

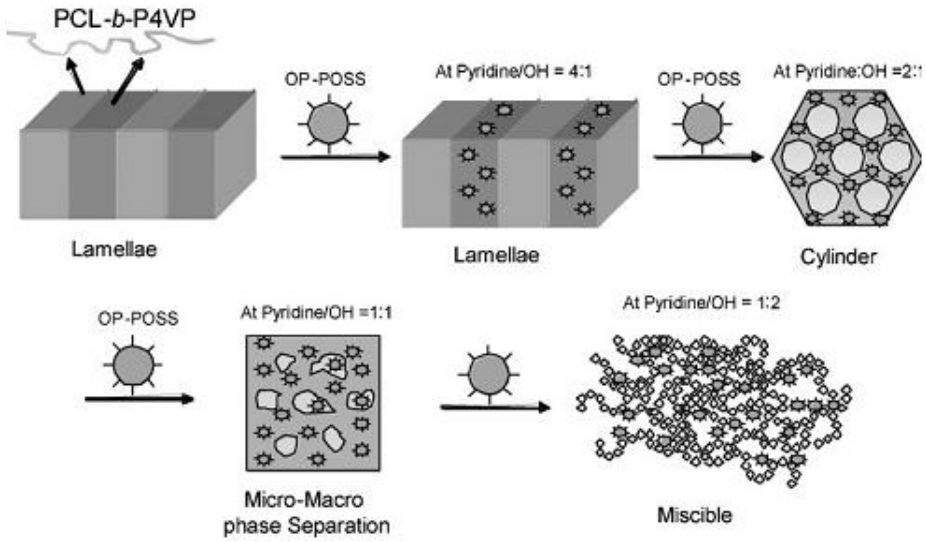

Fig 1.18 The effect of POSS content on the phase morphology of PCL-*b*-P4VP

Mixing aqueous solutions of anionic BCP micelles and of silsesquioxane NPs led to a straightforward formation of O/I nano-hybrids that responded to pH and salinity[161, 162]. Complexation in acidic media was driven by hydrogen-bonding and ionic interaction, and in alkaline media, nano-hybrids were mainly formed due to ionic interaction. The reason for the

size conservation was most probably due to the kinetically frozen micellar core and the compensation of (i) increased steric repulsion due to complexation and (ii) attractive interactions between the silsesquioxane NP and the charged PAA. Cryo-TEM micrographs indicated a core-shell-corona structure of the nano-hybrids, where the shell had a higher density of NPs than the corona.

POSS cages fully functionalized with maleamic acid or aminophenyl ligands capable of hydrogen bonding with the PEO blocks of low *MW* BCPs can induce order in the otherwise disordered BCP melts, producing well-ordered and highly filled composites with small domains[163]. The phase behavior of the composites depended significantly upon the choice of hydrogen bonding ligands, however, blends with both additives with F108 formed well-ordered cylindrical and spherical morphologies. Lamellar morphologies were accessible using Pluronic P105 as the template. Between the two ligands, maleamic acid was found to result in higher levels of incorporation than aminophenyl while maintaining the well-ordered BCP morphology. Strong order in the BCP nanostructure was maintained up to 80% loading of POSS-OAA and up to 40% loading of POSS-OAP in F108. XRD and DSC measurements indicated miscibility and compatibility of both the additives with PEO. Cross-linking of the POSS-OAA-F108 composite at 50% and 70% additive loadings upon heating to 160^{o}C followed by calcination at 650^{o}C yielded meso-porous silica with cylindrical and spherical morphologies that were templated by the presence of the BCP.

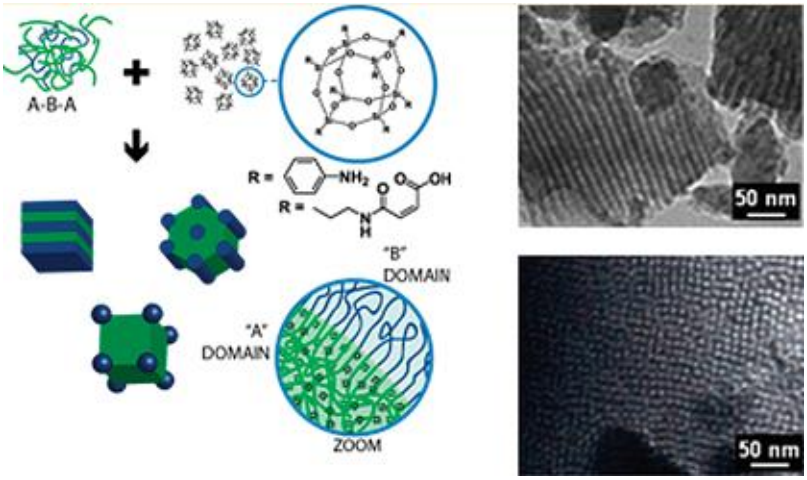

Fig 1.19 Assembly of POSS in polymer via hydrogen bonding and TEM images of meso-porous silica obtained from pyrolysis

1.3.2 Synthesis and self-assembly of POSS end-capping polymers

Kim et al[164] have investigated the morphological, microstructural, and rheological properties of amphiphilic telechelics POSS-PEO. It was found that the morphologies of the crystals were dramatically affected by POSS incorporation level and thus length of PEO block. Amphiphilic POSS telechelics showed microstructural features characteristic structure of two separate crystalline components-PEO and POSS. The amphiphilic POSS telechelics behave like triblock. The persistence of a POSS nano-crystalline phase at temperature between the melting transition of PEO and POSS led to dramatic alteration in physical properties, especially flow behavior (Fig1.20). The dynamic module of the POSS10k-tel having about 20 wt% POSS content was solid like for a wide range of temperatures above the PEO melting temperature, but apparently underwent an order disorder transition at a temperature near the apparent melting temperature for the POSS phase observed calorimetrically. Further study on the viscosity data of dilute solution of new POSS-PEO telechelics revealed the influences of polymer architecture and solvent polarity on associative behaviors of the polymers in dilute solutions[165]. It was found that the solution viscosities were strongly affected by the solvent (THF/water) composition. A polyelectrolyte-like effect was observed in H_2O, manifested as an upturn in η_{red} at low concentration, postulating the formation of micelles in the solutions. It was concluded that the associative behavior of the amphiphilic POSS telechelics could vary depending on the POSS content and the length of PEO blocks affording a significant variation in hydrophobic/hydrophilic balance as well as on solvent polarity.

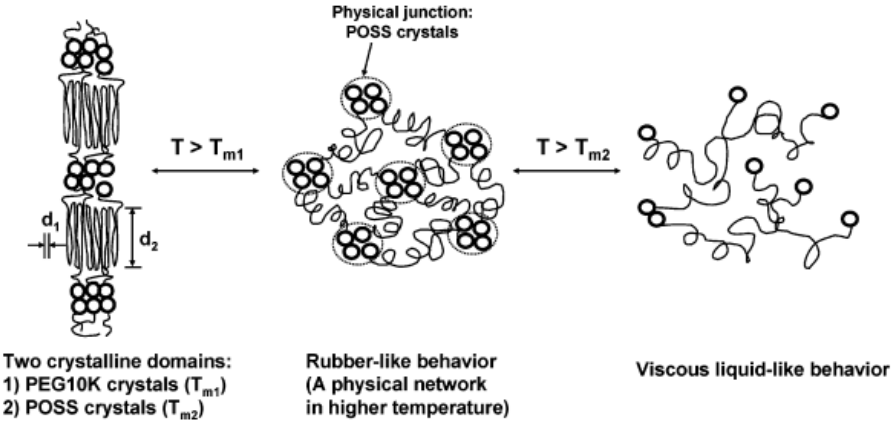

Fig1.20 Two steps molten behavior of POSS end-capped PEO

Solution behavior of telechelic styrene/sodium styrene-sulfonate copolymer P(S-*co*-SSA) with POSS as the end groups has been studied[166]. In the studied concentration range, the Tele-PSS-POSS molecules self-assembled into micelles that had a hydrophobic core mainly composed of iBuPOSS surrounded by a corona of PSS loops. With increasing Tele-PSS-POSS concentration, the micelles became increasingly interconnected, forming larger hollow supermicellar structures (Fig1.21). The uniqueness of this amphiphilic telechelic hybrid lied in the strong aggregation propensity of POSS, which induced micelle bridging even at low concentrations.

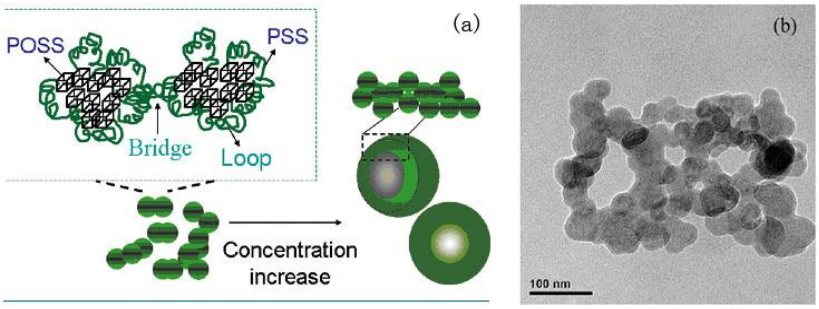

Fig 1.21 (a) Schematic illustration of self-assembly of POSS end-capped P(S-*co*-SSA) and (b) TEM image of supermicelle structure

Micellization behavior of well-defined eight armed amphiphilic cubic silsesquioxane-poly(ethylene oxide) (CSSQ-PEO) has also been studied[167]. A core-corona structure of unimolecular and aggregated CSSQ-PEO was found in aqueous solution. DLS measurements and TEM micrographs showed that unassociated unimolecular micelles coexisted with micelles aggregates at certain concentrations. The corona PEO segments were expanded and swollen in aqueous solution that may cause the CSSQ-PEO unimolecular micelles to form large-size spherical aggregates. The interconnections between the micelles aggregates led to the formation of network-like structures at higher concentration.

POSS-helical polypeptide copolymers have been synthesized through the ring-opening polymerization (ROP) of γ-benzyl-L-glutamate N-carboxyanhydride (γ-Bn-Glu NCA) using aminopropyl iBuPOSS as a macroinitiator (Fig1.22)[168]. The POSS moiety incorporated at the chain end of the PBLG unit played two important roles: (a) allowing intramolecular hydrogen

bonding to occur between the POSS and PBLG units to enhance the latter's R-helical conformations in the solid state and (b) preventing the aggregation of nanoribbons although the POSS blocks' protrusion from the ribbons results in the formation of clear gels in solution (Fig1.23). Such a hierarchical self-organization was interesting from a biomimetic point of view, and also provided a new strategy for the design of micrometer-scale superstructured materials with nanometric precision.

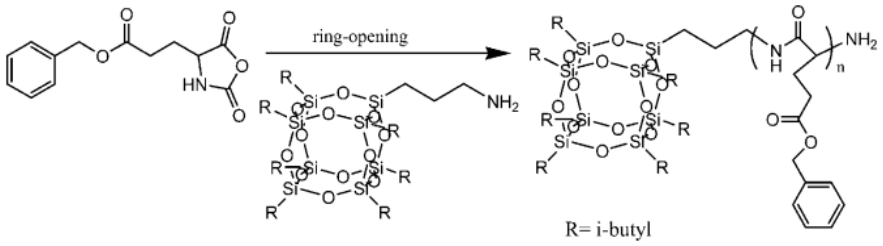

Fig 1.22 Synthesis of peptide via ring-open reaction initiated by amino POSS

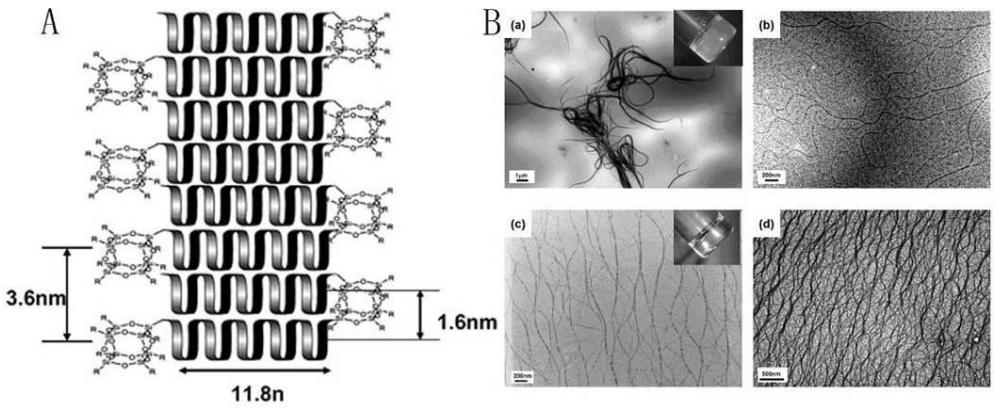

Fig 1.23 (A) Self-assembly of POSS end-capped peptide and (B) TEM of: (a) $PBLG_{53}$ homopolypeptide, and copolymers of (b) POSS-$PBLG_{18}$, (c) POSS-PBLG43, and (d) POSS-PBLG56. 0.2 wt % solution in toluene, stained by RuO

Zhang et al have designed and synthesized a novel POSS-containing CTA from aminopropyl iBuPOSS (Fig1.24). The POSS-containing RAFT agent was further applied in the RAFT polymerization of N-Isopropylacrylamide (NIPAM)[169], tert-Butyl acrylate (t-BA)[170] and St[171] to produce the tadpole-shaped O/I hybrid polymers. The tadpole-shaped O/I hybrid PNIPAM exhibited a change in volume in response to external temperature changes. P(t-BA) was further hydrolyzed into amphiphilic, tadpole-shaped POSS-PAA.

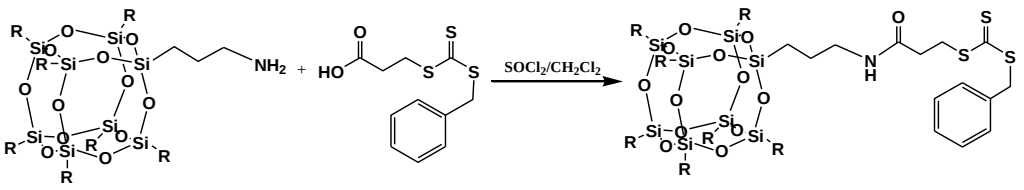

Fig 1.24 The synthesis of POSS containing CTA

Considering the polymer matrices as selective solvent, the self-assembly of (quasi)amphiphilc POSS based polymers occurred in the matrices as well as in conventional selective solvent, if not rapidly frozen by vetrification. Zheng et al have synthesized hepta(3,3,3-trifluoropropyl)POSS capped PCL[172], PEO[173] and poly(hydroxyether of bisphenol A)[174], and used them as modifier in epoxy to construct NCs via the in situ polymerization (Fig1.25). The formation of nanostructures was addressed on the basis of miscibility and phase behavior of the subcomponents of the O/I amphiphile with epoxy after and before curing reaction. It was proposed that the formation of the nanostructures followed the mechanism of self-assembly. AFM showed that there is significant migration of the POSS moiety at the surface of the thermosets. The static contact angle measurements indicated that the O/I NC displayed a significant enhancement in surface hydrophobicity (or dewettability) as well as reduction in surface free energy.

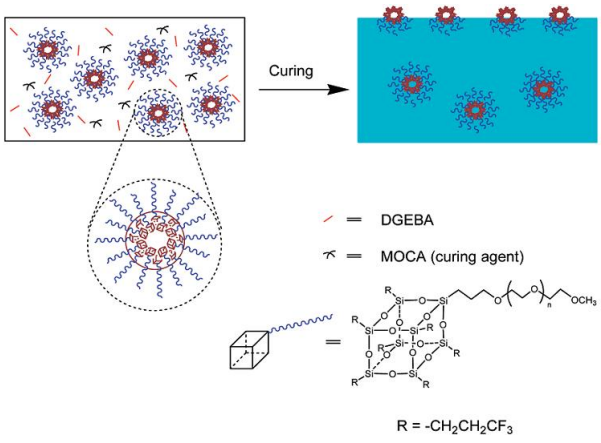

Fig 1.25 Self-organization of fluoro containing POSS end capped PEO in epoxy

In most situations, POSS acted as hydrophobic block due to their low polarity. However, in the studies of self-assembly in aqueous solution, amphiphilic molecules composed of big

hydrophilic head and long hydropobic tail was more popular. Cheng et al[175] for the first time have successfully synthesized such kind of POSS based "giant surfactant" via combination of living anionic polymerization, hydrosilylation, and thiol-ene "click" chemistry. The micellar morphology of PS-APOSS in solution changed from vesicles to wormlike cylinders andfurther to spheres as the degree of ionization of the carboxylic acid groups increased. Unexpectedly, it was found that the PS tails in the core of PS-APOSS micelles were highly stretched and the trend of the core radii of the micelles was found to be Rvesicle < Rcylinder < Rsphere, which is the opposite of that for the traditional PS-*b*-PAA BCP system. The conformational rigidity of the APOSS head groups and the strong APOSS-APOSS interactions in PS-APOSS micelles are believed to force the PS tails to stretch in order to minimize the overall free energy. This novel class of giant surfactants expands the scope of macromolecular amphiphiles and provides a platform for the study of the basic physical principles of their self-assembly behaviors. In a present publication[176], they have also reported the synthesis of other two kind of POSS end capped amphiphilics based on PLA via chain initiation from mono-hydroxyl functionalized heptavinyl POSS (VPOSS-OH) with controlled *MW* and narrow polydispersity by stannous octoate-mediated ring-opening polymerization of L-lactide, followed by by thiol-ene "click" chemistry to functionalize the POSS with various functional groups, such as carboxylic acids, hydroxyl groups, and sugars to impart tunable polarity and functionality to the head group.

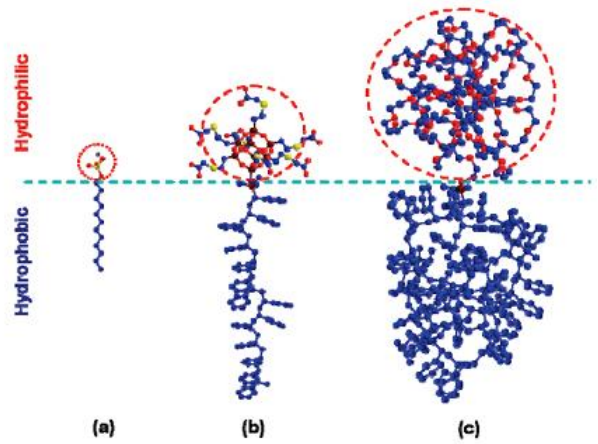

Fig 1.26 (a) Small molecular surfactant, (b) Gaint surfactant and (c) Amphiphilic BCP on the interface of water/oil

Miao et al[177] have studied the self-assembly and chain-folding in well-defined PE-*b*-PEO-*b*-POSS triblock molecules. In these triblock oligomers, both PE and POSS were crystalline, whereas PEO became amorphous due to tethering of its both ends to other two blocks. In the crystalline state, PE chains tilted 32° from the lamellar normal, and both iBuPOSS and CpPOSS molecules stacked into four-layer (ABCA) lamellar crystals, having the same trigonal (R3 hm) symmetry as in pure POSS crystals. Because the cross-sectional area for a PE chain in the PE crystals (0.216 nm^2/chain) at the interface was much smaller than that for a POSS molecule in POSS crystals (1.136 nm^2/molecule), the self-assembly and PE chain-folding were substantially affected by the sequence of PE and POSS crystallization when crystallizing from the melt. On the basis of this study, the authors concluded that confinement effect plays an important role on chain-folding of crystalline block oligomers, which in turn determines the unbalanced cross-sectional areas between chemically different blocks and finally dictates their final crystalline morphology.

Mather et al[178, 179] have reported that iBuPOSS-centered poly(ε-caprolactone) (PCL) polyol telechelics network showed evidence for microphase separation and complex crystallization competition between PCL and POSS. It was found that only those PCL networks with high POSS loading (>34 wt%) led to POSS crystalline domains as indicated by differential scanning calorimetry (DSC) and wide-angle X-ray diffraction (WAXD). Dynamic mechanical analysis showed two distinct rubbery plateaus in the sample with 42 wt% POSS loading, one between the T_g of amorphous PCL and the prominent POSS melting point, the other appearing above the POSS melting point and afforded by the covalent crosslinks. An excellent one-way shape memory response (shape fixing and recovery) was observed for these high POSS loading samples featuring POSS crystallinity. It was observed that for POSS-PCL diols there was coordination (via hydrogen bonding) between the inert corner groups of POSS and the PCL end groups, thus compromising PCL crystallization. Network formation gave rise to POSS crystals embedded in an amorphous PCL phase.

1.3.3 Synthesis and self-assembly of POSS BCPs

In contrast to that in solution, the self-assembly of end-capped POSS polymer in bulk or

film was few investigated, due to the low POSS fraction and low *MW*. BCPs were proper candidates for further investigation on bulk self-assembly behavior and application of POSS based polymer. With the developing of LCP, synthesis of POSS BCPs with high *MW* and POSS fraction and tunable composition became possible.

POSS bearing reactive double bond was one of the most popular macromer for POSS tethering polymers. New synthetic routes were applied to these POSS macromers to achieve designed structure polymers. Among which, the LCP have been attracted considerable attention due to their potential in topological design and end-functionalization. Herein, the synthesis of well defined POSS based BCPs via LCP and their self-assembly were presented individually.

Haddad et al[180] for the first time have reported on the self-assembly of AB POSS based BCPs, poly(norbornene-POSS)-*b*-poly(norbornene) prepared via ROMP. As shown in Fig1.27, the TEM images of thin sections revealed that such diblocks featured prominent micro-phase separation when the POSS content was above 10 wt%. The distinct dark POSS-rich phase, due to its higher electron density, featured the strong ordering as cylinders (Fig1.28). However, the long-range ordering of cylindrical POSS-rich micro-domain was poor, perhaps due to poor *MW* distribution. ROMP of norbornene ethyl POSS monomer (NBEPOSS) and 2-endo-3-exo-5-norbornene-2, 3-dicaboxylic acid trimethyl ester (NBETMS) was performed by Xu et al[181] as well. The BCP PNBETMS-*b*-PNBEPOSS were then converted to PNBECOOH-*b*-PNBEPOSS by hydrolysis and precipitation.

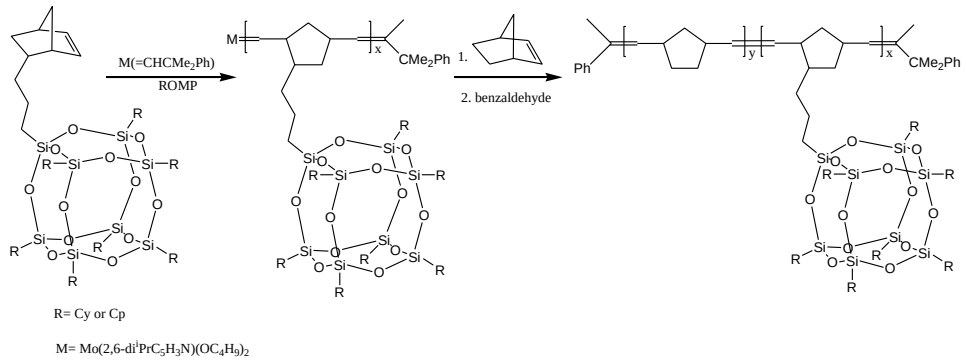

Fig 1.27 Synthesis of norbornene POSS BCP via ROMP

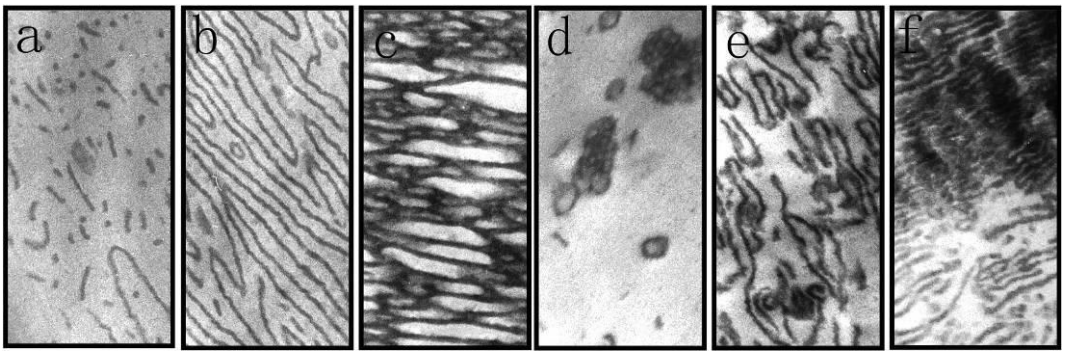

Fig1.28 Morphology of norbornene-POSS/norbornene BCPs casting film: (a)10wt%, (b)30wt%, (c)60wt% of norbornene-CpPOSS and (d)10wt%, (e)30wt%, (f)60wt% of norbornene-CyPOSS

Pyun et al[182, 183] have successfully synthesized well-defined AB diblocks and ABA triblocks PBA-*b*-PMAPOSS via ATRP (Fig1.29). TEM images obtained with selective staining of POSS revealed that microphase separation did not occur at lower POSS loadings, where the DP_n followed $PMAPOSS_6$-*b*-PBA_{481}-*b*-$PMAPOSS_6$. At a higher molar ratio $PMAPOSS_{10}$-*b*-PBA_{201}-*b*-$PMAPOSS_{10}$, strong micro-phase separation was observed but with a morphology inverse that expected: PBA cylinders were periodically distributed in a continuous PMAPOSS despite it being the larger weight fraction component. Above both T_g of the two phases, the rheological behavior showed a lack of fluidity at even the highest temperature and lowest frequency. The slope near 1/2 at lower frequency, observed for both log *G'* & *G"* vs log reduced frequency, was consistent with other rheological observations for ordered BCPs. This non-terminal rheological behavior was attributed to elasticity derived from the micro-phase separated morphology of a strongly segregated system. However, even the polymer were narrow dispersed, the DP_n can not be higher than 15 for MAiBuPOSS due to the steric hindrance, which limited the wide application of this method.

The self-asembly of amphiphilic copolymers PEG-*b*-PMAPOSS synthesized via ATRP has also been studied [184, 185]. It was found that the diblock copolymer showed tailored micellization behavior, whereas the triblock copolymer formed physical gel crosslinked by organization of POSS block (Fig1.30). Gelation was induced in micelle solution of diblock copolymer by introducing triblock copolymer chains as well. The rheological performance

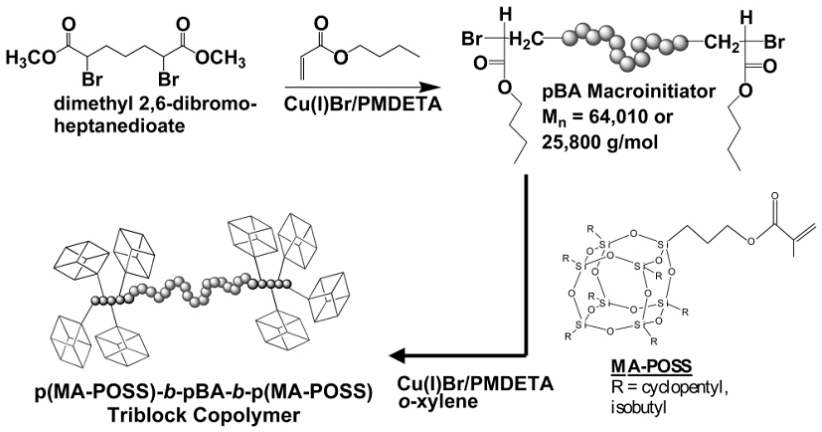

Fig 1.29 Synthesis of POSS containing ABA triblock copolymer via ATRP

even superior to that of pure triblock copolymer gel, was achieved with 40 wt % content of triblock in the mixture. The reported results could provide new tool to custom design systems with desired rheological behavior by controlling the composition of gel with the choice of di-triblock copolymers and POSS NPs. Furthermore, the research illustrated strong hydrophobicity of POSS block and its ability to self-assemble into micelles and of gel formation at relatively lower BCP concentrations. This could open up new avenues for functional POSS polymers in cosmetic and drug delivery applications.

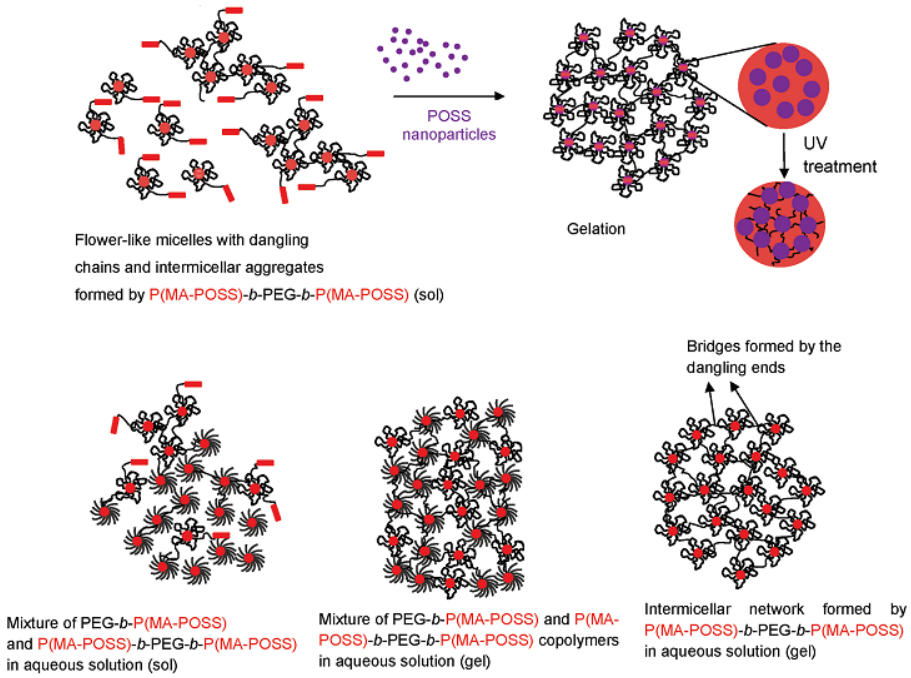

Fig1.30 Schematic presentations of intermicellar aggregates in solutions and gels

Rios-Dominguez et al[186] have attempted to synthesize hybrid BCP based on the hybrid styryl POSS by stable free radical polymerization using BPO and hydroxyl-TEMPO (Fig1.31). The POSS-TEMPO macro initiator synthesized in this work had a M_n in the order of 3900Da with a *PDI* of 1.1. The M_n for the polystyrene synthesized with different amounts of the POSS-TEMPO macro initiator increased slightly with the amount of the macro initiator, whereas the M_w showed an important increase since the *PDI* increases from 2.7 to 4 when PS was synthesized with 5 and 20wt% of the POSS-TEMPO macro initiator, respectively.

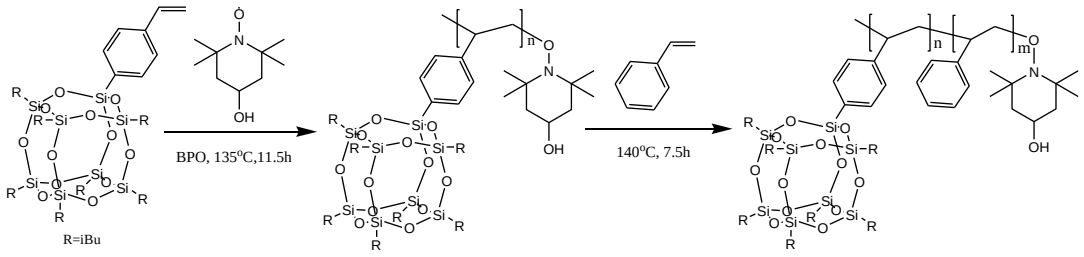

Fig 1.31 Synthesis of POSS based block copolymer via NMP

Hayakawa et al[187, 188] have investigated the LAP of methacryl POSS monomer. It was reported that LAP break the limitation in polymerization degrees caused by stereic hindrance as described in ATRP and NMP, thus hybrid BCPs with tunable composition could be easily synthesized. O/I BCPs containing POSS namely PMMA-*b*-PMAPOSS and PS-*b*-PMAPOSS were synthesized with excellent control over the POSS chain length and narrow polydispersity.

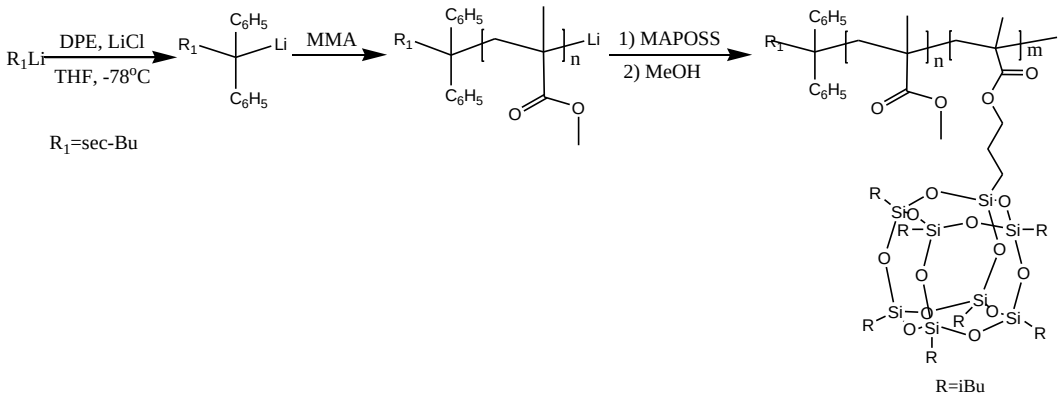

Fig 1.32 Synthesis of POSS based BCP via LAP

Both bulk samples and thin-film samples showed well-patterned structure by TEM and synchrotron X-ray scattering (Fig1.33). Because of the tunability of the PMAPOSS length by anionic polymerization, a rich range of morphologies such as spheres, cylinders, and lamellae were obtained for both sets of BCPs. In thin films, the PMAPOSS segments formed a helix-like structure to relieve the steric crowding of the POSS units. Upon thermal annealing POSS aggregation drove the helical units to pack into an orthorhombic lattice structures. The excellent self-assembling characteristics in bulk and thin films, good etch selectivity between the blocks, and access to a wide range of domain sizes and morphologies made these POSS-based BCPs ideal candidates for lithography.

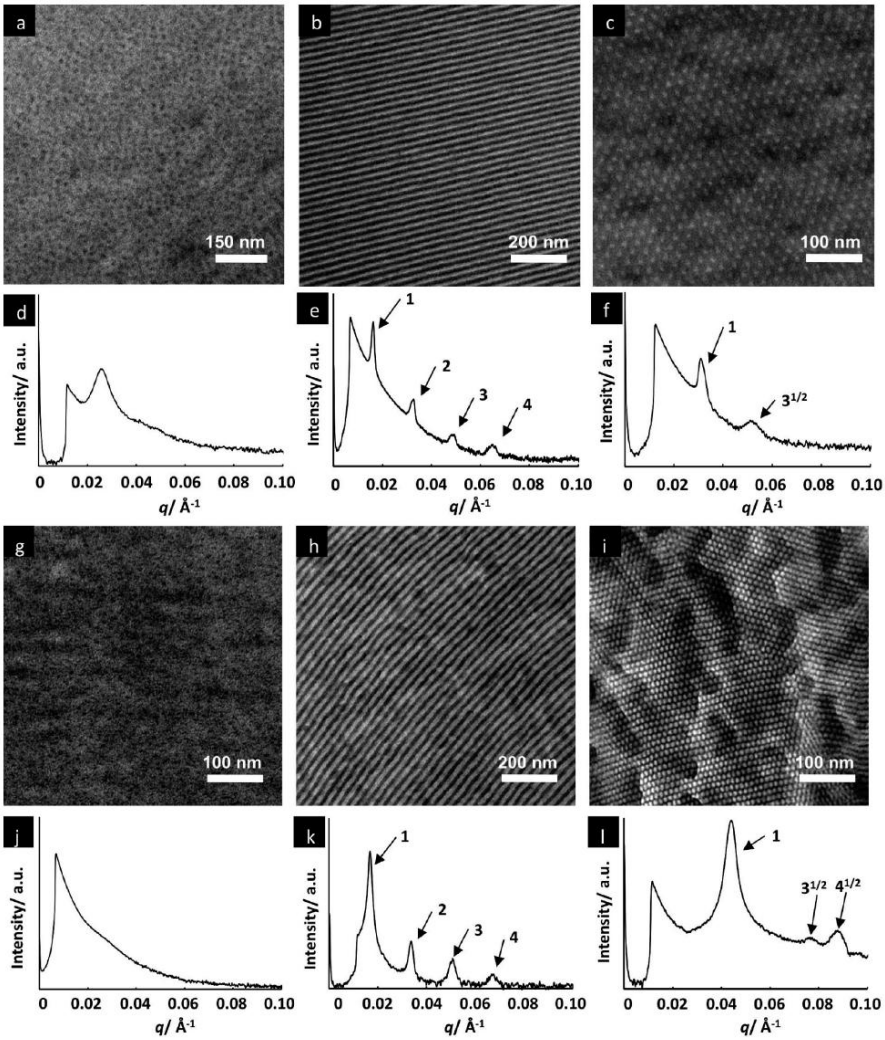

Fig 1.33 TEM and TSAXS profiles of (a, d) $PMMA_{450}$-*b*-$PMAPOSS_7$, (b, e) $PMMA_{262}$-*b*-$PMAPOSS_{23}$, (c, f) $PMMA_{52}$-*b*-$PMAPOSS_{18}$, (g, j) PS_{587}-*b*-$PMAPOSS_4$, (h, k) PS_{266}-*b*-$PMAPOSS_{20}$, and (i, l) PS_{52}-*b*-$PMAPOSS_9$

Insight studies on the POSS packing in hybrid BCPs have been carried out in nanoscale thin films of PS_{214}-*b*-$PMAPOSS_{27}$ by using in situ GIXS (GISAXS and GIWAXS) with a synchrotron radiation source[189]. Vertically oriented lamellar structure in the out-of-plane of the film with the thicknesses of the PS and PMAPOSS domain layers were 20.4 and 15.9 nm was formed in the solvent-annealed films with and without further thermal annealing. Surprisingly, it was found that in the lamellar structure, the PMAPOSS layers were composed of two sublayers, namely a densely ordered layer (13.0 nm thick) and a less ordered layer (2.9 nm thick). The block chains in the densely ordered layer formed orthorhombic crystals whereas those in the less ordered layer formed molecularly stacked layers as schemed in Fig1.35. The formation of the crystals and ordered layers might be induced by the ordering ability of the POSS moieties. Furthermore, the PMAPOSS block chains had helical conformations and thus were present as molecular cylinders, which made the formation of the crystals and ordered layers possible. However, on heating the orthorhombic crystals and the molecularly stacked layers in the PMAPOSS domains were found to melt over the range 170~190^{o}C. Because of melting, both the thicknesses and densities of the densely ordered and less ordered PMAPOSS layers in the lamellar structure varied significantly with temperature. During the subsequent cooling run, the orthorhombic crystals and molecularly stacked layers were not fully recovered, which indicated that the formation of orthorhombic crystals and stacked layers in the PMAPOSS domains required thermal annealing.

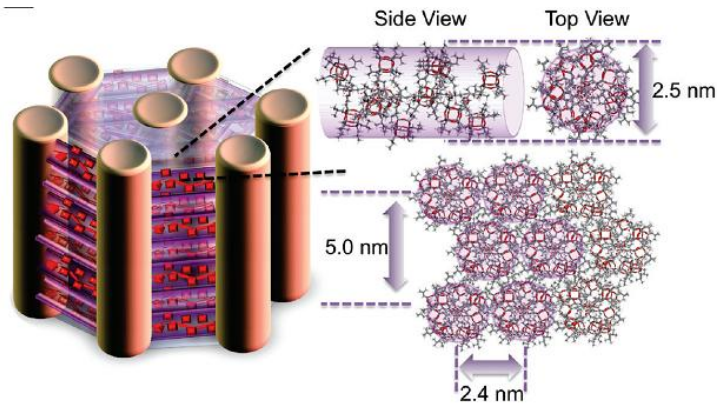

Fig 1.34 Representation of the morphology of thermally annealed $PMMA_{41}$-*b*-$PMAPOSS_{29}$, consisting of PMMA cylinders in a PMAPOSS matrix

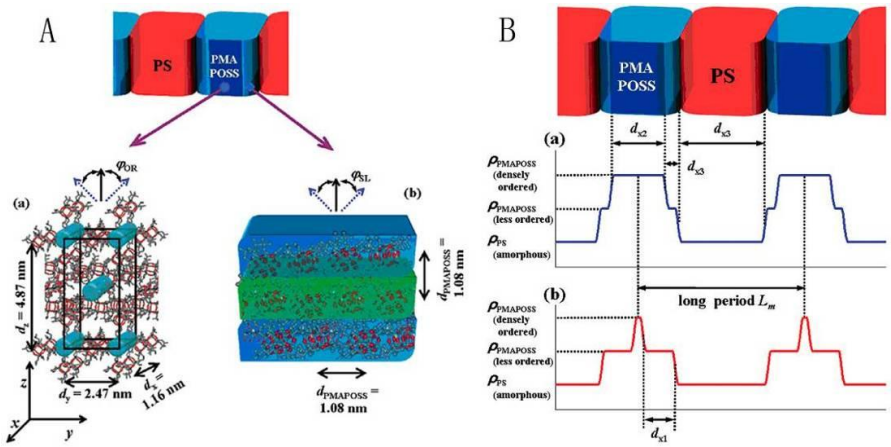

Fig1.35 (A) Schematic representation of the molecular packing structure of PMAPOSS domains in PS_{214}-*b*-$PMAPOSS_{27}$ films: (a) densely ordered layer and (b) a less ordered layer; (B) Relative electron density profile along the long period of the lamella: (a) 25°C before heating; (b) 200°C on heating. Here, d_{x1}, d_{x2}, and d_{x3} were the thicknesses of the less ordered layer, the densely ordered layer, and the amorphous PS layer, respectively

Mya et al[190] have synthesized PMAiBuPOSS homopolymer and their BCP, PMAiBuPOSS-*b*-PMMA by RAFT polymerization, for the first time, in the presence of DDTA. From the evaluation of the MAiBuPOSS polymerization kinetics, the monomer conversion was found to be ~80% and the M_n at this conversion were 24000 and 32300 Da for the [MAiBuPOSS]/[DDTA] ratios of 100 and 200, as determined by GPC. However, the high polydispersity was observed in PMAiBuPOSS homopolymers due to the presence of low *MW* species attributed by the chain termination reaction, which revealed that the RAFT polymerization was not well-controlled by using DDTA.

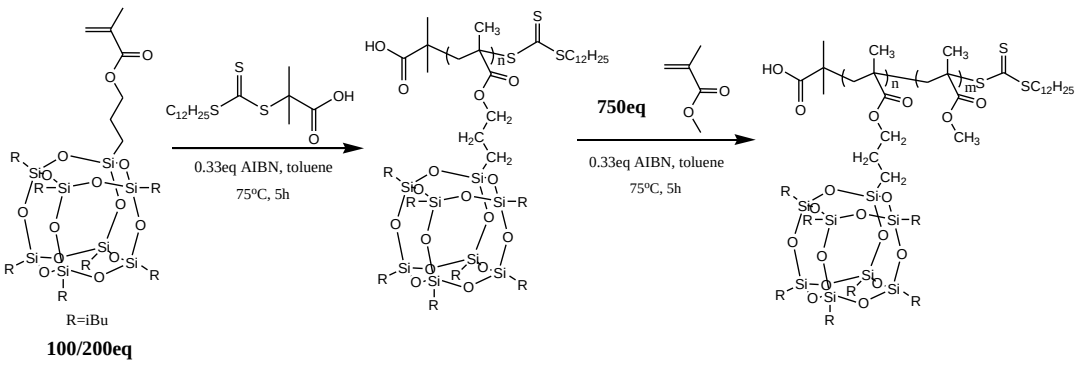

Fig 1.36 Synthesis of POSS based BCP via RAFT polymerization mediated by DDTA

1.4 Our work

This work was generally aimed to synthesize POSS based BCP and their self-assemblies via RAFT polymerization, to study on the effect of POSS self-assembly structure on the bulk properties and to prepare nanostructured hybrid epoxy via POSS based copolymer.

CRP of POSS kind monomer with bulky side group has remained a challenge in recent decades, which limited the comprehensive study of properties and application of POSS based block polymers. Herein, we have investigated the RAFT polymerization of several POSS macromers with different vertex group. Vertex group dependence was found in terms of limitation of DP_n. By optimizing the experiment condition, POSS homopolymer close to limitation with narrow *MW* distribution was synthesized. The chain extension behavior of PMACyPOSS macro CTA by several types of monomer was studied. POSS based BCPs with different topology such as AB，BAB，$(BA)_3$ and $(BA)_n$ were synthesized. The morphology and thermo-mechanical properties of POSS based BCPs as well as the structure-property relationship was investigated.

The self-assembly behavior of POSS based BCP in selective solvent was studied and self-assemblies were achieved. Dispersion RAFT polymerization in apolar solvent was studied and self-assemblies with various morphologies were obtained. Cooling induced micelle transition and the chain length effect on the pathway to vesicle were found.

Nano-construction of O/I hybrid epoxy materials based on POSS based copolymers was investigated. The effect of functional group content on miscibility of POSS based statistic copolymer and epoxy was investigated. A novel method to nanostructure epoxy hybrid from self-assembly of POSS based BCPs possessing high POSS weight ratio synthesized via RAFT polymerization in epoxy precursors was presented. Thanks to the presence of the miscible PMMA block, the BCP was capable to self-organize on a nano-scale in epoxy precursors solutions, forming micelles owning inorganic-rich POSS core and PMMA corona. The properties of resulted POSS based O/I hybrids was studied in terms of thermo-mechanical, fracture, thermal stability as well as char formation.

Reference

1. Okada, A.F., et al., *Composite material and process for manufacturing same.* [P]. US Patent 4739007, 1988.
2. Kojima, Y., et al., *Synthesis of Nylon-6-Clay Hybrid by Montmorillonite Intercalated with Epsilon-Caprolactam.* [J]. Journal of Polymer Science Part a-Polymer Chemistry, 1993. **31**(4): p. 983-986.
3. Brinker, C.J. and C. Scherer, *Sol-Gel Science.* [M]. Academic Press: San Diego,, 1990.
4. Feher, F.J. and T.A. Budzichowski, *New Polyhedral Oligosilsesquioxanes Via the Catalytic-Hydrogenation of Aryl-Containing Silsesquioxanes.* [J]. Journal of Organometallic Chemistry, 1989. **373**(2): p. 153-163.
5. Feher, F.J., et al., *A new route to heterosilsesquioxane frameworks.* [J]. Angewandte Chemie-International Edition, 1998. **37**(19): p. 2663-2666.
6. Loy, D.A. and K.J. Shea, *Bridged Polysilsesquioxanes - Highly Porous Hybrid Organic-Inorganic Materials.* [J]. Chemical Reviews, 1995. **95**(5): p. 1431-1442.
7. Scott, D.W., *Theremal Rearrangement of Branchedchain Metylpolysiloxanes.* [J]. Journal of the American society, 1946. **68**: p. 356-357.
8. Brown, J.F.J. and H.V.J. Lester, *The Polycondensation of Cyclohexylsilanetriol.* [J]. Journal of the American society, 1965. **87**: p. 4313-4317.
9. Feher, F.J., D.A. Newman, and J.F. Walzer, *Silsesquioxanes as Models for Silica Surfaces.* [J]. Journal of the American Chemical Society, 1989. **111**(5): p. 1741-1748.
10. Feher, F.J. and K.J. Weller, *Polyhedral Aluminosilsesquioxanes as Models for Aluminosilicates - Unique Synthesis of Anionic Al/Si/O Frameworks.* [J]. Organometallics, 1990. **9**(10): p. 2638-2640.
11. Martynova, T.N. and T.I. Chupakhina, *Heterofunctional Oligoorganylsilsesquioxanes.* [J]. Journal of Organometallic Chemistry, 1988. **345**(1-2): p. 11-18.
12. Calzaferri, G., et al., *The monophenylhydrosilasesquioxanes PhH(n-1)Si(n)O(1.5n) where n=8 or 10.* [J]. Journal of the Chemical Society-Dalton Transactions, 1996(15): p. 3313-3322.
13. Feher, F.J., *Polyhedral Oligometallasilsesquioxanes (Pomss) as Models for Silica-Supported Transition-Metal Catalysts - Synthesis and Characterization of (C5me5)Zr[(Si7o12)(C-C6h11)7].* [J]. Journal of the American Chemical Society, 1986. **108**(13): p. 3850-3852.
14. Feher, F.J., R. Terroba, and J.W. Ziller, *A new route to incompletely-condensed silsesquioxanes: base-mediated cleavage of polyhedral oligosilsesquioxanes.* [J]. Chemical Communications, 1999(22): p. 2309-2310.
15. Feher, F.J., D. Soulivong, and F. Nguyen, *Practical methods for synthesizing four incompletely condensed silsesquioxanes from a single R8Si8O12 framework.* [J]. Chemical Communications, 1998(12): p. 1279-1280.
16. Feher, F.J., D. Soulivong, and A.G. Eklund, *Controlled cleavage of R8Si8O12 frameworks: a revolutionary new method for manufacturing precursors to hybrid inorganic-organic materials.* [J]. Chemical Communications, 1998(3): p. 399-400.
17. Feher, F.J., et al., *Methods for effecting monofunctionalization of (CH2 = CH)(8)Si8O12.* [J]. Chemical Communications, 1999(14): p. 1289-1290.
18. Feher, F.J., et al., *A new route to incompletely condensed silsesquioxanes: acid-mediated cleavage and rearrangement of (c-C6H11)(6)Si6O9 to C-2-[(c-C6H11)(6)Si6O8X2].* [J]. Chemical Communications, 1999(17): p. 1705-1706.

19. Feher, F.J., R. Terroba, and R.Z. Jin, *Controlled partial hydrolysis of spherosilicate frameworks: syntheses of endo-[(Me3SiO)(6)Si6O7(OH)(4)] and endo-[(Me3SiO)(6)Si6O7{OSiMe2(CH=CH2)}(4)] from [(Me3SiO)(6)Si6O9]*. [J]. Chemical Communications, 1999(24): p. 2513-2514.
20. Feher, F.J., et al., *Syntheses of highly functionalized cube-octameric polyhedral oligosilsesquioxanes (R8Si8O12).* [J]. Journal of the Chemical Society-Dalton Transactions, 1999(9): p. 1491-1497.
21. Cordes, D.B., P.D. Lickiss, and F. Rataboul, *Recent Developments in the Chemistry of Cubic Polyhedral Oligosilsesquioxanes.* [J]. Chemical Reviews, 2010. **110**(4): p. 2081-2173.
22. Fina, A., O. Monticelli, and G. Camino, *POSS-based hybrids by melt/reactive blending.* [J]. Journal of Materials Chemistry, 2010. **20**(42): p. 9297-9305.
23. Kuo, S.W. and F.C. Chang, *POSS related polymer nanocomposites.* [J]. Progress in Polymer Science, 2011. **36**(12): p. 1649-1696.
24. Joshi, A. and B.S. Butola, *Studies on nonisothermal crystallization of HDPE/POSS nanocomposites.* [J]. Polymer, 2004. **45**(14): p. 4953-4968.
25. Fu, B.X., et al., *Physical gelation in ethylene-propylene copolymer melts induced by polyhedral oligomeric silsesquioxane (POSS) molecules.* [J]. Polymer, 2003. **44**(5): p. 1499-1506.
26. Chen, J.H., et al., *Isothermal crystallization behavior of isotactic polypropylene blended with small loading of polyhedral oligomeric silsesquioxane.* [J]. Polymer, 2007. **48**(6): p. 1756-1769.
27. Liu, L., et al., *Crystallization and morphology study of polyhedral oligomeric silsesquioxane (POSS)/polysiloxane elastomer composites prepared by melt blending.* [J]. Polymer, 2007. **48**(11): p. 3201-3212.
28. Soong, S.Y., R.E. Cohen, and M.C. Boyce, *Polyhedral oligomeric silsesquioxane as a novel plasticizer for poly(vinyl chloride).* [J]. Polymer, 2007. **48**(5): p. 1410-1418.
29. Soong, S.Y., et al., *Rate-dependent deformation behavior of POSS-filled and plasticized poly(vinyl chloride).* [J]. Macromolecules, 2006. **39**(8): p. 2900-2908.
30. Hao, N., M. Bohning, and A. Schonhals, *CO(2) Gas Transport Properties of Nanocomposites Based on Polyhedral Oligomeric Phenethyl-Silsesquioxanes and Poly(bisphenol A carbonate).* [J]. Macromolecules, 2010. **43**(22): p. 9417-9425.
31. Zhao, Y.Q. and D.A. Schiraldi, *Thermal and mechanical properties of polyhedral oligomeric silsesquioxane (POSS)/polycarbonate composites.* [J]. Polymer, 2005. **46**(25): p. 11640-11647.
32. Kopesky, E.T., et al., *Miscibility and viscoelastic properties of acrylic polyhedral oligomeric silsesquioxane-poly(methyl methacrylate) blends.* [J]. Polymer, 2005. **46**(13): p. 4743-4752.
33. Tanaka, K., S. Adachi, and Y. Chujo, *Side-Chain Effect of Octa-Substituted POSS Fillers on Refraction in Polymer Composites.* [J]. Journal of Polymer Science Part a-Polymer Chemistry, 2010. **48**(24): p. 5712-5717.
34. Misra, R., et al., *Molecular miscibility and chain dynamics in POSS/polystyrene blends: Control of POSS preferential dispersion states.* [J]. Polymer, 2009. **50**(13): p. 2906-2918.
35. Yei, D.R., et al., *Enhanced thermal properties of PS nanocomposites formed from inorganic POSS-treated montmorillonite.* [J]. Polymer, 2004. **45**(8): p. 2633-2640.
36. Wan, C.Y., et al., *Effect of POSS on Crystalline Transitions and Physical Properties of Polyamide 12.* [J]. Journal of Polymer Science Part B-Polymer Physics, 2009. **47**(2): p. 121-129.
37. Misra, R., et al., *POSS-Nylon 6 Nanocomposites: Influence of POSS Structure on Surface and Bulk Properties.* [J]. Journal of Polymer Science Part B-Polymer Physics, 2009. **47**(11): p. 1088-1102.

38. Cozza, E.S., O. Monticelli, and E. Marsano, *Electrospinning: A Novel Method to Incorporate POSS Into a Polymer Matrix.* [J]. Macromolecular Materials and Engineering, 2010. **295**(9): p. 791-795.
39. Kopesky, E.T., et al., *Thermomechanical properties of poly(methyl methacrylate)s containing tethered and untethered polyhedral oligomeric silsesquioxanes.* [J]. Macromolecules, 2004. **37**(24): p. 8992-9004.
40. Yen, Y.C., et al., *Effect of LiClO4 on the thermal and morphological properties of organic/inorganic polymer hybrids.* [J]. Polymer, 2008. **49**(17): p. 3625-3628.
41. Shibata, M., R. Horie, and W. Yoneta, *Intermolecular interaction of supramolecular organic-inorganic hybrid composites of sulfonated polystyrene and oligomeric silsesquioxane possessing pyridyl groups.* [J]. Polymer, 2010. **51**(24): p. 5764-5770.
42. Sheen, Y.C., et al., *Synthesis and characterization of amorphous octakis-functionalized polyhedral oligomeric silsesquioxanes for polymer nanocomposites.* [J]. Polymer, 2008. **49**(18): p. 4017-4024.
43. Carroll, J.B., et al., *"Plug and play" polymers. Thermal and X-ray characterizations of noncovalently grafted polyhedral oligomeric silsesquioxane (POSS) - Polystyrene nanocomposites.* [J]. Macromolecules, 2003. **36**(17): p. 6289-6291.
44. Lichtenhan, J.D., Y.A. Otonari, and M.J. Carr, *Linear Hybrid Polymer Building-Blocks - Mathacrylate-Functionalized Polyhedral Oligmeric Silsquioxane Monomers and Polymers.* [J]. Macromolecules, 1995. **28**(24): p. 8435-8437.
45. Haddad, T.S. and J.D. Lichtenhan, *Hybrid organic-inorganic thermoplastics: Styryl-based polyhedral oligomeric silsesquioxane polymers.* [J]. Macromolecules, 1996. **29**(22): p. 7302-7304.
46. Mather, P.T., et al., *Mechanical relaxation and microstructure of poly(norbornyl-POSS) copolymers.* [J]. Macromolecules, 1999. **32**(4): p. 1194-1203.
47. Zheng, L., R.J. Farris, and E.B. Coughlin, *Novel polyolefin nanocomposites: Synthesis and characterizations of metallocene-catalyzed polyolefin polyhedral oligomeric silsesquioxane copolymers.* [J]. Macromolecules, 2001. **34**(23): p. 8034-8039.
48. Tsuchida, A., et al., *Ethene and propene copolymers containing silsesquioxane side groups.* [J]. Macromolecules, 1997. **30**(10): p. 2818-2824.
49. Waddon, A.J., et al., *Nanostructured polyethylene-POSS copolymers: Control of crystallization and aggregation.* [J]. Nano Letters, 2002. **2**(10): p. 1149-1155.
50. Zhang, H.X., et al., *Preparation and characterization of styrene/styryl-polyhedral oligomeric silsesquioxane hybrid copolymers.* [J]. Polymer International, 2008. **57**(12): p. 1351-1356.
51. Lo Schlavo, S., et al., *Novel propylmethacrylate-monofunctionalized polyhedral oligomeric silsesquioxanes homopolymers prepared via radical bulk free polymerization.* [J]. European Polymer Journal, 2007. **43**(12): p. 4898-4904.
52. Wang, X.T., et al., *Thermal properties and liquid crystallinity of side-chain azobenzene copolymer containing pendant polyhedral oligomeric silsequioxanes.* [J]. Journal of Thermal Analysis and Calorimetry, 2010. **102**(2): p. 739-744.
53. Escude, N.C. and E.Y.X. Chen, *Stereoregular Methacrylate-POSS Hybrid Polymers: Syntheses and Nanostructured Assemblies.* [J]. Chemistry of Materials, 2009. **21**(24): p. 5743-5753.
54. Turri, S. and M. Levi, *Structure, dynamic properties, and surface behavior of nanostructured ionomeric polyurethanes from reactive polyhedral oligomeric silsesquioxanes.* [J]. Macromolecules, 2005. **38**(13): p. 5569-5574.
55. Gu, X.Z., J. Wu, and P.T. Mather, *Polyhedral Oligomeric Silsesquioxane (POSS) Suppresses*

Enzymatic Degradation of PCL-Based Polyurethanes. [J]. Biomacromolecules, 2011. **12**(8): p. 3066-3077.

56. Wu, J.A., Q. Ge, and P.T. Mather, *PEG-POSS Multiblock Polyurethanes: Synthesis, Characterization, and Hydrogel Formation.* [J]. Macromolecules, 2010. **43**(18): p. 7637-7649.
57. Lai, Y.S., et al., *Structural and electrochemical properties of polyurethanes/polyhedral oligomeric silsesquioxanes (PU/POSS) hybrid coatings on aluminum alloys.* [J]. Materials Chemistry and Physics, 2009. **117**(1): p. 91-98.
58. Lee, J., et al., *Synthesis of polyhedral oligomeric silsesquioxane-functionalized polyfluorenes: Hybrid organic-inorganic pi-conjugated polymers.* [J]. Synthetic Metals, 2006. **156**(7-8): p. 590-596.
59. Fu, B.X., A. Lee, and T.S. Haddad, *Styrene-butadiene-styrene triblock copolymers modified with polyhedral oligomeric silsesquioxanes.* [J]. Macromolecules, 2004. **37**(14): p. 5211-5218.
60. Chen, Y.W. and E.T. Kang, *New approach to nanocomposites of polyimides containing polyhedral oligomeric silsesquioxane for dielectric applications.* [J]. Materials Letters, 2004. **58**(29): p. 3716-3719.
61. Hany, R., et al., *Chemical synthesis and characterization of POSS-functionalized poly [3-hydroxyalkanoates].* [J]. Polymer, 2005. **46**(14): p. 5025-5031.
62. Wright, M.E., et al., *Chemical modification of fluorinated polyimides: New thermally curing hybrid polymers with POSS.* [J]. Macromolecules, 2006. **39**(14): p. 4710-4718.
63. Ryu, H.S., D.G. Kim, and J.C. Lee, *Polysiloxanes containing polyhedral oligomeric silsesquioxane groups in the side chains; synthesis and properties.* [J]. Polymer, 2010. **51**(11): p. 2296-2304.
64. Kim, C.K., et al., *Amphiphilic poly(vinyl alcohol) hybrids and electrospun nanofibers incorporating polyhedral oligosilsesquioxane.* [J]. Macromolecules, 2007. **40**(14): p. 4823-4828.
65. Monticelli, O., et al., *Preparation, Characterization, and Properties of Novel PSMA-POSS Systems by Reactive Blending.* [J]. Macromolecules, 2009. **42**(17): p. 6614-6623.
66. Fina, A., et al., *POSS grafting on PPgMA by one-step reactive blending.* [J]. Polymer, 2009. **50**(1): p. 218-226.
67. Zucchi, I.A., M.J. Galante, and R.J.J. Williams, *Surface energies of linear and cross-linked polymers based on isobornyl methacrylate and methacryl-heptaisobutyl POSS.* [J]. European Polymer Journal, 2009. **45**(2): p. 325-331.
68. Wu, X.R., et al., *Development of novel dental nanocomposites reinforced with polyhedral oligomeric silsesquioxane (POSS).* [J]. Dental Materials, 2010. **26**(5): p. 456-462.
69. Zeng, K., Y. Fang, and S.X. Zheng, *Organic-Inorganic Hybrid Hydrogels Involving Poly(N-isopropylacrylamide) and Polyhedral Oligomeric Silsesquioxane: Preparation and Rapid Thermoresponsive Properties.* [J]. Journal of Polymer Science Part B-Polymer Physics, 2009. **47**(5): p. 504-516.
70. Choi, J.W., et al., *Organic/inorganic imide nanocomposites from aminophenylsilsesquioxanes.* [J]. Chemistry of Materials, 2003. **15**(17): p. 3365-3375.
71. Huang, C.F., et al., *Influence of PMMA-chain-end tethered polyhedral oligomeric silsesquioxanes on the miscibility and specific interaction with phenolic blends.* [J]. Macromolecules, 2006. **39**(1): p. 300-308.
72. Mya, K.Y., et al., *Star-Like Polyurethane Hybrids with Functional Cubic Silsesquioxanes: Preparation, Morphology, and Thermomechanical Properties.* [J]. Journal of Polymer Science Part A-Polymer Chemistry, 2009. **47**(18): p. 4602-4616.

73. Wang, Z.B., et al., *Nanostructured Organic-Inorganic Copolymer Networks Based on Polymethacrylate-Functionalized Octaphenylsilsesquioxane and Methyl Methacrylate: Synthesis and Characterization.* [J]. Macromolecules, 2011. **44**(3): p. 566-574.
74. Zhang, J., R.W. Xu, and D.S. Yu, *A novel poly-benzoxazinyl functionalized polyhedral oligomeric silsesquioxane and its nanocomposite with polybenzoxazine.* [J]. European Polymer Journal, 2007. **43**(3): p. 743-752.
75. Sulca, N.M., et al., *Monitoring the synthesis of new polymer nanocomposites based on different polyhedral oligomeric silsesquioxanes using Raman spectroscopy.* [J]. Journal of Raman Spectroscopy, 2009. **40**(11): p. 1634-1640.
76. Lligadas, G., et al., *Bionanocomposites from renewable resources: Epoxidized linseed oil-polyhedral oligomeric silsesquioxanes hybrid materials.* [J]. Biomacromolecules, 2006. **7**(12): p. 3521-3526.
77. Barral, L., et al., *Thermodegradation kinetics of a hybrid inorganic-organic epoxy system.* [J]. European Polymer Journal, 2005. **41**(7): p. 1662-1666.
78. Chiu, Y.C., et al., *Morphology, Thermal and Mechanical Properties of the Polyhedral Oligomeric Silsesquioxane Side-Chain Epoxy Hybrid Material.* [J]. Journal of Applied Polymer Science, 2010. **118**(6): p. 3723-3732.
79. Ramirez, C., et al., *Organic/inorganic hybrid materials from an epoxy resin cured by an amine silsesquioxane.* [J]. Journal of Thermal Analysis and Calorimetry, 2007. **87**(1): p. 69-72.
80. Ramirez, C., et al., *Thermal behaviour of a polyhedral oligomeric silsesquioxane with epoxy resin cured by diamines.* [J]. Journal of Thermal Analysis and Calorimetry, 2003. **72**(2): p. 421-429.
81. Lin, P.H. and R. Khare, *Glass transition and structural properties of glycidyloxypropyl-heptaphenyl polyhedral oligomeric silsesquioxane-epoxy nanocomposites.* [J]. Journal of Thermal Analysis and Calorimetry, 2010. **102**(2): p. 461-467.
82. Di Luca, C., et al., *In-Situ Generation of a Dispersion of POSS Crystalline Platelets in an Epoxy Matrix Induced by Polymerization.* [J]. Macromolecules, 2010. **43**(21): p. 9014-9021.
83. Lee, A. and J.D. Lichtenhan, *Viscoelastic responses of polyhedral oligosilsesquioxane reinforced epoxy systems.* [J]. Macromolecules, 1998. **31**(15): p. 4970-4974.
84. Kumar, S.A. and A. Sasikumar, *Studies on novel silicone/phosphorus/sulphur containing nano-hybrid epoxy anticorrosive and antifouling coatings.* [J]. Progress in Organic Coatings, 2010. **68**(3): p. 189-200.
85. Choi, J., et al., *Organic/inorganic hybrid composites from cubic silsesquioxanes.* [J]. Journal of the American Chemical Society, 2001. **123**(46): p. 11420-11430.
86. Choi, J., A.F. Yee, and R.M. Laine, *Organic/inorganic hybrid composites from cubic silsesquioxanes. Epoxy resins of octa(dimethylsiloxyethylcyclohexylepoxide) silsesquioxane.* [J]. Macromolecules, 2003. **36**(15): p. 5666-5682.
87. Choi, J., S.G. Kim, and R.M. Laine, *Organic/inorganic hybrid epoxy nanocomposites from aminophenylsilsesquioxanes.* [J]. Macromolecules, 2004. **37**(1): p. 99-109.
88. Dias, N.L., et al., *Dielectric properties of thermosetting material nanocomposites.* [J]. Journal of Applied Polymer Science, 2007. **106**(1): p. 205-213.
89. Liu, Y.L., et al., *Epoxy/polyhedral oligomeric silsesquioxane nanocomposites from octakis(glycidyidimethylsiloxy)octasilsesquioxane and small-molecule curing agents.* [J]. Journal of Polymer Science Part a-Polymer Chemistry, 2006. **44**(12): p. 3825-3835.
90. Perrin, F.X., N. Chaoui, and A. Margaillan, *Effects of*

octa(3-chloroammoniumpropyl)octasilsesquioxane on the epoxy self-polymerisation and epoxy-amine curing. [J]. Thermochimica Acta, 2009. **491**(1-2): p. 97-102.

91. Liu, Y.H., S.X. Zheng, and K.M. Nie, *Epoxy nanocomposites with octa(propylglycidyl ether) polyhedral oligomeric silsesquioxane.* [J]. Polymer, 2005. **46**(25): p. 12016-12025.
92. Tucker, S.J., et al., *Ambient cure PUSS-epoxy matrices for marine composites.* [J]. Composites Part A-Applied Science and Manufacturing, 2010. **41**(10): p. 1441-1446.
93. Teo, J.K.H., et al., *Epoxy/polyhedral oligomeric silsesquioxane (POSS) hybrid networks cured with an anhydride: Cure kinetics and thermal properties.* [J]. Polymer, 2007. **48**(19): p. 5671-5680.
94. Ramirez, C., et al., *Epoxy/POSS organic-inorganic hybrids: ATR-FTIR and DSC studies.* [J]. European Polymer Journal, 2008. **44**(10): p. 3035-3045.
95. Ni, Y. and S.X. Zheng, *Epoxy resin containing octamaleimidophenyl polyhedral oligomeric silsesquioxane.* [J]. Macromolecular Chemistry and Physics, 2005. **206**(20): p. 2075-2083.
96. Ni, Y., S.X. Zheng, and K.M. Nie, *Morphology and thermal properties of inorganic-organic hybrids involving epoxy resin and polyhedral oligomeric silsesquioxanes.* [J]. Polymer, 2004. **45**(16): p. 5557-5568.
97. Lee, L.H. and W.C. Chen, *Organic-inorganic hybrid materials from a new octa(2,3-epoxypropyl)silsesquioxane with diamines.* [J]. Polymer, 2005. **46**(7): p. 2163-2174.
98. Liu, Y.H., K. Zeng, and S.X. Zheng, *Organic-in organic hybrid nanocomposites involving novolac resin and polyhedral oligomeric silsesquioxane.* [J]. Reactive & Functional Polymers, 2007. **67**(7): p. 627-635.
99. Huang, J.C., et al., *Organic-inorganic nanocomposites from cubic silsesquioxane epoxides: direct characterization of interphase, and thermomechanical properties.* [J]. Polymer, 2005. **46**(18): p. 7018-7027.
100. Abad, M.J., et al., *Epoxy networks containing large mass fractions of a monofunctional polyhedral oligomeric silsesquioxane (POSS).* [J]. Macromolecules, 2003. **36**(9): p. 3128-3135.
101. Liu, Y.L. and G.P. Chang, *Novel approach to preparing epoxy/polyhedral oligometric silsesquioxane hybrid materials possessing high mass fractions of polyhedral oligometric silsesquioxane and good homogeneity.* [J]. Journal of Polymer Science Part A-Polymer Chemistry, 2006. **44**(6): p. 1869-1876.
102. Zucchi, I.A., et al., *Monofunctional epoxy-POSS dispersed in epoxy-amine networks: Effect of a prereaction on the morphology and crystallinity of POSS domains.* [J]. Macromolecules, 2007. **40**(4): p. 1274-1282.
103. Xu, Y.T., et al., *Morphology and thermal properties of organic-inorganic hybrid material involving monofunctional-anhydride PUSS and epoxy resin.* [J]. Materials Chemistry and Physics, 2011. **125**(1-2): p. 174-183.
104. Camino, G., A. Fina, and D. Tabuani, *High Performance Fillers for Polymer Composites* [J]. International Conference, 4th, Barcelona, Spain, Mar. 4-5, 2009. **15**: p. 1-6.
105. Joshi, M., et al., *Rheological and viscoelastic behavior of HDPE/octamethyl-POSS nanocomposites.* [J]. Macromolecules, 2006. **39**(5): p. 1839-1849.
106. Wu, J., et al., *Rheological behavior of entangled polystyrene-polyhedral oligosilsesquioxane (POSS) copolymers.* [J]. Macromolecules, 2007. **40**(3): p. 544-554.
107. Romo-Uribe, A., et al., *Viscoelastic and morphological behavior of hybrid styryl-based polyhedral oligomeric silsesquioxane (POSS) copolymers.* [J]. Journal of Polymer Science Part B-Polymer Physics, 1998. **36**(11): p. 1857-1872.

108. Lee, A., J. Xiao, and F.J. Feher, *New approach in the synthesis of hybrid polymers grafted with polyhedral oligomeric silsesquioxane and their physical and viscoelastic properties.* [J]. Macromolecules, 2005. **38**(2): p. 438-444.
109. Romero-Guzman, M.E., et al., *Viscoelastic properties of POSS-styrene nanocomposite blended with polystyrene.* [J]. Rheologica Acta, 2009. **48**(6): p. 641-652.
110. Wu, J., T.S. Haddad, and P.T. Mather, *Vertex Group Effects in Entangled Polystyrene-Polyhedral Oligosilsesquioxane (POSS) Copolymers.* [J]. Macromolecules, 2009. **42**(4): p. 1142-1152.
111. Bizet, S., J. Galy, and J.F. Gerard, *Structure-property relationships in organic-inorganic nanomaterials based on methacryl-POSS and dimethacrylate networks.* [J]. Macromolecules, 2006. **39**(7): p. 2574-2583.
112. Brus, J., M. Urbanova, and A. Strachota, *Epoxy networks reinforced with polyhedral oligomeric silsesquioxanes: Structure and segmental dynamics as studied by solid-state NMR.* [J]. Macromolecules, 2008. **41**(2): p. 372-386.
113. Bizet, S., J. Galy, and J.F. Gerard, *Molecular dynamics simulation of organic-inorganic copolymers based on methacryl-POSS and methyl methacrylate.* [J]. Polymer, 2006. **47**(24): p. 8219-8227.
114. Xu, H.Y., et al., *Glass transition temperatures of poly(hydroxystyrene-co-vinylpyrrolidone-co-isobutylstyry1 polyhedral oligosilsesquioxanes).* [J]. Polymer, 2002. **43**(19): p. 5117-5124.
115. Xu, H.Y., et al., *Preparation, thermal properties, and T-g increase mechanism of poly(acetoxystyrene-co-octavinyl-polyhedral oligomeric silsesquioxane) hybrid nanocomposites.* [J]. Macromolecules, 2005. **38**(25): p. 10455-10460.
116. Ruiz-Perez, L., et al., *Toughening by nanostructure.* [J]. Polymer, 2008. **49**(21): p. 4475-4488.
117. Liu, H. and S. Zheng, *Polyurethane Networks Nanoreinforced by Polyhedral Oligomeric Silsesquioxane.* [J]. Macromolecular Rapid Communications, 2005. **26**(3): p. 196-200.
118. Huang, J.-M., et al., *Preparation and characterization of epoxy/polyhedral oligomeric silsesquioxane hybrid nanocomposites.* [J]. Journal of Polymer Science Part B: Polymer Physics, 2009. **47**(19): p. 1927-1934.
119. Strachota, A., et al., *Epoxy networks reinforced with polyhedral oligomeric silsesquioxanes (POSS). Thermomechanical properties.* [J]. Macromolecules, 2004. **37**(25): p. 9457-9464.
120. Liu, Y., et al., *Preparation, Characterization, and Properties of Novel Polyhedral Oligomeric Silsesquioxane-Polybenzimidazole Nanocomposites by Friedel-Crafts Reaction.* [J]. Macromolecules, 2010. **43**(16): p. 6731-6738.
121. Fu, B.X., et al., *Structural development during deformation of polyurethane containing polyhedral oligomeric silsesquioxanes (POSS) molecules.* [J]. Polymer, 2001. **42**(2): p. 599-611.
122. Kim, G.M., et al., *Hybrid epoxy-based thermosets based on polyhedral oligosilsesquioxane: Cure behavior and toughening mechanisms.* [J]. Journal of Polymer Science Part B-Polymer Physics, 2003. **41**(24): p. 3299-3313.
123. Jones, I.K., et al., *Effect of polyhedral-oligomeric-sil-sesquioxanes on thermal and mechanical behavior of SC-15 epoxy.* [J]. Express Polymer Letters, 2008. **2**(7): p. 494-501.
124. Kopesky, E.T., G.H. McKinley, and R.E. Cohen, *Toughened poly(methyl methacrylate) nanocomposites by incorporating polyhedral oligomeric silsesquioxanes.* [J]. Polymer, 2006. **47**(1): p. 299-309.
125. Mantz, R.A., et al., *Thermolysis of polyhedral oligomeric silsesquioxane (POSS) macromers and*

POSS-siloxane copolymers. [J]. Chemistry of Materials, 1996. **8**(6): p. 1250-1259.

126. Bolln, C., et al., *Thermal properties of the homologous series of 8-fold alkyl-substituted octasilsesquioxanes.* [J]. Chemistry of Materials, 1997. **9**(6): p. 1475-1479.
127. Fina, A., et al., *Polyhedral oligomeric silsesquioxanes (POSS) thermal degradation.* [J]. Thermochimica Acta, 2006. **440**(1): p. 36-42.
128. Liu, Y.R., Y.D. Huang, and L. Liu, *Effects of TriSilanolIsobutyl-POSS on thermal stability of methylsilicone resin.* [J]. Polymer Degradation and Stability, 2006. **91**(11): p. 2731-2738.
129. Liu, Y.R., Y.D. Huang, and L. Liu, *Thermal stability of POSS/methylsilicone nanocomposites.* [J]. Composites Science and Technology, 2007. **67**(13): p. 2864-2876.
130. Amir, N., A. Levina, and M.S. Silverstein, *Nanocomposites through copolymerization of a polyhedral oligomeric silsesquioxane and methyl methacrylate.* [J]. Journal of Polymer Science Part A-Polymer Chemistry, 2007. **45**(18): p. 4264-4275.
131. Camino, G., A. Fina, and D. Tabuani, *POSS as Fire Retardants.* [C]. MoDeSt-Workshop 08 on Nano-filled Fire Retardant Polymers and Polymeric Composites Beijing (China), 2008. **16-17**.
132. Song, L., et al., *Study on thermal degradation and combustion behaviors of PC/POSS hybrids.* [J]. Polymer Degradation and Stability, 2008. **93**(3): p. 627-639.
133. Wu, K., et al., *Synthesis and characterization of a functional polyhedral oligomeric silsesquioxane and its flame retardancy in epoxy resin.* [J]. Progress in Organic Coatings, 2009. **65**(4): p. 490-497.
134. Franchini, E., et al., *Influence of POSS structure on the fire retardant properties of epoxy hybrid networks.* [J]. Polymer Degradation and Stability, 2009. **94**(10): p. 1728-1736.
135. Dasari, A., et al., *Roles of graphite oxide, clay and POSS during the combustion of polyamide 6.* [J]. Polymer, 2009. **50**(6): p. 1577-1587.
136. Liu, S.M., et al., *Study on flame-retardant mechanism of polycarbonate containing sulfonate-silsesquioxane-fluoro retardants by TGA and FTIR.* [J]. Polymer Degradation and Stability, 2006. **91**(8): p. 1808-1814.
137. Zhang, W.C., X.M. Li, and R.J. Yang, *Novel flame retardancy effects of DOPO-POSS on epoxy resins.* [J]. Polymer Degradation and Stability, 2011. **96**(12): p. 2167-2173.
138. Zhang, W.C., X.M. Li, and R.J. Yang, *Pyrolysis and fire behaviour of epoxy resin composites based on a phosphorus-containing polyhedral oligomeric silsesquioxane (DOPO-POSS).* [J]. Polymer Degradation and Stability, 2011. **96**(10): p. 1821-1832.
139. Zhang, W.C., et al., *Mechanical and thermal properties and flame retardancy of phosphorus-containing polyhedral oligomeric silsesquioxane (DOPO-POSS)/polycarbonate composites.* [J]. Polymer Degradation and Stability, 2010. **95**(12): p. 2541-2546.
140. Vannier, A., et al., *The use of POSS as synergist in intumescent recycled poly(ethylene terephthalate).* [J]. Polymer Degradation and Stability, 2008. **93**(4): p. 818-826.
141. Fina, A., et al., *Metal functionalized POSS as fire retardants in polypropylene.* [J]. Polymer Degradation and Stability, 2006. **91**(10): p. 2275-2281.
142. Wang, X., et al., *Thermal Degradation Behaviors of Epoxy Resin/POSS Hybrids and Phosphorus-Silicon Synergism of Flame Retardancy.* [J]. Journal of Polymer Science Part B-Polymer Physics, 2010. **48**(6): p. 693-705.
143. Gerard, C., G. Fontaine, and S. Bourbigot, *Synergistic and antagonistic effects in flame retardancy of an intumescent epoxy resin.* [J]. Polymers for Advanced Technologies, 2011. **22**(7): p. 1085-1090.
144. Wu, Q., et al., *Combustion and thermal properties of epoxy/phenyltrisilanol polyhedral oligomeric*

silsesquioxane nanocomposites. [J]. Journal of Thermal Analysis and Calorimetry, 2010. **100**(3): p. 1009-1015.

145. Eon, D., et al., *Plasma oxidation of polyhedral oligomeric silsesquioxane polymers.* [J]. Journal of Vacuum Science & Technology B, 2006. **24**(6): p. 2678-2688.
146. Tegou, E., et al., *Polyhedral oligomeric silsesquioxane (POSS) acrylate copolymers for microfabrication: properties and formulation of resist materials.* [J]. Microelectronic Engineering, 2004. **73-4**: p. 238-243.
147. Gonzalez, R.I., *Synthesis and in-situ atomic oxygen erosion studies of space-survivable hybrid organic/inorganic POSS polymers.* [D]. Chemical Engineering Department, University of Florida, 2002.
148. Lin, H.M., K.H. Hseih, and F.C. Chang, *Characterization of negative-type photoresists containing polyhedral oligomeric silsesquioxane methacrylate.* [J]. Microelectronic Engineering, 2008. **85**(7): p. 1624-1628.
149. Moon, J.H., et al., *Direct fabrication of 3D silica-like microstructures from epoxy-functionalized polyhedral oligomeric silsesquioxane (POSS).* [J]. Journal of Materials Chemistry, 2009. **19**(27): p. 4687-4691.
150. Ro, H.W., et al., *Cubic Silsesquioxanes as a Green, High-Performance Mold Material for Nanoimprint Lithography.* [J]. Advanced Materials, 2011. **23**(3): p. 414-420.
151. Hirai, T., et al., *One-Step Direct-Patterning Template Utilizing Self-Assembly of POSS-Containing Block Copolymers.* [J]. Advanced Materials, 2009. **21**(43): p. 4334-+.
152. Eon, D., et al., *Surface segregation of photoresist copolymers containing polyhedral oligomeric silsesquioxanes studied by x-ray photoelectron spectroscopy.* [J]. Journal of Vacuum Science & Technology B, 2004. **22**(5): p. 2526-2532.
153. Hosaka, N., et al., *Structure and dewetting behavior of polyhedral oligomeric silsesquioxane-filled polystyrene thin films.* [J]. Langmuir, 2007. **23**(2): p. 902-907.
154. Hosaka, N., et al., *Influence of the addition of silsesquioxane on the dewetting behavior of polystyrene thin film.* [J]. Composite Interfaces, 2004. **11**(4): p. 297-306.
155. Miyamoto, K., et al., *Stabilization of polystyrene thin films against dewetting by silsesquioxane-terminated polystyrene additives.* [J]. Chemistry Letters, 2006. **35**(10): p. 1098-1099.
156. Wanke, C.H., et al., *Tuning of polypropylene wettability by plasma and polyhedral oligomeric silsesquioxane modifications.* [J]. Polymer, 2011. **52**(8): p. 1797-1802.
157. Dai, L.Z., et al., *Preparation of novel methyl methacrylate/fluorinated silsesquioxane copolymer film with low surface energy.* [J]. Science China-Chemistry, 2010. **53**(9): p. 2000-2005.
158. Gao, Y., et al., *Novel water and oil repellent POSS-based organic/inorganic nanomaterial: Preparation, characterization and application to cotton fabrics.* [J]. Polymer, 2010. **51**(25): p. 5997-6004.
159. Xu, Y.Y., J.Y. Yuan, and A.H.E. Muller, *Single-molecular hybrid nano-cylinders: Attaching polyhedral oligomeric silsesquioxane covalently to poly(glycidyl methacrylate) cylindrical brushes.* [J]. Polymer, 2009. **50**(25): p. 5933-5939.
160. Lu, C.H., et al., *The Self-Assembled Structure of the Diblock Copolymer PCL-b-P4VP Transforms Upon Competitive Interactions with Octaphenol Polyhedral Oligomeric Silsesquioxane.* [J]. Macromolecular Rapid Communications, 2009. **30**(24): p. 2121-2127.
161. Schumacher, M., et al., *Smart Organic-Inorganic Nanohybrids Based on Amphiphilic Block*

Copolymer Micelles and Functional Silsesquioxane Nanoparticles. [J]. Langmuir, 2009. **25**(6): p. 3407-3417.

162. Schumacher, M., et al., *Smart organic-inorganic nanohybrid stars based on star-shaped poly(acrylic acid) and functional silsesquioxane nanoparticles.* [J]. Polymer, 2009. **50**(8): p. 1908-1917.
163. Daga, V.K., et al., *Hydrogen Bond Assisted Assembly of Well-Ordered Polyhedral Oligomeric Silsesquioxane-Block Copolymer Composites.* [J]. Macromolecules, 2011. **44**(17): p. 6793-6799.
164. Kim, B.S. and P.T. Mather, *Morphology, microstructure, and rheology of amphiphilic telechelics incorporating polyhedral oligosilsesquioxane.* [J]. Macromolecules, 2006. **39**(26): p. 9253-9260.
165. Kim, B.S. and P.T. Mather, *Amphiphilic telechelics with polyhedral oligosilsesquioxane (POSS) end-groups: Dilute solution viscometry.* [J]. Polymer, 2006. **47**(17): p. 6202-6207.
166. Wei, J., et al., *Self-Assembly Behaviors of Telechelic Poly(styrene-ran-sodium styrenesulfonate) with Polyhedral Oligomeric Silsesquioxane as End Groups.* [J]. Journal of Physical Chemistry B, 2011. **115**(9): p. 1929-1935.
167. Mya, K.Y., et al., *Core-corona structure of cubic silsesquioxane-poly(ethylene oxide) in aqueous solution: Fluorescence, light scattering, and TEM studies.* [J]. Journal of Physical Chemistry B, 2005. **109**(19): p. 9455-9462.
168. Kuo, S.W., et al., *Solid State and Solution Self-Assembly of Helical Polypeptides Tethered to Polyhedral Oligomeric Silsesquioxanes.* [J]. Macromolecules, 2009. **42**(5): p. 1619-1626.
169. Zhang, W.A., et al., *Synthesis and Self-Assembly of Tadpole-Shaped Organic/Inorganic Hybrid Poly(N-isopropylacrylamide) Containing Polyhedral Oligomeric Silsesquioxane via RAFT Polymerization.* [J]. Journal of Polymer Science Part A-Polymer Chemistry, 2008. **46**(21): p. 7049-7061.
170. Zhang, W.A., et al., *Synthesis via RAFT Polymerization of Tadpole-Shaped Organic/Inorganic Hybrid Poly(acrylic acid) Containing Polyhedral Oligomeric Silsesquioxane (POSS) and Their Self-assembly in Water.* [J]. Macromolecules, 2009. **42**(7): p. 2563-2569.
171. Zhang, W.A., et al., *Preparation and characterization of organic/inorganic hybrid polymers containing polyhedral oligomeric silsesquioxane via RAFF polymerization.* [J]. Reactive & Functional Polymers, 2009. **69**(2): p. 124-129.
172. Zeng, K., et al., *Self-assembly behavior of hepta(3,3,3-trifluoropropyl) polyhedral oligomeric silsesquioxane-capped poly(epsilon-caprolactone) in epoxy resin: Nanostructures and surface properties.* [J]. Polymer, 2009. **50**(2): p. 685-695.
173. Zeng, K. and S.X. Zheng, *Nanostructures and surface dewettability of epoxy thermosets containing hepta(3,3,3-trifluoropropyl) polyhedral oligomeric silsesquioxane-capped poly(ethylene oxide).* [J]. Journal of Physical Chemistry B, 2007. **111**(50): p. 13919-13928.
174. Zeng, K., L. Wang, and S.X. Zheng, *Nanostructures and surface hydrophobicity of epoxy thermosets containing hepta(3,3,3-trifluropropyl) polyhedral oligomeric silsesquioxane-capped poly(hydroxyether of bisphenol A) telechelics.* [J]. Journal of Colloid and Interface Science, 2011. **363**(1): p. 250-260.
175. Yu, X.F., et al., *A Giant Surfactant of Polystyrene-(Carboxylic Acid-Functionalized Polyhedral Oligomeric Silsesquioxane) Amphiphile with Highly Stretched Polystyrene Tails in Micellar Assemblies.* [J]. Journal of the American Chemical Society, 2010. **132**(47): p. 16741-16744.
176. Zhang, W.B., et al., *Synthesis of Shape Amphiphiles Based on Functional Polyhedral Oligomeric Silsesquioxane End-Capped Poly(L-Lactide) with Diverse Head Surface Chemistry.* [J].

Macromolecules, 2011. **44**(8): p. 2589-2596.

177. Miao, J.J., et al., *Self-assembly and chain-folding in hybrid coil-coil-cube triblock oligomers of polyethylene-b-poly(ethylene oxide)-b-polyhedral oligomeric silsesquioxane.* [J]. Macromolecules, 2007. **40**(15): p. 5460-5470.
178. Lee, K.M., et al., *Polycaprolactone-POSS chemical/physical double networks.* [J]. Macromolecules, 2008. **41**(13): p. 4730-4738.
179. Alvarado-Tenorio, B., A. Romo-Uribe, and P.T. Mather, *Microstructure and Phase Behavior of POSS/PCL Shape Memory Nanocomposites.* [J]. Macromolecules, 2011. **44**(14): p. 5682-5692.
180. Timothy S. Haddad, et al., *Hybrid Inorganic/Organic Diblock Copolymers. Nanostructure in Polyhedral Oligomeric Silsesquioxane Polynorbornenes;*. [C]. Materials Research Society Symposium Proceeding, 2001, **628,** CC2.6.1-CC2.6.7.
181. Xu, W.T., C.H. Chung, and Y.W. Kwon, *Synthesis of novel block copolymers containing polyhedral oligomeric silsesquioxane (POSS) pendent groups via ring-opening metathesis polymerization (ROMP).* [J]. Polymer, 2007. **48**(21): p. 6286-6293.
182. Pyun, J. and K. Matyjaszewski, *The synthesis of hybrid polymers using atom transfer radical polymerization: Homopolymers and block copolymers from polyhedral oligomeric silsesquioxane monomers.* [J]. Macromolecules, 2000. **33**(1): p. 217-220.
183. Pyun, J., et al., *ABA triblock copolymers containing polyhedral oligomeric silsesquioxane pendant groups: synthesis and unique properties.* [J]. Polymer, 2003. **44**(9): p. 2739-2750.
184. Hussain, H., et al., *Micelle Formation and Gelation of (PEG P(MA-POSS)) Amphiphilic Block Copolymers via Associative Hydrophobic Effects.* [J]. Langmuir, 2010. **26**(14): p. 11763-11773.
185. Tan, B.H., H. Hussain, and C.B. He, *Tailoring Micelle Formation and Gelation in (PEG-P(MA-POSS)) Amphiphilic Hybrid Block Copolymers.* [J]. Macromolecules, 2011. **44**(3): p. 622-631.
186. Rios-Dominguez, H., et al., *Syntheses and evaluation of gas transport properties in polystyrene-POSS membranes.* [J]. Journal of Membrane Science, 2006. **271**(1-2): p. 94-100.
187. Hirai, T., et al., *Hierarchical Self-Assembled Structures from POSS-Containing Block Copolymers Synthesized by Living Anionic Polymerization.* [J]. Macromolecules, 2009. **42**(22): p. 8835-8843.
188. Hirai, T., et al., *Hierarchical nanostructures of organosilicate nanosheets within self-organized block copolymer films.* [J]. Macromolecules, 2008. **41**(13): p. 4558-4560.
189. Ahn, B., et al., *Hierarchical Structure in Nanoscale Thin Films of a Poly(styrene-b-methacrylate grafted with POSS) (PS_{214}-b-$PMAPOSS_{27}$).* [J]. Macromolecules, 2010. **43**(24): p. 10568-10581.
190. Mya, K.Y., et al., *Time-Dependent Polymerization Kinetic Study and the Properties of Hybrid Polymers with Functional Silsesquioxanes.* [J]. Journal of Physical Chemistry B, 2010. **114**(28): p. 9119-9127.

Chapter 2 POSS based BCPs: Synthesis, Morphology and Properties

2.1 Introduction

POSS was a new class of organo-silicon compound with a nano-scale cubic structure (1~3nm) which were also named "molecule silica", whose chemical structure followed the basic composition of $(RSiO_{1.5})_n$, typically n=8. The main structure of POSS was inorganic siloxane cage externally covered by organic subsistent, by which the dispersion and compatibility could be controlled in a wide range of polymer systems. The POSS synthesis, application and development in the past two decades were well reviewed by Cordes et al[1] in a recent publication. The incorporation of POSS moieties into polymeric systems would modify the molecular interactions, molecular conformations and segment mobility, which dominated the macroscopic properties of polymer such like thermal stability, mechanical properties, flame retardant and surface properties etc. [2-5].

As a kind of "building block", POSS was concerned to construct nano-hybrids by assembly or aggregation of POSS cages in "bottom up" way. Supramolecular structure by self-assembly of POSS moieties gained much concern presently. Previous research on POSS based copolymer was focused on polymer with tethering POSS, which included random tethered polymers, end-capped tele-chelics polymers and BCPs. Works on POSS based polymers and their properties were well reviewed by Wu et al[6, 7] and Kuo et al[8]. POSS has gained increasing interest in the past decades due to its inner-molecular hybrid characteristics and potential application in high performance materials. Recently the research on structure-properties relationship of such kind of nano-hybrids rose up as a hot issue in polymer chemistry and physics. In the pursuit to understand the relationship between morphology and properties of POSS base polymer, the synthesis of well-defined molecular architecture polymers for morphology control became particularly important. BCPs containing POSS block was an alternative kind of well-defined POSS based polymer. Since the POSS block might play a role as rigid "rod" which could result in special properties, the synthesis of POSS based BCPs has recently gained attention as a route to prepare novel NCs.

POSS BCPs were firstly synthesized by Mather et al[9] via ROMP and Pyun et al via ATRP[10, 11]. Due to the synthetic limitation, even some interesting character such as microstructure separation, thermal properties and rheology of POSS BCP were observed, properties based on POSS BCPs were few studied. Hussain et al[12] have synthesized AB diblocks and ABA triblocks containing POSS block and PEG block, and POSS block in ABA tri-blocks played a role as crosslink in gelation in solution. Xu et al[13] have synthesized POSS based amphiphilic BCPs via RMOP. Quite recently, Hirai et al[14] successfully synthesized POSS based BCPs without DP_n limitation via LAP. Both nice micro structures and corresponding application in nano-materials manufacturing were reported in their publications[15-19].

It is well-known that LCP is common method to synthesize well-defined BCPs. Due to the mild condition, CRP has seen increasing interest from industry and academia in recent years as it gives similar control of polymerization to that in more drastic systems such as LAP. Therefore, they were extensively applied to generate well-defined architectures, such as polymers with well-known DP_n, *MW* distributions, end functionalities, chain architectures and compositions. Among the CRP techniques, RAFT polymerization appeared to be the most versatile processes in terms of the reaction conditions, the variety of monomers for which polymerization can be controlled, tolerance to functionalities, and the range of polymeric architectures that can be produced[20]. Therefore, since the first publication in 1998[21], multi group efforts have been made and hundreds of monomers were well mediated by different kinds of CTAs. Quite recently, Mya et al[22] have studied the RAFT polymerization of MAiBuPOSS mediated by dodecyl (dimethylacetic acid) trithiocarbonate (DDTA). However, this system seems to be poor controlled, resulting polymer with high *PDI* and irregular morphology.

In this chapter, we presented the RAFT Polymerization of POSS macromers mediated by CDB. The steric hindrance of bulky side group on chain transfer was investigated by comparing two macromers with different vertex group in terms of DP_n limitation. Chain extension of POSS homo-polymer macro CTA by three typical conventional monomers, MMA, BuA, St and their mixture were studied. Well defined BCPs with low *PDI* and various topologies were obtained. The morphology and properties of those polymers were investigated as well.

2.2 Experimental

2.2.1 Materials

Bromide benzene, carbon disulfide, Mg, I_2, CPAD, α-methyl styrene, dicyclohexyl carbodiimide (DCC), 4-di(methylamino) pyridine (DMAP), trimethylol propane (TMP), AIBN was purchased from Aldrich and used as received. MAiBuPOSS, MACyPOSS and MAPhPOSS were purchased from Hybrid Plastics and used as received. MMA, BuA and St were purified by passing through a column of basic aluminium oxide to remove inhibitors. Toluene was purchased from Aldrich and used as received.

2.2.2 Synthesis

2.2.2.1 Synthesis of CTAs

CDB was synthesized according to the procedure described in literature[20] as shown in Fig2.1. Mg (2.5g, 105mmol) and a catalytic amount of I_2 were put into a 250mL a three neck flask equipped with pressure equalizing addition funnel and stir bar. 10mL of Anhydrous THF (50mL) and bromobenzene(10.5mL, 15.7g, 100mmol) mixture was then added into the flask under argon, and was heated to 35^{o}C for 15min, then the rest of mixture was added through the funnel. After kept at 50^{o}C for 2h, the resulted dark green solution was cooled to 0^{o}C and CS_2（6.02ml, 7.6g,100mmol）in 30mL anhydrous THF was added in through the funnel, the solution turned to dark red. After heat at 50^{o}C for 1h, the residual magnesium was removed by filter and the THF in filtrate was removed by rotation evaporation. The dithio-acid was purified by repeated extraction with ether (80mL) and 2M HCl (100mL) and washed by 0.4M NaOH (240mL) was added in to extract the aqueous phase. After acidizing by 2M HCl (100mL). After dried by $MgSO_4$, ether was removed, and then CCl_4 (60ml) and α-methyl styrene (13.02ml, 11.8g, 100mmol) was added in and then kept at 70^{o}C for 8h. After passing a H60 silica column eluted by petroleum ether, the red oil was frozen to solid and re-crystallized from hexane three times.

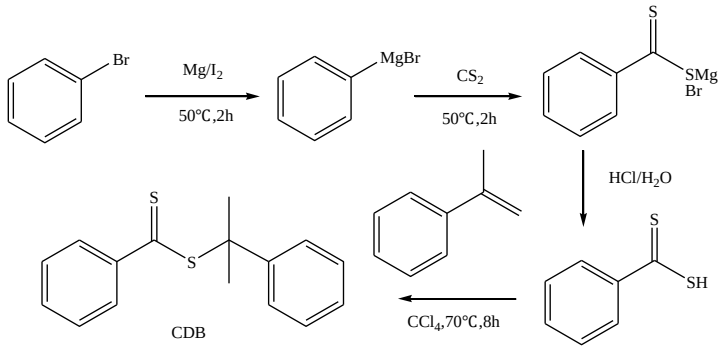

Fig 2.1 Synthesis protocol of CDB

Synthesis of multi-functional RAFT agent through esterification of CPAD (Fig2.2): CPAD 1.18g (4mmol) was put into a two neck flask equipped with addition funnel. The atmosphere was replaced to argon, then 50ml anhydrous THF was added in by syringe via addition fennel. After the CPAD was well dissolved, the solution was cool to 0℃, then DCC 1.65g (8mmol) in 10ml THF was added in the flask by dropwise. After stirring for 15 min, DMAP 4.0mg (0.032mmol) + THMP 134mg (1mmol) in 20ml THF was added in by dropwise. Then the mixture was allowed at room temperature for 18h. After evaporated the THF, EtOAc was added in to wash the precipitate and the filter, the filtrate was concentrated. After pass a column eluted by c-hexane: ethyl acetate =7:3 (*v/v*), red fractions were collected and concentrated for SEC and NMR analysis to confirm their structures.

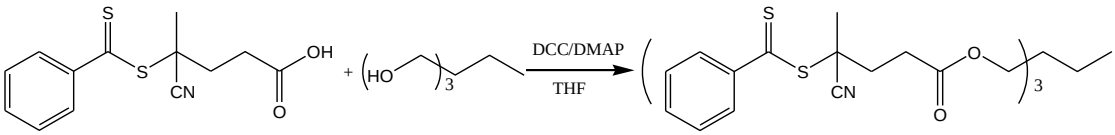

Fig 2.2 Synthesis of tri-functionalized CTA based on the esterification of CPAD

2.2.2.2 Homopolymerization of POSS macromers

The formulation was shown in Fig2.3. In a typical experiment, MACyPOSS (1.351g, 1.2mmol), CDB (10.9mg, 0.04mmol) and AIBN (2.2mg, 0.0133mmol) were dissolved in 1.8 mL of toluene and placed in a schlenk tube which were thoroughly deoxygenated by five consecutive freeze-pump-thaw cycles. The tubes were subsequently placed in an oil bath

thermostated at 65°C. Aliquots were drawn at regular intervals from the reaction mixture, plunged into iced water and analyzed by ^{1}H NMR and SEC. The reaction was stopped by plunging the tubes into liquid nitrogen.

PMACyPOSS polymers were subsequently precipitated twice into acetone/ethyl acetate 8/2 (v/v) mixture in order to eliminate residual monomer. Pure PMAiBuPOSS was obtained from repeated precipitations from ethyl acetate/methanol 1/6~8 (*v/v*) mixtures. PMAPhPOSS was synthesized in THF, and precipitated twice from acetone: ethanol=1:1(*v/v*) (1% of residual POSS monomer after purification).

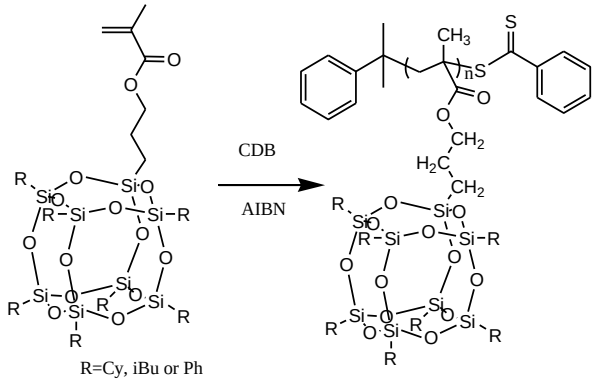

Fig 2.3 RAFT polymerization of POSS monomer

2.2.2.3 Preparation of hybrid BCPs

The formulation was shown in Fig2.4. In a typical experiment, MMA(1.2mL,11.33mmol), St(0.15mL, 1.27mmol), P2(0.4g, 2×10^{-5}mol) and AIBN(1×10^{-6}mol) were dissolved in 0.5mL toluene in Schlenk tube, which were thoroughly deoxygenated by five consecutive freeze-pump-thaw cycles. The tubes were subsequently placed in an oil bath thermo-stated at 65°C. Aliquots were drawn at regular intervals from the reaction mixture, plunged into iced water and analyzed by ^{1}H NMR and SEC. The reaction was stopped by plunging the tubes into liquid nitrogen. The resulting BCPs were obtained as pink powders after twice precipitation from methanol. For BCPs containing pure PMMA block, selective solvent, for instance, cyclohexane was used to extract the residual of POSS homo-polymer macro CTA.

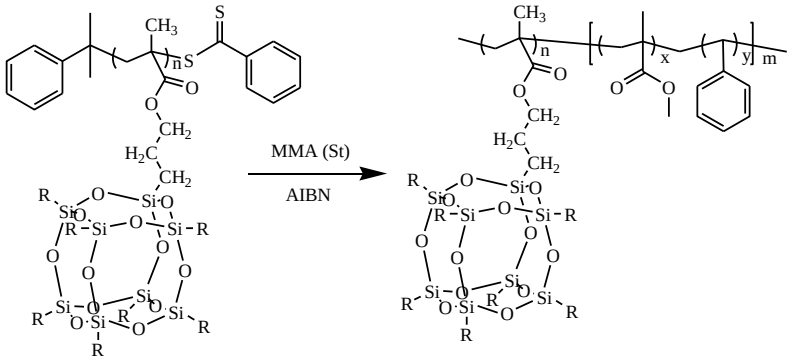

Fig 2.4 Chain extension of POSS homo-polymer macro-CTA

2.2.3 Characterization methods

^{1}H and ^{13}C NMR spectra were recorded on a Bruker AVANCE250 (250 MHz) or AVANCE400 (400 MHz) spectrometer using $CDCl_3$ as solvent if not specially mentioned.

Fourier Transformed Infrared Spectroscopy (FTIR): FTIR measurements were conducted on an AVATAR 360 FTIR (Nicolet Instrument) at room temperature (25 ◦C). The sample was prepared by casting diluted solution on KBr. In all cases, 32 scans at a resolution of $4cm^{-1}$ were used to record the spectra.

Size Exclusion Chorography (SEC) analysis were performed in THF at 25°C (flow rate: 1 $mL{\cdot}min^{-1}$) on a Shimadzu DGU-20A apparatus equipped with a Shimadzu RID-10A refractive-index detector and a Viscotek 270 viscosimetry/RALS dual detection, and fitted with (A) three Waters HR5E or (B) a series of HR0.5, HR2 and HR3 columns (for high and small *MW* respectively).

Wide Angle X-ray Scattering (WAXS): WAXS was performed on Rigaku D/max-2500 using Kα radiation of Cu target (0.154nm) under 40kV×100mA.

Differential Scanning Calorimetric (DSC) analysis was carried out on a DSC Q20, the heating rate was 10°C/min from 0°C to 250°C, and the second heating cycle was used for glass transition analysis.

Thermo-Gravimetric Analysis (TGA) was carried out on a TGA Q500. All of the thermal analyses were conducted in nitrogen atmosphere from ambient temperature to 600℃ at the heating rate of $20℃/min^{-1}$. The thermal degradation temperature was taken as the highest

weight loss rate temperature.

Dynamic Mechanical Thermal Analysis (DMTA) was carried out on a Dynamic Mechanical Thermal Analyzer (DMTA) (MKⅣ, Rheometric Scientific Inc. USA) using single cantilever model with the temperature range from 30℃ to 200℃, the frequency used is 1.0 Hz at the heating rate 3.0℃/min.

Transmission Electron Microscopy (TEM) was performed on a Philips 120 high-resolution transmission electron microscope at the accelerating voltage of 120 kV and JEM2100 200kV. Samples were trimmed using an ultra-microtome, and the slice (60~70 nm in thickness) were placed in 200 mesh copper grids for observation.

2.3 Result and discussion

2.3.1 Characterization of POSS monomers and their homopolymer

The ^{1}H NMR spectrum of MACyPOSS and all the signal assignment was shown in Fig2.5. After polymerization, the signal for the protons on double bond disappeared and that for the methylene protons on ester group shifted to low chemical shift as shown in Fig2.6. Same changes happened for MAiBuPOSS and MAPhOSS (Fig2.7~10). The conversion was determined by ^{1}H NMR in $CDCl_3$ by relative integrations of the polymer ester group methylene protons (CH_2-O, 2nH, = 3.8 ppm~4.15ppm for the monomer- where n is the degree of polymerization) and the characteristic vinyl protons of the residual monomer (5.58 and 6.15ppm, 2H) using monomer as standards. Theoretical degree of polymerization $\overline{DP_n}_{\text{th}}$ was straightforwardly calculated from monomer conversion. $\overline{DP_n}_{\text{NMR}}$ was calculated from the ^{1}H NMR spectrum of the pure polymer by integration of the signals from the aromatic protons of the CTA's benzyl group and polymer ester group methylene protons (CH_2-O, 2nH, 3.85ppm). Due to the interruption of aromatic protons from PMAPhPOSS unit, $\overline{DP_n}_{\text{NMR}}$ can not be calculated.

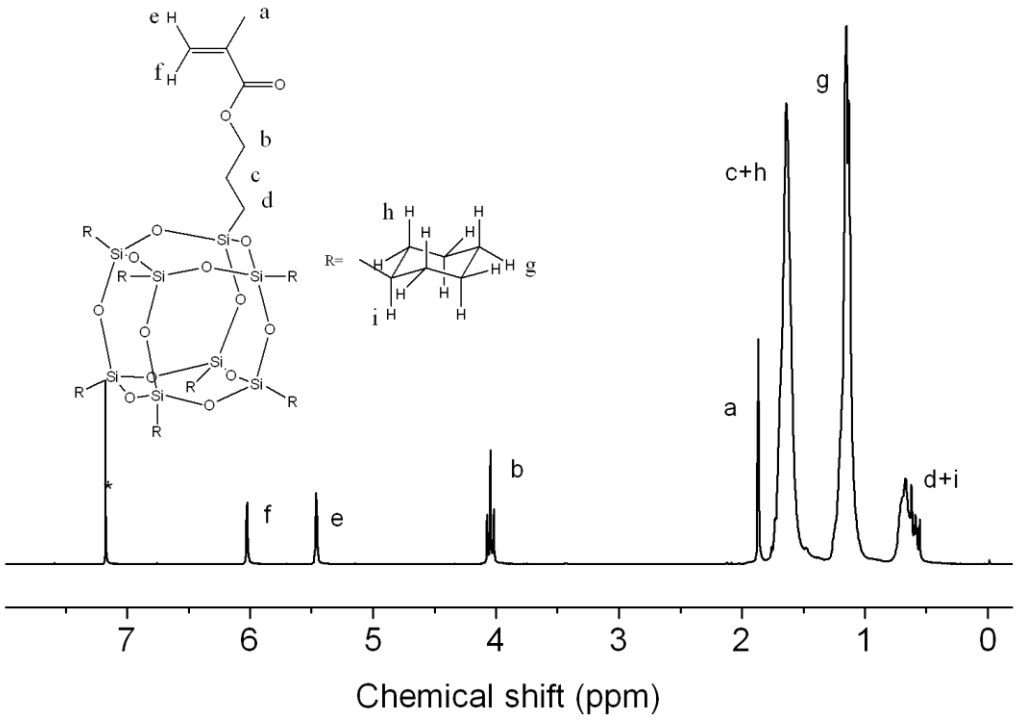

Fig 2.5 ^{1}H NMR spectrum and peak assignment of MACyPOSS, Bruker 250M, *d*-chloroform

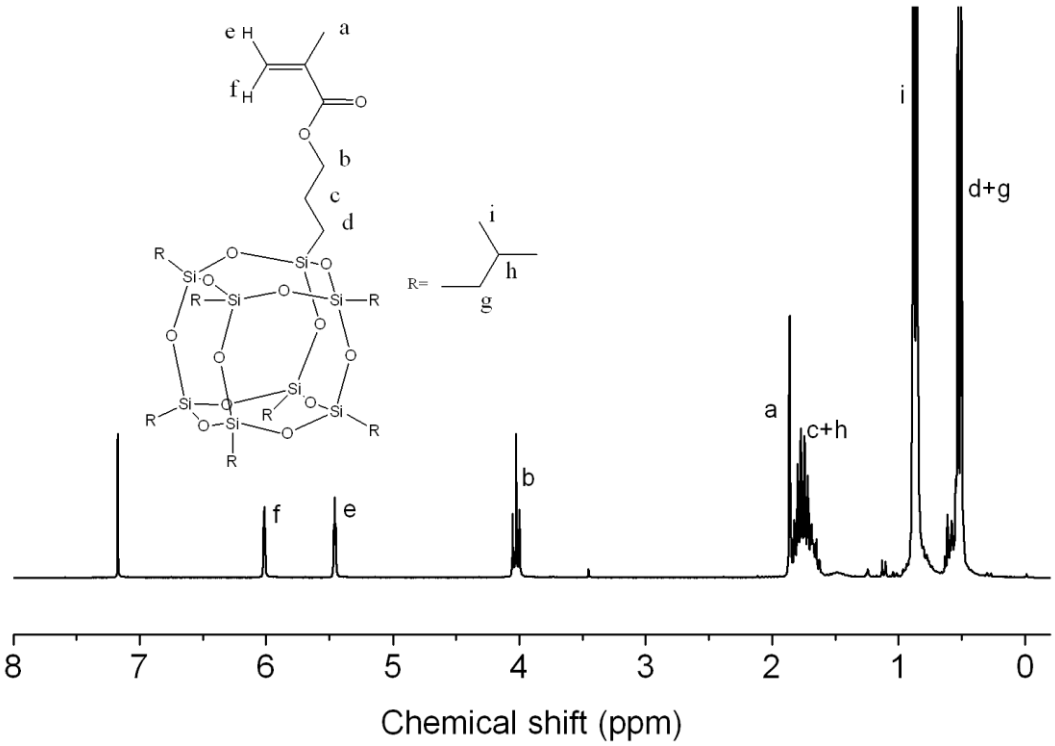

Fig 2.6 ^{1}H NMR spectrum and peak assignment of MAiBuPOSS, Bruker 250M, *d*-chloroform

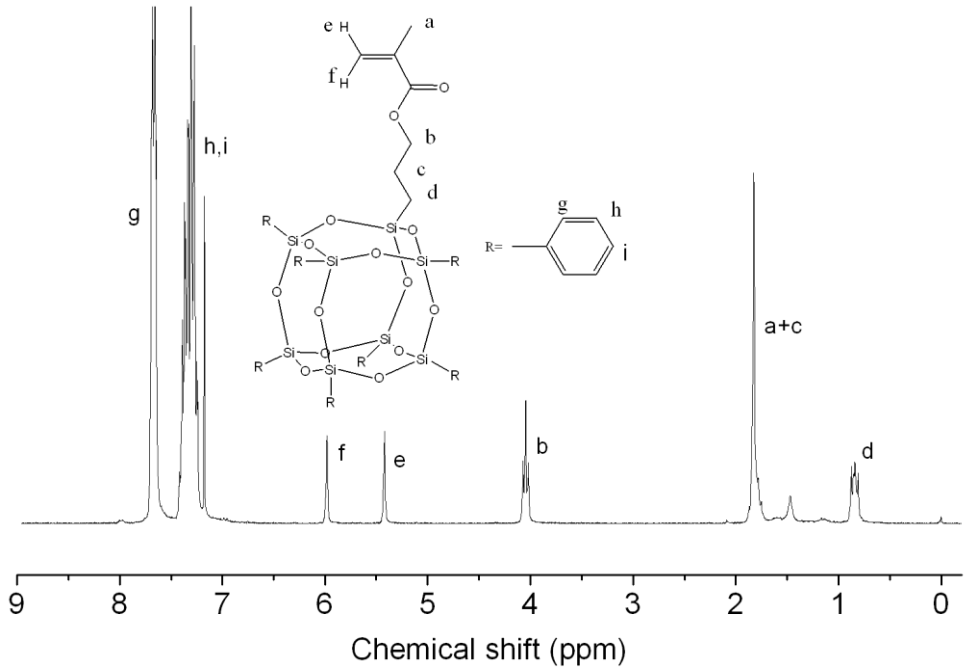

Fig 2.7 ^{1}H NMR spectrum and peak assignment of MAPhPOSS, Bruker 250M, *d*-chloroform

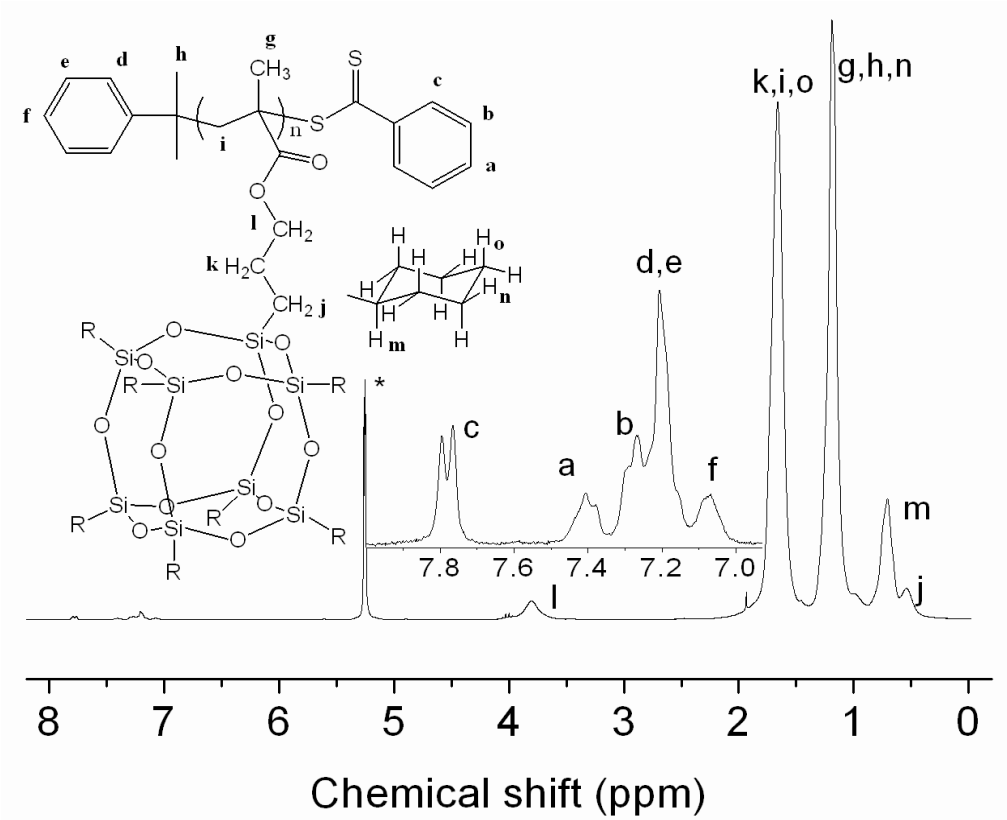

Fig 2.8 ^{1}H NMR spectrum and peak assignment of PMACyPOSS, Bruker 250M, *d*-dichloromethane

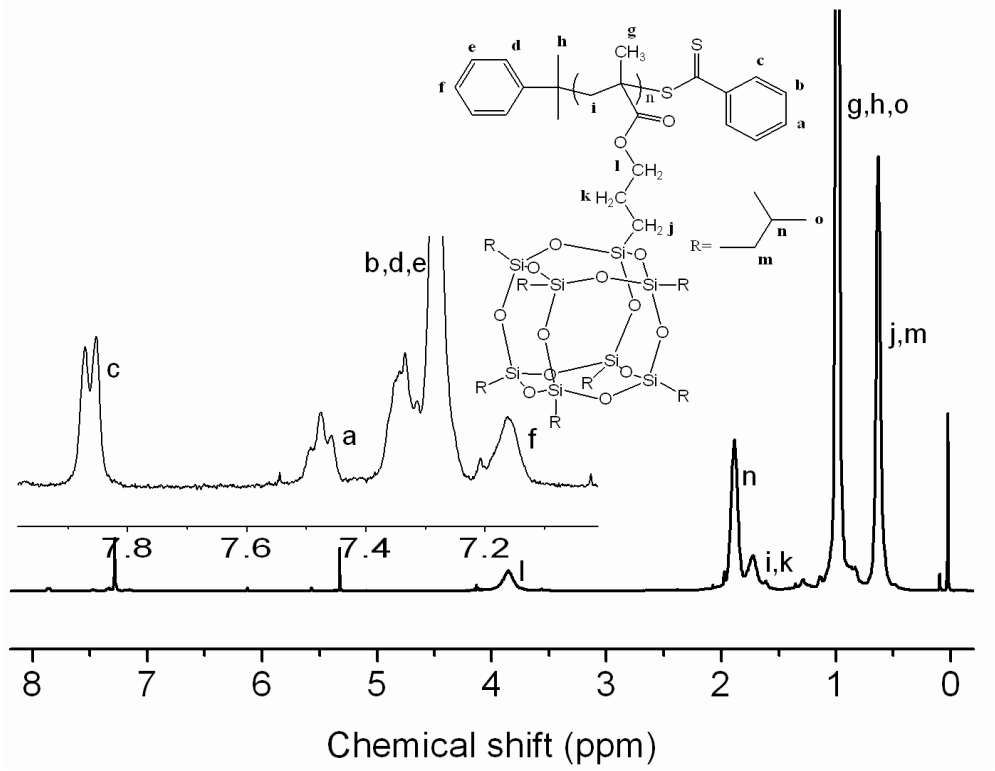

Fig 2.9 ^{1}H NMR spectrum and peak assignment of PMAiBuPOSS, Bruker 250M, *d*-chloroform

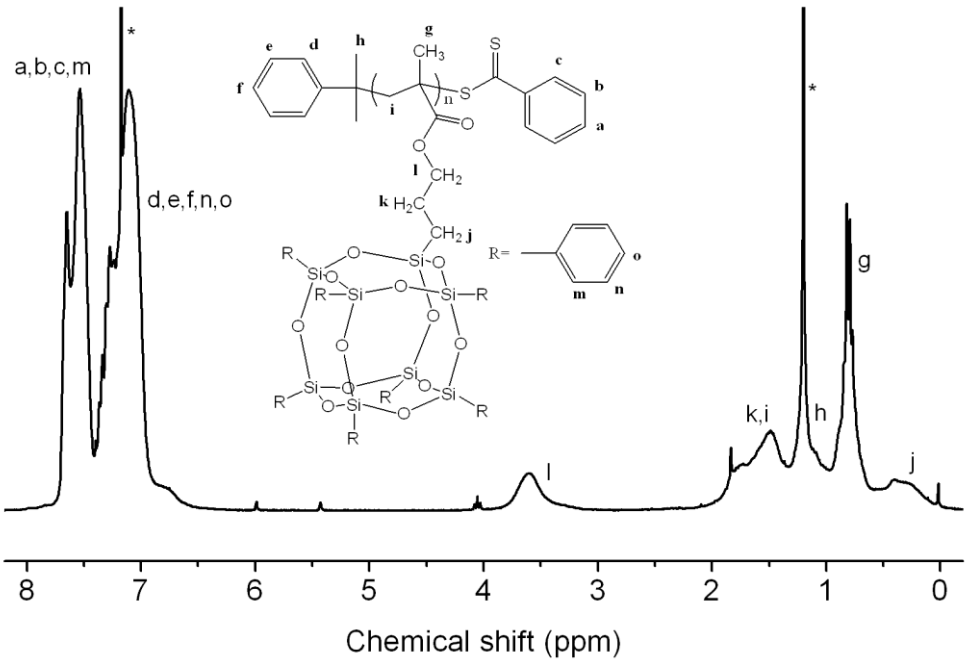

Fig 2.10 ^{1}H NMR spectrum and peak assignment of PMAPhPOSS, Bruker 250M, *d*-chloroform

WAXS analysis was also carried out to tell the crystalline behaviour of POSS monomers as shown in Fig2.11. For MACyPOSS, the patterns showed sharp scattering peak at 2θ=7.83, 10.46, 11.61, 18.14, and 18.80°. The assignment of these peaks to the crystal planes and interplanar crystal spacing were shown in Table2-1[23].

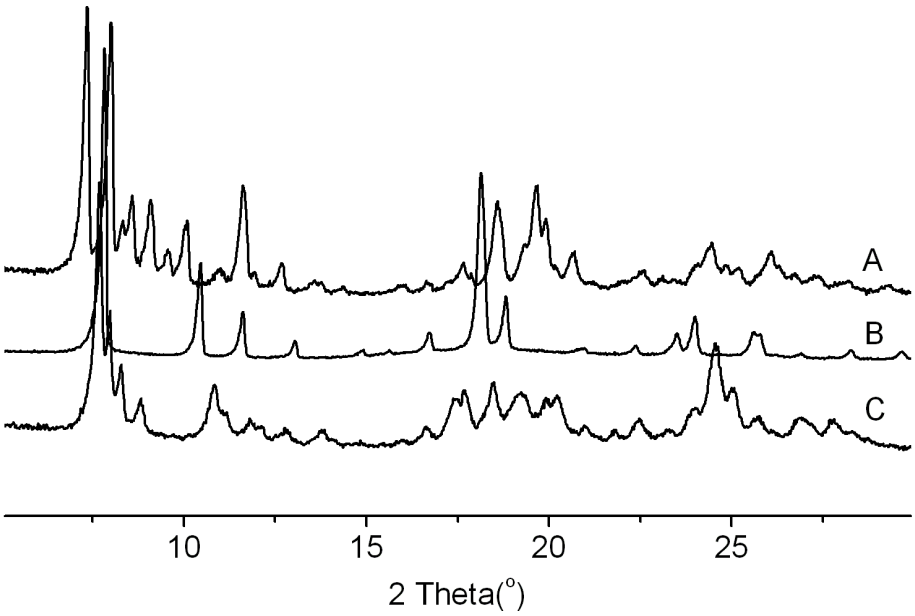

Fig 2.11 WAXS spectra of (A) MAiBuPOSS, (B) MACyPOSS, (C) MAPhPOSS

Table 2-1 Assignment of WAXS peak and distance calculated of MACyPOSS

h, k, l	2 theta (°)	Distance (Å)
101	7.83	11.28
110	10.47	8.44
102	11.61	7.61
021	13.05	6.78
030/113/122	16.72/18.14/18.82	5.30/4.88/4.71
312	24.00	3.70
124/105	25.60/25.76	3.48/3.45

2.3.2 Synthesis and characterization of RAFT agent

2.3.2.1 Synthesis and characterization of CDB

The FTIR spectrum of CDB was shown in Fig2.12. One can clearly resolve the signal of Ph (3030 cm^{-1}), methyl (2970, 2870, 1382, 1362 cm^{-1}) and dithioester group (1218, 1042 and 867 cm^{-1}). The purity of CDB was estimated by ^{1}H NMR. As shown in Fig2.13, the signal of aromatic protons was well resolved, no detectable impurity was observed in ^{1}H NMR.

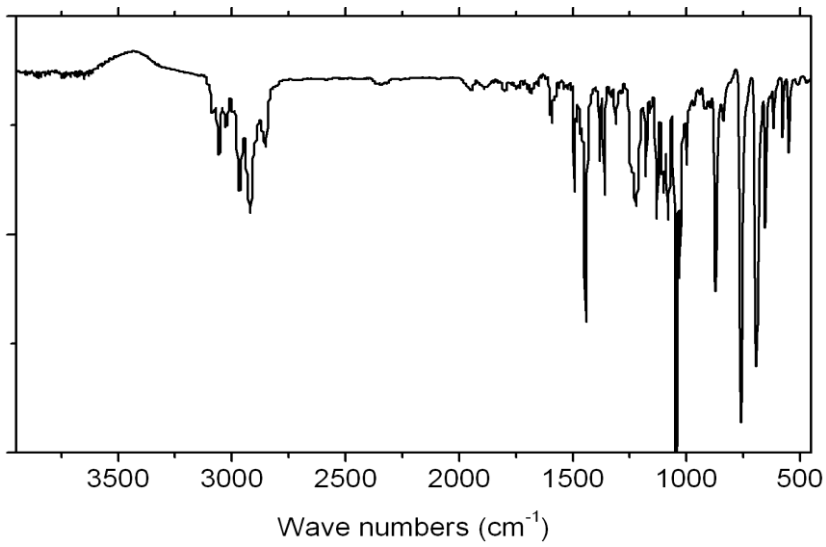

Fig 2.12 FT-IR spectrum of CDB

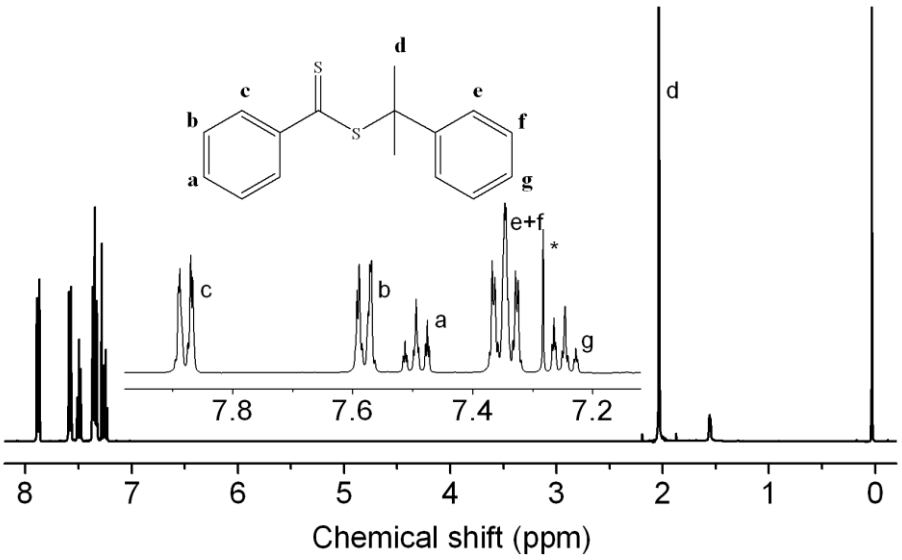

Fig 2.13 ^{1}H NMR spectrum and peak assignment of CDB, Bruker 400M, *d*-chloroform

2.3.2.2 Synthesis and characterization of T1 and B1

The structure and ^{1}H NMR spectrum of CPAD were shown in Fig2.14. It is a common dithiobenzoate moiety for the synthesis of multiple functional CTA via esterification of carboxyl group. As CPAD/DCC intermediate was very sensitive to base (such as DMAP), a yellow byproduct resulted from the degradation of CPAD was obtained. The chemical shift of aromatic protons became poor resolved, which indicated the damage of dithiobenzoate. The condition was optimized to diminish the produce of such byproduct.

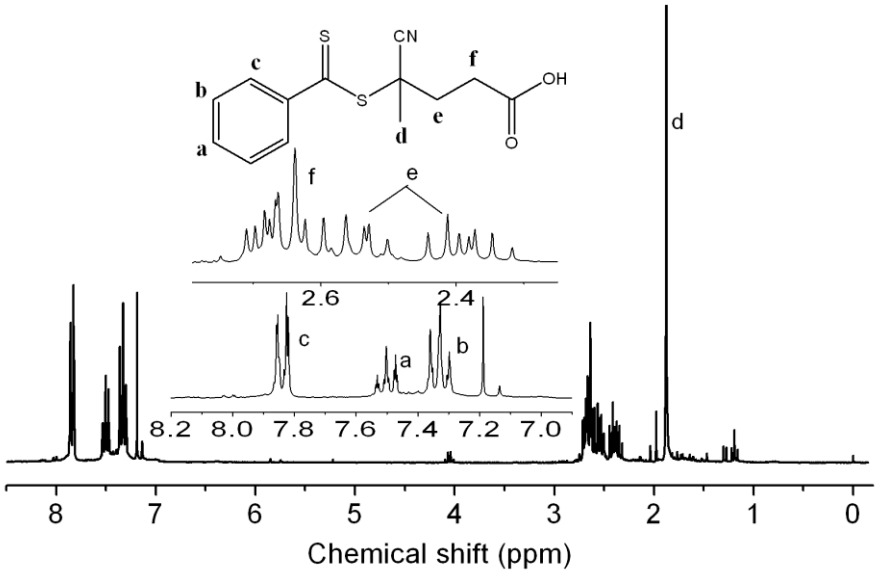

Fig 2.14 ^{1}H NMR spectrum and peak assignment of CPAD, Bruker 250M, *d*-chloroform

The conversion of CPAD could be easily estimated by SEC with UV signal, as dithiobenzoate was the main UV sensitive moiety. The SEC trace of the reacted mixture was shown in Fig2.15A, in which five main peaks were resolved as marked. By passing through a silica column eluted by c-hexane: ethyl acetate =7:3, three red fractions were obtained in sequence (named R1, R2 and R3 respectively), which are corresponding to peak 3, 1and 2 as shown in Fig2.15 B, C and D respectively. Red viscous oils were obtained by evaporating solvent and dried under vacuum then analyzed by ^{1}H NMR. The ^{1}H NMR spectra of these three fractions were shown in Fig2.16 and their possible structures were shown in Fig2.17. R2 and R3 were named to be T1 and B1 respectively, whereas R1 was supposed to be acrylurea.

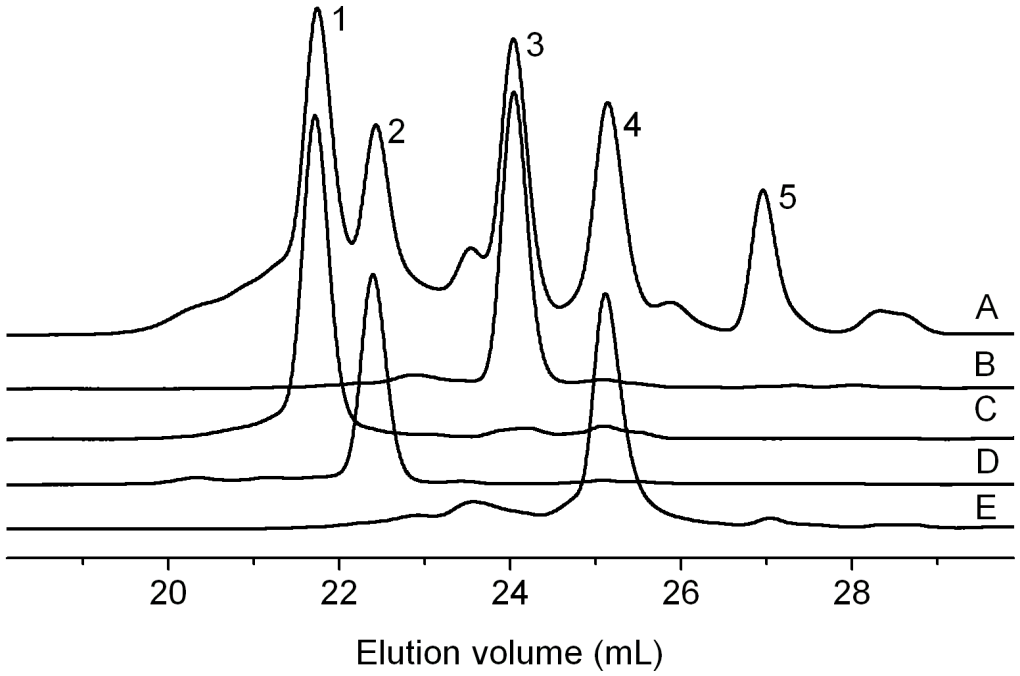

Fig 2.15 SEC curves of (A) mixture after esterification, (B) first red fraction R1, (C) second red fraction R2, (D) third red fraction R3 and (E) CPAD. Column series B

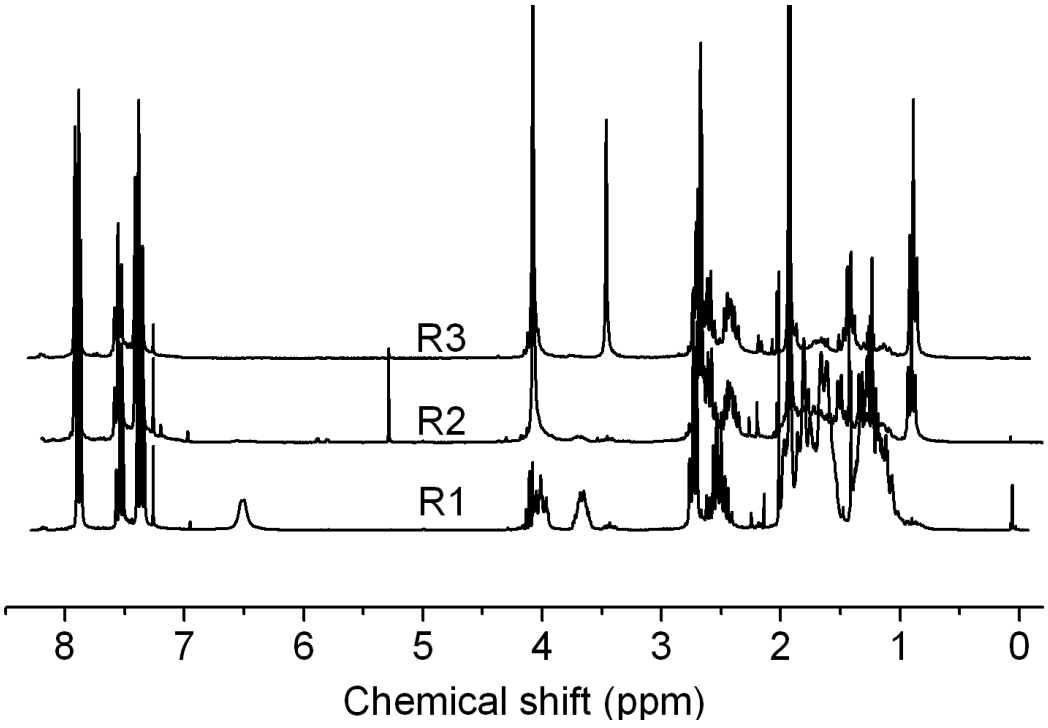

Fig 2.16 ^{1}H NMR spectra of R1, R2 and R3, Bruker 250M, *d*-chloroform

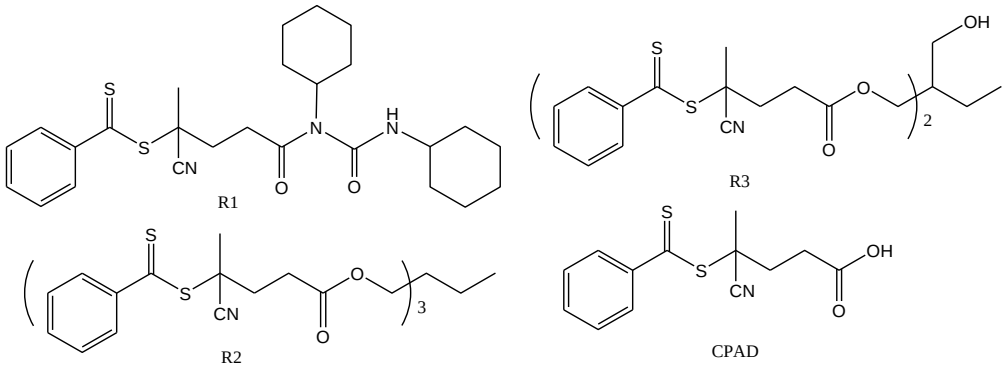

Fig 2.17 Molecular structures of R1, R2, R3 and CPAD

2.3.3 RAFT-mediated homo-polymerization of POSS macromers

2.3.3.1 Polymerization kinetic study

The main mechanism of RAFT polymerization was shown in Fig2.18[24], the transfer of the CTA between growing radical chains present at a very low concentration and dormant polymeric chains present at a higher concentration, will regulate the growth of the *MW* and limit the termination reactions. The rapid exchange between active and dormant chains ensured equal probability for all chains to propagate, therefore leading to narrow *MW* distribution. The prediction of *MW* depended on C_{tr} of CTA in pre-equilibrium process, whereas the *MW* distribution relied on the C_{tr} of living polymer in main-equilibrium process. Both two parameters are crucial for systems owning living/control characteristic.

The CRP of POSS has been previously reported to be highly challenging owing to steric hindrance issues. Aiming at generating tailor-made hybrid BCPs with high inorganic content, the homopolymerization behaviour of POSS methacrylates possessing either iBu or Cy substituents on the Si/O cage vertices (MACyPOSS and MAiBuPOSS) was initially investigated in detail in the presence of CDB to determine conditions of polymerization affording macromolecules with optimal *MW* distribution and well-defined structure.

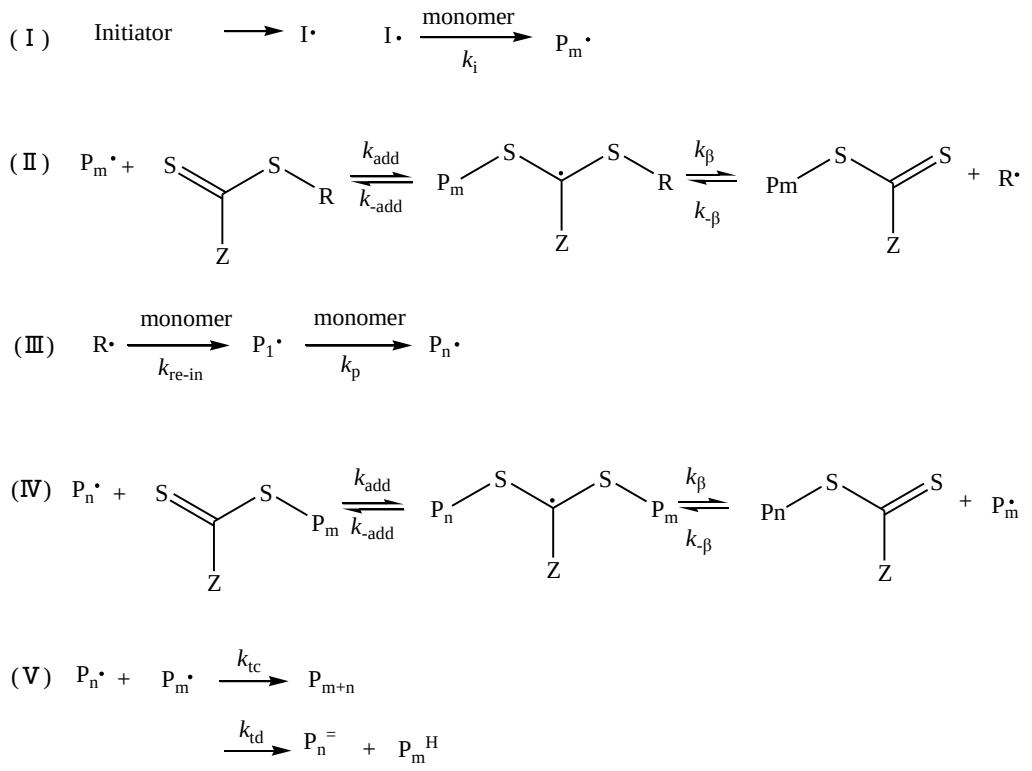

Fig 2.18 General mechanism of RAFT polymerization

Usually, the kinetic study was used to check the living/control characteristic and to determine the polymerization condition. For an ideal LCP, the rate coefficient should keep at a constant and semilogarithmic should be linear, because the chain propagation is a first order reaction evolved with the concentration of monomer. However, in most case, "living/control" always decorated with quotation mark, which it only owns a "pseudo" living/control system i.e. CRP was defined under the assumption that the bi-radical termination rate was low enough to be "ignored". In RAFT polymerization, normal initiator i.e. AIBN was used as free radical resource to construct the pre-equilibrium and supply the free radical consumed by termination. Theoretical M_n for POSS homopolymer and BCP was calculated by the equation as follows: $M_{n,th} = \frac{[monomer]_0}{[CTA]_0} \times conversion \times M_m + M_0$, in which M_m and M_0 represent the *MW* of monomer and CTA (CDB or first block) respectively (M_m=1126 and 946.3 for MACyPOSS and MAiBuPOSS respectively, M_0=272.4 for CDB).

We firstly investigated the effect of monomer concentration on polymer kinetics in which [MAiBuPOSS]/[CDB]/[AIBN]=30/3/1 and the [MAiBuPOSS]=0.4, 0.5 and 0.6 mol/L were

used respectively. Polymerization exhibited an ideal behaviour up to very high conversions. Good linearity was observed for all the kinetic curves as shown in Fig2.19. It was found that increase the monomer concentration could increase the rate constant. SEC analysis of all fractions showed narrow and symmetric distribution. A typical time evolution SEC traces as shown in Fig2.20 indicates a narrow and symmetric distribution. The relationship between *MW* and conversion was shown in Fig2.21.

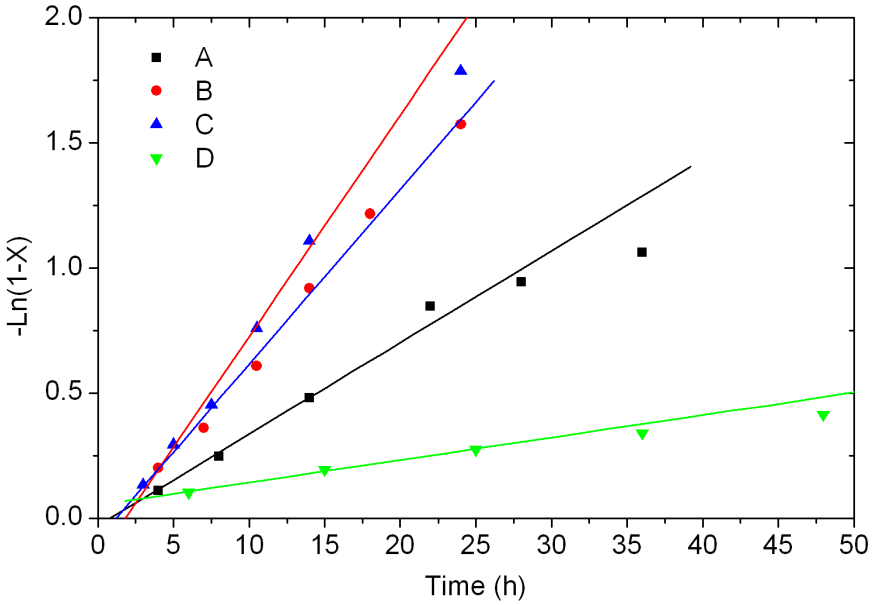

Fig 2.19 Semilogarithmic kinetic curves homopolymerization of MAiBuPOSS, [M]/[CDB]/[AIBN]=30/1/0.333 in different $[M]_0$: (A) 0.4M, (B) 0.5M and (C) 0.6M, and (D) $[M]_0$=0.47M, [M]/[CDB]/[AIBN]=60/1/0.05

In the conversion range for which a linear relationship between -ln(1-conv) vs time was observed, the chains grew with monomer conversion and polydispersity indices remained below 1.2 (see Fig2.21). At this point it should be noted that owing to very different solution behaviors of PS and Cy/iBu POSS functionalized polymethacrylates in THF, molar masses and *PDI* evaluated by SEC with PS standards are underestimated[25]. Therefore, absolute molar masses (M_w) were also determined by static light scattering. As previously described by Han et al[26] for MMA polymerization mediated with relatively high amounts of CDB, measured molar masses were higher than theoretical values at early stages of the polymerization owing to incomplete consumption of CDB due to the relatively low CTE. In

accord with a progressive conversion of the CTA, these values gradually converged in the course of the polymerization (See Fig2.21).

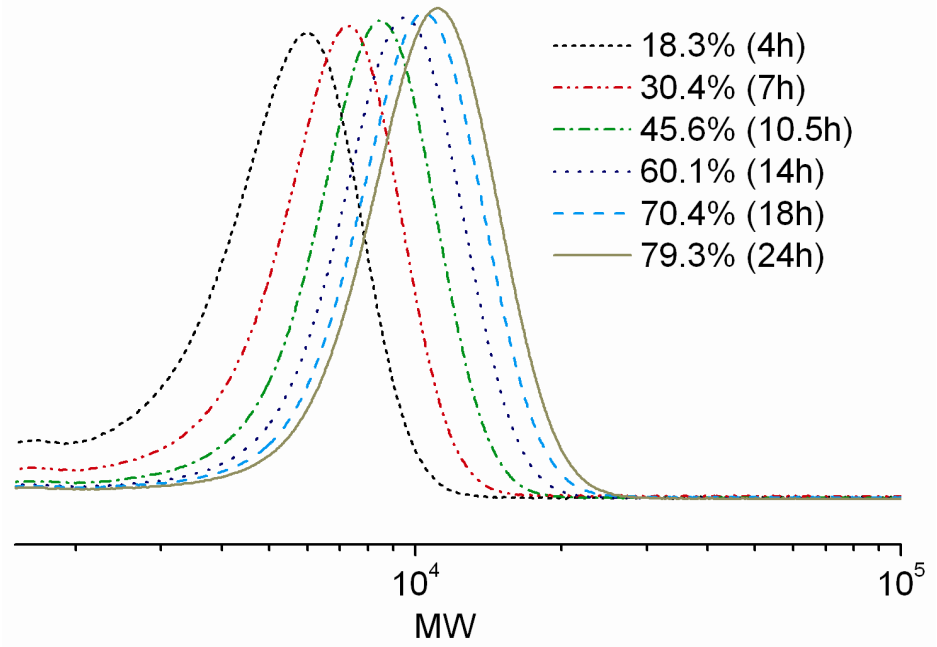

Fig 2.20 SEC curves of PMAiBuPOSS at different conversion in kinetic study. [M]/[CDB]/[AIBN]=30/1/0.333, $[M]_0$=0.5M

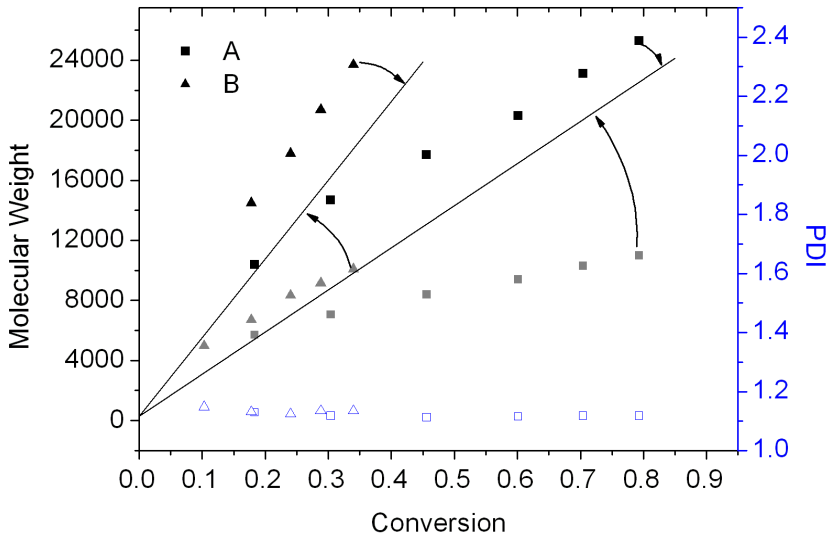

Fig 2.21 *MW* and *PDI* vs conversion in homopolymerization of MAiBuPOSS: (A) $[M]_0$ = 0.5M, [M]/[CDB]/[AIBN] = 30/1/0.333; (B) $[M]_0$ = 0.465M, [M]/[CDB]/[AIBN] = 60/1/0.05). Black: M_w by LS; grey: M_n by SEC; hollow: *PDI*

The polymerization kinetic of MACyPOSS under various [CDB]/[AIBN] ratio was shown in Fig2.22, the Semilogarithmic kinetic curves showed good linearity at low conversion. The SEC curves and *MW*-conversion relationship was very similar with MAiBuPOSS.

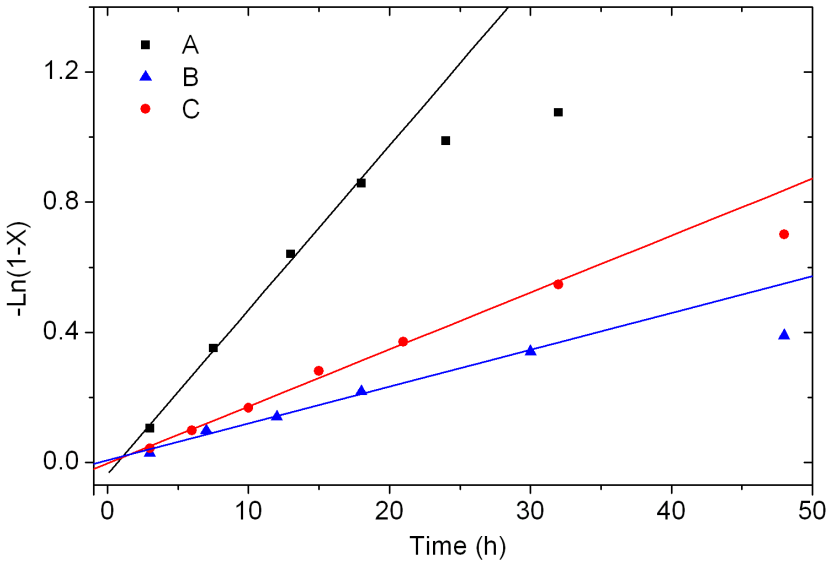

Fig 2.22 Semilogarithmic kinetic curves of homopolymerization of MACyPOSS with defferent [CDB]/[AIBN]: (A) 3, (B) 10, (C) 20. [M]/[CDB] =30/1, $[M]_0$=0.42M

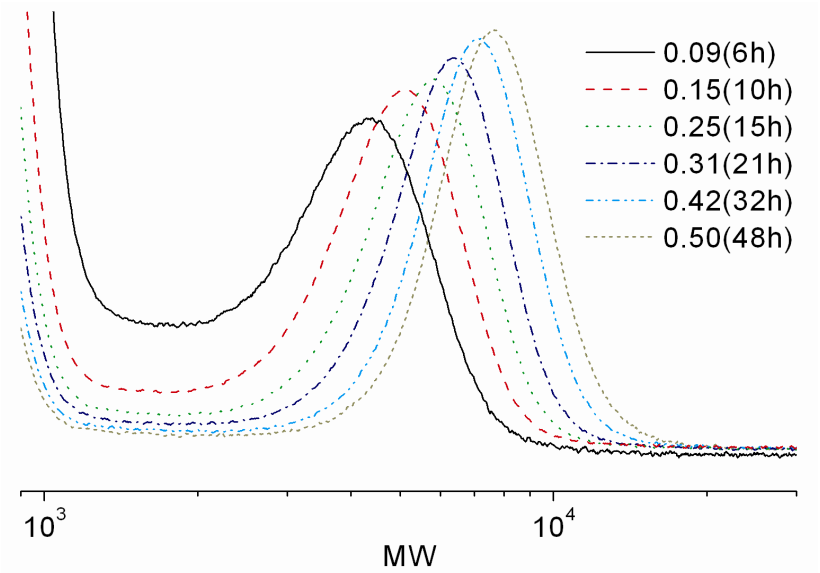

Fig 2.23 SEC curves of PMACyPOSS at different conversion in kinetic study. [M]/[CDB]/[AIBN]=30/1/0.1, $[M]_0$=0.42M

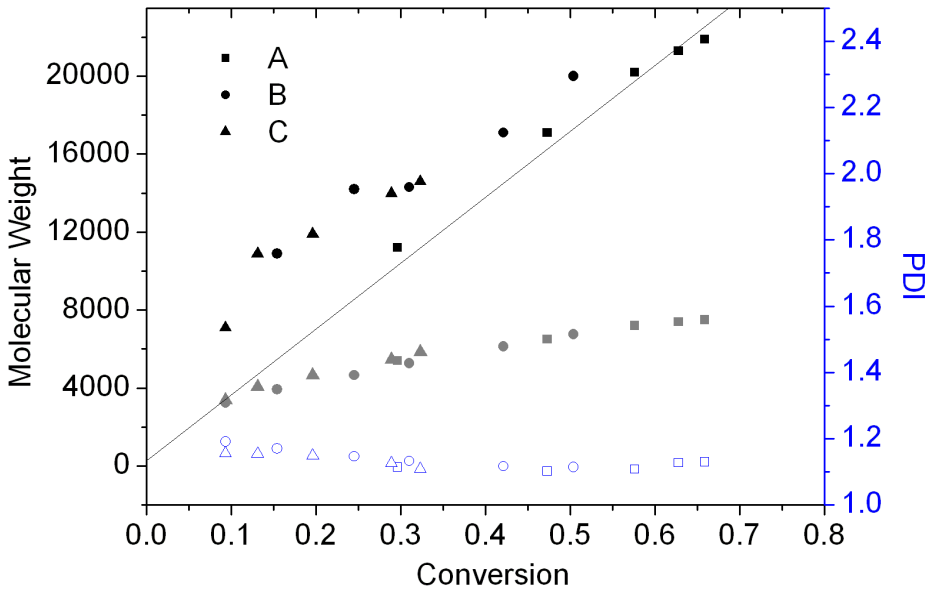

Fig 2.24 *MW* and *PDI* vs conversion in homopolymerization of MACyPOSS with deffrent [CDB]/[AIBN] (A) 3; (B) 10; (C)20. [M]/[CDB]=30, $[M]_0$ = 0.416mol/L. Black: M_w by LS; grey: M_n by SEC; hollow: *PDI*

Thus, there two factors effect the *MW* during the polymerization: on one hand, the incomplete converse of CTA makes the M_n calculated from conversion was underestimated; on the other hand, the termination of free radical generated during the polymerization to maintain the polymerization rate produced dead chains with out living group, which makes the theoretical value overestimated. To get rid of the affect of dead chains, homo-polymer for analysis was synthesized at high [CDB]/[AIBN] (20/1) so that ^{1}H NMR can be used to calculate the DP_n. Typical ^{1}H NMR spectrum of PMACyPOSS homopolymer was shown in Fig2.5. Protons on aromatic of terminate group can be clearly resolved when CCl_2D_2 was used as solvent. PMACyPOSS with M_n=7300, *PDI*=1.10 by SEC vs PS standards and M_w=20000 by light scattering was successfully synthesized in the condition of [M]/[CDB]/[AIBN]=40/1/0.05 in a conversion of 39.1%. ^{1}H NMR analysis shows the DP_n of the product is 17.5.

2.3.3.2 Limit of DP_n in RAFT polymerization

Depicts the kinetics of polymerization at relatively low feed ratio of bulky monomers to

CTA (30), whereas a very satisfactory linear fit was obtained in the early period of the polymerization for both MACyPOSS and MAiBuPOSS at [M]/[CTA]=30, on the contrary to MAiBuPOSS, a deviation to linearity reflecting a loss of control was observed for MACyPOSS at relatively moderate conversion (around 60%). Such discrepancy illustrated the considerable influence of the substituent attached to the POSS cages on the control of the polymerization and suggests in particular that the steric congestion generated by the bulky Cy groups significantly affected the efficiency of the addition-fragmentation process. Consistent with this explanation, the *MW* distribution of PMACyPOSS chains generated at [M]/[CDB]=30 tended to broaden asymmetrically at moderate conversion (~60%, DP_n~18) whereas a narrow monomodal molar mass distribution was observed throughout the polymerization of MAiBuPOSS chains under similar [M]/[CDB] conditions (See Figure 2a and 2c). Increasing [M]/[CDB] ratio to 60 also revealed a significant enlargement of PMAiBuPOSS peaks at about 50% conversion suggestive of a loss of control for MAiBuPOSS polymerization for degrees of polymerization close to 30 (Figure 2d). This limitation of DP_n was consistent with that as reported in ATRP in a previous publication but had a higher value.

The probable mechanism for the limitation was due to the bulk side group which hindered the accesses of chain free radical to the end group of living polymer chain, thus the chain free radical reached a certain DP_n becomes more difficult to be captured by the dithioester than the shorter ones. This chain length dependent chain transfer behavior is due to the huge cubes tightly tied on a main chain which makes it's difficult to be accommodated via adjusting the chain conformation. Therefore, POSS cages in the terminal were expelled by that pendent in main chain, which embedded the free radical in a certain extent. However, the chain propagation was not so affected as chain transfer since the hindrance for the access of monomer was weaker. The incapability in free radical capture also increases the concentration of free radical, in which more dead chains generated.

The details of POSS homopolymer synthesized in this chapter were shown in Table2-2.

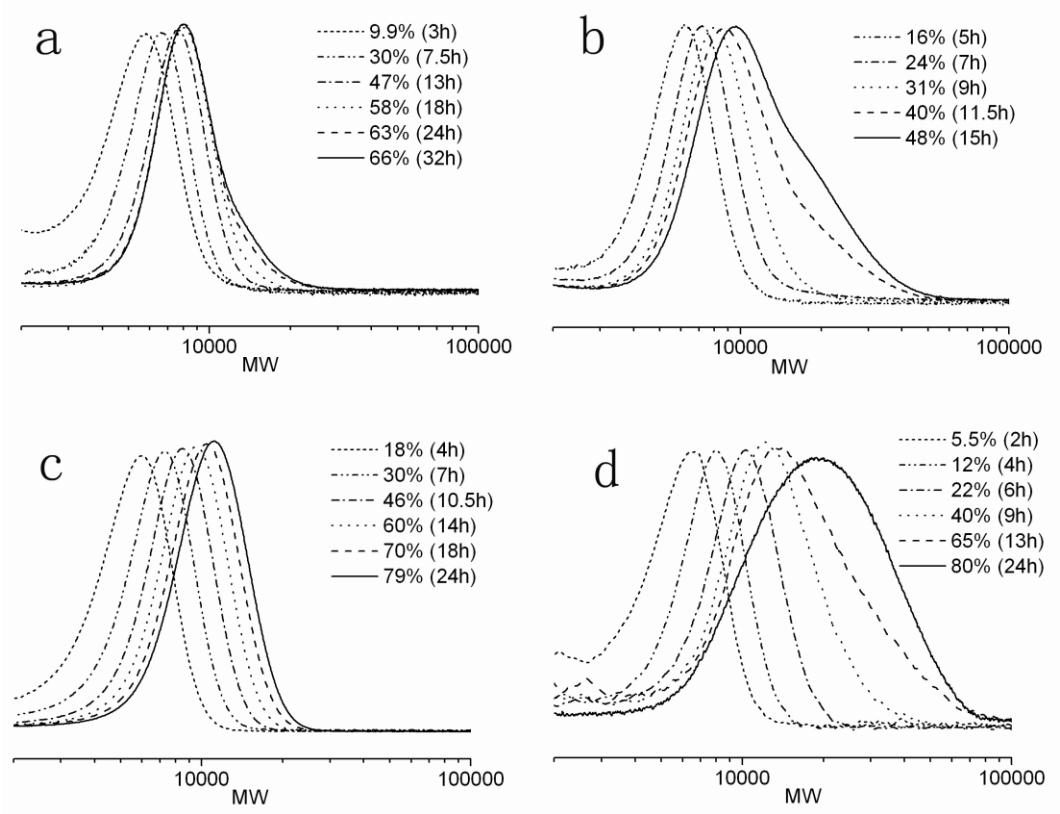

Fig 2.25 Illustration of DP_n limitation in CDB mediated homopolymerization of MACyPOSS: (a) [M]/[CDB]/[AIBN] = 30/1/0.333; (b) M]/[CDB]/[AIBN] = 60:1/0.333) and MAiBuPOSS: (c) [M]/[CDB]/[AIBN] = 30/1/0.333; (d) [M]/[CDB]/[AIBN] = 60/1/0.333

Table 2-2 Properties of the POSS based homopolymers

Exp	M	$[M]_0/[CDB]_0$	Conversion (%)	DP_n [b]	M_n [c] ($\times 10^3$)	M_w [d] ($\times 10^3$)	*PDI*
P1	Cy	30	37	15	6.2	17 (13)[e]	1.12
P2	Cy	40	39	17.5	7.3	20 (18)[e]	1.10
P3	Cy	40	41	18.6	7.9	n.a. (19)[e]	1.10
P4	iBu	28	93	n.a.	12	28 (24)[e]	1.15
P5	iBu	25	73	19.0	8.4	n.a. (19)[e]	1.05

(a) Polymerizations carried out at 65°C at [CDB]/[AIBN]=20 for P1-4 and [CDB]/[AIBN]=3 for P5; (b) Calculated from ^{1}H NMR after purification; (c) Estimated from SEC analysis calibrated with PS standards; (d) Determined by SLS; (e) Theoretical molar masses

2.3.4 Synthesis of BCP via chain extension

2.3.4.1 Polymerization kinetics

Firstly, Three typical conventional monomers: St which has lower propagation rate and low steric bulk of consequent free radical allowing the RAFT polymerization to be well controlled, BuA which has a very reactive propagating radical with low steric bulk leading to fast polymerizations and MMA whose steric hindrance makes it difficult for the bulky tertiary propagating radical to add to the C=S of the CTA, were used for chain extension. The macro CTA PMACyPOSS used for chain extension kinetic study was synthesized in condition [M]/[CDB]/[AIBN]=30/1/0.05 achieved 37.1% conversion. Conversion of St was calculated by ratio of integration from 4.8ppm to 6.1ppm assigned to double bond protons (5.61ppm, 1H and 5.18ppm, 1H) and integration from 0.4ppm to 1ppm assigned to methylene and methyl protons in PMACyPOSS. Conversion of n-BuA was calculated by ratio of integration from 5.5ppm to 6.6ppm assigned to double bond protons (6.43ppm, 1H; 6.05ppm, 1H and 5.80ppm, 1H,) and integration from 3.4ppm to 4.35ppm assigned to methylene protons of ester group in PMACyPOSS at high chemical shift (3.85ppm, 2H)and methyl protons in BuA and p(n-BuA) (4.15ppm ,3H for n-BuA and 3.95ppm, 2H for PBuA). Conversion of MMA in chain extension was calculated by ratio of integration from 5.1ppm to 6.4ppm assigned to double bond protons (6.15ppm, 1H and 5.58ppm, 1H) and integration from 3.4ppm to 4.15ppm assigned to methylene protons of ester group in PMACyPOSS at high chemical shift (3.85ppm, 2H) and methyl protons in MMA and PMMA (3.75ppm, 3H for MMA and 3.6ppm 3H for PMMA).

As shown in Fig2.26, The polymerization kinetics of chain extension by these three monomers showed good linearity, which seems indicated that the chain extension was very successful. Form the kinetic curves, one can conclude that the polymerization of BuA was much faster than other two monomer, especially St even the monomer concentration of St was the highest and temperature at 80^{o}C.

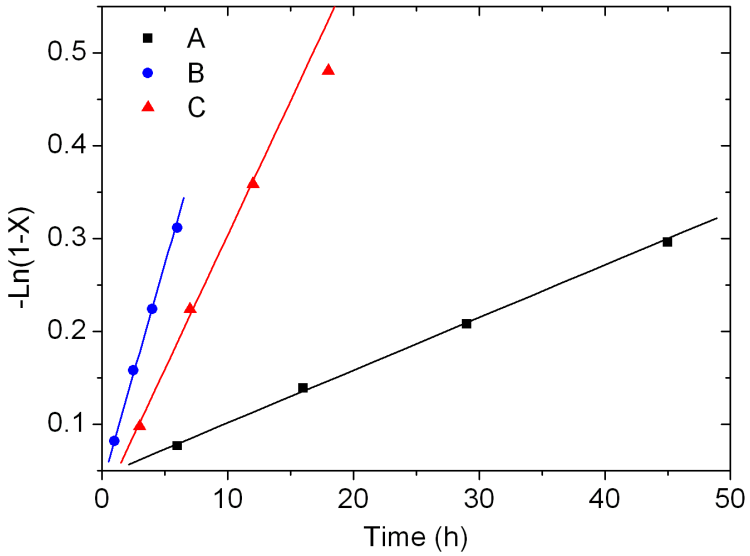

Fig 2.26 Semilogarithmic kinetic curves for chain extension of PMACyPOSS by: (A) St $[M]_0$=5.4M, [M]/[CTA] =727; (B) BuA, $[M]_0$=4.0M, [M]/[CTA] =592 and (C) MMA $[M]_0$=5.0M, [M]/[CTA] =567. [CTA]/[AIBN]=20

However, the linearity of kinetic curves didn't mean all; further investigation in chain extension behavior should be carried out to tell the living characteristic. SEC spectra of different monomer conversion during the chain extension by MMA shown in Fig2.27 showed that the macro CTA was slowly consumed during the polymerization, and much homo-polymer resided even at 38.2% conversion when the polymerization halted. As disclosed in Figure 3a, in contrast to previous reports on polymethacrylates chain extension with MMA[24, 27], chain extension of well-defined PMACyPOSS (P1, M_w=17000 g.mol^{-1}, *PDI*=1.12, 37% of conversion) afforded BCP material (E1, M_w=42000 g.mol^{-1}, *PDI*=1.49, 38% of conversion) together with non negligible amounts of PMACyPOSS homopolymer. The chain extension behavior for BuA were very similar with that of MMA as shown in Fig2.28 even the macro CTA was consumed much faster due to higher CTE. However, this behavior could be attributed to both incomplete converse of macro CTA due to the low efficiency and dead chains generated in POSS homopolymerization.

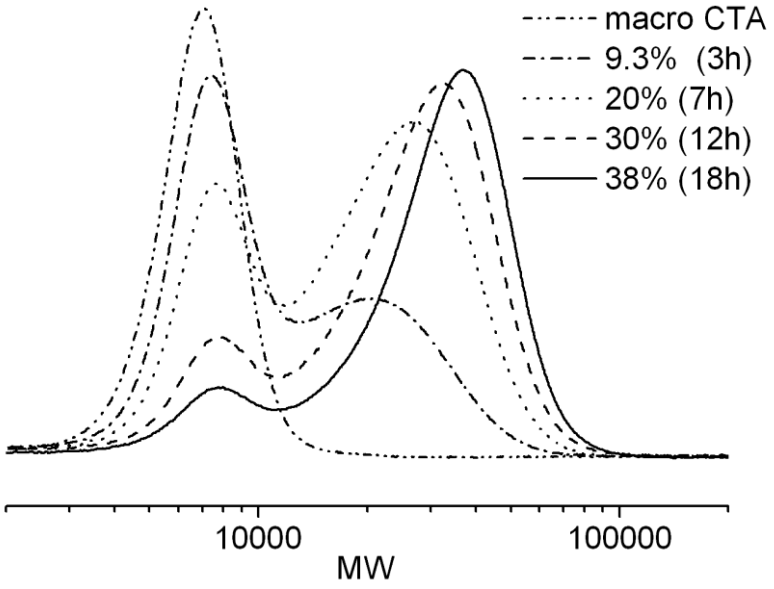

Fig 2.27 SEC curves of fractions in chain extension of PMACyPOSS by MMA.

[M]/[CTA]/[AIBN]=567/1/0.05, $[M]_0$=5.0M

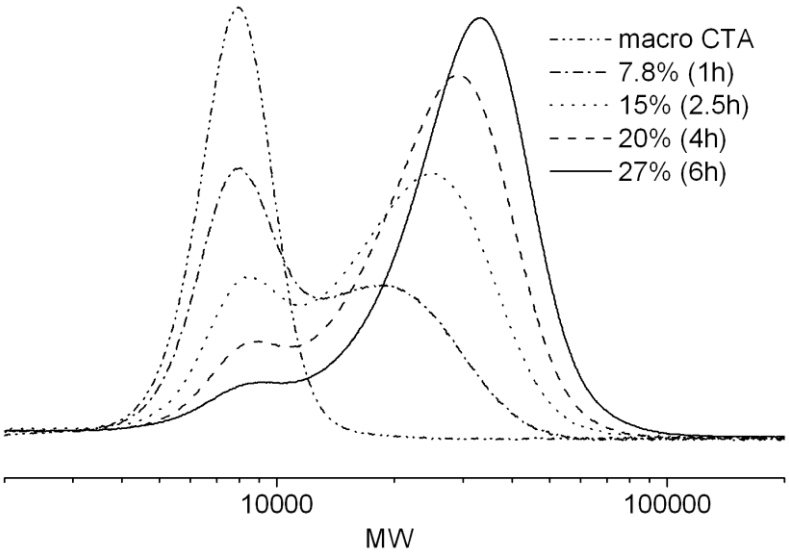

Fig 2.28 SEC curves of fractions in chain extension of PMACyPOSS by BuA.

[M]/[CTA]/[AIBN]=592/1/0.05, $[M]_0$=4.0M

To clearly assign the presence of this low molar mass shoulder to steric hindrance driven decrease of the C_{tr} or to abundant termination events during the polymerization of MACyPOSS, chain extension was further conducted with styrene, a monomer that should promote the efficiency of the macro RAFT agent (Fig2.29)[28]. BCPs exhibiting monomodal

distribution, narrow molar mass distribution and experimental molar mass concurring with predicted values were then obtained (E2, M_w=36000 g.mol^{-1}, *PDI*=1.17, 26% of conversion). In contrast with PMACyPOSS-*b*-PMMA, no low molar mass shoulder could be detected suggesting that most of the chains are indeed functionalized with dithiobenzoate groups and that the PMACyPOSS RAFT agents are quantitatively involved in the chain extension process thanks to more favorable C_{tr}. Therefore, the residual of first block can be approximately attributed to incomplete converse of macro CTA only. The macro CTA was consumed with the converse of the monomer, which is the typical characteristic for RAFT polymerization mediated by CTA with low C_{tr}. This behavior may be attributed to steric hindrance which sharply decreased the C_{tr} due to the bulky side group in PMACyPOSS–SC(S)Ph. C_{tr} became relatively low to well mediate polymerization of MMA, but still high enough for styrene. Similar behavior was observer in the case of RAFT polymerization of methacrylate with other bulky side groups[29].

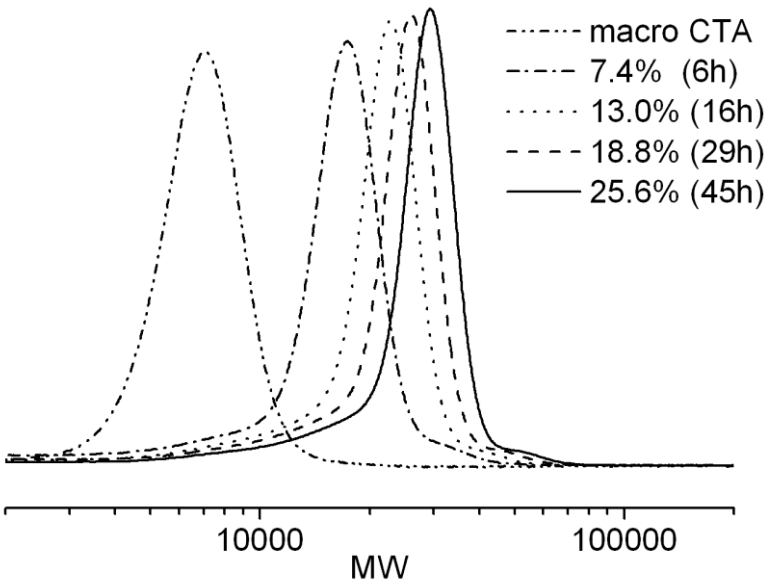

Fig 2.29 SEC curves of fractions in chain extension of PMACyPOSS by St. [M]/[CTA]/[AIBN]=727/1/0.05, $[M]_0$=5.4M

Since the refractive index increment dn/dc of PMMA and PMACyPOSS in THF are similar (0.0870, 0868 by the multi detector respectively), the peak ratio of RI signal in SEC

spectra was used to estimate the efficiency of macro CTA and C_{tr}^{app} by the equation C_{tr}^{app}= d(ln[CTA]$_t$)/d(ln[M]$_t$). The final conversion of macro CTA was 79.4% and C_{tr}^{app} =3.2 from the SEC spectra as shown in Fig2.30 a. ^{1}H NMR was also used to calculate the efficiency of macro CTA. ^{1}H NMR analysis on PMACyPOSS $_{14.5}$-*b*-PMMA$_{216}$ as prepared and after purification by cyclohexane to remove the POSS homopolymer showed that the composition shift from 0.0718 to 0.0561(mol ratio POSS unit to MMA unit), indicating that the efficiency of micro CTA was 78.1% under a conversion of 38.2% in chain extension by MMA, which shows good agreement with that from SEC analysis (Fig2.30b).

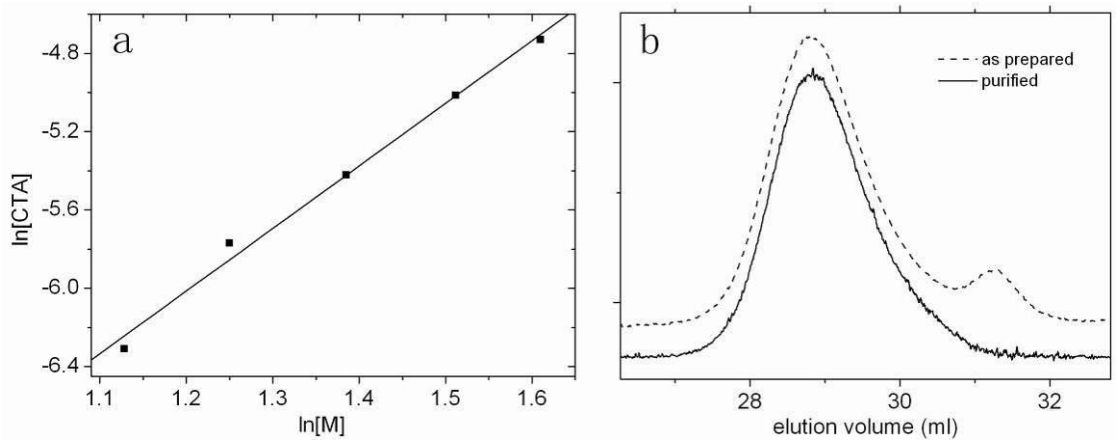

Fig 2.30 （a）Solution of C_{tr}^{app} by d(ln[CTA]$_t$)/d(ln[M]$_t$); (b) SEC traces comparison of PMACyPOSS$_{18}$-*b*-PMMA$_{283}$ as-prepared and after purification

An alternative route to POSS containing BCP is chain extension of normal coil chain macro CTA. However, due to the requirement of R group for effective chain transfer[27], only polymethacrylates macro CTA are appropriate to mediating the polymerization of methacryl POSS monomers. However, due to the high *MW* and low polarity of POSS monomer, high monomer concentration to achieve acceptable polymerization rate will reduce the polarity thus the macro CTA no longer soluble therein, i.e. MACyPOS solution in a moderate concentration (e.g. 0.3mol/L) was poor to dissolve PMMA-S-C(S)-Ph (M_n=12000, *PDI*=1.23) for chain extension when attempting to prepare BCP via chain extension of PMMA by MACyPOSS. In contrast, chain extension of PMACyPOSS by MMA was applicable due to the solubility of MMA for macro CTA.

2.3.4.2 CTE in chain extension

Considered that the consecutive nano-structured epoxy hybrid, DGEBA soluble block i.e. PMMA was required. Due to the incomplete converse of macro CTA, it's difficult to precisely predict the *MW* and composition by conversion, as well as to tune the chain length of second block. Even the residual of POSS polymer macro CTA was proved to be easily removed, in the case of synthesis of POSS containing BCPs with high POSS fraction or complicate topology (like ABA tri-blocks $(AB)_3$ tri-arm stars and comb like polymer brushes), this low CTE becomes the crucial factor. Therefore, the CTE must be improved. It was reported that the control of in a tri-thiocarbonate mediated MMA system was obviously improved in the introduce of small amount of St, which wasn't remarkably effect solubility parameter of the second block[30]. That gives us the inspiration to use a mixed monomer of MMA and Styrene in chain extension of POSS homo-polymers.

In an attempt to simultaneously achieve a more efficient chain extension with MMA and preserve the solubility character of PMMA block, a small percentage of St was thus incorporated as a co-monomer (up to 10% mol). The kinetics for chain extension were shown in Fig2.31 indicated that the rate of polymerization of mixed monomer were slow down in contrast to that of MMA. St conversed much faster than MMA (almost 2 folds) during the polymerization. In the pre-equilibrium step, both St and MMA was equal to be initiated by primary free radicals to form short chain free radicals which would be captured by CTA to release PMACyPOSS free radical for chain extension. However, due to the high CTE, St ended free radicals prefer chain transfer whereas MMA ended free radicals prefer to further propagation. Therefore, the CTE was dominated by St, which was much higher than that of MMA.

The copolymerization resulted in a clear shift of the SEC peaks towards higher *MW* corroborating the growth of a second P(MMA-*co*-St) block as shown in Fig2.32 and Fig2.33. In analogy with the chain extension with St, the trace corresponding to PMACyPOSS homopolymers fainted in the course of the polymerization owing to higher C_{tr}^{app} to PMACyPOSS macro CTA in the copolymerization system. The excellent agreement with theoretical values (see Table 2 E3, $M_{n,th}$=42600 g.mol^{-1}, M_w=43100 g.mol^{-1}, *PDI*=1.24, 34%

of conversion) as well as the decrease of *PDI* with conversion further pointed toward the synthesis of well-defined hybrid PMACyPOSS-*b*-P(MMA-*co*-St) copolymers possessing high POSS weight ratio.

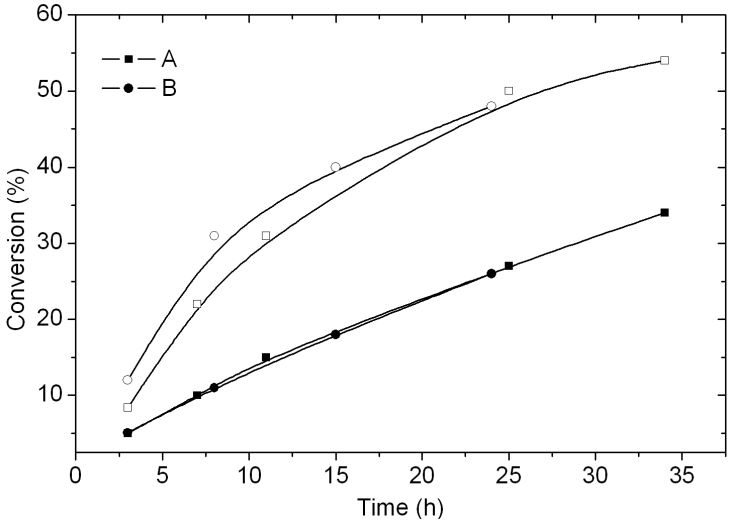

Fig 2.31 Kinetic curves for chain extension of PMACyPOSS by:
(A) MMA+5mol%St, $[MMA]_0$=5.0M, [MMA]/[CTA]/[I]=567/1/0.05, and
(B) MMA+10mol%St, $[MMA]_0$=5.0M, [MMA]/[CTA]/[I]=567/1/0.05.
Black symbol: MMA and hollow symbol: St

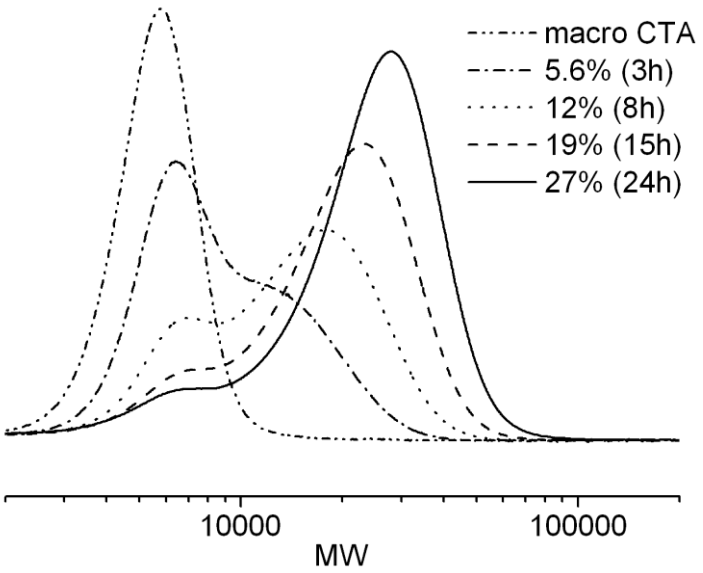

Fig 2.32 SEC curves of fractions in chain extension of PMACyPOSS by MMA+5mol%St.
$[MMA]_0$=5.0M, [MMA]/[CTA]/[AIBN]=567/1/0.05

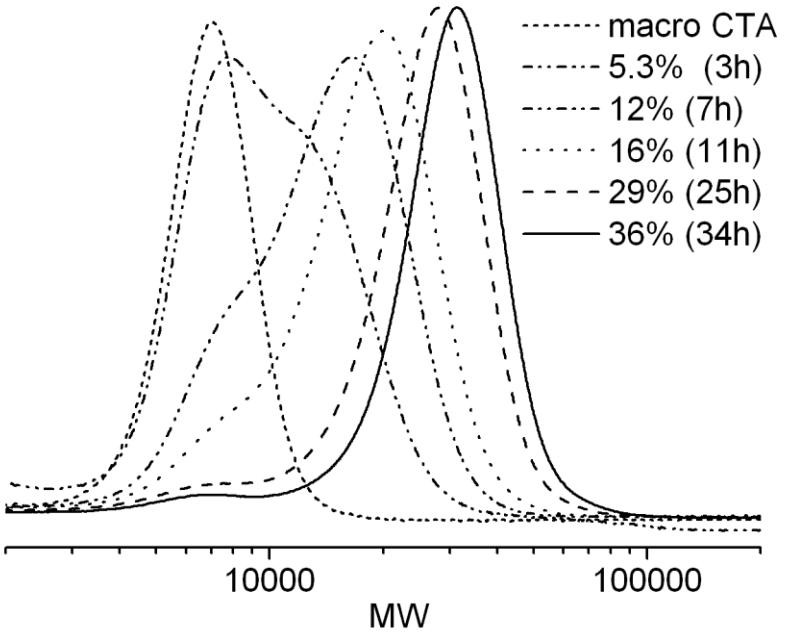

Fig 2.33 SEC curves of fractions in chain extension of PMACyPOSS by MMA+10mol%St. $[MMA]_0$=5.0M, [MMA]/[CTA]/[AIBN]=567/1/0.05

The experimental details of chain extension were shown in Table2-3, in which BCP contains pure PMMA block was purified by extracting the residual POSS block in selective solvent i.e. cyclohexane. Data in bracket corresponds to the purified sample, while others correspond to sample as prepared.

2.3.5 Synthesis of POSS based copolymer with different topology

Efforts have also been made to synthesize POSS based BCP complex topological structure. BAB tri-block and $(BA)_3$ tri-arm were synthesized using multi-functionalized CTA B1 and T1. Semilogarithmic kinetic curves and SEC curves during MACyPOSS polymerization mediated by a T1 were shown in Fig2.34 and 2.35 respectively. In the low conversion range, a linear relationship between -ln(1-conv) vs time was observed. The SEC curves shifted to high *MW* as the monomer conversion increased. *PDI* remained relatively low particularly for that with shorter chain as shown in Table2-4.

Table2-3 Experimental condition and result for chain extension

Expt	Macro CTA	Monomer	$[M]_0$ (mol/L)	$[CTA]_0$ (10^{-3}mol/L)	*Time* (h)	*Conv.* (%)	$M_{n,th}$ (10^3)	M_n [b] (10^3)	*PDI*	M_w [c] (10^3)	f_{POSS} [d] (wt%)
E1	P1	MMA	5.12	9.03	3	9.3	21.6	9.15	1.58		
					7	20	27.7	13.0	1.61		
					12	30	33.4	17.4	1.54		
					18	38	38.0	21.1 (28.4)	1.49 (1.25)	42.2	38.7
E2	P1	95mol%MMA +5mol%St	5.28	8.85	3	5.6	19.7	8.42	1.35		
					8	12	23.5	12.1	1.43		
					15	19	27.9	15.7	1.44		
					24	27	32.4	19.3	1.43	35.3	48.2
E3	P2	90mol%MMA +10mol%St	5.22	8.26	3	5.3	23.3	10.1	1.38		
					7	12	27.3	12.9	1.31		
					11	16	30.4	16.0	1.29		

					25	29	38.5	23.1	1.26		
					34	36	42.6	26.5	1.24	43.1	47.0
E4	P1	St	5.40	7.42	6	7.4	21.9	11.7	1.32		
					16	13	26.1	16.3	1.22		
					29	19	30.6	18.2	1.23		
					45	26	35.6	21.9	1.17	32.4	47.2
E5	P2	MMA	5.0	7.6	18	43	48.4	28.6 （36.5）	1.47 (1.23)	53.4	36.9
E6	P5[d]	MMA	4.90	7.41	18	39	50.0	45.2	1.15	75.8	(40.4)
E7	P3	90mol%MMA +10mol%St	5.0	5.98	25h	25	41.0	30.8	1.24		49.4

(a) All the chain extension was carried out under [CTA]/[AIBN]=20 at 65^{o}C except E4 at 80^{o}C; (b) Against PS standards; (c) Purified polymer analyzed by multi detector combine with RI, RALS and LALS; (d) Calculated by 1H NMR after purification; (e) P5 mixture was used for chain extension directly without any further purification

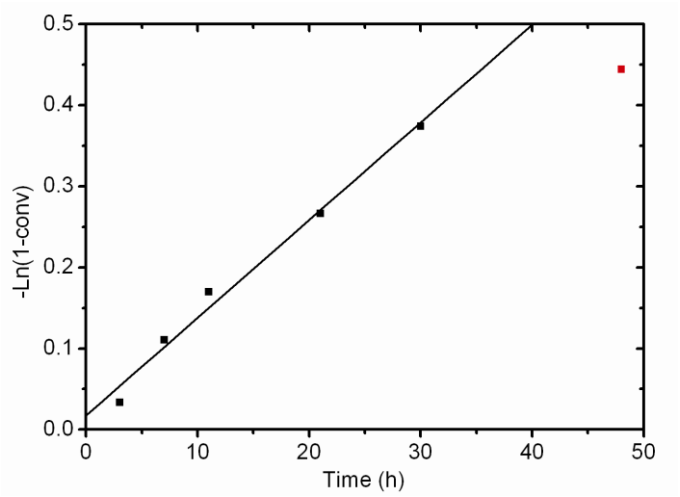

Fig 2.34 Semilogarithmic kinetic curves for T1 mediated homopolymerization of MACyPOSS, [M]/[CTA]/[AIBN]=98/1/0.333, $[M]_0$=0.42M

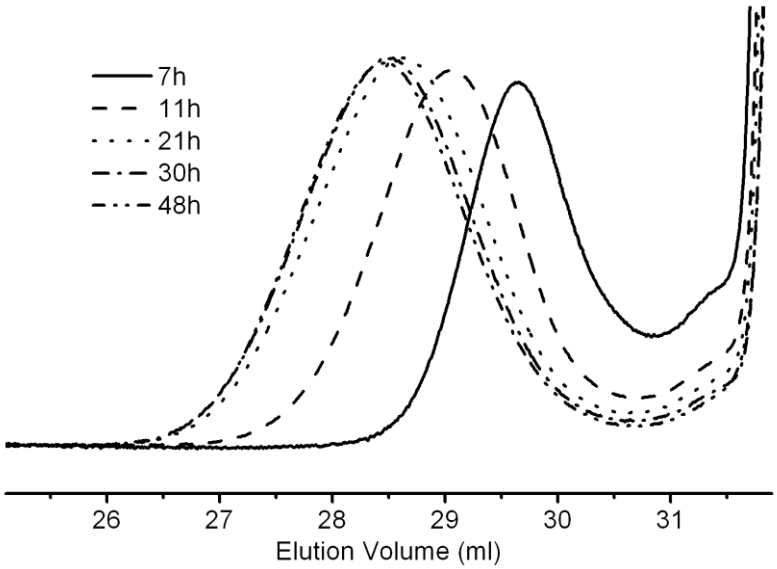

Fig 2.35 SEC curves of PMACyPOSS at different conversion in kinetic study, [M]/[CTA]/[AIBN]=98/1/0.333, $[M]_0$=0.42M

Table 2-4 Properties of the POSS based homopolymers

Sample	CTA	[M]/[CTA]	Conversion (%)	$DP_{n,\,NMR}$	M_n (10^3)	*PDI*	$M_{n,th}$ (10^3)
B1A	B1	86	36	19×2	15	1.35	35
T1A	T1	130	31	17×3	18	1.29	45
T1B	T1	130	40	25×3	21	1.43	59

For the macro CTA described above, chain extension was carried out by mix monomer containing 10mol% St and 90mol% MMA. The SEC curves of sample before and after chain extension was shown in Fig2.36. It was clear that the kinetic curve was of good linearity and the *MW* increased with the conversion. Narrow and symmetric distribution was observed for single chain shorter than 18 but became a broaden peak for long chain as interpreted above. The SEC curves of BCPs obtained by consecutive chain extension showed good *MW* distribution without visible first block residual except for that from T1B, in which a tail was observed. The details were shown in Table2-5.

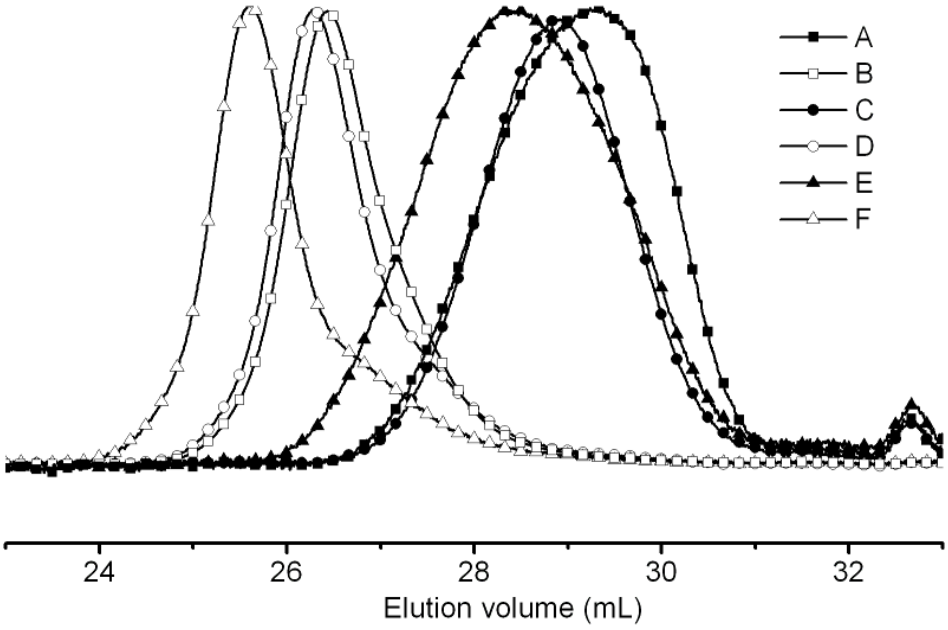

Fig 2.36 SEC curves of (A) B1A, (C) T1A, (E) T1B and the corresponding curves after chain extension (B), (D) and (F)

Table 2-5 Characterization of the POSS based BCPs

Sample	$M_{n,SEC}$ (10^3)	*PDI*	$M_{w,LS}$ (10^3)	POSS (wt%)
B1A-BCP	65	1.258	121	40.1
T1A-BCP	68	1.289	138	46.5
T1B-BCP	105	1.383	223	39.9

2.3.6 Molecular structure and morphology characterization of BCP

2.3.6.1 Molecular structure characterization

The ^{1}H NMR spectra of representative POSS based BCPs were shown in Fig2.37. Composition of PMAiBuPOSS$_x$-*b*-PMMA$_y$ was calculated by the integration of 0.6ppm (PMAiBuPOSS, 16xH) and 3.4~4.2ppm ((2xH for PMAiBuPOSS and 3yH for PMMA); Composition of PMACyPOSS$_x$-*b*-PMMA$_y$ was calculated by the integration ratio of 0.6~2.2ppm (86xH for PMACyPOSS and 5yH for PMMA) and 3.4~4.2ppm ((2xH for PMAiBuPOSS and 3yH for PMMA), so does the P(MACyPOSS$_x$-*co*-MMA$_y$); Composition of PMACyPOSS$_x$-*b*-P(MMA$_y$-*co*-St$_z$) was calculated by the integration ratio of 0.6~2.2ppm (86xH for PMACyPOSS and 5yH for PMMA and 3zH for PSt), 2.2~4.2ppm ((2xH for PMAiBuPOSS and 3yH for PMMA)[31] and 6.6~7.2ppm (5zH for PS). The characterization data of relative polymer was shown in Table2-7.

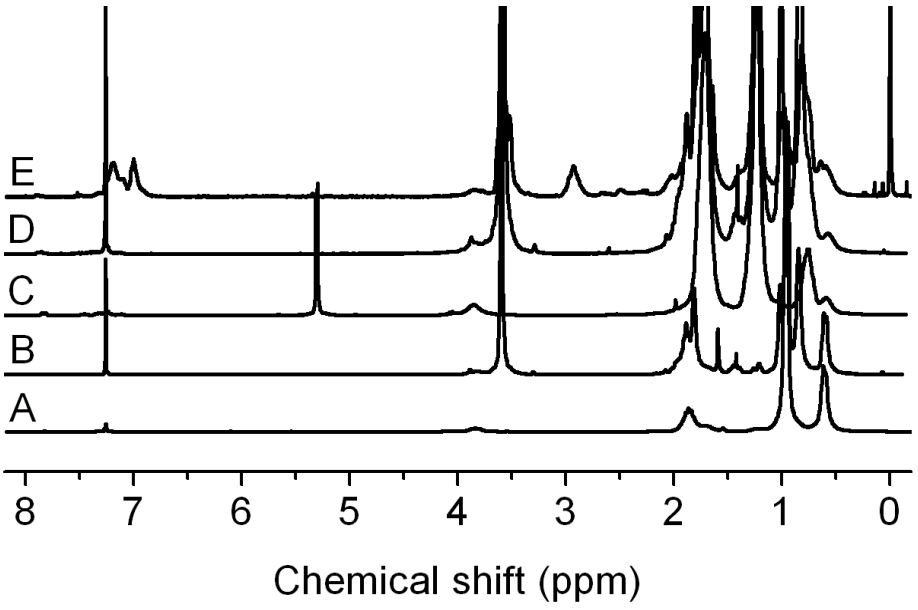

Fig 2.37 ^{1}H NMR spectra of POSS homo-polymers and block copolymers: (A) PMAiBuPOSS$_{27}$, (B) PMAiBuPOSS$_{26}$-*b*-PMMA$_{385}$, (C) PMACyPOSS$_{17.5}$, (D) PMACyPOSS$_{17.5}$-*b*-PMMA$_{335}$, (E) PMACyPOSS$_{18.6}$-*b*-P(MMA$_{175}$-*co*-St$_{33}$). ^{1}H NMR analysis were carried out in *d*-chloroform except (C) in *d*-dichloromethane

Table 2-6 Molecular details of polymers and thermal properties in this chapter

Sample	M_n[a] (10^3)	PDI[a]	M_w[b] (10^3)	f_{POSS}[c] (wt%)	T_g[d] (^oC)	ΔC_p[d] ($J \cdot g^{-1} \cdot K^{-1}$)	T_d[e] (^oC)	Char[e] (wt%)
MACyPOSS	-	-		-	-	-	439	22.3
$PMACyPOSS_{18.6}$	7.3	1.12	20	-	-	-	427	12.0
$PMMA_{293}$	30	1.18	-	0	112.6	0.353	355	0.14
$PMACyPOSS_{17.5}$-*b*-$PMMA_{335}$	36	1.22	53	37	128.1	0.171	361	3.7
$PMACyPOSS_{14.5}$-*b*-PSt_{186}	22	1.17	32	47	100.5	0.147	417	3.1
$PMAiBuPOSS_{26}$-*b*-$PMMA_{385}$	45	1.15	76	40	125.4	0.138	366	0.15
$PMACyPOSS_{18.6}$-*b*-$P(MMA_{175}$-*co*-$St_{33})$	31	1.24	38	49	116.4	0.138	402	5.2
$P(MACyPOSS_{20}$-*co*-$MMA_{388})$	42	1.18	-	38	125.5	0.219	362	3.2

(a) Determined by SEC against PS standards; (b) calculated from multi detector; (c) calculated from ^1H NMR; (d) middle transition step measured by DSC, (e) max weight loss temperature by TGA in N_2

2.3.6.2 Morphology

The morphology of BCPs was analyzed by TEM of cast film prepared by casting 3mg/mL BCP/toluene solution on the grid then slowly evaporated the solvent. Well-defined lamellar morphology but with poor long distance order structure and irregular arrangement was observed for PMACyPOSS$_{17.5}$-*b*-PMMA$_{335}$ as shown in Fig2.38a and its insert. The dark area was attributed to POSS domain due to the high electron density of Si. The morphology of PMACyPOSS$_{18.6}$-*b*-P(MMA$_{175}$-*co*-St$_{33}$) was shown in Fig2.38b and its insert. In contrast to that of PMACyPOSS$_{17.5}$-*b*-PMMA$_{335,}$ the lamellar structure was better resolved and more regular. The size of POSS domain was in 10~12nm. Few impurities were observed in TEM observation.

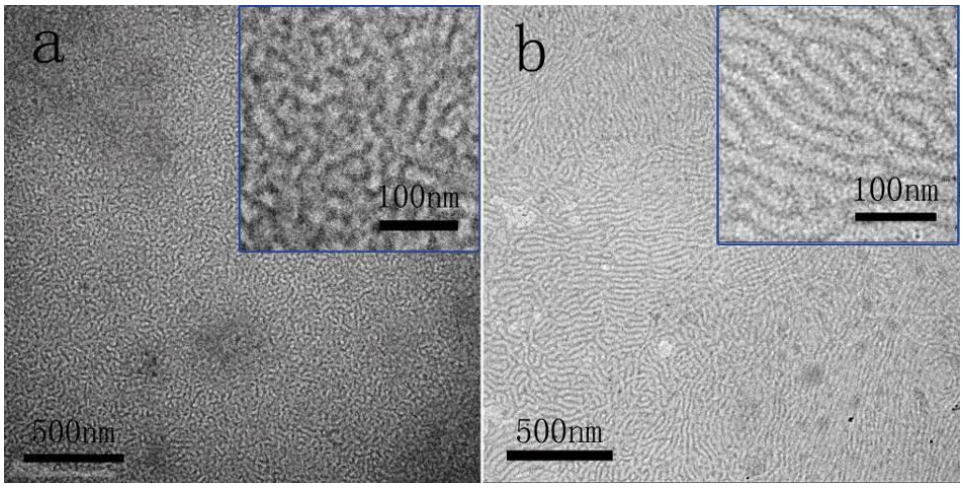

Fig 2.38 TEM image of casting thin film of (a) PMACyPOSS$_{17.5}$-*b*-PMMA$_{335}$ and (b) PMACyPOSS$_{18.6}$-*b*-P(MMA$_{175}$-*co*-St$_{33}$)

The WAXS patterns of MACyPOSS and its homopolymer and copolymer were shown in Fig2.39. The monomer showed sharp reflections at 2θ=7.83, 10.46, 11.61, 18.14, and 18.80, whereas the corresponding reflection in homopolymer only shows a broaden peak. Statistic copolymer with MMA shows a sharp reflection at 2θ = 7.78^{o} after thermal annealing, indicating the presence of crystalline structure in the polymer. WAXS patterns show that in the BCPs no matter with similar or even higher

POSS content only show a broaden peak, which corresponding to poor crystallinity, which was different from that of MAiBuPOSS in previous report[11]. It was clear that ability to crystallization of PMACyPOSS was inhibited after polymerization due to the bulky side group and strong interaction. The POSS in statistic copolymer could form nanocrystal with the motion of PMMA chain above T_g.

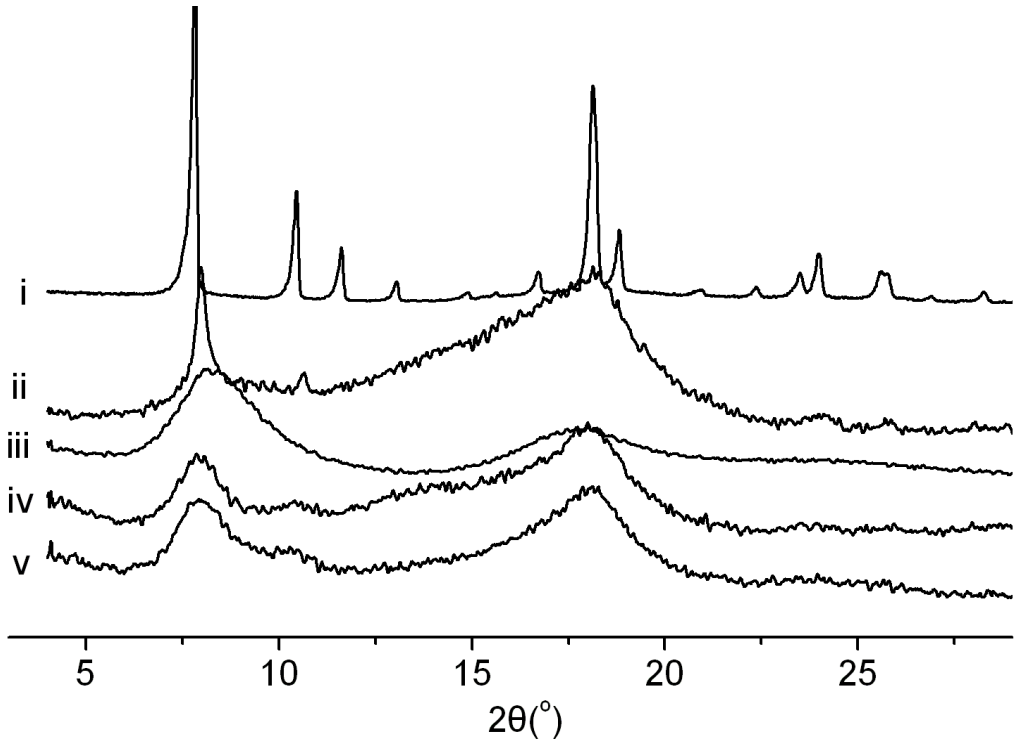

Fig 2.39 Wide-angle X-ray scattering (WAXS) using Cu K_α radiation (λ=0.15418nm) for (i) MACyPOSS powder, (ii) P(MACyPOSS$_{20}$-*co*-MMA$_{388}$) , (iii) PMACyPOSS$_{18}$, (iv) PMACyPOSS$_{17.5}$-*b*-PMMA$_{335}$ and (v) PMACyPOSS$_{18.6}$-*b*-P(MMA$_{175}$-*co*-St$_{33}$). Samples were annealing at 140°C for 1 week except MACyPOSS monomer

2.3.7 Thermal-mechanical properties of BCPs

2.3.7.1 Glass transition

Generally, the T_g of polymers was affected by the *MW*, side chain interaction, rigidity of main chain, steric barrier and free volume fraction. The effect of POSS on T_g depended on the net contribution of steric effect on chain motion, additional free

volume fraction and POSS polymeric segment interactions. POSS cages are undoubtedly rigid and bulk, which can prevent the chain motions, and the semi-crystalline POSS aggregates offer additional physical cross-linkage. Both of them had positive contribution on T_g. On the other hand, random tethering POSS cages in main chain increased the density of chain ends and free volume, potentially lowering T_g by internal plasticization.

It has been previously reported that MAiBuPOSS, MACyPOSS monomers and their copolymers display very disparate thermal behavior. MAiBuPOSS exhibiting weak interaction between molecules due to the flexible vertex groups, have a melt point at 109°C. PMAiBuPOSS homopolymer proves to be slightly crystallization under certain treatment and exhibits a T_g around 40~50°C[32]. For most case of random copolymers，the introduction of MAiBuPOSS unit negatively affected the T_g, due to the bulky side group and weak interaction which provides extra free volume to the PMMA system[33]. Conversely, no transition or melting has been detected yet for MACyPOSS monomer and homopolymers before decomposition due to the strong interaction of well packed vertex group in crystals. For MACyPOSS containing random copolymer, the increase of glass transitions was observed extensively. This vertex group effect on thermal transition was extensively investigated in previous works[9, 32, 34-39]. However, the morphology effect from random and BCPs owning POSS with different vertex group was rarely studied.

Thermal properties of the hybrid BCPs were given in Fig2.40 and Table2-7. Herein, DSC thermograms of the copolymers did not reveal transitions directly assignable to POSS containing blocks (data not showed). However, the presence of PMACyPOSS or PMAiBuPOSS blocks was emphasized by the increase of the T_g corresponding to the PMMA phase from 112°C to 128°C and 125°C respectively. As a comparison, a similar enhancement (125°C) was observed for a random P(MACyPOSS$_{20}$-*co*-MMA$_{388}$) copolymer with equivalent POSS content. However, in contrast with the random incorporating of MAiBuPOSS, the introduction of PMAiBuPOSS block increases the T_g of PMMA to 125℃ as well which was sustained in a present publication[22]. On the other hand, the incorporation of St unit in

the second block afforded copolymers (PMACyPOSS$_{18.6}$-*b*-P(MMA$_{175}$-*co*-St$_{33}$)) having intermediate T_g (116°C) in spite of very high POSS content (~ 50 % wt) due to the lower T_g of P(MMA-*co*-St) matrix.

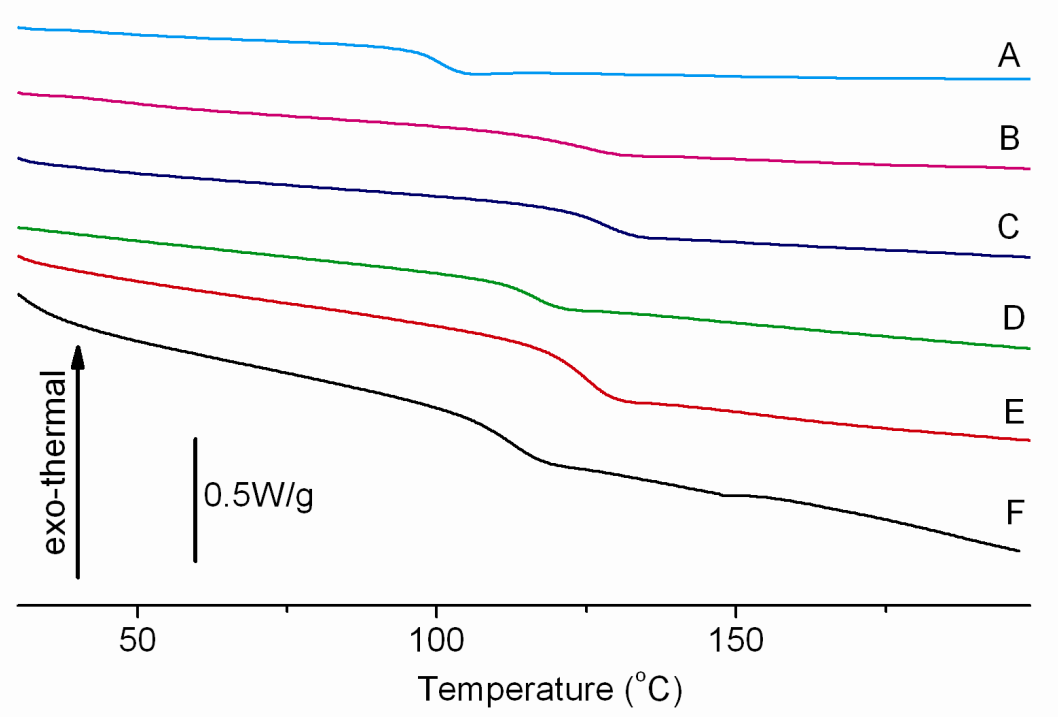

Fig 2.40 DSC curves of (A) PMCyPOSS$_{14.5}$-*b*-PSt$_{186}$, (B) PMAiBuPOSS$_{26}$-*b*-PMMA$_{385}$, (C) PMACyPOSS$_{17.5}$-*b*-PMMA$_{335}$, (D) PMACyPOSS$_{18.6}$-*b*-P(MMA$_{175}$-*co*-St$_{33}$), (E) P(MACyPOSS$_{20}$-*co*-MMA$_{388}$) and (F) PMMA$_{293}$. 10°C/min from 25°C to 250°C (200°C for PMMA), 2nd heating cycle

To compare the POSS aggregation behavior of BCP and statistic copolymer as shown in the WAXS, sample annealing at 160°C for 4days were analyzed by DSC as well. The temperature processing was set as 10°C/min from 25°C~160°C~ 25°C~250 °C. As shown in Fig2.41, DSC curves shows no obvious deference before and after thermal treat for BCP, whereas a small endo-thermal peak with ΔH=2.26 J/g was observed after thermal treat for statistic copolymer. Similar result was observed by Amichi et al[40].

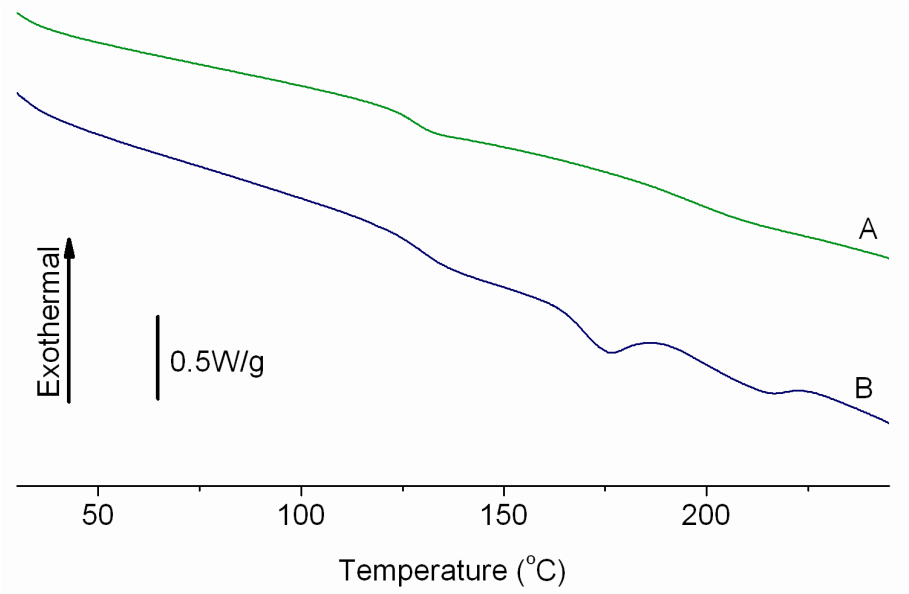

Fig 2.41 DSC curves of A: PMACyPOSS$_{17.5}$-*b*-PMMA$_{335}$, and B: P(MACyPOSS$_{20}$-*co*-MMA$_{388}$) after annealing

2.3.7.2 Thermo-mechanical properties

To investigate the effect of POSS in different type and conformation on thermo-mechanical properties, DMTA analysis was performed. Samples for DMTA were prepared by solution casting. The temperature was increased step by step very slowly to avoid the bubble of solvent. Then the samples were heated at 140℃ for one week. Pure PMMA (M_n=29900, *PDI*=1.22) was not managed to prepare DMTA sample as the sample became brittle after solvent evaporation.

Dynamic mechanical properties of the hybrid copolymers were given in Fig2.42. PMAiBuPOSS$_{26}$-*b*-PMMA$_{385}$ displays the typical curves like BCP with the presence of two damping peaks and a two-step drop of modulus (*E'*). The first damping peak, with a maximum at *T*~70 °C, was due to the glass transition of the PMAiBuPOSS block that could not be observed by DSC. The drop of modulus associated to this transition was around half a decade. The modulus subsequently exhibited a plateau-like behaviour until the appearance of the second transition. The second damping peak, with a maximum at *T*~140 °C, could be assigned to the glass transition

of the PMMA block. At the same time the modulus showed a strong decrease, close to two decades, and reached 1 MPa at 200 °C.

The behaviour of BCPs synthesized from MACyPOSS was completely different. Only one transition was observed at 130 °C and 115 °C for PMACyPOSS$_{17.5}$-*b*-PMMA$_{335}$ and PMACyPOSS$_{18.6}$-*b*-P(MMA$_{175}$-*co*-St$_{33}$), corresponding to the glass transition of MMA block and MMA/St block respectively. No transition associated to PMACyPOSS could be observed in this range of temperature. Of particular interest was the high value of modulus at high temperature displayed by PMACyPOSS$_{17.5}$-*b*-PMMA$_{335}$ and PMACyPOSS$_{18.6}$-*b*-P(MMA$_{175}$-*co*-St$_{33}$) copolymers and the absence of flow which could be associated to the assembly of PMACyPOSS block in cohesive nano-domains as previously reported for random and BCPs[11, 41, 42], which played a role as crosslink phase. This high temperature resistant material, which was strong enough to hold its shape even at 200℃, might have potential application as high performance materials.

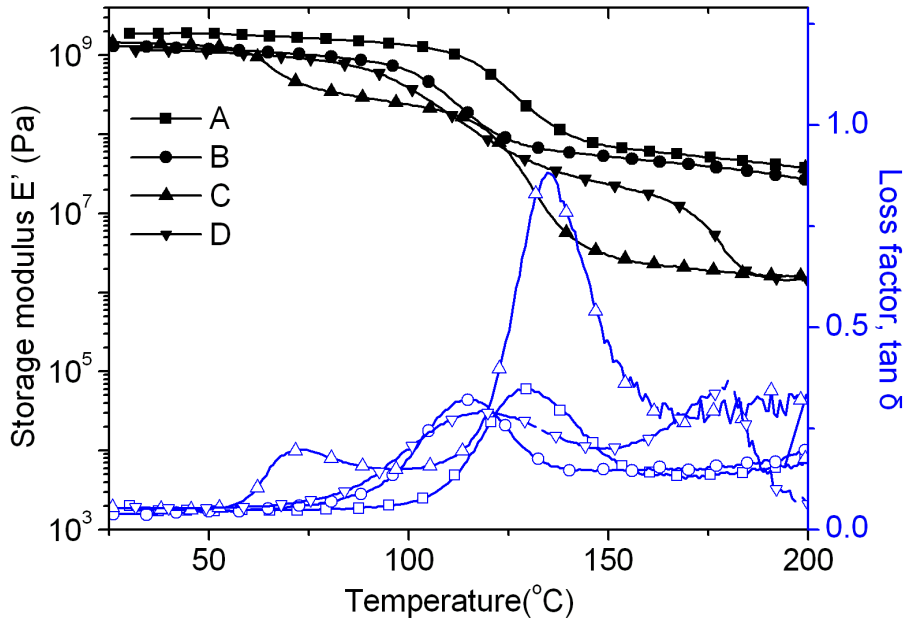

Fig 2.42 Dynamic mechanical thermal analysis (DMTA) of copolymers at 1Hz (bending mode): (A) PMACyPOSS$_{17.5}$-*b*-PMMA$_{335}$, (B) PMAiBuPOSS$_{26}$-*b*-PMMA$_{385}$, (C) PMACyPOSS$_{18.6}$-*b*-P(MMA$_{175}$-*co*-St$_{33}$) and (D) P(MACyPOSS$_{20}$-*co*-MMA$_{388}$). Black symbols: storage modulus E'; hollow symbols: loss factor tan δ

For comparison, the behaviour of P(MACyPOSS$_{20}$-*co*-MMA$_{388}$) random copolymer was also studied by DMTA. The copolymer showed one broad damping peak with a maximum at 125°C corresponding to the glass transition. Interestingly, the presence of physical inter-chain interactions promoted by the POSS units prevented from a complete flow of the polymer after T_g. These interactions were finally disrupted at 170°C leading to polymer flow. These results clearly illustrated how the presence of highly cohesive inorganic domains impacts the modulus above the transition of the organic phase.

2.3.7.3 Thermal stability and flame retardancy

TGA analysis was also carried out to investigate the thermal stability. As shown in Fig2.43, both MACyPOSS and its homopolymer showed similar decomposition stage when heated in N_2 atmosphere. However, the homopolymer showed a 25^{o}C decrease of T_d when compared to the monomer. This observation confirmed that the morphology played a very important role in thermal stability. The monomer proved to be full crystallized by WAXS, whereas the homo-polymer was amorphous due to the poor chain motion caused by the crowd bulky side POSS group. The strong interaction between POSS cages in crystals would prevent the inner POSS from decomposition and "evaporation". For the homo-polymer, once the main chain was unzipped, the POSS cage would be easily decomposition and evaporated, resulting low T_d and residual char. Much higher T_d as well as different degradation behavior was observed for MACyPOSS-MMA copolymer with POSS loading up to 90wt% in literature[32], which probably due to the high *MW* and good crystallinity.

The TGA of polymers was shown in Fig2.44. The fist loss step was attributed to the residual of solvent and decomposition of end group. TGA analysis showed only a slightly increase (375℃) on the decomposition temperature (T_d, defined when 50% mass loss) when compare to the PMMA (364℃) but much lower than PMACyPOSS (429℃). The TGA curve of PMACyPOSS was very closed to that of $Cy_8Si_8O_{12}$[43], showed a higher T_d than that in the other work[31], this discrepancy might attribute to

the short but regular chain length of POSS homo-polymer in this work. The char residual of both homo-polymer and copolymers were much lower than the Si content (in terms of SiO_2) as well.

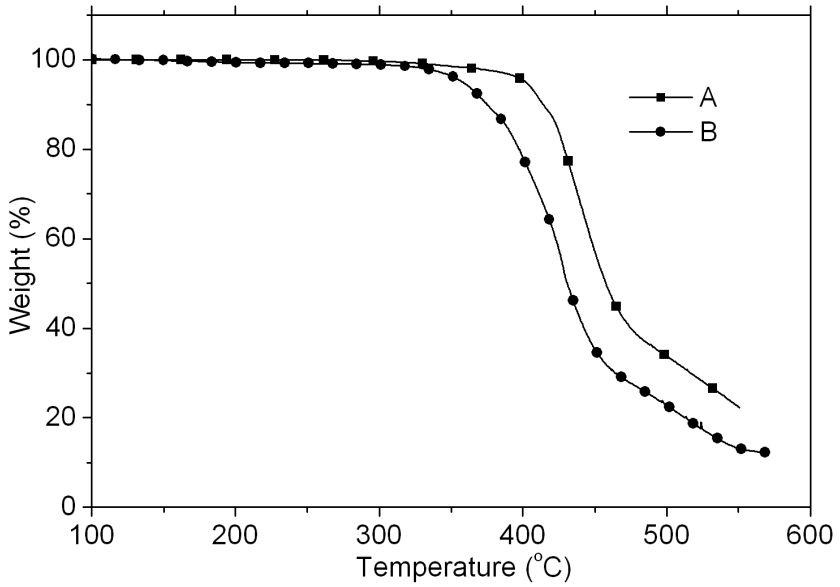

Fig 2.43 TGA curves of: (A) MACyPOSS monomer and (B) PMACyPOSS. 20°C/min, from 25°C~600°C, in N_2

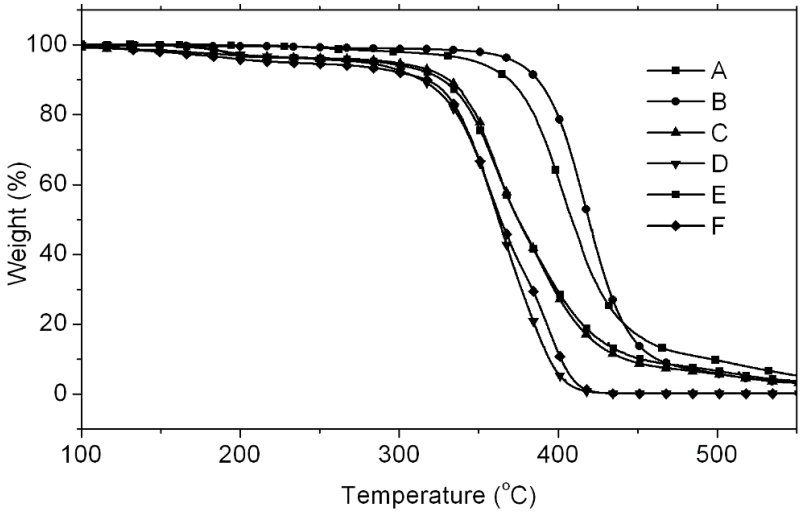

Fig 2.44 TG and DTG curves of: (A) $PMACyPOSS_{17.5}$-*b*-$PMMA_{335}$, (B) $PMCyPOSS_{14.5}$-*b*-PSt_{186}, (C) P($MACyPOSS_{20}$-*co*-MMA_{388}) , (D) $PMAiBuPOSS_{26}$-*b*-$PMMA_{385}$, (E) $PMACyPOSS_{18.6}$-*b*-P(MMA_{175}-*co*-St_{33}) and (F) $PMMA_{293}$. 20°C/min, from 25°C~600°C, in N_2

As a kind of I/O nano-object, POSS cage was expected to have promising future in synergetic flam-retardant[3, 44, 45]. POSS has been proved to enhance the thermo-oxidation resistance, attributed to the formation of the inert silica-like layer on the surface, which can prevent the further oxidation of the inner part of the matrix[45]. To further investigate the flame retardancy, TGA in air was carried out as well. All polymers showed dramatically weight loss at 280°C when combustion occurred. Samples containing St unit showed good char forming character before 500°C, but finally to silica as well as other polymer. The residual char was very close to the theoretical Si content (in terms of SiO_2). From this point of view, silica formation is truly occurred in combustion of POSS based polymer, but single POSS addition dose not offer good flam retardancy in terms of char formation. The most important effect of POSS is the synergy effect in char structure improvement. Synergy effect of multi-element attracts a lot of attentions, because the silicon forming chars at high temperature which is prevented by the evaporation of char.

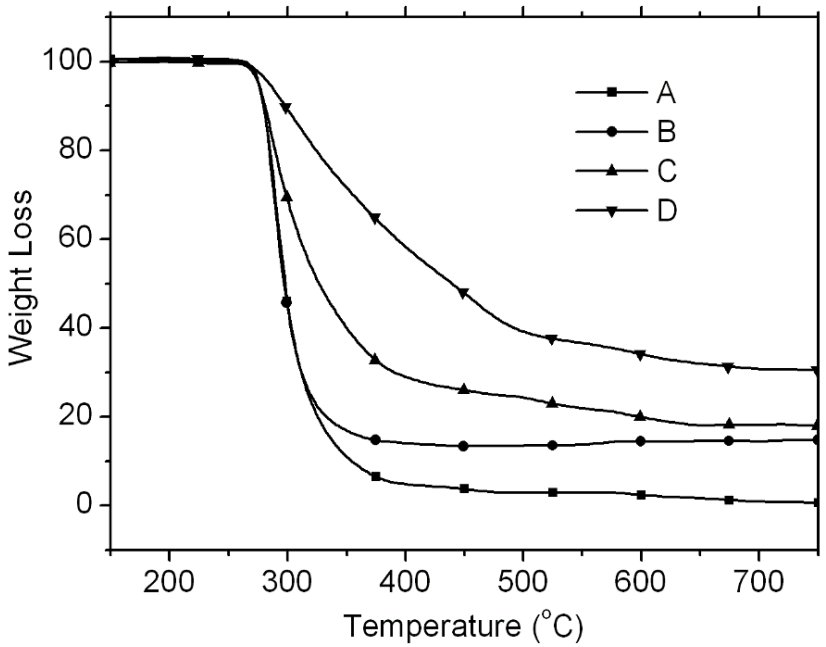

Fig 2.45 TGA curves of: (A) PMMA, (B) PMACyPOSS$_{17.5}$-*b*-PMMA$_{335}$, (C) PMACyPOSS$_{18.6}$-*b*-P(MMA$_{175}$-*co*-St$_{33}$), (D) PMACyPOSS$_{18.6}$-*b*-P(MMA$_{90}$-co -St$_{17}$). 10°C/min, from 25°C~800°C, in air

The morphology of resulted silica was analyzed by TEM. As shown in Fig2.46a, b, and c, the residual of PMACyPOSS$_{11}$-*b*-P(MMA$_{515}$-*co*-St$_{60}$) composed of two kind of structure: one is 3D packed silk worm like nanorods, the other is the hierarchical structure composed of silica grid. 3D packed nanorods formed micro particles with meso-porous therein and could be re-dispersed with grinding, the silk worm structure with 7nm in size and 5~10nm in distance could be observed on the edge, whereas the hierarchical structure formed cage like NP in the size of ~200nm composed of grid in the size of 7nm. The TEM of residual from BCP containing higher POSS fraction, PMACyPOSS$_{18.6}$-*b*-P(MMA$_{90}$-*co*-St$_{17}$)was shown in Fig2.46(d), 2.46(e). Nano-lamella composed of meso-porous silica was obtained. Due to the heat resistance of POSS domain, no soften but direct oxidation occurred during heating process, leaving the siloxane structure therein, while the organic part was oxidized and evaporated, leaving meso-porous.

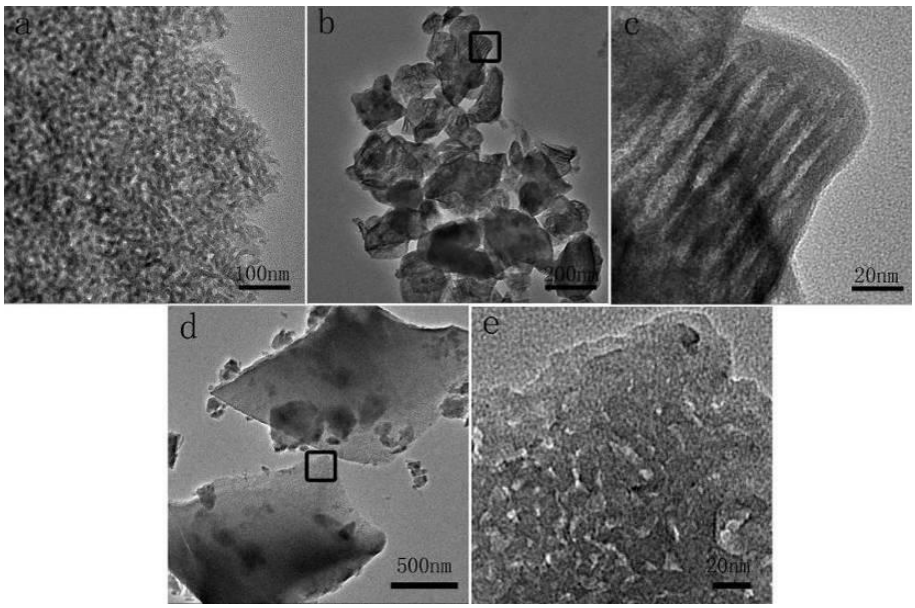

Fig 2.46 TEM images of char of: (a), (b), (c) PMACyPOSS$_{11}$-*b*-P(MMA$_{515}$-*co*-St$_{60}$); and (d), (e) PMACyPOSS$_{18.6}$-*b*-P(MMA$_{90}$-*co*-St$_{17}$)

2.4 Conclusion

CRP of POSS monomers with bulky side group has remained a challenge in recent decades, which limited the comprehensive study of properties and application of POSS based block polymers. Herein, we have investigated the RAFT polymerization of several POSS monomers with different vertex groups. Vertex group dependence was found in terms of limitation of polymerization degree, for instance, DP_n limitation was approximately 18 for MACyPOSS and 30 for MAiBuPOSS. The system was well-controlled below DP_n limitation, whereas *MW* distribution became asymmetrically broaden when limitation approaching because of the lower capability in free radical capturing of higher *MW* fraction. By optimizing the experiment condition, POSS homo-polymer close to limitation with narrow *MW* distribution was synthesized.

The chain extension behavior of PPOSS macro CTA by several types of monomer was studied. It was found that the steric hindrance of POSS dramatically decreased the CTE, leading a low *MW* shoulder peak. By introducing in a small amount of St co-monomer, the efficiency was obviously increased and POSS based BCP with different topology such as AB，BAB and $(BA)_3$ were synthesized.

By comparing the effect of POSS type and their aggregation state on the thermo-mechanical properties, the structure-property relationship was investigated. It was found that the properties of BCPs was completely different from statistic copolymer, for instance: the introduction of MAiBuPOSS would decrease the T_g of its statistic copolymer with MMA，while the PMAiBuPOSS block will increase the T_g of PMMA due to the motion hindering. For MACyPOSS，even the same trend on T_g was observed for statistic and BCP, the rubbery plateau was much more broaden for BCP due to the tough POSS domain. The presence of physical inter-chain interactions promoted by the POSS units in statistic copolymer prevented from a complete flow of the polymer after T_g but finally disrupted at 170 °C leading to polymer flow. The vertex group of POSS was found to obviously affect the properties of their copolymer, for instance, the PMAiBuPOSS block has a transition at 70^oC due to the weak

interaction, decreasing the module in half decade, whereas the strong interaction between PMACyPOSS block made it cross linking phase, reinforcing the matrix.

The thermal degradation behavior of POSS based polymers analyzed by TGA indicated that both char formation and evaporation of POSS occurred in N_2. However, mainly silica formed in air, which was confirmed to be meso-porous structure after pyrolysis by TEM analysis.

Reference

1. Cordes, D.B., P.D. Lickiss, and F. Rataboul, *Recent Developments in the Chemistry of Cubic Polyhedral Oligosilsesquioxanes.* [J]. Chemical Reviews, 2010. **110**(4): p. 2081-2173.
2. Ikeda, M. and H. Saito, *Improvement of polymer performance by cubic-oligosilsesquioxane.* [J]. Reactive & Functional Polymers, 2007. **67**(11): p. 1148-1156.
3. Camino, G., A. Fina., and D. Tabuani, *POSS as Fire Retardants.* MoDeSt-Workshop 08 on Nano-filled Fire Retardant Polymers and Polymeric Composites Beijing (China), 2008. 16-17.
4. Kopesky, E.T., G.H. McKinley, and R.E. Cohen, *Toughened poly(methyl methacrylate) nanocomposites by incorporating polyhedral oligomeric silsesquioxanes.* [J]. Polymer, 2006. **47**(1): p. 299-309.
5. Kopesky, E.T., et al., *Thermomechanical properties of poly(methyl methacrylate)s containing tethered and untethered polyhedral oligomeric silsesquioxanes.* [J]. Macromolecules, 2004. **37**(24): p. 8992-9004.
6. Li, G.Z., et al., *Polyhedral oligomeric silsesquioxane (POSS) polymers and copolymers: A review.* [J]. Journal of Inorganic and Organometallic Polymers, 2001. **11**(3): p. 123-154.
7. Wu, J. and P.T. Mather, *POSS Polymers: Physical Properties and Biomaterials Applications.* [J]. Polymer Reviews, 2009. **49**(1): p. 25-63.
8. Kuo, S.W. and F.C. Chang, *POSS related polymer nanocomposites.* [J]. Progress in Polymer Science, 2011. **36**(12): p. 1649-1696.
9. Haddad, T.S. and J.D. Lichtenhan, *Hybrid organic-inorganic thermoplastics: Styryl-based polyhedral oligomeric silsesquioxane polymers.* [J]. Macromolecules, 1996. **29**(22): p. 7302-7304.
10. Pyun, J. and K. Matyjaszewski, *The synthesis of hybrid polymers using atom transfer radical polymerization: Homopolymers and block copolymers from polyhedral oligomeric silsesquioxane monomers.* [J]. Macromolecules, 2000. **33**(1): p. 217-220.
11. Pyun, J., et al., *ABA triblock copolymers containing polyhedral oligomeric silsesquioxane pendant groups: synthesis and unique properties.* [J]. Polymer, 2003. **44**(9): p. 2739-2750.

12. Hussain, H., et al., *Micelle Formation and Gelation of (PEG P(MA-POSS)) Amphiphilic Block Copolymers via Associative Hydrophobic Effects.* [J]. Langmuir, 2010. **26**(14): p. 11763-11773.
13. Xu, W.T., C.H. Chung, and Y.W. Kwon, *Synthesis of novel block copolymers containing polyhedral oligomeric silsesquioxane (POSS) pendent groups via ring-opening metathesis polymerization (ROMP).* [J]. Polymer, 2007. **48**(21): p. 6286-6293.
14. Hirai, T., et al., *Hierarchical nanostructures of organosilicate nanosheets within self-organized block copolymer films.* [J]. Macromolecules, 2008. **41**(13): p. 4558-4560.
15. Hirai, T., et al., *Hierarchical Self-Assembled Structures from POSS-Containing Block Copolymers Synthesized by Living Anionic Polymerization.* [J]. Macromolecules, 2009. **42**(22): p. 8835-8843.
16. Hirai, T., et al., *One-Step Direct-Patterning Template Utilizing Self-Assembly of POSS-Containing Block Copolymers.* [J]. Advanced Materials, 2009. **21**(43): p. 4334-+.
17. Hayakawa, T., et al., *Fabrication of hierarchically ordered hybrid structures over multiple length scales via direct etching of self-organized polyhedral oligomeric silsesquioxane (POSS) functionalized block copolymer films.* [J]. Polymer Journal, 2006. **38**(6): p. 567-576.
18. Ishida, Y., et al., *Directed Self-Assembly of Cage Silsesquioxane Containing Block Copolymers via Graphoepitaxy Techniques.* [J]. Journal of Photopolymer Science and Technology, 2010. **23**(2): p. 155-159.
19. Jin, S., et al., *Synchrotron Grazing Incidence X-ray Scattering Study of the Morphological Structures in Thin Films of a Polymethacrylate Diblock Copolymer Bearing POSS Moieties.* [J]. Journal of Physical Chemistry B, 2010. **114**(24): p. 8033-8042.
20. Moad, G., E. Rizzardo, and S.H. Thang, *Radical addition-fragmentation chemistry in polymer synthesis.* [J]. Polymer, 2008. **49**(5): p. 1079-1131.
21. Chiefari, J., et al., *Living free-radical polymerization by reversible addition-fragmentation chain transfer: The RAFT process.* [J]. Macromolecules, 1998. **31**(16): p. 5559-5562.
22. Mya, K.Y., et al., *Time-Dependent Polymerization Kinetic Study and the Properties of Hybrid Polymers with Functional Silsesquioxanes.* [J]. Journal of Physical Chemistry B, 2010. **114**(28): p. 9119-9127.
23. Bizet, S.,Nanomatériaux hybrides organique/inorganique par copolymérisation de polysilsesquioxanes polyédriques (POSS^{TM}) avec de monomère méthacrylate. [D]. Institue Nationale de Science Appliquee, Lyon, 2006.
24. Chong, Y.K., et al., *A more versatile route to block copolymers and other polymers of complex architecture by living radical polymerization: The RAFT process.* [J]. Macromolecules, 1999. **32**(6): p. 2071-2074.
25. Guillaneuf, Y. and P. Castignolles, *Using apparent molecular weight from SEC in controlled/living polymerization and kinetics of polymerization.* [J]. Journal of Polymer Science Part A-Polymer Chemistry, 2008. **46**(3): p. 897-911.
26. Han, X.Q., et al., *Direct observation of the RAFT polymerization process by chromatography.* [J]. Macromolecules, 2007. **40**(15): p. 5618-5624.
27. Legge, T.M., A.T. Slark, and S. Perrier, *Novel difunctional reversible addition fragmentation chain transfer (RAFT) agent for the synthesis of telechelic and ABA*

triblock methacrylate and acrylate copolymers. [J]. Macromolecules, 2007. **40**(7): p. 2318-2326.

28. Chong, Y.K., et al., *Thiocarbonylthio compounds [S=C(Ph)S-R] in free radical polymerization with reversible addition-fragmentation chain transfer (RAFT polymerization). Role of the free-radical leaving group (R).* [J]. Macromolecules, 2003. **36**(7): p. 2256-2272.
29. Nguyen, M.N., C. Bressy, and A. Margaillan, *Synthesis of novel random and block copolymers of tert-butyldimethylsilyl methacrylate and methyl methacrylate by RAFT polymerization.* [J]. Polymer, 2009. **50**(14): p. 3086-3094.
30. Stoffelbach, F., et al., *Surfactant-Free, Controlled/Living Radical Emulsion Polymerization in Batch Conditions Using a Low Molar Mass, Surface-Active Reversible Addition-Fragmentation Chain-Transfer (RAFT) Agent.* [J]. Macromolecules, 2008. **41**(21): p. 7850-7856.
31. Kirci, B., J.F. Lutz, and K. Matyjaszewski, *Synthesis of well-defined alternating copolymers poly(methyl methacrylate-alt-styrene) by RAFT polymerization in the presence of Lewis acid.* [J]. Macromolecules, 2002. **35**(7): p. 2448-2451.
32. Lichtenhan, J.D., Y.A. Otonari, and M.J. Carr, *Linear Hybrid Polymer Building-Blocks - Methacrylate-Functionalized Polyhedral Oligomeric Silsesquioxane Monomers and Polymers.* [J]. Macromolecules, 1995. **28**(24): p. 8435-8437.
33. Bizet, S., J. Galy, and J.F. Gerard, *Molecular dynamics simulation of organic-inorganic copolymers based on methacryl-POSS and methyl methacrylate.* [J]. Polymer, 2006. **47**(24): p. 8219-8227.
34. Wu, J., T.S. Haddad, and P.T. Mather, *Vertex Group Effects in Entangled Polystyrene-Polyhedral Oligosilsesquioxane (POSS) Copolymers.* [J]. Macromolecules, 2009. **42**(4): p. 1142-1152.
35. Bizet, S., J. Galy, and J.F. Gerard, *Structure-property relationships in organic-inorganic nanomaterials based on methacryl-POSS and dimethacrylate networks.* [J]. Macromolecules, 2006. **39**(7): p. 2574-2583.
36. Mather, P.T., et al., *Mechanical relaxation and microstructure of poly(norbornyl-POSS) copolymers.* Macromolecules, 1999. **32**(4): p. 1194-1203.
37. Lichtenhan, J.D., et al., *Silsesquioxane Siloxane Copolymers from Polyhedral Silsesquioxanes.* [J]. Macromolecules, 1993. **26**(8): p. 2141-2142.
38. Xu, H.Y., et al., *Preparations, thermal properties, and T-g increase mechanism of inorganic/organic hybrid polymers based on polyhedral oligomeric silsesquioxanes.* [J]. Macromolecules, 2002. **35**(23): p. 8788-8793.
39. Xu, H.Y., et al., *Glass transition temperatures of poly(hydroxystyrene-co-vinylpyrrolidone-co-isobutylstyry1 polyhedral oligosilsesquioxanes).* [J]. Polymer, 2002. **43**(19): p. 5117-5124.
40. Amici, M., *hybrid inorganic/organic polymers based on methacrylate – polyhedral oligmeric silsesquioxanes (POSS)—— morphology and structure-properties relationships.* [D]. Institue Nationale de Science Appliquee, Lyon, 2006.
41. Zhang, W.H., et al., *Effect of methyl methacrylate/polyhedral oligomeric silsesquioxane random copolymers in compatibilization of polystyrene and poly(methyl methacrylate) blends.* [J]. Macromolecules, 2002. **35**(21): p. 8029-8038.

42. Timothy S. Haddad, et al., *Hybrid Inorganic/Organic Diblock Copolymers. Nanostructure in Polyhedral Oligomeric Silsesquioxane Polynorbornenes;*. [C]. Materials Research Society Symposium Proceeding, 2001. **628**, CC2.6.1-CC2.6.7.
43. Mantz, R.A., et al., *Thermolysis of polyhedral oligomeric silsesquioxane (POSS) macromers and POSS-siloxane copolymers.* [J]. Chemistry of Materials, 1996. **8**(6): p. 1250-1259.
44. Chigwada, G., et al., *Fire retardancy of vinyl ester nanocomposites: Synergy with phosphorus-based fire retardants.* [J]. Polymer Degradation and Stability, 2005. **89**(1): p. 85-100.
45. Zhang, Z.P., et al., *Thermo-oxygen degradation mechanisms of POSS/epoxy nanocomposites.* [J]. Polymer Degradation and Stability, 2007. **92**(11): p. 1986-1993.

Chapter3 In-Situ Self-assembly of POSS Based BCPs via RAFT Dispersion Polymerization

3.1 Introduction

O/I hybrid nano-materials have attracted a great deal of attention in the last decades due to their remarkable performances from the synergistic combination of organic polymers and inorganic materials properties[1-3]. A traditional approach to hybrid self-assemblies was based on self assembly of BCPs containing alkoxysilanes followed by cross-link via conventional sol-gel process involving hydrolysis and condensation reactions[4-6]. Recently, another promising route to O/I hybrid materials involves tailor-made inorganic clusters such as POSS, 1-3 nm $(SiO_{1.5})_n$ structures that can be considered as the tiniest silica nano-objects[7-9]. Reactive or non-reactive organic substituent could be easily attached to the Si/O cage vertices to facilitate the incorporation of POSS units into polymer matrices and impart novel properties to common classes of macromolecular materials. So far, efforts to achieve well defined structured POSS based polymers including end tethering polymers[10-23], star polymers[24, 25], brushes[26] and BCPs[25, 27-32] as well as their self-assemblies in solution[11, 15, 33-37] have been made.

The self-assembly of amphiphilic BCPs in selective solvents provides a defined route to a variety of supramolecular assemblies, including spherical micelles, worm-like micelles, vesicles, multi-compartment micelles, toroids, and helices[38-46]. Various factors such as BCP structure, selectivity of solvent and the way of sample preparation etc. are crucial to the discovery of such self-assembled nanostructures. Among these structures, vesicle was of special interest due to its extensive potential applications in catalysis, biology, medical, nano-reactors, and food industries[47-50].

We have investigated the self-assembly behavior of POSS based BCP in selective solvent, for instance in acetone and cyclohexane respectively. TEM images of micelles of $PMACyPOSS_{18.6}$-*b*-$P(MMA_{175}$-*co*-$St_{33})$ formed in those selective solvent and the DLS results inserts were shown in Fig3.1. Narrow dispersed regular spherical micelles were formed in

cyclohexane, with Rh=13.5nm and relative deviation=0.095 by DLS; whereas coexistence of spherical and rod-like micelles were observed in acetone, with Rh=18.3nm and relative deviation=0.203 by DLS. By comparing the results from TEM and DLS, it was easily found that the size of micelles in cyclohexane obtained from TEM and DLS showed good agreement whereas that in acetone showed great deviation. Considered that the DLS result related to dynamic volume, while TEM result correspond to electron density, we supposed that different core-shell structure were formed in these two solvent. The tremendous difference in DLS indicated that the effect of solvent change on hydrodynamic volume of coil chain was different from that of rod chain.

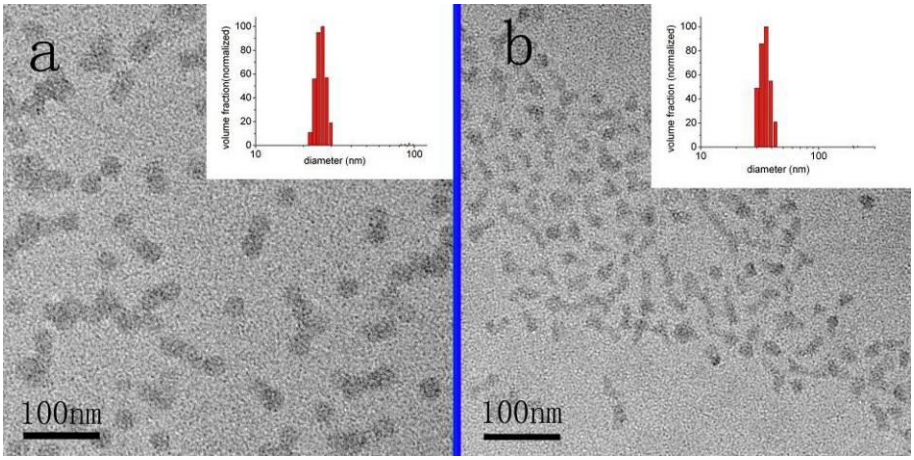

Fig 3.1 TEM of micelles (3mg/ml) of PMACyPOSS$_{18.6}$-*b*-P(MMA$_{175}$-*co*-St$_{33}$) formed in: (a) cyclohexane and (b) acetone; the inserts were the DLS results

Considering that the rod PMACyPOSS chain might bring difference in assembly behavior from normal coil chain BCP, herein, efforts have been made to synthesize POSS based self-assemblies. However, the route that preparing self-assemblies of BCPs in selective solvent was limited by the difficulties of mass production due to the low concentration of nanomaterials formed and its time consuming. A more convenient strategy was desired to solve this problem. CRP of vinyl monomers in a selective solvent of the macro CTA were investigated, but only spherical micelles were formed[51-57]. Recently, micelles with various morphologies were successfully synthesized via one pot method, which named polymerization induced self-assembly and re-organization (PISR)[58-63].

Firstly, we attempted to mediate MMA polymerization with $PMACyPOSS_{11}$ macro CTA in cyclohexane. As shown in Fig3.2, regular and uniform spheres and vesicles could be obtained by simply adjust the initial dosage. No uniform nano-fiber but only nano-rod was observed. SEC results showed that small amount of macro CTA resided even the PMMA chain reached 1600 DP_n, indicating that a low efficiency system can not achieve good morphology controllability of self-assemblies.

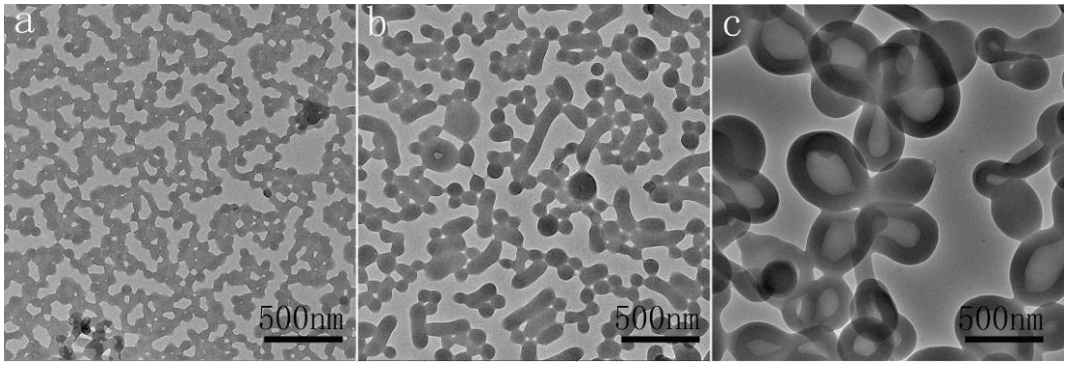

Fig 3.2 TEM images of morphologies from different feed ratio of [MMA]/[CTA]: (a) 940, (b) 1410, (c) 1880; MMA/cyclohexane=1:2 (*v/v*), [CTA]/[AIBN]=10:1, 65^{o}C 20h, conversion=90%

Herein, we presented a simple route to hybrid self-assemblies via thermal initiated RAFT polymerization of styrene mediated by POSS homo-polymer macro CTA in octane which was a selective solvent for PMAiBuPOSS. As the mixture is a moderate solvent at the polymerization temperature, for instance 120^{o}C for PS block, systems kept homogeneous (or opalescent) when appropriate conversion reached during the polymerization period, and self-assembled hybrid nanomaterials were obtained via cooling induced micelle formation and transition under stirring. The pathway of the formation of different morphologies was investigated as well by trapping the intermediate. The pathways selection of spontaneous vesicle formation was discussed during cooling induced micelle transition synthesized from macro CTA with different chain lengths.

3.2 Experimental

3.2.1 Materials

AIBN (Aldrich, 99%) was used as received. CDB was synthesized according to the procedure described in literature[64] and re-crystallized from hexane after two columns, ^{1}H NMR (7.86ppm, d, 2H; 7.56ppm, d, 2H; 7.46 ppm, t, 1H; 7.36ppm, t, 4H; 7.21ppm, t, 1H; 2.03ppm, s, 6H). MAiBuPOSS and MACyPOSS were purchased from Hybrid Plastics and used as received. St was purified by passing base alumina column to remove the inhibitor before use. Toluene was purchased from sinoreagent and was washed by concentrate sulfate acid and water consequently, then distilled in the present of calcium hydride before use. Octane (CP grade) was obtained from sinoreagent and used as received.

3.2.2 Synthesis

Synthesis of PMAiBuPOSS macro CTA

In a typical experiment, MAiBuPOSS (3.774g, 4mmol), CDB (109mg, 0.4mmol) and AIBN (3.3mg, 0.02mmol) were dissolved in toluene (2.2mL) in schlenk tube, and then the solution was degassed with five consecutive freezing-pump-thawing cycles and then filled with argon. The tube was sealed and then placed in oil bath thermo-stated at 65^{o}C for 48h, Conversion=80%. PMAiBuPOSS was obtained by repeated precipitated from methanol: ethyl acetate=8:1, M_n=6200, *PDI*=1.05 by SEC and DP_n=13 by ^{1}H NMR, named PMAiBuPOSS$_{13}$. Another PMAiBuPOSS macro CTA with higher DP_n were synthesized in the condition of [MAiBuPOSS]/[CDB]/[AIBN] =[25]/[1]/[0.05] at conversion=73%, achieving homo-polymer with M_n=8400, *PDI*=1.05 by SEC and DP_n=19 by ^{1}H NMR, named PMAiBuPOSS$_{19}$.

RAFT dispersion polymerization of St mediated with PMAiBuPOSS macro CTA

A typical procedure was described as follows. PMAiBuPOSS (62mg, 0.005 mmol) was dissolved in St (1mL, 8.5mmol), and octane (2mL). The solution was added to a 15 mL schlenk tube with a magnetic bar, and then the system was degassed by four freeze-pump-thaw cycles and filled with argon. The tube was sealed and placed in oil bath thermo-stated at 120^{o}C under stirring. After polymerization was carried out for preset time,

the reaction mixture was slowly cooled to room temperature (~1^{o}C/min) under fast stirring. Then the polymer mixture was taken out for conversion and *MW* analysis. The as-formed nanostructure was frozen by octane, and the nanomaterials were purified via repeat centrifugation and re-dispersion in octane to remove un-reacted styrene. The recipe of experiment was shown in Table3-1.

3.2.3 Characterization methods

^{1}H Nuclear Magnetic Resonance spectroscopy (NMR): ^{1}H NMR measurements were carried out on a Bruker AV400MHz NMR spectrometer. The samples were dissolved with *d*-chloroform and the solutions were measured with tetramethylsilane (TMS) as the internal reference.

Size Exclusion Chromatography (SEC): SEC was performed in tetrahydrofuran using a series of Waters styragel HR2, HR4 and HR5 under the flow rate of 1mL/min. Calculations of apparent molar mass were determined using Waters Breeze software from a calibration based on linear polystyrene standards (from PSS). RI detector was used to calculate the *MW*.

Transmission Electron Microscopy (TEM): TEM was performed on a JEM2100 high-resolution Transmission Electron Microscope at the accelerating voltage of 200kV. Samples were prepared by diluting several drops of mixture in 3mL octane, and then picked by copper 400 mesh grids.

Scanning Electron Microscopy (SEM): SEM of fracture surface was performed on LEO-1530 Field Emission Scanning Electron Microscope at an activation voltage of 20 kV. Samples were prepared by casting diluted solution on glass slide.

Dynamic Laser Scattering (DLS): DLS analysis was performed on Plus90 particle size analyzer (Brookhaven) at 25^{o}C. Samples were prepared by diluting solution with octane into translucent.

Table3-1 Experimental details in preparation of self-assemblies

Exp.	CTA	$[M]_0/[CTA]$	St/octane (*v/v*)	*Time* (h)	*Conv.* (%)	M_n [a] (10^3)	*PDI*[a]	Morphology[b]
E1	$PMAiBuPOSS_{13}$	1700	1/2	6	17	29	1.23	S
				10	21	32	1.29	S+C
				15	24	33	1.39	C
				25	32	44	1.36	V
				40	46	48	1.49	V
E2	$PMAiBuPOSS_{13}$	2550	1/2	15	24	44	1.45	C+V to V
E3	$PMAiBuPOSS_{13}$	3400	1/2	15	25	51	1.44	LCV
E4	$PMAiBuPOSS_{19}$	2550	1/2	15	25	63	1.59	S
E5	$PMAiBuPOSS_{19}$	2550	1/1.5	16	35	53	1.65	S+H
				24	38	56	1.91	S+V
				40	51	69	1.60	V +S
E6	$PMAiBuPOSS_{19}$	3800	1/1.5	15	29	68	1.60	S+H+V
				25	35	74	1.65	V

(a) by SEC vs PS standards; (b) S, C, V, H and LCV represent spheres, cylinders, vesicles, hollow particles and large compound vesicles respectively

3.3 Result and discussion

3.3.1 Preparation of PMAiBuPOSS macro CTA

As molecular silica, POSS was one of the most studied hybrid nano-building blocks. In a previous work[65], we have presented the RAFT polymerization of POSS monomers mediated by CDB. The structure was analyzed by ^{1}H NMR as shown in Fig3.3. DP_n was calculated by the integration ratio of protons in ester methylene group (3.85ppm, 2H, m) and ortho-aromatic protons in the functional end group (7.85ppm, 2H, d).

The $DP_{n,\ NMR}$ of PMAiBuPOSS is 13 (corresponding to M_n=12300), which was much higher than that from SEC ($M_{n,SEC}$=6200, PDI=1.05) due to the hydrodynamic difference between PS standards and PMAiBuPOSS. This point of view has been confirmed by result from SEC and light scattering as well-presented in the previous work[32, 65]. The $DP_{n,\ NMR}$ was much higher than the theoretical value as well due to the relatively low CTE of CDB in mediating polymerization of methacrylates, especially in condition of low [monomer]/ [CTA][66]. Another probable reason was, the purification some kind liked fractionation, especially for low *MW* homo-polymer. For PMAiBuPOSS$_{19}$, the discrepancy between $DP_{n,NMR}$ and theoretical value (calculated from conversion) (19 and 18) was much smaller, indicating higher CTE (~95%). The functionality for both PMAiBuPOSS macro CTAs was confirmed to be nearly 100% by followed chain extension of styrene from the lack of residual of PMAiBuPOSS homopolymer.

3.3.2 Preparation of hybrid self-assemblies

In the preparation of nanomaterials from self-assembly of amphiphilic BCPs, the control of polymer structures at the molecular level, the nature of solvent and the way for preparation are crucial in morphology control. Octane (δ= 15.5 MPa$^{0.5}$) was used as solvent which is good solvent for PMAiBuPOSS ($\delta_{Octa\ \ iBu\text{-}POSS}$=17.45 MPa$^{0.5}$)[67,68], but a non-solvent for PS (δ=17.8-18.7) at room temperature. Moreover, its boiling point is 125.7^{o}C, which is high enough for thermal polymerization of St under normal pressures. Firstly, PMAiBuPOSS$_{13}$ was used as macro CTA, and the initial molar feed ratio was St/CTA=1700, St/octane=1:2(*v/v*).

The system kept transparent during the polymerization for 15h. The mixture was cooled in liquid nitrogen and allowed the oxygen in to quench the polymerization and then rapidly heated to 120°C. By slowly cooling the solution to temperature under rapid stirring, the mixture became translucent. The appearance change strongly suggested the formation of self-assemblies.

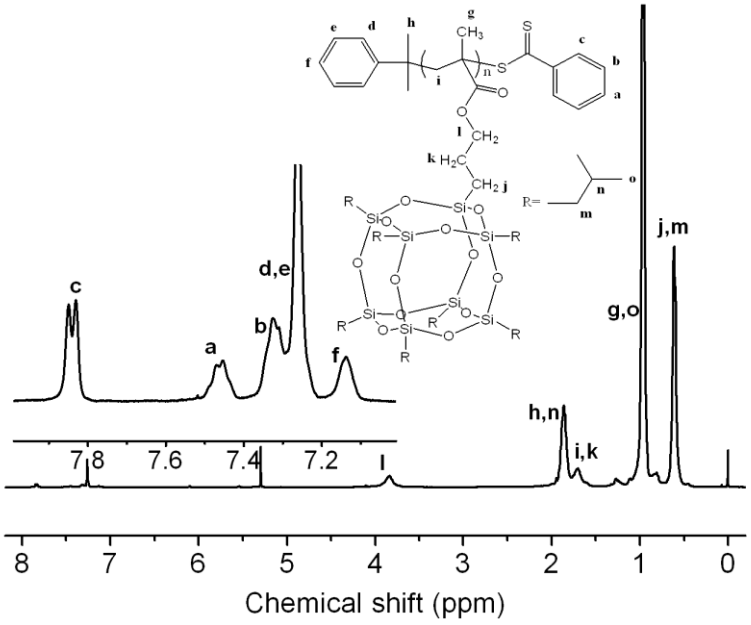

Fig 3.3 Chemical structure and ^{1}H NMR spectrum with peak assignment of PMAiBuPOSS macro CTA

Recently, it has been reported that the micelle formation and transition occurred with the increase of chain length of insoluble block during the polymerization in selective solvent[52]. As the micelle formed at quite beginning, the polymerization was compressed dramatically. In this work, the polymerization kinetics during the whole period was investigated. The solution kept transparent before 25h and became slightly cloudy at 40h due to the moderate solubility of solvent mixture at high temperature. As shown in Fig3.4, the polymerization rate kept a high value during the whole polymerization period. The good polymerization rate might be attributed to both high initiation rate and better homogeneity of the system as the final nano-materials were obtained by cooling procedure rather than in-situ formation.

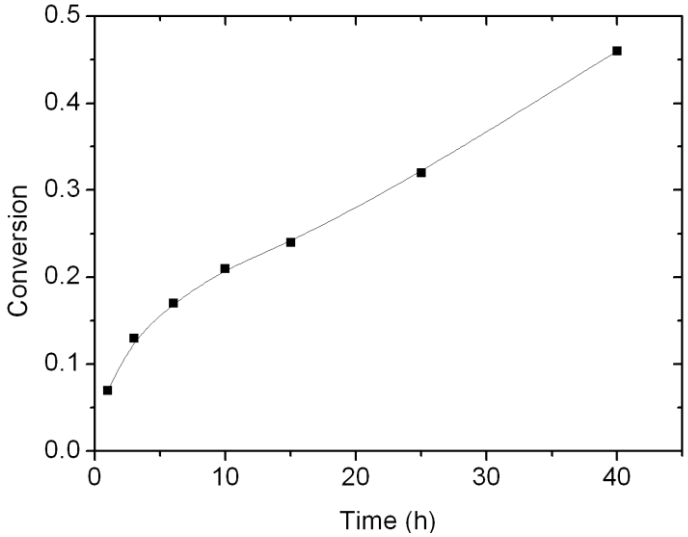

Fig 3.4 Polymerization kinetic of E1, St/octane (v/v) =1/2, [St]/[PMAiBuPOSS$_{13}$]=1700, 120^{o}C

Fig3.5 showed the *MW* and *PDI* evolution during polymerization. It was obvious that M_n and *PDI* increased with the increase of conversion along with increasingly deviates from the theoretical values. Because of the relatively high initiation rate of thermal polymerization at 120^{o}C, free radicals generated rapidly, causing a shoulder of high *MW* which was attributed to the combination termination and a big tail of low *MW* by newly generated radical addition and chain exchange (see Fig3.6).

After cooling to room temperature, clear evolution of appearance with the increase of polymerization time was observed. The appearance of product changed from transparent, opalescent, translucent, then to milk-like emulsion with the increase of conversion (Fig3.7). To confirm the morphologies corresponded to different appearance, DLS, TEM and SEM analysis were performed. As shown in Fig3.8, DLS results showed that spherical micelles with Rh=19.2nm were formed at 3h, then the Rh for nano-aggregates increased with the increase of conversion. As shown in Fig3.9, TEM images showed the morphology transition from spheres (Fig3.9a) to branched rods (Fig3.9b), fibers (Fig3.9c), vesicles (Fig3.9d) and deformed vesicles (Fig3.9e). The SEM results corresponding Fig3.9 were shown in Fig3.10.

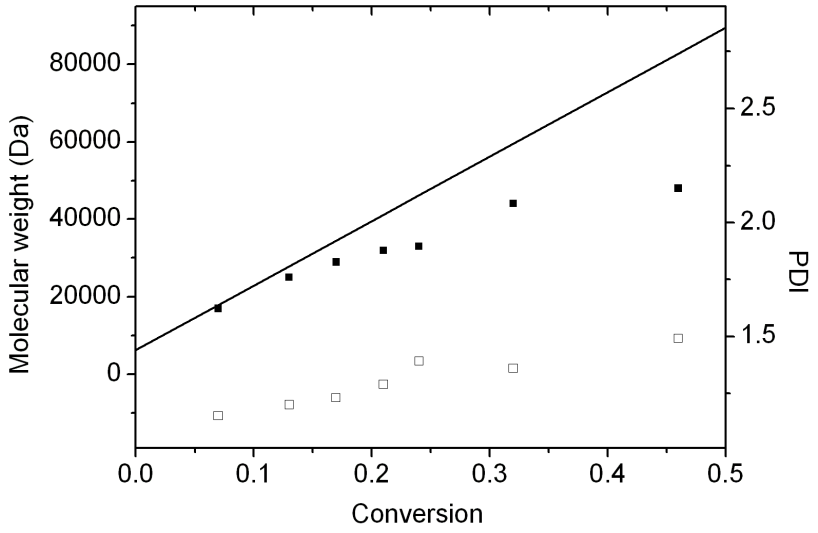

Fig 3.5 Conversion evolution of *MW* and *PDI* in E1: St/octane (*v/v*) =1/2, [St]/[PMAiBuPOSS$_{13}$]=1700, 120^{o}C

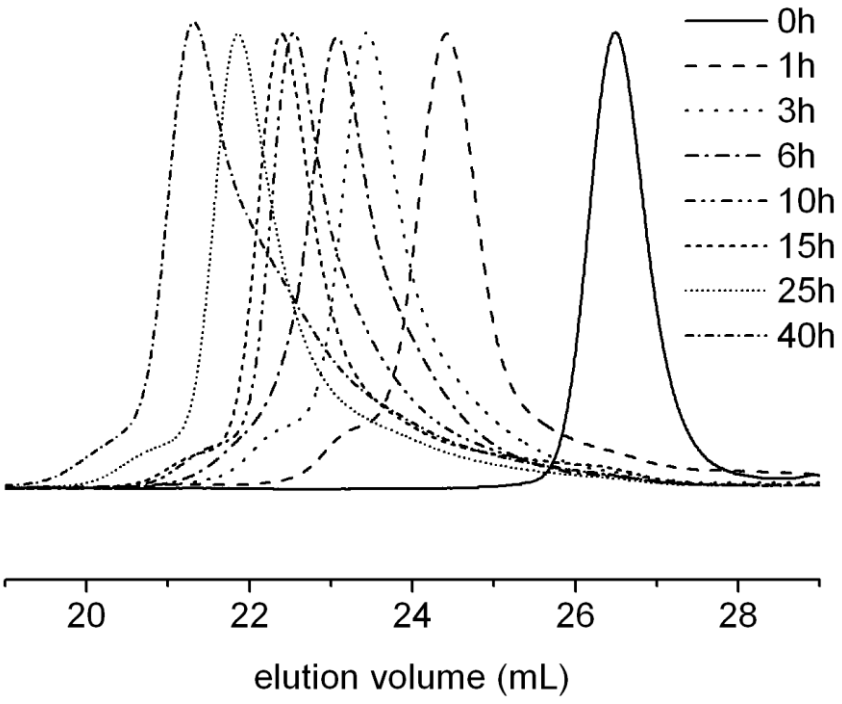

Fig 3.6 SEC curves of fraction during polymerization of E1. St/octane (*v/v*) =1/2, [St]/[PMAiBuPOSS$_{13}$]=1700, 120^{o}C

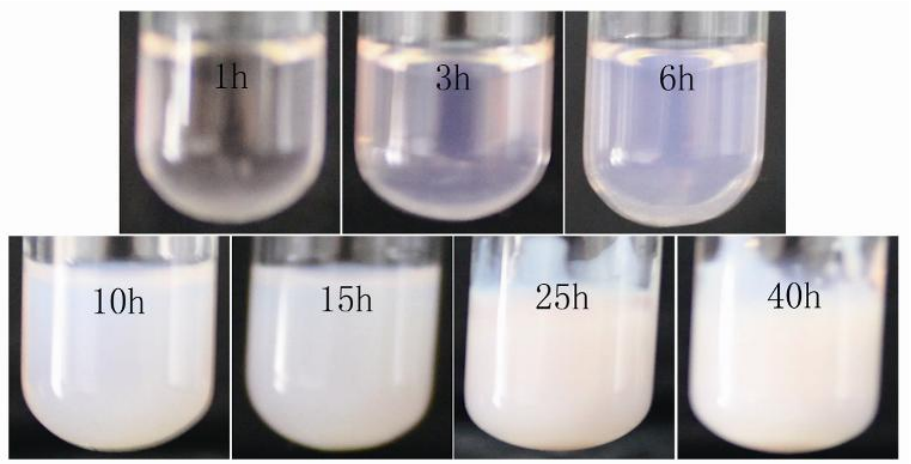

Fig 3.7 Time evolution of optical appearance of E1 after cooling to room temperature. St/octane (*v/v*) =1/2, [St]/[PMAiBuPOSS$_{13}$]=1700, 120^{o}C

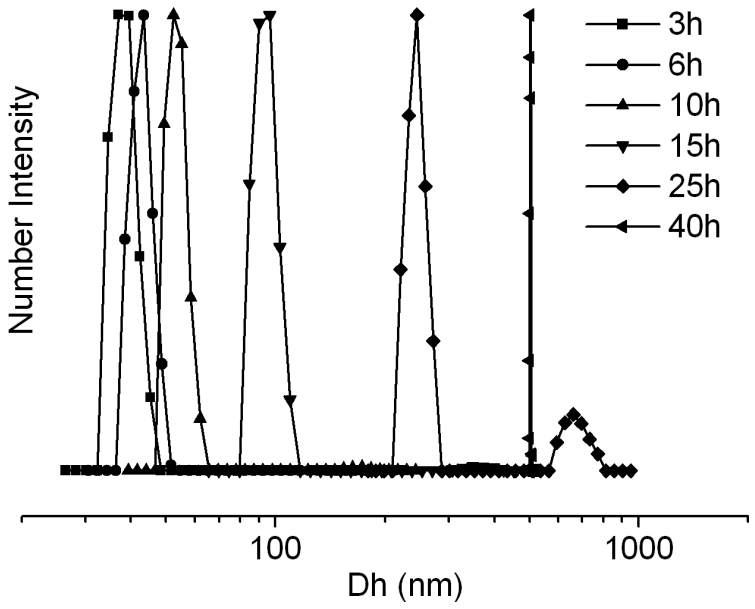

Fig 3.8 DLS curves of micelles from different polymerization time of E1: St/octane (v/v) =1/2, [St]/[PMAiBuPOSS$_{13}$]=1700, 120^{o}C

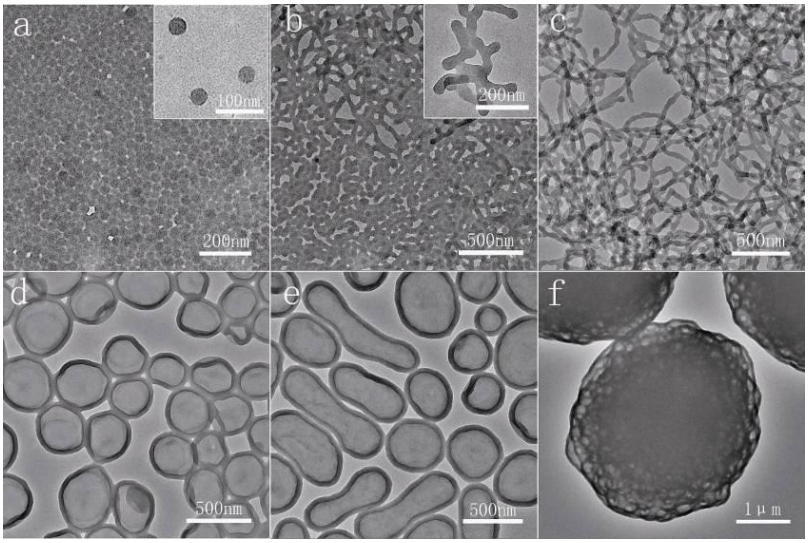

Fig 3.9 TEM images of morphologies of E1: St/octane (*v/v*) =1/2, [St]/[PMAiBuPOSS$_{13}$]=1700, 120^{o}C, (a) 6h, (b) 10h, (c) 15h, (d) 25h, (e) 40h and (f) E3: St/octane (v/v) =1/2, [St]/[PMAiBuPOSS$_{13}$]=3400, 120^{o}C, 15h

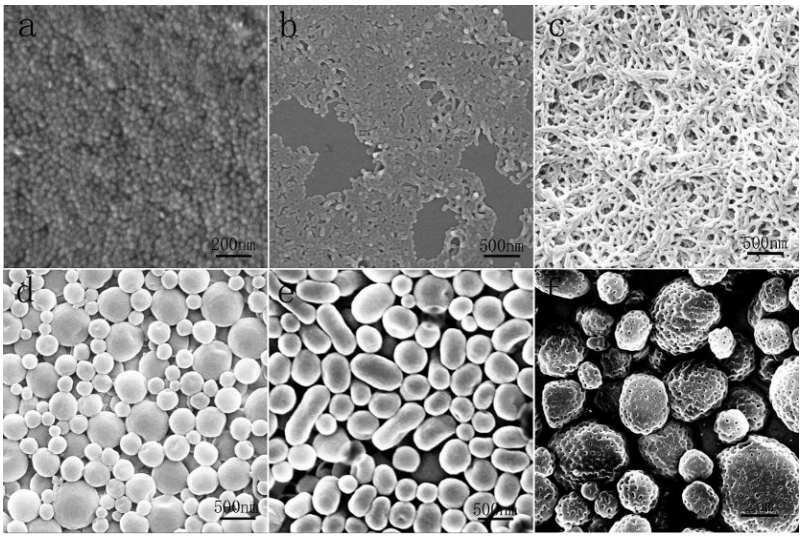

Fig 3.10 SEM images of morphologies of E1: St/octane (*v/v*) =1/2, [St]/[PMAiBuPOSS$_{13}$]=1700, 120^{o}C, (a) 6h, (b) 10h, (c) 15h, (d) 25h, (e) 40h and (f) E3: St/octane (*v/v*) =1/2, [St]/[PMAiBuPOSS$_{13}$]=3400, 120^{o}C, 15h

To further investigate the effect of PS block chain length on the morphology, initial molar feed ratio St/CTA=2550 and 3400 with the same solvent composition were used respectively. During cooling procedure, the appearance switched from opalescent to milk-like dispersion. Both TEM and SEM results showed well formed but collapsed vesicles (Fig3.14a and d). By

increasing the feed ratio to 3400, the mixture became slightly cloudy at 120°C after 15h, large compound vesicles (Fig3.9f and Fig3.10f) were formed and the dispersion tended to precipitation at room temperature. The porous microspheres were confirmed to be perforated vesicles composed of a highly folded bilayer membrane continuous in 3 dimensions, but the holes on vesicle surface which are interconnected inside, and there are isolated spaces inside as well[69]. The successively evolution of microstructure of micelles via increasing the chain length of insoluble block was attributed to the increase of *critical packing parameter* [v/ ($a_0 l_c$)] as described in other surfactant system[70].

Efforts to synthesize nanomaterials using higher *MW* macro CTA, for instance, $PMAiBuPOSS_{19}$, have been made as well. When kept the monomer to octane ratio =1/2 (*v/v*) and [M]/[CTA] =2550 (E4), Only spherical micelles were observed under similar conversion after cooling procedure, which was in accordance with that in PS-*b*-PAA/ dioxane/water system reported previously. System became out of control when high conversion reached in order to obtained vesicles, causing styrene polymerized outside of micelles which brought about the precipitation. After cooling to room temperature, large aggregates of spheres and hollow particles were obtained (data not shown), which was agreed with that in AIBN initiated system when high amount of initiator was used[71].

Thus, to make sure the system was better controlled under the preset conversion, the monomer to octane ratio was tuned from 1/2 to 1/1.5 (*v/v*). However, cylindrical micelles can't be observed any more during polymerization or cooling procedure. The polymerization time evolution of morphologies was shown in Fig3.11. Core-shell spheres were formed soon when cooled to room temperature at relatively low conversion after 6h (data not shown). As the conversion increased with polymerization time, spheres grew to larger irregular particles through aggregation and holes were observed in them (Fig3.11a). The hollow particles (or semi-vesicles) grew to vesicles by adsorbing other spheres or aggregates and chain rearrangement (Fig3.11b). Interestingly, even after 40h, few spheres still existed with vesicles and the mean size of vesicles was even smaller than that of 24h (Fig3.11c). The decrease of size might caused by fusion and diffusion process between vesicles, which also can elucidate the narrower size distribution. By increasing the St/CTA feed ratio to 3800, even spheres and vesicles coexisted at 29% conversion after 15h (Fig3.11d), well formed vesicles were

obtained at 35% conversion after 25h (Fig3.11e). The vesicles obtained from macro CTA with higher DP_n were obviously much tougher than that from lower one and no collapsed vesicle was observed. All the SEM images corresponding to Fig3.11 as shown in Fig3.12 further confirmed the morphologies.

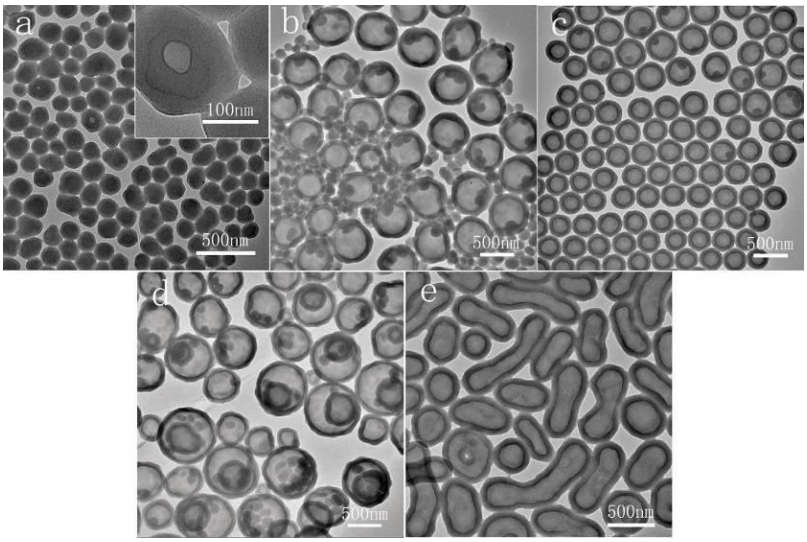

Fig3.11 TEM images of morphologies of E5: St/octane (*v/v*) =1/1.5, [St]/[PMAiBuPOSS$_{19}$]=2550, 120^{o}C, (a)15h, (b)24h, (c)40h and E6: St/octane (*v/v*) =1/1.5, [St]/[PMAiBuPOSS$_{19}$]=3800, 120^{o}C, (d)15h, (e)25h

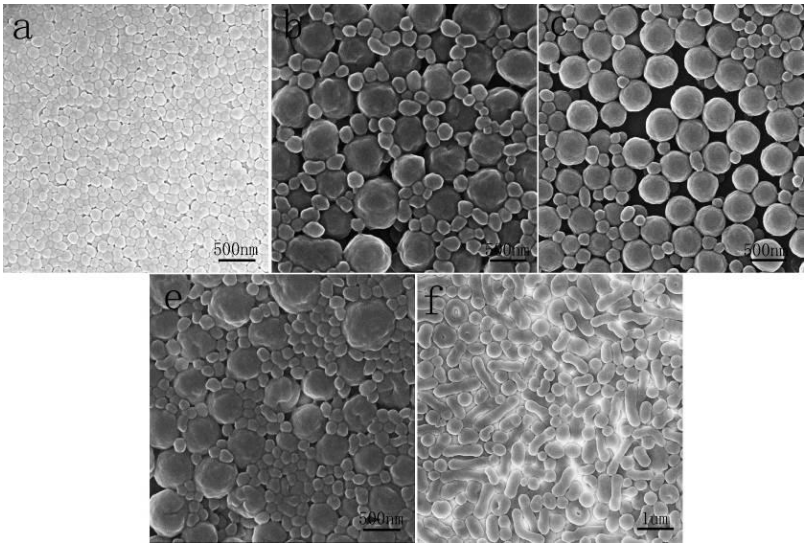

Fig3.12 SEM images of morphologies of E5: St/octane (*v/v*) =1/1.5, [St]/[PMAiBuPOSS$_{19}$]=2550, 120^{o}C, (a)15h, (b)24h, (c)40h and E6: St/octane (*v/v*) =1/1.5, [St]/[PMAiBuPOSS$_{19}$]=3800, 120^{o}C, (d)15h, (e)25h

3.3.3 Reversible cooling induced morphology transition

We were quite curious about the obvious change of appearance during cooling process for all polymerization mixture. As an example, while cooling the mixture of E2, the appearance transited from slightly blue light (opalescent) to translucent at about 90^{o}C then to milk-like at room temperature. Moreover, this change was thermal reversible. The optical photographs of appearance at different temperatures were shown in Fig3.13. The opalescent appearance at 120^{o}C stated spherical micelles dispersion. As temperature decreases, gradually transition to milk-like appearance indicated the generation of larger scale aggregates, from spherical micelles, through cylindrical micelles and finally to vesicle. However, precipitation (or phase separation) occurred rapidly at 70~80^{o}C without stirring, making the transition difficult to be tracked on line. Judging from different appearance of the mixture with different feed ratio, the critical chain length of PS block in the mixture solvent at 120^{o}C was estimated to be about 400 DP_n, which was much higher than that at room temperature. From this point of view, the micelle formation and transition were thermal dynamically driven by the difference of critical chain length at different temperatures.

Fig3.13 Optical appearance of E2: St/octane (*v/v*) =1/2, [St]/[PMAiBuPOSS$_{13}$]=2550，120^{o}C , 15h at different temperature during cooling

The nature of solvent was one of the most crucial factors in morphology control which was usually continuously tuned by the addition of selective solvent. In some circumstance, variation of temperature was used to tune the interaction parameter between polymer and solvent effectively and continuously thus to change the morphologies of BCPs. Ylitalo et al firstly observed the effect of temperature on micelle formation in the PEP-PS/(octane + styrene) system and attributed it to the decrease of interaction parameter of solvent and PS

block, i.e. an increase in the solvent quality with increasing temperature[72]. Thermal induced morphology transition was firstly observed in PS-*b*-PAA dissolved in single low alkanols (methanol to n-butanol) solvent under elevated pressures[73]. Recently, temperature effect on morphologies was extensively studied in BCPs containing thermal sensitive block[74-77].

As the vesicles were spontaneously formed from spherical micelles during cooling, the effect of cooling procedure on the morphology was then investigated. It was found that the cooling procedure strongly affected the morphology of E2. When the mixture was slowly cooling (natural cooling in oil bath, ~1^{o}C/min) from 120^{o}C to room temperature, well formed but irregular and collapsed vesicles were observed (Fig3.14a and c), whereas coexist of cylindrical micelles and vesicles were obtained by rapid cooling in ice bath or acetone/liquid nitrogen bath. However, no frozen spherical micelle was observed no matter how rapid the cooling was due to the faster sphere-cylinder transition in contrast to cylinder-vesicle transition.

To further investigate the effect of kinetic factors on morphology transition, rapid step cooling including an additional annealing time at different temperatures was then applied. Mixture at 120^{o}C was firstly cooled in water thermo-stated at 80^{o}C, 70^{o}C and 60^{o}C respectively and held for 20 minutes, and then rapidly cooled in ice bath under fast stirring. However, in all cases, coexist of vesicles and cylindrical micelles were observed. Interestingly, mainly cylindrical micelles with only very few vesicles were observed for the last treatment (Fig3.14c and f).

As the preparation of single well formed morphology was failed in rapid step cooling, we improved the procedure by slowly cool the mixture after hold at 70^{o}C for 20 minutes. Finally, regular and uniform vesicles with relatively narrower size distribution were obtained (Fig3.14b and e). The cooling procedure dependence of morphology could be well understood by kinetic concern. As the cylinder-vesicle transition was slowly enough (in the time scale of tens minutes depending on a lot of factors such as *MW* and concentration of BCP as well as solvent characteristic), the intermediate could be obtained by freezing route[78]. Long equilibrium time and proper chain motion were required in the formation of uniform vesicles. In the case of rapid step cooling at 60^{o}C，cylindrical micelles were well formed during cooling and annealing, and the PS core was almost frozen to verification state. In this case, fusion of

PS core was hardly occurred and the formation of vesicle was suppressed, thus nanofibers were mainly obtained. Compared to slow cooling, the addition annealing time at 70°C provided an equilibrium time to form the intermediate such as octopus and jelly fish-like structure (will be discussed later). Annealing at higher temperature provided no assistance for vesicle formation, while the system was not dynamically favorable for morphology transition.

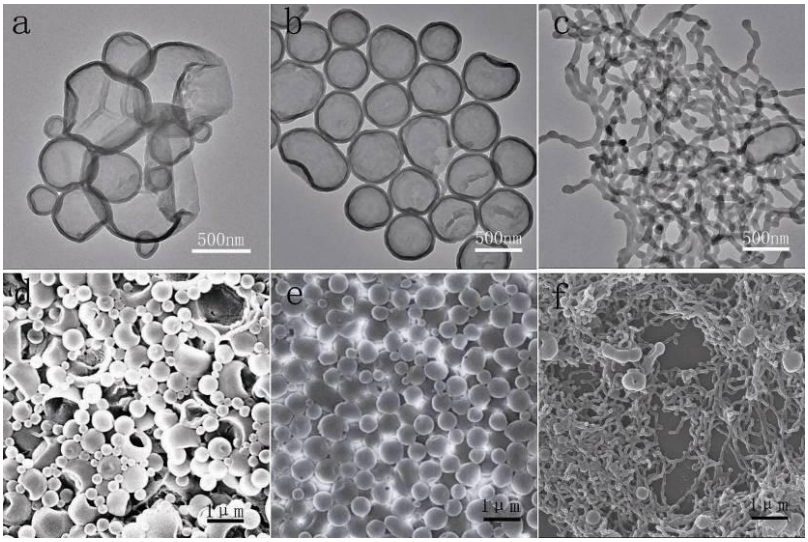

Fig 3.14 TEM (a, b, c) and SEM (d, e, f) images of E2: St/octane (*v/v*) =1/2, [St]/[PMAiBuPOSS$_{13}$]=2550，120°C , 15h from: (a, d) slowly cooled to room temperature; (b, e) rapid cooled to 70°C then held for 20minutes followed by slowly cooled to RT; (c, f) rapid cooled to 60°C then held for 20minutes then followed by rapidly cooled in ice bath

3.3.4 The pathway of spontaneous vesicle formation

It was reported extremely asymmetric amphiphilic BCP can form vesicles in certain condition. Two mechanisms for spontaneous formation of vesicles for BCPs were confirmed both experimentally and theoretically according to previous research[79-82]. Mechanism Ⅰ, the amphiphilic BCPs aggregate into small spherical micelles rapidly and then grew to cylindrical micelles by collision with spheres in one dimension. The cylinder micelles collision and entangled to jelly fish-like micelles and finally closed up to vesicles[83]. Mechanism Ⅱ, the rapidly formed spherical micelles grew up to large spherical micelles by collision and fusion process in three dimensions. The energetically unfavorable large spherical micelles took the

solvents in and transited to hollow spheres. By persistent taking solvent in and collision with other spheres, the hollows spheres increased to vesicles via chain rearrangement.

However, the factors on the choice of pathways to vesicle remain unclear. It was reported that various factors such as the nature of solvent[79], addition rate of selective solvent[80], chain length[81] etc. affected the pathways in spontaneous vesicle formation. As vesicles spontaneously formed in both two pathways in this work, the factor on the applied mechanism in each way was discussed. The transition mechanism was usually experimentally studied by trapping intermediate morphologies during the transition process. Step rapidly cooling at 70^{o}C for E2 15h mentioned above was used to trap the intermediate morphologies. As shown in Fig5, morphologies trapped such as octopus-like (Fig3.15a), jelly fish-like (Fig3.15b) and unclosed vesicles (Fig3.15c) were observed in the same slice as well as well formed cylindrical micelles and vesicles, which further confirmed that the formation of vesicles was consistent with mechanism Ⅰ for E1 and E2. Vesicles formed after cylindrical micelles in the time evolution of morphologies of E1 further confirmed this mechanism. Similar trapping route was applied for E6 15h, but only irregular particles, hollow spheres and vesicles were observed. Thus, we hypothesized that the formation of vesicles was consistent with mechanism Ⅱ for E5 and E6.

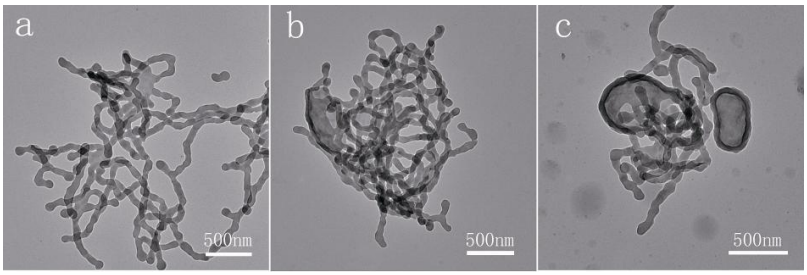

Fig 3.15 TEM images of intermediate of E2: St/octane (*v/v*) =1/2, [St]/[PMAiBuPOSS$_{13}$]=2550，120^{o}C , 15h obtained from rapid cooled to 70^{o}C then held for 20minutes followed by rapidly cooled in ice bath

The difference of adjusted mechanism could be attributed to the balance of kinetic and dynamic factors, for instance, the difference of collision rate of POSS corona and fusion rate of PS core. As the chain length of PS block reached the critical value, spherical micelles

formed rapidly, and then tend to collision driven by thermal motion. If the fusion rate was comparable to the collision, energy favorable state will be soon established. When using macro CTA with low *MW*, relatively shorter chain length of PS is enough for the evolution of morphology dynamically, and easier for fusion by chain motion, one dimension string formed and then transformed to cylindrical micelles (sometimes branched rods), thus there was no obvious kinetic constrain. However, in the case of high *MW* macro CTA, spheres formed rapidly and the fusion process was lagged behind, thus the particles aggregated in three dimensions to form large particles and took solvent in. Since the large particles were not energy favorable as the temperature decreases, it's not stable any more dynamically and phase separation occurred to form hollow spheres. By persistently taking solvent in and collision with other spheres, the hollows spheres grew to vesicles via chain rearrangement. This pathways selection might attribute to the transition from thermal dynamic to kinetic constrain. Poorer solvent was thermal-dynamically required for higher morphology (i.e. Vesicular), but better solvent condition was necessary for well controlled chain extension and morphology transition. This paradox between kinetics and dynamics can't be well mediated in dispersion polymerization as the polymerization rate can't be indefinitely slowed down in preparation of diluted solution of BCP. Thus, we believe that a proper chain length of macro CTA and solvent composition were very important in the synthesis of multiple self-assembly morphologies in dispersion polymerization. Even though the chain length effect on spontaneous vesicles formation in concentrate BCP/solution system was theoretically investigated[81], as far as we know, this is the first time to experimentally confirm this argument. The Illustration of pathway selection to vesicle in this work was shown in Fig3.16.

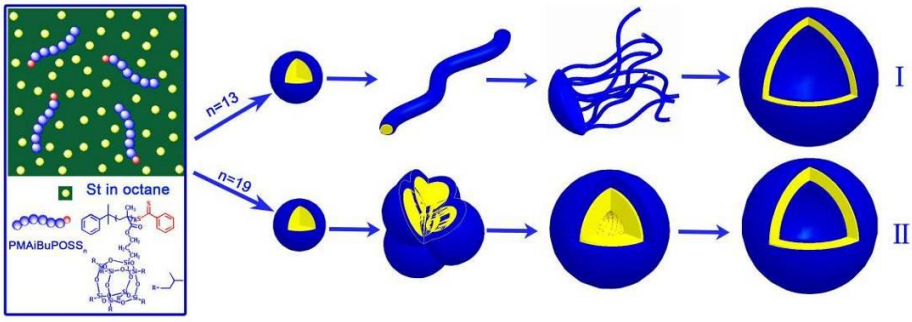

Fig 3.16 Illustration of pathway selection to vesicle in dispersion polymerization

3.4 Conclusion

POSS containing O/I self-assemblies were synthesized via thermal initiated RAFT dispersion polymerization mediated by PMAiBuPOSS macro CTA. Different from PISR procedure reported previously, various morphologies were obtained via reversible cooling induced micellization and/or morphology transition. By tuning the initial feed ratio or conversion, continuous morphology transition could be observed. Moreover, the effect of chain length of macro CTA on the pathways selection of spontaneous vesicle formation was studied. So far as we know, it was the first time observing the effect of chain length of macro CTA on the pathway from mechanism Ⅰ (through cylindrical micelle) to mechanism Ⅱ (through Ostwald ripening). This discovery will be helpful in extensive synthesis of nanomaterials, particularly cylindrical micelles, as well as theoretical studies on BCP self-assembly area.

Reference

1. Paul, D.R. and L.M. Robeson, *Polymer nanotechnology: Nanocomposites.* [J]. Polymer, 2008. **49**(15): p. 3187-3204.
2. Sanchez, C., et al., *Applications of hybrid organic-inorganic nanocomposites.* [J]. Journal of Materials Chemistry, 2005. **15**(35-36): p. 3559-3592.
3. Nicole, L., L. Rozes, and C. Sanchez, *Integrative Approaches to Hybrid Multifunctional Materials: From Multidisciplinary Research to Applied Technologies.* [J]. Advanced Materials, 2010. **22**(29): p. 3208-3214.
4. Du, J.Z. and Y.M. Chen, *Organic-inorganic hybrid nanoparticles with a complex hollow structure.* [J]. Angewandte Chemie-International Edition, 2004. **43**(38): p. 5084-5087.
5. Du, J.Z. and Y.M. Chen, *Preparation of organic/inorganic hybrid hollow particles based on gelation of polymer vesicles.* [J]. Macromolecules, 2004. **37**(15): p. 5710-5716.
6. Du, J.Z., et al., *Organic/inorganic hybrid vesicles based on a reactive block copolymer.* [J]. Journal of the American Chemical Society, 2003. **125**(48): p. 14710-14711.
7. Scott, D.W., *Theremal Rearrangement of Branchedchain Metylpolysiloxanes.* [J]. Journal of the American society, 1946. **68**: p. 356.
8. Cordes, D.B., P.D. Lickiss, and F. Rataboul, *Recent Developments in the Chemistry of Cubic Polyhedral Oligosilsesquioxanes.* [J]. Chemical Reviews, 2010. **110**(4): p. 2081-2173.
9. Baney, R.H., et al., *Silsesquioxanes.* [J]. Chemical Reviews, 1995. **95**(5): p. 1409-1430.
10. Kim, B.S. and P.T. Mather, *Morphology, microstructure, and rheology of amphiphilic telechelics incorporating polyhedral oligosilsesquioxane.* [J]. Macromolecules, 2006. **39**(26): p. 9253-9260.
11. Kim, B.S. and P.T. Mather, *Amphiphilic telechelics with polyhedral oligosilsesquioxane (POSS)*

end-groups: Dilute solution viscometry. [J]. Polymer, 2006. **47**(17): p. 6202-6207.

12. Wei, J., et al., *Self-Assembly Behaviors of Telechelic Poly(styrene-ran-sodium styrenesulfonate) with Polyhedral Oligomeric Silsesquioxane as End Groups.* [J]. Journal of Physical Chemistry B, 2011. **115**(9): p. 1929-1935.
13. Mya, K.Y., et al., *Star-Like Polyurethane Hybrids with Functional Cubic Silsesquioxanes: Preparation, Morphology, and Thermomechanical Properties.* [J]. Journal of Polymer Science Part A-Polymer Chemistry, 2009. **47**(18): p. 4602-4616.
14. Kuo, S.W., et al., *Solid State and Solution Self-Assembly of Helical Polypeptides Tethered to Polyhedral Oligomeric Silsesquioxanes.* [J]. Macromolecules, 2009. **42**(5): p. 1619-1626.
15. Zhang, W.A., et al., *Synthesis via RAFT Polymerization of Tadpole-Shaped Organic/Inorganic Hybrid Poly(acrylic acid) Containing Polyhedral Oligomeric Silsesquioxane (POSS) and Their Self-assembly in Water.* [J]. Macromolecules, 2009. **42**(7): p. 2563-2569.
16. Zhang, W.A., et al., *Synthesis and Self-Assembly of Tadpole-Shaped Organic/Inorganic Hybrid Poly(N-isopropylacrylamide) Containing Polyhedral Oligomeric Silsesquioxane via RAFT Polymerization.* [J]. Journal of Polymer Science Part A-Polymer Chemistry, 2008. **46**(21): p. 7049-7061.
17. Zhang, W.A., et al., *Preparation and characterization of organic/inorganic hybrid polymers containing polyhedral oligomeric silsesquioxane via RAFF polymerization.* [J]. Reactive & Functional Polymers, 2009. **69**(2): p. 124-129.
18. Zeng, K., L. Wang, and S.X. Zheng, *Nanostructures and surface hydrophobicity of epoxy thermosets containing hepta(3,3,3-trifluropropyl) polyhedral oligomeric silsesquioxane-capped poly(hydroxyether of bisphenol A) telechelics.* [J]. Journal of Colloid and Interface Science, 2011. **363**(1): p. 250-260.
19. Zeng, K., et al., *Self-assembly behavior of hepta(3,3,3-trifluoropropyl) polyhedral oligomeric silsesquioxane-capped poly(epsilon-caprolactone) in epoxy resin: Nanostructures and surface properties.* [J]. Polymer, 2009. **50**(2): p. 685-695.
20. Zeng, K. and S.X. Zheng, *Nanostructures and surface dewettability of epoxy thermosets containing hepta(3,3,3-trifluoropropyl) polyhedral oligomeric silsesquioxane-capped poly(ethylene oxide).* [J]. Journal of Physical Chemistry B, 2007. **111**(50): p. 13919-13928.
21. Yu, X.F., et al., *A Giant Surfactant of Polystyrene-(Carboxylic Acid-Functionalized Polyhedral Oligomeric Silsesquioxane) Amphiphile with Highly Stretched Polystyrene Tails in Micellar Assemblies.* [J]. Journal of the American Chemical Society, 2010. **132**(47): p. 16741-16744.
22. Zhang, W.B., et al., *Synthesis of Shape Amphiphiles Based on Functional Polyhedral Oligomeric Silsesquioxane End-Capped Poly(L-Lactide) with Diverse Head Surface Chemistry.* [J]. Macromolecules, 2011. **44**(8): p. 2589-2596.
23. Miao, J.J., et al., *Self-assembly and chain-folding in hybrid coil-coil-cube triblock oligomers of polyethylene-b-poly(ethylene oxide)-b-polyhedral oligomeric silsesquioxane.* [J]. Macromolecules, 2007. **40**(15): p. 5460-5470.
24. Pyun, J. and K. Matyjaszewski, *Synthesis of nanocomposite organic/inorganic hybrid materials using controlled/"living" radical polymerization.* [J]. Chemistry of Materials, 2001. **13**(10): p. 3436-3448.
25. Pyun, J. and K. Matyjaszewski, *The synthesis of hybrid polymers using atom transfer radical polymerization: Homopolymers and block copolymers from polyhedral oligomeric silsesquioxane monomers.* [J]. Macromolecules, 2000. **33**(1): p. 217-220.

26. Chen, R.X., et al., *Surface-initiated atom transfer radical polymerization of polyhedral oligomeric silsesquioxane (POSS) methacrylate from flat silicon wafer.* [J]. Polymer, 2006. **47**(4): p. 1119-1123.
27. Haddad, T.S. and J.D. Lichtenhan, *Hybrid organic-inorganic thermoplastics: Styryl-based polyhedral oligomeric silsesquioxane polymers.* [J]. Macromolecules, 1996. **29**(22): p. 7302-7304.
28. Xu, W.T., C.H. Chung, and Y.W. Kwon, *Synthesis of novel block copolymers containing polyhedral oligomeric silsesquioxane (POSS) pendent groups via ring-opening metathesis polymerization (ROMP).* [J]. Polymer, 2007. **48**(21): p. 6286-6293.
29. Pyun, J., et al., *ABA triblock copolymers containing polyhedral oligomeric silsesquioxane pendant groups: synthesis and unique properties.* [J]. Polymer, 2003. **44**(9): p. 2739-2750.
30. Mya, K.Y., et al., *Time-Dependent Polymerization Kinetic Study and the Properties of Hybrid Polymers with Functional Silsesquioxanes.* [J]. Journal of Physical Chemistry B, 2010. **114**(28): p. 9119-9127.
31. Hirai, T., et al., *Hierarchical nanostructures of organosilicate nanosheets within self-organized block copolymer films.* [J]. Macromolecules, 2008. **41**(13): p. 4558-4560.
32. Hirai, T., et al., *Hierarchical Self-Assembled Structures from POSS-Containing Block Copolymers Synthesized by Living Anionic Polymerization.* [J]. Macromolecules, 2009. **42**(22): p. 8835-8843.
33. Kim, C.K., et al., *Amphiphilic poly(vinyl alcohol) hybrids and electrospun nanofibers incorporating polyhedral oligosilsesquioxane.* [J]. Macromolecules, 2007. **40**(14): p. 4823-4828.
34. Kim, B.S. and P.T. Mather, *Amphiphilic telechelics incorporating polyhedral oligosilsesquioxane: 1. Synthesis and characterization.* [J]. Macromolecules, 2002. **35**(22): p. 8378-8384.
35. Zhang, L., et al., *Synthesis, Characterization and Self-Assembly of Novel Amphiphilic Block Copolymers with a Polyhedral Oligomeric Silsesquioxanes Moiety Attached at the Junction of the Two Blocks.* [J]. Macromolecular Rapid Communications, 2009. **30**(12): p. 1015-1020.
36. Hussain, H., et al., *Synthesis, Micelle Formation, and Bulk Properties of Poly(ethylene glycol)-b-Poly(pentafluorostyrene)-g-polyhedral Oligomeric Silsesquioxane Amphiphilic Hybrid Copolymers.* [J]. Journal of Polymer Science Part A-Polymer Chemistry, 2010. **48**(1): p. 152-163.
37. Hussain, H., et al., *Micelle Formation and Gelation of (PEG P(MA-POSS)) Amphiphilic Block Copolymers via Associative Hydrophobic Effects.* [J]. Langmuir, 2010. **26**(14): p. 11763-11773.
38. Zhang, L.F. and A. Eisenberg, *Muliple Morphologies of Crew-Cut Aggregates of Polystyrene-b-Poly(Acrylic Acid) Block-Copolymers.* [J]. Science, 1995. **268**(5218): p. 1728-1731.
39. Yu, Y.S. and A. Eisenberg, *Control of morphology through polymer-solvent interactions in crew-cut aggregates of amphiphilic block copolymers.* [J]. Journal of the American Chemical Society, 1997. **119**(35): p. 8383-8384.
40. Yu, K., L.F. Zhang, and A. Eisenberg, *Novel morphologies of "crew-cut" aggregates of amphiphilic diblock copolymers in dilute solution.* [J]. Langmuir, 1996. **12**(25): p. 5980-5984.
41. Yu, Y.S., L.F. Zhang, and A. Eisenberg, *Morphogenic effect of solvent on crew-cut aggregates of apmphiphilic diblock copolymers.* [J]. Macromolecules, 1998. **31**(4): p. 1144-1154.
42. Zhang, L.F. and A. Eisenberg, *Morphogenic effect of added ions on crew-cut aggregates of polystyrene-b-poly(acrylic acid) block copolymers in solutions.* [J]. Macromolecules, 1996. **29**(27): p. 8805-8815.
43. Yu, K. and A. Eisenberg, *Multiple morphologies in aqueous solutions of aggregates of polystyrene-block-poly(ethylene oxide) diblock copolymers.* [J]. Macromolecules, 1996. **29**(19): p. 6359-6361.

44. Shen, H.W., L.F. Zhang, and A. Eisenberg, *Thermodynamics of crew-cut micelle formation of polystyrene-b-poly(acrylic acid) diblock copolymers in DMF/H2O mixtures.* [J]. Journal of Physical Chemistry B, 1997. **101**(24): p. 4697-4708.
45. Zhang, L.F. and A. Eisenberg, *Formation of crew-cut aggregates of various morphologies from amphiphilic block copolymers in solution.* [J]. Polymers for Advanced Technologies, 1998. **9**(10-11): p. 677-699.
46. Zhang, L.F. and A. Eisenberg, *Thermodynamic vs kinetic aspects in the formation and morphological transitions of crew-cut aggregates produced by self-assembly of polystyrene-b-poly(acrylic acid) block copolymers in dilute solution.* [J]. Macromolecules, 1999. **32**(7): p. 2239-2249.
47. Kim, H., S.M. Jeong, and J.W. Park, *Electrical Switching between Vesicles and Micelles via Redox-Responsive Self-Assembly of Amphiphilic Rod-Coils.* [J]. Journal of the American Chemical Society, 2011. **133**(14): p. 5206-5209.
48. Yu, S.Y., et al., *"Breathing" Vesicles.* [J]. Journal of the American Chemical Society, 2009. **131**(30): p. 10557-10566.
49. Mai, Y. and A. Eisenberg, *Controlled Incorporation of Particles into the Central Portion of Vesicle Walls.* [J]. Journal of the American Chemical Society, 2010. **132**(29): p. 10078-10084.
50. Hickey, R.J., et al., *Controlling the Self-Assembly Structure of Magnetic Nanoparticles and Amphiphilic Block-Copolymers: From Micelles to Vesicles.* [J]. Journal of the American Chemical Society, 2011. **133**(5): p. 1517-1525.
51. Ji, W.X., et al., *In situ and online monitoring polymerization-induced micellization.* [J]. Macromolecules, 2008. **41**(13): p. 4914-4919.
52. Zheng, G.H. and C.Y. Pan, *Reversible addition-fragmentation transfer polymerization in nanosized micelles formed in situ.* [J]. Macromolecules, 2006. **39**(1): p. 95-102.
53. Yang, L.P. and C.Y. Pan, *One-pot synthetic strategy to core cross-linked micelles with pH-sensitive cross-linked cores and temperature-sensitive shells through RAFT polymerization.* [J]. Australian Journal of Chemistry, 2006. **59**(10): p. 733-736.
54. Wan, W.M. and C.Y. Pan, *Atom transfer radical dispersion polymerization in an ethanol/water mixture.* [J]. Macromolecules, 2007. **40**(25): p. 8897-8905.
55. Zheng, Q., G.H. Zheng, and C.Y. Pan, *Preparation of nano-sized poly(ethylene oxide) star microgels via reversible addition-fragmentation transfer polymerization in selective solvents.* [J]. Polymer International, 2006. **55**(9): p. 1114-1123.
56. Yamauchi, K., et al., *Direct observation of polymerization-reaction-induced molecular self-assembling process: In-situ and real-time SANS measurements during living anionic polymerization of polyisoprene-block-polystyrene.* [J]. Macromolecules, 2006. **39**(13): p. 4531-4539.
57. Lee, J.M., S.E. Shim, and S. Choe, *Dispersion polymerization of MMA using polystyrene-block-poly(4-vinylpyridine) prepared by a RAFT.* [J]. Journal of Industrial and Engineering Chemistry, 2006. **12**(4): p. 648-651.
58. Wan, W.M., C.Y. Hong, and C.Y. Pan, *One-pot synthesis of nanomaterials via RAFT polymerization induced self-assembly and morphology transition.* [J]. Chemical Communications, 2009(39): p. 5883-5885.
59. Wan, W.M., X.L. Sun, and C.Y. Pan, *Formation of Vesicular Morphologies via Polymerization Induced Self-Assembly and Re-Organization.* [J]. Macromolecular Rapid Communications, 2010.

31(4): p. 399-404.

60. Wan, W.M. and C.Y. Pan, *One-pot synthesis of polymeric nanomaterials via RAFT dispersion polymerization induced self-assembly and re-organization.* [J]. Polymer Chemistry, 2010. **1**(9): p. 1475-1484.
61. Cai, W.M., et al., *Morphology transitions in RAFT polymerization.* [J]. Soft Matter, 2010. **6**(21): p. 5554-5561.
62. Wan, W.M., X.L. Sun, and C.Y. Pan, *Morphology Transition in RAFT Polymerization for Formation of Vesicular Morphologies in One Pot.* [J]. Macromolecules, 2009. **42**(14): p. 4950-4952.
63. He, W.D., et al., *Multiple Morphologies of PAA-b-PSt Assemblies throughout RAFT Dispersion Polymerization of Styrene with PAA Macro-CTA.* [J]. Macromolecules, 2011. **44**(9): p. 3358-3365.
64. Moad, G., E. Rizzardo, and S.H. Thang, *Radical addition-fragmentation chemistry in polymer synthesis.* [J]. Polymer, 2008. **49**(5): p. 1079-1131.
65. Deng, Y.M., et al., *Nanostructured Hybrid Polymer Networks From In Situ Self-Assembly of RAFT-Synthesized POSS-Based Block Copolymers.* [J]. Journal of Polymer Science Part A-Polymer Chemistry, 2011. **49**(20): p. 4343-4352.
66. Han, X.Q., et al., *Direct observation of the RAFT polymerization process by chromatography.* [J]. Macromolecules, 2007. **40**(15): p. 5618-5624.
67. Misra, R., et al., *Molecular miscibility and chain dynamics in POSS/polystyrene blends: Control of POSS preferential dispersion states.* [J]. Polymer, 2009. **50**(13): p. 2906-2918.
68. Lim, S.K., et al., *Polyhedral oligomeric silsesquioxane and polyethylene nanocomposites and their physical characteristics.* [J]. Journal of Industrial and Engineering Chemistry, 2010. **16**(2): p. 189-192.
69. Chen, Y.M., et al., *Perforated block copolymer vesicles with a highly folded membrane.* [J]. Macromolecules, 2007. **40**(13): p. 4389-4392.
70. Shen, H.W. and A. Eisenberg, *Block length dependence of morphological phase diagrams of the ternary system of PS-b-PAA/dioxane/H2O.* [J]. Macromolecules, 2000. **33**(7): p. 2561-2572.
71. Wan, W.M. and C.Y. Pan, *Formation of Polymeric Yolk/Shell Nanomaterial by Polymerization-Induced Self-Assembly and Reorganization.* [J]. Macromolecules, 2010. **43**(6): p. 2672-2675.
72. Ylitalo, D.A. and C.W. Frank, *The effect of pressure on block copolymer micelle formation: Fluorescence and light scattering studies of poly(styrene-b-ethylene propylene) in heptane.* [J]. Polymer, 1996. **37**(22): p. 4969-4978.
73. Desbaumes, L. and A. Eisenberg, *Single-solvent preparation of crew-cut aggregates of various morphologies from an amphiphilic diblock copolymer.* [J]. Langmuir, 1999. **15**(1): p. 36-38.
74. Bryskhe, K., et al., *Spontaneous vesicle formation in a block copolymer system.* [J]. Journal of Physical Chemistry B, 2004. **108**(28): p. 9710-9719.
75. Cai, Y., K.B. Aubrecht, and R.B. Grubbs, *Thermally Induced Changes in Amphiphilicity Drive Reversible Restructuring of Assemblies of ABC Triblock Copolymers with Statistical Polyether Blocks.* [J]. Journal of the American Chemical Society, 2011. **133**(4): p. 1058-1065.
76. Chen, Q., H. Schonherr, and G.J. Vancso, *Encapsulation and Release of Molecular Cargos via Temperature-Induced Vesicle-To-Micelle Transitions.* [J]. Small, 2010. **6**(23): p. 2762-2768.
77. Bhargava, P., et al., *Temperature-induced reversible morphological changes of polystyrene-block-poly(ethylene oxide) micelles in solution.* [J]. Journal of the American Chemical

Society, 2007. **129**(5): p. 1113-1121.

78. Chen, L., H.W. Shen, and A. Eisenberg, *Kinetics and mechanism of the rod-to-vesicle transition of block copolymer aggregates in dilute solution.* [J]. Journal of Physical Chemistry B, 1999. **103**(44): p. 9488-9497.
79. Huang, J.H., Y. Wang, and C.J. Qian, *Simulation study on the formation of vesicle and influence of solvent.* [J]. Journal of Chemical Physics, 2009. **131**(23).
80. Han, Y.Y., et al., *Effect of Selective Solvent Addition Rate on the Pathways for Spontaneous Vesicle Formation of ABA Amphiphilic Triblock Copolymers.* [J]. Journal of the American Chemical Society, 2010. **132**(3): p. 1144-1150.
81. He, X.H. and F. Schmid, *Dynamics of spontaneous vesicle formation in dilute solutions of amphiphilic diblock copolymers.* [J]. Macromolecules, 2006. **39**(7): p. 2654-2662.
82. Sevink, G.J.A. and A.V. Zvelindovsky, *Self-assembly of complex vesicles.* [J]. Macromolecules, 2005. **38**(17): p. 7502-7513.
83. Blanazs, A., et al., *Mechanistic Insights for Block Copolymer Morphologies: How Do Worms Form Vesicles?* [J]. Journal of the American Chemical Society, 2011. **133**(41): p. 16581-16587.

Chapter4 Nano-structured Epoxy with POSS Based Copolymer

4.1 Introduction

A major challenge in polymer science consisted in continuously designing functional materials with improved and/or unusual features to fulfill the expectations of expanding technology. In this context, polymer-based O/I NCs which exhibited remarkable performances stemming from the synergistic combination of organic polymers and inorganic materials properties have attracted a great deal of attention in the last decades[1-3]. A straightforward route to this class of hybrid materials relied on the dispersion of pre-formed nanoscaled inorganic materials, i.e. silica, metal or metal oxides, into polymer matrice[4, 5]. However, the scope of this non-covalent blending approach was somewhat limited by the tendency of the purely inorganic materials to aggregate as well as their poor compatibility with the polymer. Surface organic functionalization of the inorganic materials was thus often mandatory to achieve homogeneous dispersions and significant properties improvements. Another powerful approach to hybrid materials was based on a conventional sol-gel process involving hydrolysis and condensation reactions from metal alkoxides, commonly alkoxysilanes[6]. Organic/inorganic hybrid systems having weak interactions between mineral and organic domains could be conveniently prepared by directly growing inorganic components in a polymer solution or in polymer precursors, i.e. epoxy/amine mixture, methacrylates etc. to be cured[7, 8]. Alternatively, hybrid materials with covalent linkages between organic and inorganic components could be obtained from organically modified metal oxides bearing polymerizable moieties[9-14]. This simple, low cost and versatile sol-gel strategy gave birth to a large panel of NC materials but the resulting sol-gel derived hybrid materials were generally polydisperse in size and heterogeneous in chemical composition.

Recently, A third promising route to hybrid materials involved tailor-made inorganic clusters such as polyhedral oligomeric silsesquioxanes (POSS), 1-3 nm $(SiO_{1.5})_n$ structures that can be considered as the tiniest silica nano-objects[15-17]. Reactive or non-reactive organic substituents could be easily attached to the Si/O cage vertices to facilitate the incorporation of

POSS units into polymer matrices and impart novel properties to common classes of macromolecular materials[18-27]. Polymer-based hybrid materials could be generated through direct blending of POSS cages within reactive blends[28] or polymers[29]. POSS cages could also be covalently connected to polymer backbones through grafting approaches[30-44] or via (co)polymerization of POSS-functionalized monomers[45], resulting in homopolymers[46-48], random copolymers[49-51], star polymers[34, 52], polymer brushes[53] or thermosets[54-64].

Epoxy resin became one of the most popular commercial resin, and POSS/epoxy hybrid materials were attracted much attention among POSS/polymer hybrid materials[65-67]. The incorporation of POSS into the epoxy rein offered the opportunity to enhance the physical properties for advanced electronic, aerospace and automotive applications[68, 69]. During the past decades, a lot of researches have been done, among which, using a mono-functionalized POSS as co-precursor was one of the most popular way due to reaction controllability. However, due to the relatively low reactivity, the aggregation between POSS usually dominated the competition as compared with reaction for reactive POSS. One pot mixing and curing procedure always results micro phase separation in the scale range from 100nm to tens um. To conquer this critical problem, enhanced extent of reaction between POSS and precursors of matrices was required. Pre-reaction between POSS and precursors was an efficient route to enhance the extent of reaction. Maria J. Abad et al[70] have incorporated large mass fractions of monofunctional POSS into an epoxy network following a two-step procedure. In a first step the POSS was completely reacted with a diamine, using a 1:1 molar ratio of both reactants. SEC results of products from reaction between POSS and BSA showed the formation of POSS-diamine mixture possessing 1, 2 and 3 POSS moieties. The resulting POSS diamine precursor exhibited a distribution of species close to the ideal one. In a second step the POSS diamine precursor was reacted with a stoichiometric amount of a diepoxide leading to the final POSS-modified epoxy network. Through this route, high POSS mass fraction up to 51.8 wt % POSS could be incorporated in the polymer network in well dispersion. Liu et al[71] have also prepared Epoxy–POSS hybrid materials exhibiting good homogeneity containing a high mass fraction (up to 50 wt %) of POSS. The use of curing agents made of small molecules effectively avoided macrophase separation and enhanced the thermal properties of the hybrid materials. Similar results were achieved by other groups

when POSS with mono amino[58] or anhydride[72] group were introduced into epoxy.

In this chapter, firstly, POSS based statistic copolymer was used to construct nano-hybrid epoxy system. It was found that the introduction of GMA unit in copolymer will improve the miscibility between copolymer and epoxy. However, the effect of POSS on properties was complicated by additional reactive group in copolymer. Therefore, we turned to the nano-construction based on self-assembly which was slightly affected by cure process. Self-assembly of (quasi)amphiphilc POSS based polymer in epoxy provides an alternative route to nano-structured hybrid epoxy network, if we consider the polymer matrices as selective solvent. Zheng et al have synthesized hepta(3,3,3-trifluoropropyl)POSS capped PCL[73], PEO[74] and poly(hydroxyether of bisphenol A)[75], and used them as modifier in epoxy to construct NCs via the in situ polymerization. The formation of nanostructures was addressed on the basis of miscibility and phase behavior of the subcomponents of the organic/inorganic amphiphilie with epoxy after and before curing reaction. AFM showed that there is significant migration of the POSS moiety at the surface of the thermosets. Herein, we reported a novel method to nanostructured epoxy hybrid based on hybrid BCPs possessing high POSS weight ratio synthesized via RAFT polymerization. Thanks to the presence of the miscible block, the BCP was capable to self-organize on a nanometer scale in epoxy precursors solutions, forming inorganic-rich POSS core covered with miscible corona. The present work aims at demonstrating that blending such hybrid BCPs within epoxy precursors and subsequent curing can afford the preparation of transparent hybrid nanostructured epoxy-amine networks.

4.2 Experimental

4.2.1 Raw materials

AIBN and Benzoyl peroxide (BPO) in AR grade were purchased from Sinoreagent and recrystallized before use. MAiBuPOSS, MACyPOSS and MAPhPOSS were purchased from Hybrid Plastics and used as received. MMA, St and GMA were passed through base alumina column to remove the inhibitor before use. Diglycidyl ether of bisphenol A (DGEBA):

Shell Epon828 (MW=376) and Dow Chemical DER332 (MW=346). Cure agent: 4,4'-methylene-bis(2-chloroaniline) (MOCA) and 4,4'-Methylenebis- (3-chloro-2,6-diethylaniline) (MCDEA) were in technical grade. The chemical structure of DGEBA and cure agent was shown in Fig4.1. Unless specially indicated, other reagents were of analytical pure grade used as received.

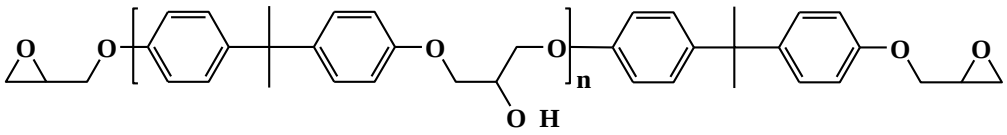

DGEBA

EPON 828, n=0.13, MW=376; DER 332, n=0.02, MW=346

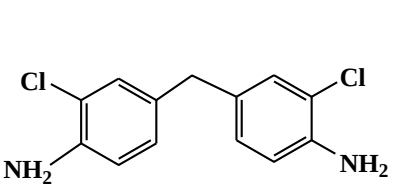

MOCA

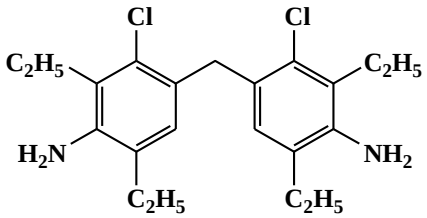

MCDEA

Fig 4.1 Molecular structure of precursors of epoxy: DGEBA, MOCA and MCDEA

4.2.2 Synthesis and preparation

4.2.2.1 Synthesis of POSS containing statistic copolymers

MMA, GMA, MAPhPOSS and toluene in preset ratio were put into a two neck flask equipped with condenser under Ar. After heating to 75℃, 1mol% (to monomer) of BPO in toluene was injected in. Polymer was obtained by repeated precipitation in methanol after polymerization for 24h. After dried, polymer was characterized by ^{1}H NMR (Fig4.2 and Table4-1).

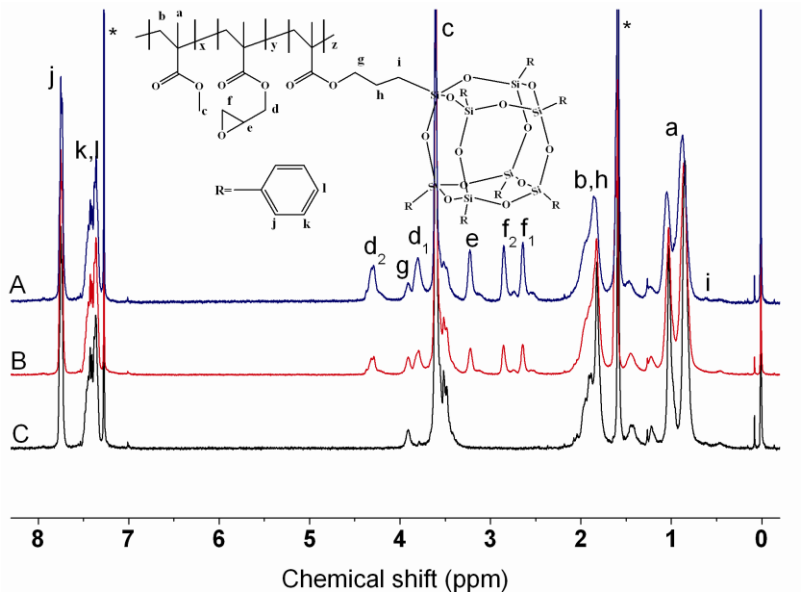

Fig 4.2 ^{1}H NMR and peak assignment of (A) SCP3, (B) SCP2 and (C) SCP1

Table4-1 Composition and structure information of statistic copolymers

Sample	Composition (mol%)			POSS (wt%)	T_g (^{o}C)
	MMA	GMA	POSS		
SCP1	94.2	0	5.77	39.9	136.9
SCP2	78.7	15.2	6.08	39.7	128.1
SCP3	58.2	35.0	6.78	40.7	123.8

4.2.2.2 Synthesis of POSS based BCPs

In a typical experiment, the MACyPOSS monomer (10.134g, 9mmol), CDB (61.3mg, 0.225mmol) and AIBN (1.85mg, 0.01125mmol) were dissolved in 13.5 mL toluene and placed in schlenk tubes which were thoroughly deoxygenated by five consecutive freeze-pump-thaw cycles. The tubes were subsequently placed in an oil bath thermostated at 65°C for 48h. The reaction was stopped by plunging the tubes into liquid nitrogen. PMACyPOSS polymers were subsequently precipitated twice into an acetone/ethyl acetate 8/2 (v/v) mixture in order to eliminate residual monomer (1wt% of residual POSS monomer after purification).

MMA(1.2mL, 11.33mmol), St(0.15mL, 1.27mmol), PMACyPOSS (0.4g, 2×10^{-5}mol) and AIBN(1×10^{-6}mol) dissolved in 0.5mL toluene in schlenk tube were deoxygenated by five consecutive freeze-pump-thaw cycles. The tubes were subsequently placed in an oil bath thermostated at 65°C. The polymerization was stopped by plunging the tubes into liquid nitrogen. The resulted BCP was obtained as pink powder after precipitation from methanol twice. For BCPs containing pure PMMA block, selective solvent, for instance, cyclohexane was used to extract the residual of POSS homo-polymer macro CTA. The chemical structure of BCPs was shown in Fig4.3 and the characterization results were shown in Table4-2.

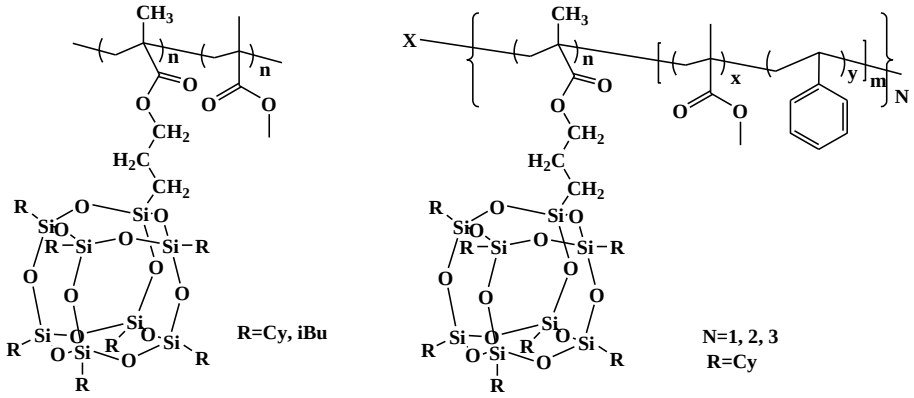

Fig 4.3 Molecular structure of POSS based BCPs

Table4-2 Composition and structure information of POSS based BCPs

Sample	Composition[a]	M_n (10^3) [b]	*PDI* [b]	M_w (10^3) [c]	f_{POSS} (wt%) [d]
BCP1	$PCy_{17.5}$-*b*-PM_{335}	36	1.22	53	37
BCP2	$PCy_{18.6}$-*b*-P(M_{175}-*co*-S_{33})	31	1.24	38	49
BCP3	X[PCy_{19}-*b*-P(M_{275}-*co*-S_{45})]$_2$	65	1.26	121	40
BCP4	X[PCy_{17}-*b*-P(M_{190}-*co*-S_{35})]$_3$	68	1.29	138	46
BCP5	$PiBu_{26}$-*b*-PM_{385}	45	1.15	76	40

(a) Cy: MACyPOSS; M: MMA, S: St, iBu: MAiBuPOSS; the number of subscript revealing the chain length was calculated by ^{1}H NMR, the number 2 and 3 for P3 and P4 revealing the arms of BCP from the ester center X; (b) by SEC against PS standards; (c) by SEC detected with multi detector combined with IR, RALS and SALS; (d) by ^{1}H NMR.

4.2.2.3 Preparation of epoxy samples

Preparation of DGEBA/MOCA/SCP samples: DGEBA, MOCA and SCP were mixed by solution blending, and then the solvent was evaporated at 80^{o}C under vacuum. The blend was cured under 150^{o}C2h+180^{o}C4h+200^{o}C2h.

Preparation of POSS BCP/DGEBA/MCDEA samples: The networks were prepared as previously described[66, 67]. Blends containing low BCP amounts (5 and 10 parts per hundred epoxy resin-phr) and DGEBA were prepared by mechanical stirring in a glass reactor at 135 °C for 12 h leading to a homogeneous premix. The preparation of networks possessing higher BCP content (20 phr) required the preliminary addition of THF (to achieve moderately viscous solutions) that was totally evaporated under vacuum before curing. The diamine (MCDEA) was then added over 5 min at 135 °C and the mixture was then casted on 50mm×50mm×1.5mm Teflon mould. The mould was finally cured at 135 °C for 12h (for neat), 14h (5 phr BCP), 18h (for 10 phr BCP) and 24h (for 20 phr BCP) and post-reacted for 4h at 190°C.

4.2.3 Characterization methods

^{1}H Nuclear magnetic resonance spectroscopy (NMR): ^{1}H NMR measurements were carried out on a Bruker AV400MHz NMR spectrometer. The samples were dissolved with d-chloroform and the solutions were measured with tetramethylsilane (TMS) as the internal reference.

Size Exclusion Chorography (SEC): SEC analysis were performed in THF at 25°C (flow rate: 1 mL·min^{-1}) on a Shimadzu DGU-20A apparatus equipped with a Shimadzu RID-10A refractive-index detector and a Viscotek 270 viscosimetry/RALS dual detection, and fitted with three Waters HR5E column.

Thermogravimetric analysis (TGA): Simultaneous Thermal Analysis (NETZSCH STA 409EP) was used to investigate the thermal stability of the hybrid material. All of the thermal analysis was conducted in air from ambient temperature to 800 ◦C at the heating rate of 10 ^{o}C min^{-1}.

Dynamic mechanical thermal analysis (DMTA): The DMTA was carried out on a

Dynamic Mechanical Thermal Analyzer (DMTA) (MKIV, Rheometric Scientific Inc., USA) in single cantilever model with the temperature ranging from 30 to 250 ◦C. The frequency used is 1.0 Hz at the heating rate 3.0^{o}C min^{-1}. The specimen dimension was 30mm×6mm×1.5mm.

Transmission Electron Microscopy (TEM) was performed on a Philips 120 high-resolution Transmission Electron Microscope at the accelerating voltage of 80 kV. Samples were trimmed using an ultra-microtome, and the slice (60~70 nm in thickness) were placed in 200 mesh copper grids for observation.

Scanning Electron Microscopy (SEM): SEM of fracture surface was performed on LEO-1530 Field Emission Scanning Electron Microscope at an activation voltage of 20 kV. The fracture surfaces were etched in dichloromethane if necessary, and then coated with thin layers of gold of about 100 Å before observation.

4.3 Result and discussion

4.3.1 Morphology study

4.3.1.1 Nanostructured epoxy with SCPs

Neat PMMA was well-dissolved in DGEBA/MOCA premix and preserved transparent after cure, indicating that no cure induced phase separation occurred. However, when ~6mol% (40wt%) of MAPhPOSS was incorporated into PMMA, samples were no longer transparent after cure, indicating that MAPhPOSS will reduce the miscibility. To solve this problem and obtain nano-dispersed epoxy hybrid, GMA unit was incorporated into polymer chain. The resulted hybrid epoxy became translucent when 15mol% of GMA was introduced in and turned to transparent when GMA rise up to 35mol%. High-resolved SEM of fracture surface of hybrid epoxy after etching was shown in Fig4.4. As comparison, very smooth surface was observed for neat epoxy (Fig4.4a), while phase separation structure was observed for that from SCP1 modified epoxy. As shown in Fig4.4b, c, and d, the size of micro domain of dispersed phase increased from 0.5 to 2um as the content increased from 5wt% to 15 wt%. it was clear that no phase separation structure was observed for epoxy modified with SCP2 and

SCP3 as shown in Fig4.4e and f. that could be attributed to the higher reactivity of GMA, so that could react with diamine prior to DGEBA. Therefore, phase separation was inhibited.

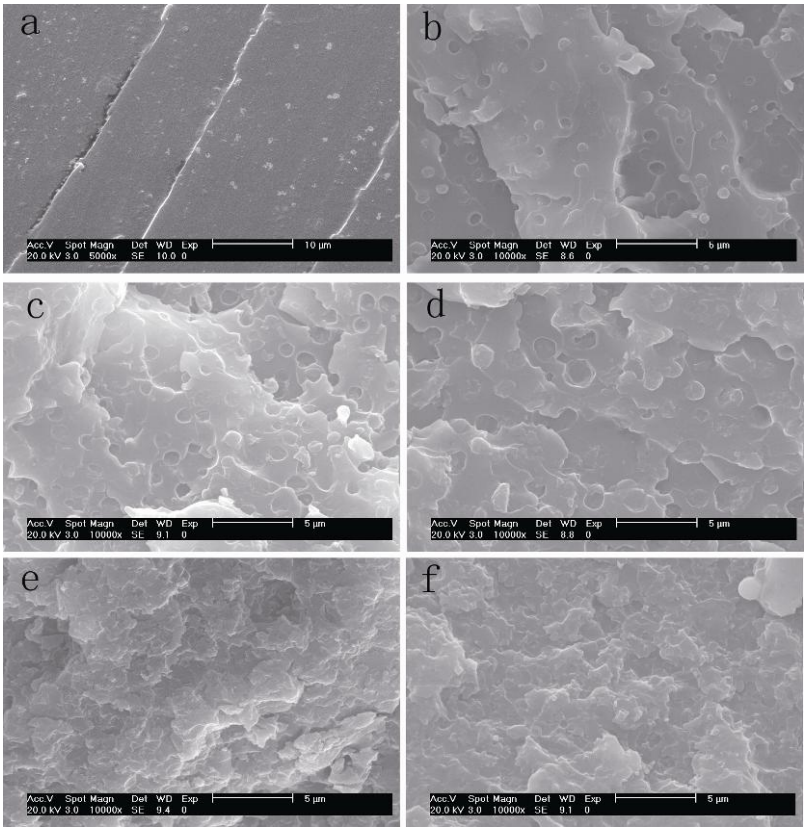

Fig 4.4 SEM images of fracture surface of: (a) neat epoxy, epoxy modified with (b) 5wt%, (c) 10wt%, (d) 15wt% of SCP1, 10wt% of (e) SCP2 and (f) SCP3

4.3.1.2 Nanostructured epoxy with BCPs

The entry to a transparent solution of MACyPOSS or its homopolymer was not successful and only cloudy dispersion was obtained even at 135°C. Therefore, we concluded that neither MACyPOSS nor its homopolymer was soluble in DGEBA due to their low polarity in contrast to DGEBA. As previously mentioned[76, 77], DGEBA was an excellent solvent for PMMA. In the present case, the PMMA block was miscible with the DGEBA and the amine hardener (MCDEA) according to their solubility parameters (δ_{PMMA}=21.52MPa$^{0.5}$; δ_{DGEBA}=20.9MPa$^{0.5}$; δ_{MCDEA}=22MPa$^{0.5}$)[78-80] whereas the poly(POSS) blocks are not miscible with the reactive mixture and remain immiscible during curing (i.e. $\delta_{OctaiBu\text{-}POSS}$=17.45

MPa0.5)[81-82]. Thus, the epoxy resin could be used as a reactive selective solvent, in which the micelle structure formed would be frozen by the following cure procedure. It was reported that epoxy modified with nano-fillers in well dispersed state would simultaneously increased both the toughness and thermal properties[83]. Different from normal coil BCP, POSS formed rigid inorganic rich aggregates due to the strong interaction, being expected to increase the T_g, toughness and modulus simultaneously. Moreover, the epoxy obtained in this work was O/I hybrid, in which the inorganic phase could play a synergetic role in some properties such as flam retardant or be selective etched to result in super porous materials. This controllable, facile nano-construction of O/I hybrid combined uniformity and homogeneity of nanostructured epoxy with BCPs and the hybrid characteristic inorganic NPs reinforced system.

For this purpose, we subsequently investigated the generation of nanostructured hybrid epoxy thermosets from hybrid BCPs. In a preliminary step, transparent solutions were obtained from mechanical blending of the hybrid BCPs with DGEBA at 135°C for 12 hours at concentrations ranging from 5 to 20 phr, suggesting a self-organization of the copolymers at the nanometer scale in the reactive solution. The hybrid copolymers self-assembled into micelles consisting in soluble PMMA blocks forming a swollen corona and non miscible PMACyPOSS or PMAiBuPOSS blocks constituting the core. MCDEA was used as cure agent due to its low reaction rate with epoxy and resulted product good compatibility with PMMA. Relying on a previous contribution of Pascault and coworkers dealing with SBM triBCPs/epoxy-diamine blends that stressed that PMMA is not phase separating during the network formation in a DGEBA/MCDEA epoxy system, we hypothesized that the resulting self-organization of the hybrid BCPs would be frozen during the curing process.

The optical photographs of epoxy samples were shown in Fig4.5. The transparency of the samples prepared with the BCPs was preserved throughout the polymerization whatever their nature and their concentration (up to 20 phr), which means no macro phase separation occurred during cure procedure. Whereas, curing of epoxy formulations containing statistic hybrid copolymer generated opaque materials, indicating the presence of well-dispersed domains beyond the nanometer range. For further understanding of micro-structure of BCPs dispersed in the epoxy, TEM analysis of slices was carried out.

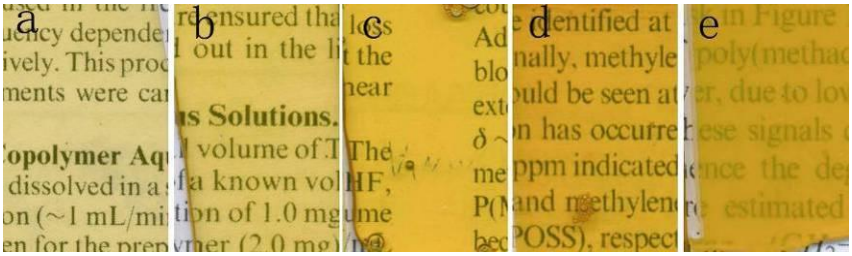

Fig 4.5 Optical appearance of epoxy samples: (a) neat epoxy; epoxy modified with 10phr of (b) BCP1, (c) BCP5, (d) BCP2 and (e) P(MMA_{388}-*co*-$MACyPOSS_{20}$)

The TEM images of ultra-thin (~70nm) slice of epoxy modified with different amounts of BCP1 shown in Fig4.6 perfectly demonstrated the formation of nanostructured epoxy networks with the hybrid BCPs self-assembled into nano-objects homogeneously dispersed in the epoxy matrix. The objects were composed of undiluted block PMACyPOSS that generate inorganic nanodomains with diameters on the order of 20 nm (dark domains corresponding to the core of the micelles) and PMMA blocks embedded in the epoxy network. Interestingly, incorporating 5 phr of BCP1 (Fig4.6a) afforded POSS nanodomains (dark domains) with a high degree of heterogeneity in terms of shape (spheres and worm like structures) and size (ranging from 15 to 100 nm). Increasing the hybrid copolymer content of BCP1 to 10 phr somewhat favored their organization in the epoxy matrix as illustrated by the exclusive presence of highly regular spherical domains (Fig4.6b). Higher BCP1 content (20 phr) afforded less organized inorganic nanodomains (Fig4.6c). The vicinity between nanostructures was in the same scale with nanostructure, showing a significant characteristic of so-called "interface dominated" materials[84].

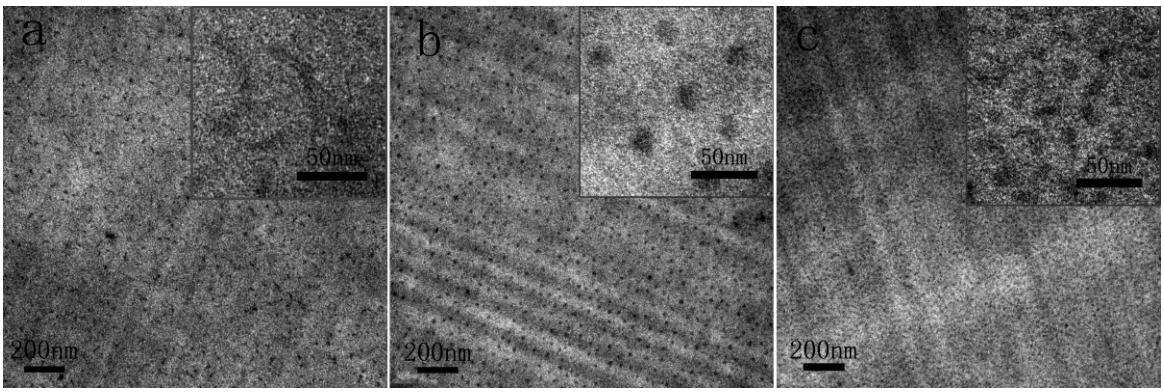

Fig 4.6 TEM of nanostructured epoxy modified with (a) 5, (b) 10 and (c) 20 phr of BCP1

The TEM images of epoxy modified with other BCPs at 10phr loading were shown in Fig4.7. Similar regular spherical morphology dispersed in matrix was observed for BCP5. Well dispersed silkworm like micelle with diameter of about 20nm and length of approximately 100nm was observed for epoxy modified BCP2. Samples modified ABA tri-block BCP3 and $(BA)_3$ tri-arm BCP4 showed spherical and mixture of spherical and cylindrical morphology respectively. It was clearly that the POSS content of BCP strongly affected on the final nanostructure. However, the topology of BCPs had slightly effect on the morphology. It might because of that the center block was composed of POSS block, which was immiscible with epoxy and formed the core of micelle finally. Therefore, different morphologies could be constructed by simple tuning the composition of BCPs.

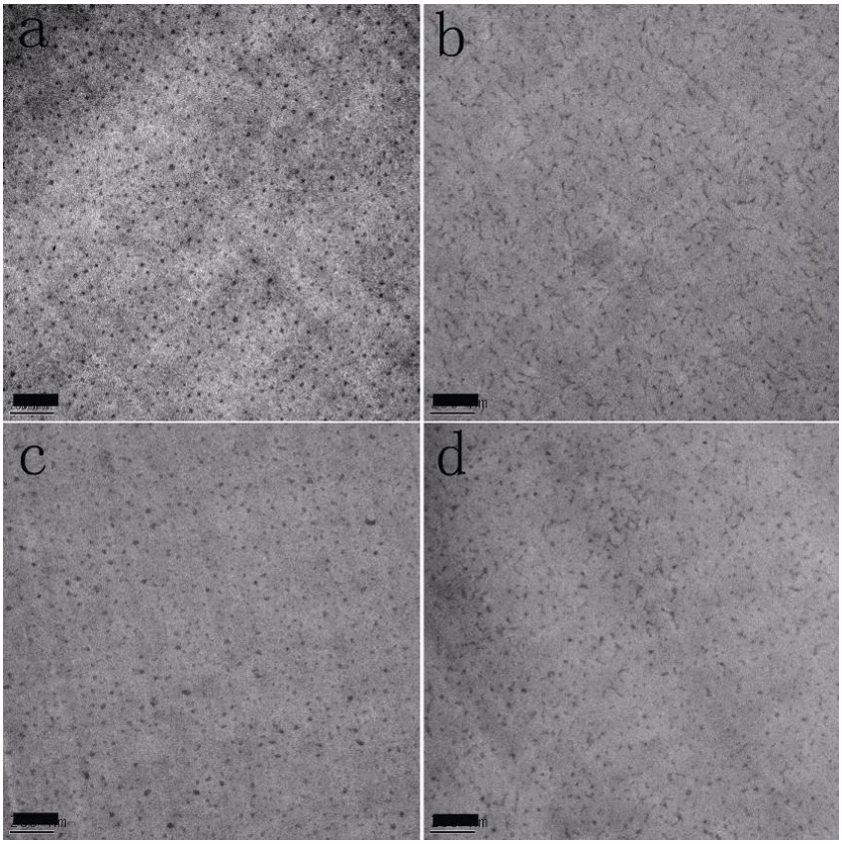

Fig 4.7 TEM of nanostructured epoxy networks generated from 10phr of hybrid block copolymers: (a) BCP5, (b) BCP2, (c) BCP3, (d) BCP4. (scale bar: 200nm)

The SEM analysis of etched fracture surface was also carried out. As shown in Fig4.8, the self-assembled BCP aggregates could be etched out, leaving holes in 20 nanometer scales.

Fig4.8a shows the etched surface of epoxy modified with 20phr BCP1. Round holes which correspond to the spoor of spherical micelles were observed clearly, but the density of holes distribution was obliviously less than that from TEM image. However, as shown in Fig4.8b, dense distribution of round holes and grooves corresponding to the spoor of silk-worm like micelles were observed for fracture surface of epoxy modified with 10phr BCP2. It's seemed that the micelles for later was easier to be etched out. This might attribute to the weaker interaction of coil chains due to the short chain length which couldn't entangle with the network and the weaker miscibility due to the incorporation of St units.

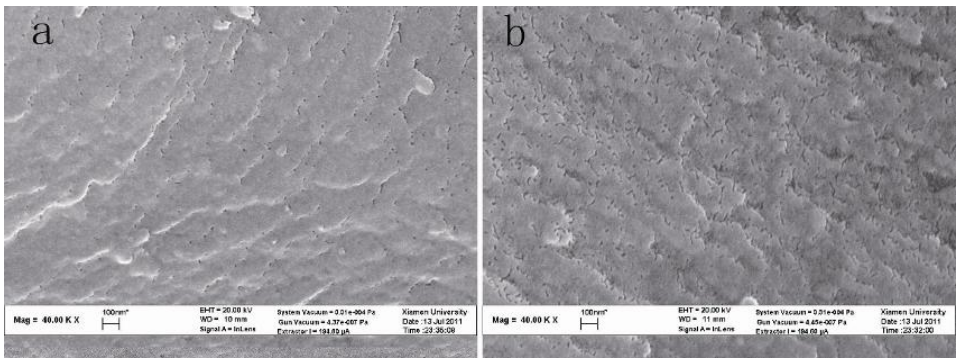

Fig 4.8 SEM images of fracture surface of epoxy modified with: (a) 20 phr of BCP1 and (b) 10 phr of BCP2. Surface was etched in dichloromethane

4.3.2 Fracture behavior

The brittleness was one of the fatal disadvantages of commercial epoxy resin which restrict their widely application in more fields. For several decades, one of the most important purposes in epoxy modification is toughening. There were much indicators to gauge the toughness, most of which was related to damaged mechanical measurements such as fracture energy, extension strength, maximum of elongation, critical stress intensity factor and critical strain energy release rate etc. a mass of samples were needed for these test due to the poor reproducibility as its very sensitive to defect. Herein, we can only qualitatively evaluate the toughness by fracture surface because of limited experimental condition.

4.3.2.1 Epoxy modified with SCPs

SEM of fracture surface in low magnification as shown in Fig 4.9 showed smooth surface with only a few crack for neat epoxy, while rough surface for modified epoxy. Epoxy modified with SCP1 showed a scales-like fracture surface. However, the fracture energy might decrease because of the weak interaction even the surface area increased. The inter-phase in micro scale trend to developed to crack, thus weaker the toughness. In contrast, epoxy modified with SCP2 and SCP3 showed rough fracture surface along with tough crack tip, indicating the transition from brittle to ductile fracture behavior.

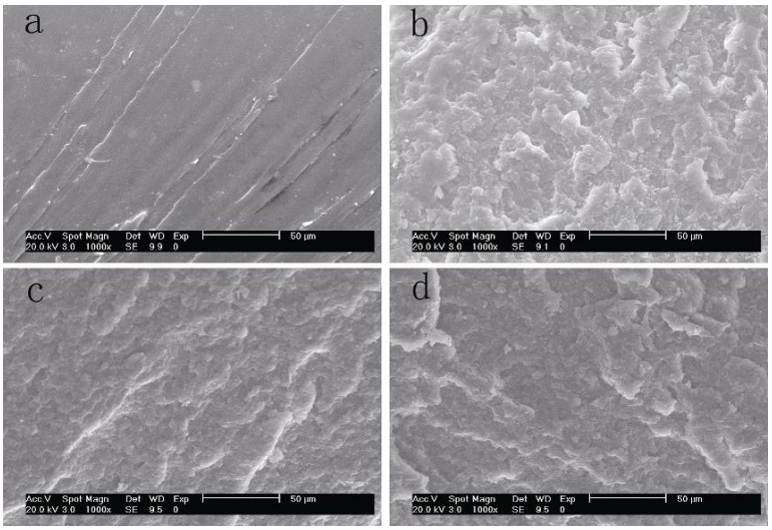

Fig 4.9 SEM images of fracture surface of epoxy modified with: (a) neat epoxy, epoxy modified with 10wt% of (b) SCP1 (c) SCPS2 and (d) SCP3

4.3.2.2 Epoxy modified with BCP

SEM of fracture surface of epoxy modified with BCPs in low magnification was shown in Fig 4.10. As shown in Fig4.10a, crack forking and feather markings were observed, and the fracture surfaces had a brittle appearance for neat epoxy. The addition of BCPs gave an apparent increase in the roughness observed by SEM as shown in Fig4.10b-f, which meant the increase of fracture energy. Different from SCPs modified samples, the addition of BCPs increased the density of crack, and the crack tip became curly as the BCPs loading increased.

Since the physical miscibility between matrix and modifiers, samples showed fracture behavior different from either the phase separation system or the chemical bonded system. Highly resolved SEM showed that each crack itself preserved smooth as the neat sample but the increase of crack density. It seemed that the incorporation of BCPs increased the fracture surface area without decreasing the inter-phase interaction or introducing in defects, thus increased the toughness.

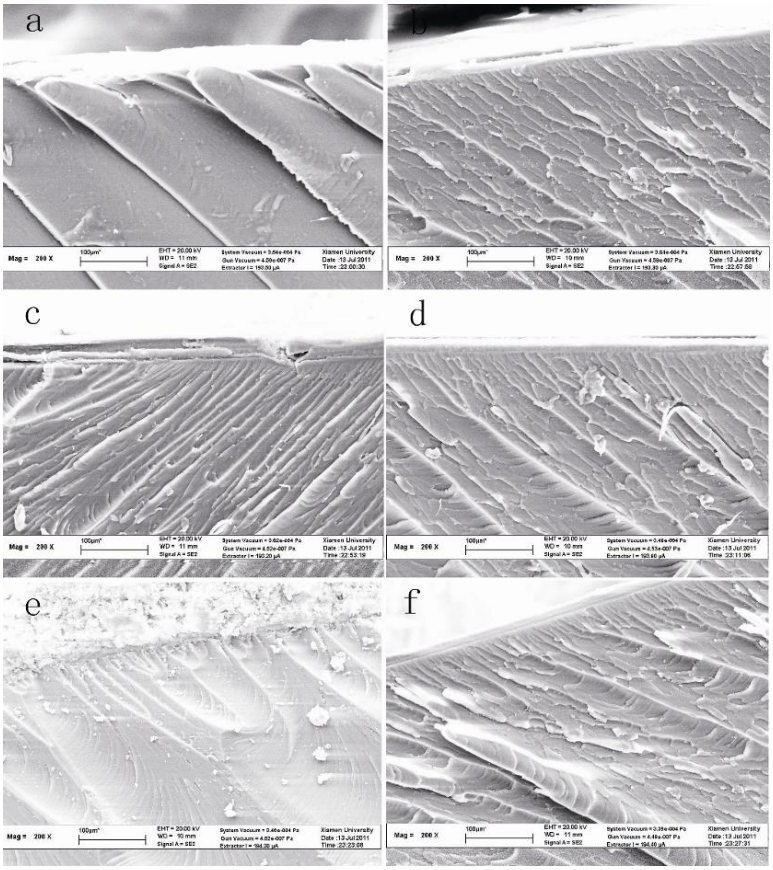

Fig 4.10 SEM images of fracture surface of (a) neat epoxy, epoxy modified with (b) 5phr, (c) 10phr, (d) 20phr of BCP1, (e) 5phr and (f) 10phr of BCP2

4.3.3 Thermo-mechanical properties

4.3.3.1 Epoxy modified with SCPs

DMTA curves of epoxy modified with 10wt% of SCPs were shown in Fig4.11. From Fig4.11 and Table4-3, the modified sample seems slightly different from the neat one. Only

that modified with SCP3 showed a slightly increase in T_g, probably due to the increase of cross link density brought from GMA, which was confirmed by higher rubbery modulus. The incorporation of GMA unit increased the miscibility and T_g, however, decreased the modulus at the same time. The results indicated that nano-reinforcement can not be well-performed by controlling the cure induced phase separation system. Meanwhile, the incorporation of GMA unit will complicate the system in property study.

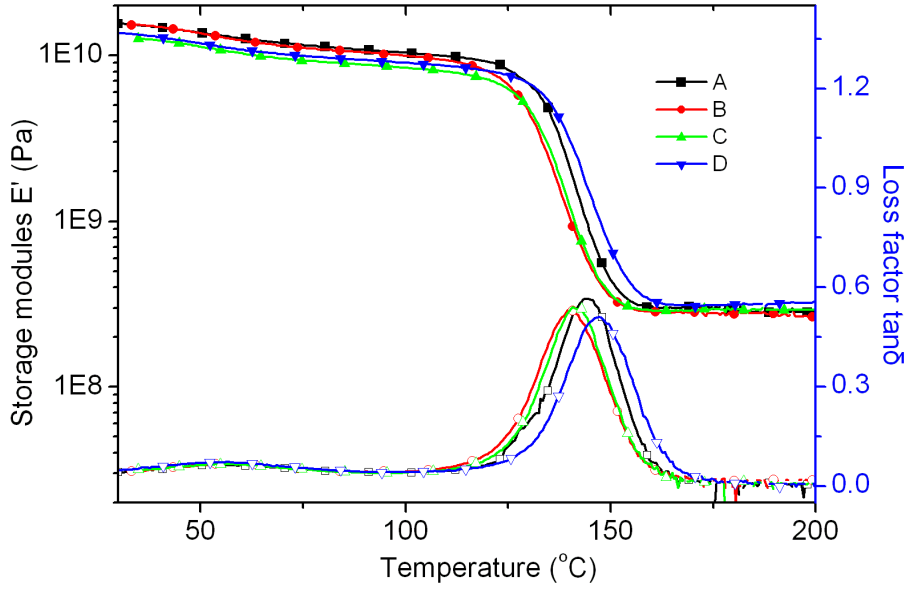

Fig 4.11 DMTA curves of (A) neat epoxy and epoxy modified with 10wt% of (B) SCP1 (C) SCP2 and (D) SCP3

Table 4-3 DMTA results of POSS based statistic copolymer modified epoxy

Sample	Composition	DMTA		
		Tg (°C)	E'-50°C (GPa)	E'-180 °C (MPa)
1	neat	144.4	1.37	28.9
2	5wt% SCP1	145.1	1.31	31.3
3	5wt% SCP2	146.8	1.31	28.6
4	5wt% SCP3	147.6	1.36	32.6
5	10wt% SCP1	139.5	1.36	27.4
6	10wt% SCP2	144.1	1.13	29.3

7	10wt% SCP3	147.7	1.18	31.5
8	15wt% SCP1	137.8	1.30	28.3
9	15wt% SCP2	142.1	1.12	27.5
10	15wt% SCP3	147.3	0.93	31.7

4.3.3.2 Epoxy modified with BCP

Dynamic mechanical analysis of networks containing different amounts of BCP1 was given in Fig4.12. All samples exhibited a single transition at high temperature confirming that the PMMA organic block remains soluble into the epoxy matrix during curing. At low BCP content, i.e. 5 phr, a slight increase of T_g and rubbery modulus were observed. Additional incorporation of BCPs did not improve the properties of the network. Indeed, whereas hybrid networks at 10 phr finally exhibited similar properties as neat materials, further increase of BCP content (20 phr) led to a significant shift towards lower T_g and rubbery modulus. This trend actually stemmed from the concomitant influence of two opposite effects. Nanostructured inorganic domains behaved in a similar manner as nanofillers restricting the mobility of polymer chains in their vicinity[85], while the soluble PMMA blocks exhibited a plasticizing effect due to their relatively low T_g in comparison with the epoxy network. Depending on the weight fraction of copolymer, one of these effects was predominant over the other. At low copolymer content, the impact of the inorganic domains seemed to be preponderant whereas, at high copolymer content, the plasticizing effect of PMMA appears to play the main role. The influence of the other copolymer structure is shown in Table4-4. The addition of 5 phr of copolymer, BCP1 or BCP2, resulted in the increase of the matrix T_g but the effect was more significant for BCP1. Even though this increase was not outstandingly high, this result was quite unusual and remarkable since most of the studies dealing with the influence of BCPs on network behavior report a decrease of T_g and rubbery modulus. It is also worth noting that this improvement of the network properties only requires 5 phr of O/I BCP thus avoiding the processing problems related to the typically high viscosities of copolymer-modified epoxy systems.

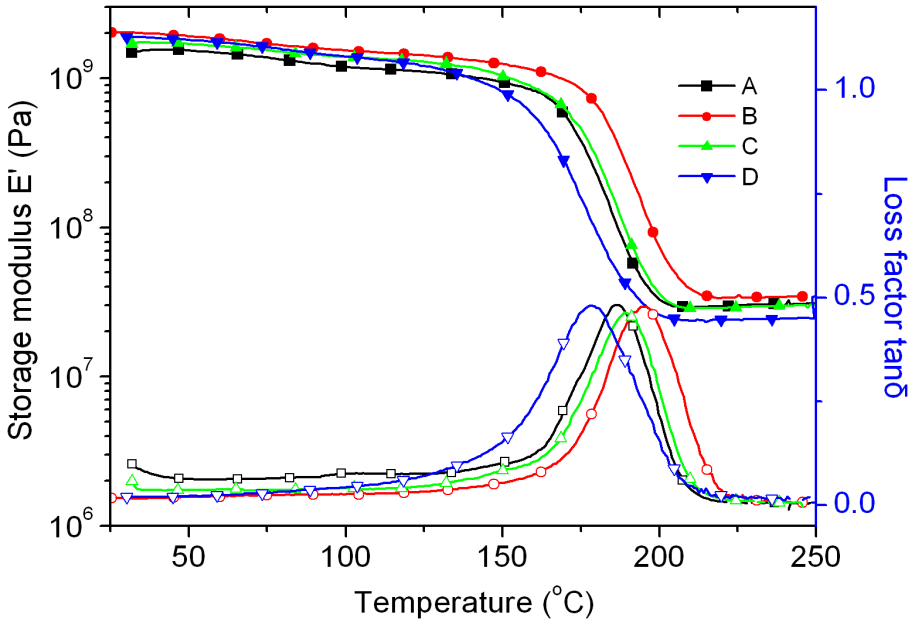

Fig 4.12 DMTA curves of (A) neat epoxy, epoxy modified with (B) 5phr, (C) 10phr and (D) 20 phr of BCP1

Table 4-4 DMTA results of POSS based BCPs modified epoxy

Sample	Composition[a]	DMTA		
		Tg (°C)	E-50°C (GPa)	E'-220°C (MPa)
A	neat	186.8	1.53	29.5
B	5phr BCP1	195.4	1.90	33.7
C	10phr BCP1	189.2	1.70	28.8
D	20phr BCP1	178.3	1.81	23.9
E	5phr BCP2	190.7	1.96	32.7
F	10phr BCP2	188.5	1.60	24.3
G	10phr BCP3	199.4	1.44	31.6
H	10phr BCP4	197.5	1.7	30.6
I	10phr BCP5	192.4	1.87	35.7

(a) phr: per hundred DGEBA

4.3.4 Thermal stability and flame retardancy

As a kind of I/O nano-object, POSS cage was expected to have promising future in synergetic flam-retardant[86, 87]. POSS has been proved to enhance the thermo-oxidation resistance, attributed to the formation of the inert silica-like layer on the surface, which can prevent the further oxidation of the inner part of the matrix[88]. There were many reports focused on the fire retardancy of POSS[89], in thermoplastic and thermosetting polymer systems. Synergy effect of multi-element attracted a lot of attentions, because the silicon formed chars at high temperature which was prevented by the evaporation of char. To investigate the effect of POSS BCP incorporation on the thermal stability and flame retardancy, TGA in air atmosphere were carried out.

4.3.4.1 Epoxy modified with statistic copolymer

TGA curves of epoxy modified with 10wt% of SCP were shown in Fig4.13. It was clear that the modified samples showed a obvious improvement in thermal stability. The initial degradation temperature (named as 10% weight loss) increased 10~30^{o}C when compared with neat epoxy. The temperature of the second loss stage increased 30~70^{o}C. The final char resided also increased to 4~10wt% from a negligible level. The GMA content on the stability was complicate and irregular, probably due to the incompletely reacted GMA which played a role of weak link.

TGA curves of samples modified with different amount of SCP3 were shown in Fig4.14. Obviously, the increase of POSS3 loading increased the degradation temperature, particularly for the second step. Meanwhile, loading higher than 10wt% didn't make further improvement in char formation. Even though, the char residual was much higher than theoretical value in terms of SiO_2, indicating that the POSS might synergistically promoted the char formation, thus implicated in flame retardant.

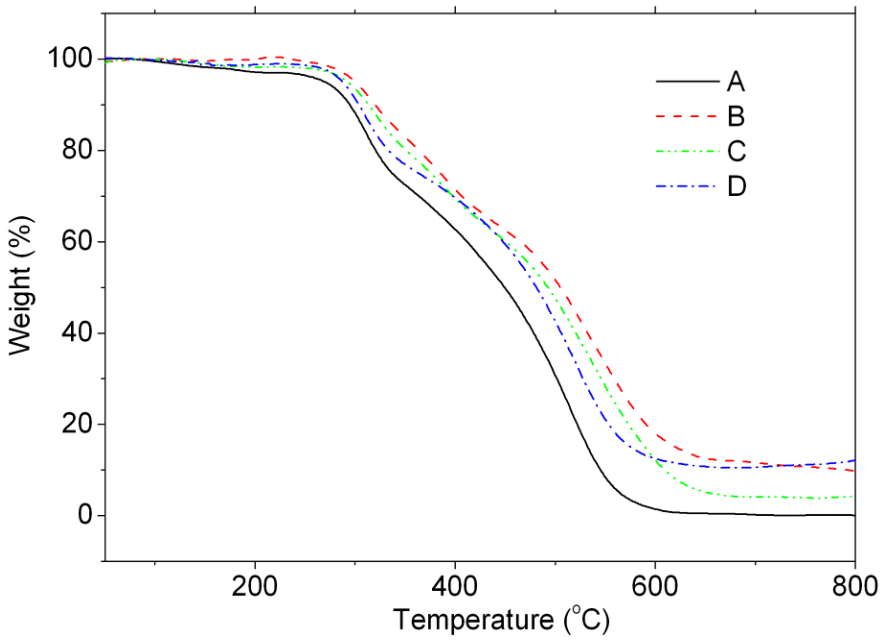

Fig 4.13 TGA curves of (A) neat epoxy, epoxy modified with 10wt% of: (B) SCP1, (C) SCP2 and (D) SCP3

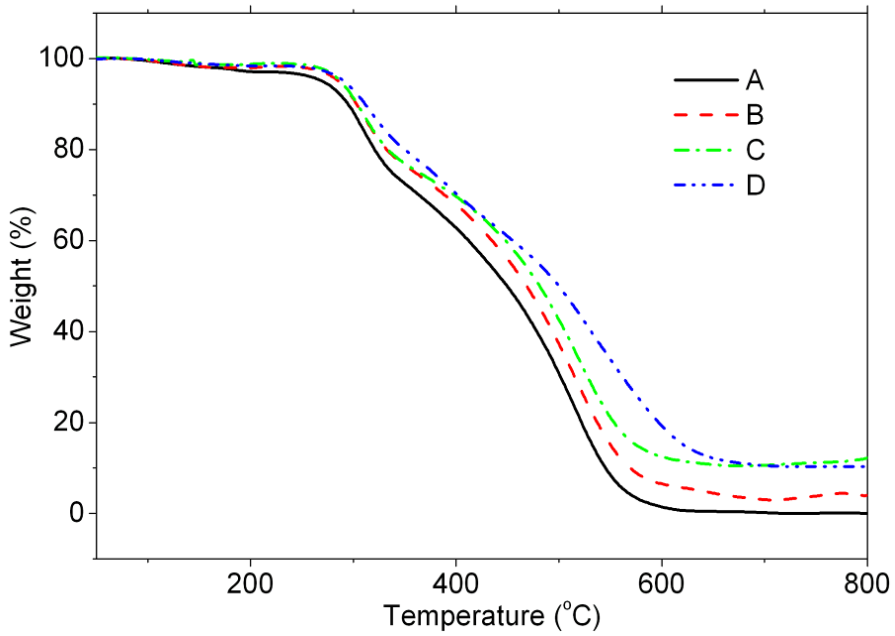

Fig 4.14 TGA curves of (A) neat epoxy, epoxy modified with: (B) 5wt%, (C) 10wt% and (D) 15wt% of SCP3

4.3.4.2 Epoxy modified with BCPs

TGA results of epoxy modified with different amount of BCP1 were shown in Fig4.15, which revealed that the incorporation of POSS in low concentration had slight effect on the decomposition behavior of epoxy matrix, whereas higher loading (20phr) obviously decreased the weight loss rate in the second step. More importantly, the char content was increased with the increase of POSS content. One should notice that the char content was much higher than the SiO_2 derived from POSS, i.e. for sample modified with 20phr of BCP1, the char content was 7.3wt%, in contrast to the SiO_2 content (less than 2 wt%). Obviously, the incorporation of POSS BCP would helpful in the char formation and slow down the oxidation rate of the formed char, which was potential in the application as synergetic flam-retardant.

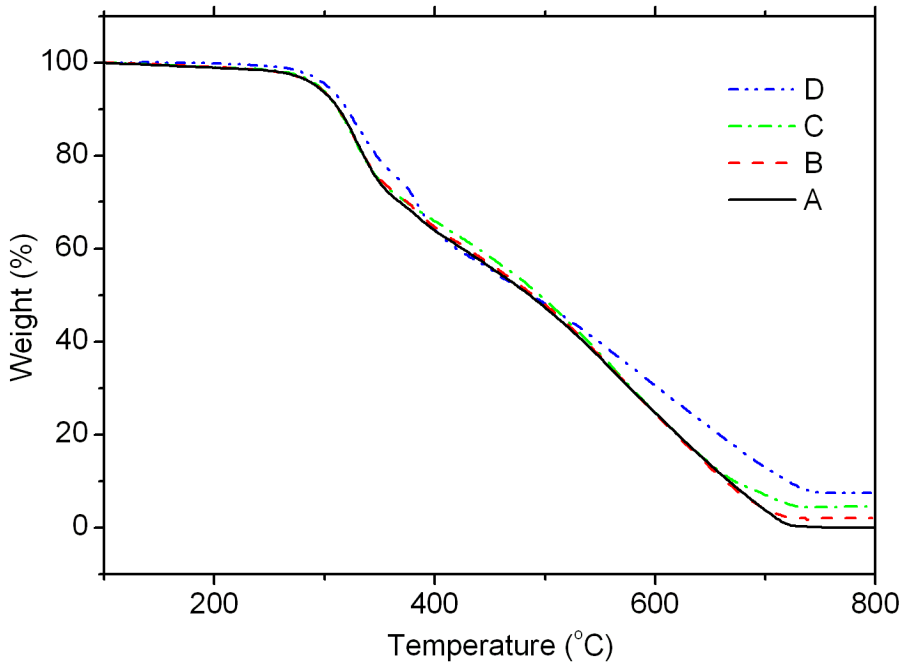

Fig 4.15 TGA curves of (A) neat epoxy, epoxy modified with: (B) 5phr, (C) 10phr and (D) 20phr of BCP1

4.4 Conclusion

Nano-structured O/I hybrid epoxy materials based on POSS based copolymers was

prepared. The effect of functional group content on miscibility of POSS based statistic copolymer and epoxy was investigated. It was found that the incorporation of GMA improved the miscibility of modifier and matrix as well as complicacy of properties.

Nano-construction of hybrid epoxy based on self-assembly of POSS based BCP in DGEBA precursor was prepared. Thanks to the presence of the miscible block, the BCP is capable to self-organize on a nanometer scale in epoxy precursors solutions, forming micelles owning inorganic-rich POSS core covered with miscible corona (Fig4.16). The O/I system from this method possess high homogeneity and well size/morphology control when compared with that from traditional sol-gel process. The results showed that the nano phase formed by POSS was homogeneously dispersed in matrix, thus the transparency preserved. The measurements indicated that the thermo-mechanical, fracture and char formation properties of resulted POSS based O/I hybrids were well improved and the thermal stability was slightly affected.

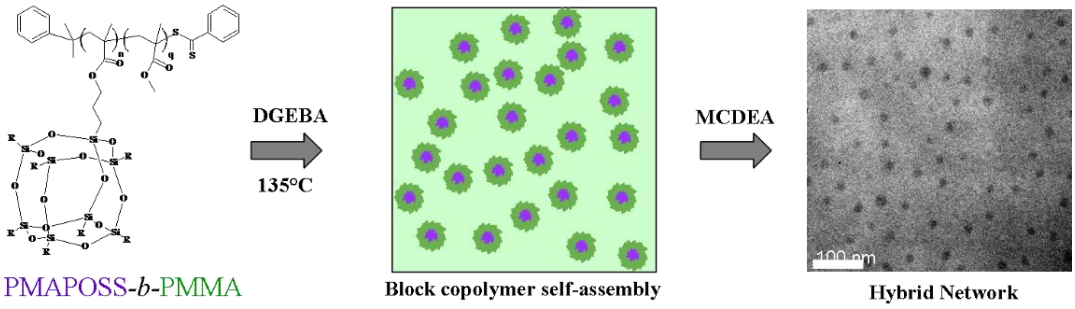

Fig 4.16 Graphical illustration of the nanostractation of O/I hybrids

Reference

1. Paul, D.R. and L.M. Robeson, *Polymer nanotechnology: Nanocomposites.* [J]. Polymer, 2008. **49**(15): p. 3187-3204.
2. Sanchez, C., et al., *Applications of hybrid organic-inorganic nanocomposites.* [J]. Journal of Materials Chemistry, 2005. **15**(35-36): p. 3559-3592.
3. Nicole, L., L. Rozes, and C. Sanchez, *Integrative Approaches to Hybrid Multifunctional Materials: From Multidisciplinary Research to Applied Technologies.* [J]. Advanced Materials, 2010. **22**(29): p. 3208-3214.
4. Okada, A.F., et al. *Composite material and process for manufacturing same*. [P]. US Patent 4739007, 1988.

5. Kojima, Y., et al., *Synthesis of Nylon-6-Clay Hybrid by Montmorillonite Intercalated with Epsilon-Caprolactam.* [J]. Journal of Polymer Science Part A-Polymer Chemistry, 1993. **31**(4): p. 983-986.
6. Brinker, C.J. and C. Scherer, *Sol-Gel Science.* [M]. Academic Press: San Diego,, 1990.
7. Spirkova, M., et al., *Preparation and characterization of hybrid organic-inorganic epoxide-based films and coatings prepared by the sol-gel process.* [J]. Journal of Applied Polymer Science, 2004. **92**(2): p. 937-950.
8. Innocenzi, P., T. Kidchob, and T. Yoko, *Hybrid organic-inorganic sol-gel materials based on epoxy-amine systems.* [J]. Journal of Sol-Gel Science and Technology, 2005. **35**(3): p. 225-235.
9. Philipp, G. and H. Schmidt, *New Materials for Contact-Lenses Prepared from Si-Alkoxides and Ti-Alkoxides by he Sol-Gel Process.* [J]. Journal of Non-Crystalline Solids, 1984. **63**(1-2): p. 283-292.
10. Philipp, G. and H. Schmidt, *The Reactivity of TiO_2 and ZrO_2 in Organically Modified Silicates.* [J]. Journal of Non-Crystalline Solids, 1986. **82**(1-3): p. 31-36.
11. Mellon, W., et al., *Block copolymers of gamma-methacryloxypropyltrimethoxysilane and methyl methacrylate by RAFT polymerization. A new class of polymeric precursors for the sol-gel process.* [J]. Macromolecules, 2005. **38**(5): p. 1591-1598.
12. Gamys, C.G., E. Beyou, and E. Bourgeat-Lam, *Micellar Behavior of Well-Defined Polystyrene-Based Block Copolymers with Triethoxysilyl Reactive Groups and Their Hydrolysis-Condensation.* [J]. Journal of Polymer Science Part A-Polymer Chemistry, 2010. **48**(4): p. 784-793.
13. Mullner, M., et al., *Water-Soluble Organo-Silica Hybrid Nanotubes Templated by Cylindrical Polymer Brushes.* [J]. Journal of the American Chemical Society, 2010. **132**(46): p. 16587-16592.
14. Zhang, K., L. Gao, and Y.M. Chen, *Organic/inorganic nanoobjects with controlled shapes from gelable triblock copolymers.* [J]. Polymer, 2010. **51**(13): p. 2809-2817.
15. Scott, D.W., *Theremal Rearrangement of Branchedchain Metylpolysiloxanes.* [J]. Journal of the American society, 1946. **68**: p. 356.
16. Baney, R.H., et al., *Silsesquioxanes.* [J]. Chemical Reviews, 1995. **95**(5): p. 1409-1430.
17. Cordes, D.B., P.D. Lickiss, and F. Rataboul, *Recent Developments in the Chemistry of Cubic Polyhedral Oligosilsesquioxanes.* [J]. Chemical Reviews, 2010. **110**(4): p. 2081-2173.
18. Feher, F.J., S.H. Phillips, and J.W. Ziller, *Facile and remarkably selective substitution reactions involving framework silicon atoms in silsesquioxane frameworks.* [J]. Journal of the American Chemical Society, 1997. **119**(14): p. 3397-3398.
19. Zhang, C.X., et al., *Highly porous polyhedral silsesquioxane polymers. Synthesis and characterization.* [J]. Journal of the American Chemical Society, 1998. **120**(33): p. 8380-8391.
20. Zhang, C.X. and R.M. Laine, *Hydrosilylation of allyl alcohol with HSiMe2OSiO1.5 (8): Octa(3-hydroxypropyldimethylsiloxy)octasilsesquioxane and its octamethacrylate derivative as potential precursors to hybrid nanocomposites.* [J]. Journal of the American Chemical Society, 2000. **122**(29): p. 6979-6988.
21. Laine, R.M., J.W. Choi, and I. Lee, *Organic-inorganic nanocomposites with completely defined interfacial interactions.* [J]. Advanced Materials, 2001. **13**(11): p. 800-+.
22. Krishnan, P.S.G., C.B. He, and C.T.S. Shang, *Synthesis, characterization, and curing kinetics of novel ladder-like polysilsesquioxanes containine side-chain maleimide groups.* [J]. Journal of Polymer Science Part A-Polymer Chemistry, 2004. **42**(16): p. 4036-4046.

23. Krishnan, P.S.G. and C.B. He, *Octa(maleimido phenyl) silsesquioxane copolymers.* [J]. Journal of Polymer Science Part A-Polymer Chemistry, 2005. **43**(12): p. 2483-2494.
24. Choi, J.W., et al., *Organic/inorganic imide nanocomposites from aminophenylsilsesquioxanes.* [J]. Chemistry of Materials, 2003. **15**(17): p. 3365-3375.
25. Lee, L.H. and W.C. Chen, *Organic-inorganic hybrid materials from a new octa(2,3-epoxypropyl)silsesquioxane with diamines.* [J]. Polymer, 2005. **46**(7): p. 2163-2174.
26. Lai, Y.S., et al., *Structural and electrochemical properties of polyurethanes/polyhedral oligomeric silsesquioxanes (PU/POSS) hybrid coatings on aluminum alloys.* [J]. Materials Chemistry and Physics, 2009. **117**(1): p. 91-98.
27. Kim, H.U., et al., *Morphology and mechanical properties of PET by incorporation of amine-polyhedral oligomeric silsesquioxane.* [J]. Composites Science and Technology, 2008. **68**(13): p. 2739-2747.
28. Tanaka, K., S. Adachi, and Y. Chujo, *Side-Chain Effect of Octa-Substituted POSS Fillers on Refraction in Polymer Composites.* [J]. Journal of Polymer Science Part A-Polymer Chemistry, 2010. **48**(24): p. 5712-5717.
29. Lee, Y.J., et al., *Miscibility, specific interactions, and self-assembly behavior of phenolic/polyhedral oligomeric silsesquioxane hybrids.* [J]. Journal of Polymer Science Part B-Polymer Physics, 2004. **42**(6): p. 1127-1136.
30. Costa, R.O.R., et al., *Organic/inorganic nanocomposite star polymers via atom transfer radical polymerization of methyl methacrylate using octafunctional silsesquioxane cores.* [J]. Macromolecules, 2001. **34**(16): p. 5398-5407.
31. Kim, K.M., D.K. Keum, and Y. Chujo, *Organic-inorganic polymer hybrids using polyoxazoline initiated by functionalized silsesquioxane.* [J]. Macromolecules, 2003. **36**(3): p. 867-875.
32. Ohno, K., et al., *Living radical polymerization by polyhedral oligomeric silsesquioxane-holding initiators: Precision synthesis of tadpole-shaped organic/inorganic hybrid polymers.* [J]. Macromolecules, 2004. **37**(23): p. 8517-8522.
33. Huang, C.F., et al., *Influence of PMMA-chain-end tethered polyhedral oligomeric silsesquioxanes on the miscibility and specific interaction with phenolic blends.* [J]. Macromolecules, 2006. **39**(1): p. 300-308.
34. Pyun, J. and K. Matyjaszewski, *Synthesis of nanocomposite organic/inorganic hybrid materials using controlled/"living" radical polymerization.* [J]. Chemistry of Materials, 2001. **13**(10): p. 3436-3448.
35. Lee, K.M., et al., *Polycaprolactone-POSS chemical/physical double networks.* [J]. Macromolecules, 2008. **41**(13): p. 4730-4738.
36. Ge, Z.S., et al., *Synthesis of Organic/Inorganic Hybrid Quatrefoil-Shaped Star-Cyclic Polymer Containing a Polyhedral Oligomeric Silsesquioxane Core.* [J]. Macromolecules, 2009. **42**(8): p. 2903-2910.
37. Zhang, W.A., et al., *Synthesis via RAFT Polymerization of Tadpole-Shaped Organic/Inorganic Hybrid Poly(acrylic acid) Containing Polyhedral Oligomeric Silsesquioxane (POSS) and Their Self-assembly in Water.* [J]. Macromolecules, 2009. **42**(7): p. 2563-2569.
38. Kim, B.S. and P.T. Mather, *Amphiphilic telechelics incorporating polyhedral oligosilsesquioxane: 1. Synthesis and characterization.* [J]. Macromolecules, 2002. **35**(22): p. 8378-8384.
39. Cardoen, G. and E.B. Coughlin, *Hemi-telechelic polystyrene-POSS copolymers as model systems for the study of well-defined inorganic/organic hybrid materials.* [J]. Macromolecules, 2004.

37(13): p. 5123-5126.

40. Kim, B.S. and P.T. Mather, *Morphology, microstructure, and rheology of amphiphilic telechelics incorporating polyhedral oligosilsesquioxane.* [J]. Macromolecules, 2006. **39**(26): p. 9253-9260.
41. Miao, J.J., et al., *Self-assembly and chain-folding in hybrid coil-coil-cube triblock oligomers of polyethylene-b-poly(ethylene oxide)-b-polyhedral oligomeric silsesquioxane.* [J]. Macromolecules, 2007. **40**(15): p. 5460-5470.
42. Xu, Y.Y., J.Y. Yuan, and A.H.E. Muller, *Single-molecular hybrid nano-cylinders: Attaching polyhedral oligomeric silsesquioxane covalently to poly(glycidyl methacrylate) cylindrical brushes.* [J]. Polymer, 2009. **50**(25): p. 5933-5939.
43. Hussain, H., et al., *Synthesis, Micelle Formation, and Bulk Properties of Poly(ethylene glycol)-b-Poly(pentafluorostyrene)-g-polyhedral Oligomeric Silsesquioxane Amphiphilic Hybrid Copolymers.* [J]. Journal of Polymer Science Part A-Polymer Chemistry, 2010. **48**(1): p. 152-163.
44. Gungor, E., et al., *Multiarm Star Polymers with POSS at the Periphery.* [J]. Journal of Polymer Science Part a-Polymer Chemistry, 2010. **48**(21): p. 4835-4841.
45. Li, G.Z., et al., *Polyhedral oligomeric silsesquioxane (POSS) polymers and copolymers: A review.* [J]. Journal of Inorganic and Organometallic Polymers, 2001. **11**(3): p. 123-154.
46. Lichtenhan, J.D., Y.A. Otonari, and M.J. Carr, *Linear Hybrid Polymer Building-Blocks-Mathacrylate-Functionalized Polyhedral Oligmeric Silsesquioxane Monomers and Polymers* [J]. Macromolecules, 1995. **28**(24): p. 8435-8437.
47. Haddad, T.S. and J.D. Lichtenhan, *Hybrid organic-inorganic thermoplastics: Styryl-based polyhedral oligomeric silsesquioxane polymers.* [J]. Macromolecules, 1996. **29**(22): p. 7302-7304.
48. Lo Schlavo, S., et al., *Novel propylmethacrylate-monofunctionalized polyhedral oligomeric silsesquioxanes homopolymers prepared via radical bulk free polymerization.* [J]. European Polymer Journal, 2007. **43**(12): p. 4898-4904.
49. Zhang, W.H., et al., *Effect of methyl methacrylate/polyhedral oligomeric silsesquioxane random copolymers in compatibilization of polystyrene and poly(methyl methacrylate) blends.* [J]. Macromolecules, 2002. **35**(21): p. 8029-8038.
50. Zheng, L., et al., *X-ray characterizations of polyethylene polyhedral oligomeric silsesquioxane copolymers.* [J]. Macromolecules, 2002. **35**(6): p. 2375-2379.
51. Mather, P.T., et al., *Mechanical relaxation and microstructure of poly(norbornyl-POSS) copolymers.* [J]. Macromolecules, 1999. **32**(4): p. 1194-1203.
52. Pyun, J. and K. Matyjaszewski, *The synthesis of hybrid polymers using atom transfer radical polymerization: Homopolymers and block copolymers from polyhedral oligomeric silsesquioxane monomers.* [J]. Macromolecules, 2000. **33**(1): p. 217-220.
53. Chen, R.X., et al., *Surface-initiated atom transfer radical polymerization of polyhedral oligomeric silsesquioxane (POSS) methacrylate from flat silicon wafer.* [J]. Polymer, 2006. **47**(4): p. 1119-1123.
54. Lee, A. and J.D. Lichtenhan, *Viscoelastic responses of polyhedral oligosilsesquioxane reinforced epoxy systems.* [J]. Macromolecules, 1998. **31**(15): p. 4970-4974.
55. Li, G.Z., et al., *Viscoelastic and mechanical properties of epoxy/multifunctional polyhedral oligomeric silsesquioxane nanocomposites and epoxy/ladderlike polyphenylsilsesquioxane blends.* [J]. Macromolecules, 2001. **34**(25): p. 8686-8693.
56. Matejka, L., et al., *Epoxy networks reinforced with polyhedral oligomeric silsesquioxanes (POSS). Structure and morphology.* [J]. Macromolecules, 2004. **37**(25): p. 9449-9456.

57. Bizet, S., J. Galy, and J.F. Gerard, *Structure-property relationships in organic-inorganic nanomaterials based on methacryl-POSS and dimethacrylate networks.* [J]. Macromolecules, 2006. **39**(7): p. 2574-2583.
58. Zucchi, I.A., et al., *Monofunctional epoxy-POSS dispersed in epoxy-amine networks: Effect of a prereaction on the morphology and crystallinity of POSS domains.* [J]. Macromolecules, 2007. **40**(4): p. 1274-1282.
59. Di Luca, C., et al., *In-Situ Generation of a Dispersion of POSS Crystalline Platelets in an Epoxy Matrix Induced by Polymerization.* [J]. Macromolecules, 2010. **43**(21): p. 9014-9021.
60. Isayeva, I.S. and J.P. Kennedy, *Amphiphilic membranes crosslinked and reinforced by POSS.* [J]. Journal of Polymer Science Part A-Polymer Chemistry, 2004. **42**(17): p. 4337-4352.
61. Gunji, T., et al., *Preparation and properties of alkoxy(methyl)silsesquioxanes as coating agents.* [J]. Journal of Polymer Science Part A-Polymer Chemistry, 2004. **42**(15): p. 3676-3684.
62. Wahab, M.A., I. Kim, and C.S. Ha, *Microstructure and properties of 3,3 ',4,4 '-biphenyltetracarboxylic dianhydride (BPDA)-p-phenylene diamine (PDA) polyimide/poly(vinylsilsesquioxane) hybrid nanocomposite films.* [J]. Journal of Polymer Science Part A-Polymer Chemistry, 2004. **42**(20): p. 5189-5199.
63. Li, G.Z., et al., *Synthesis and properties of poly(isobutyl methacrylateco-butanediol dimethacrylate-co-methacryl polyhedral oligomeric silsesquioxane) nanocomposites.* [J]. Journal of Polymer Science Part A-Polymer Chemistry, 2005. **43**(2): p. 355-372.
64. Liang, K.W., et al., *Synthesis, morphology, and viscoelastic properties of cyanate ester/polyhedral oligomeric silsesquioxane nanocomposites.* [J]. Journal of Polymer Science Part A-Polymer Chemistry, 2005. **43**(17): p. 3887-3898.
65. Choi, J., et al., *Organic/inorganic hybrid composites from cubic silsesquioxanes.* [J]. Journal of the American Chemical Society, 2001. **123**(46): p. 11420-11430.
66. Fu, B.X., M. Namani, and A. Lee, *Influence of phenyl-trisilanol polyhedral silsesquioxane on properties of epoxy network glasses.* [J]. Polymer, 2003. **44**(25): p. 7739-7747.
67. Kim, G.M., et al., *Hybrid epoxy-based thermosets based on polyhedral oligosilsesquioxane: Cure behavior and toughening mechanisms.* [J]. Journal of Polymer Science Part B-Polymer Physics, 2003. **41**(24): p. 3299-3313.
68. Lu, T., et al., *Blended hybrids based on Silsesquioxane-OH and epoxy resins.* [J]. Journal of Applied Polymer Science, 2007. **106**(6): p. 4117-4123.
69. Liu, H.Z., S.X. Zheng, and K.M. Nie, *Morphology and thermomechanical properties of organic-inorganic hybrid composites involving epoxy resin and an incompletely condensed polyhedral oligomeric silsesquioxane.* [J]. Macromolecules, 2005. **38**(12): p. 5088-5097.
70. Abad, M.J., et al., *Epoxy networks containing large mass fractions of a monofunctional polyhedral oligomeric silsesquioxane (POSS).* [J]. Macromolecules, 2003. **36**(9): p. 3128-3135.
71. Liu, Y.L. and G.P. Chang, *Novel approach to preparing epoxy/polyhedral oligometric silsesquioxane hybrid materials possessing high mass fractions of polyhedral oligometric silsesquioxane and good homogeneity.* [J]. Journal of Polymer Science Part A-Polymer Chemistry, 2006. **44**(6): p. 1869-1876.
72. Xu, Y.T., et al., *Morphology and thermal properties of organic-inorganic hybrid material involving monofunctional-anhydride PUSS and epoxy resin.* [J]. Materials Chemistry and Physics, 2011. **125**(1-2): p. 174-183.
73. Zeng, K., et al., *Self-assembly behavior of hepta(3,3,3-trifluoropropyl) polyhedral oligomeric*

silsesquioxane-capped poly(epsilon-caprolactone) in epoxy resin: Nanostructures and surface properties. [J]. Polymer, 2009. **50**(2): p. 685-695.

74. Zeng, K. and S.X. Zheng, *Nanostructures and surface dewettability of epoxy thermosets containing hepta(3,3,3-trifluoropropyl) polyhedral oligomeric silsesquioxane-capped poly(ethylene oxide).* [J]. Journal of Physical Chemistry B, 2007. **111**(50): p. 13919-13928.
75. Zeng, K., L. Wang, and S.X. Zheng, *Nanostructures and surface hydrophobicity of epoxy thermosets containing hepta(3,3,3-trifluropropyl) polyhedral oligomeric silsesquioxane-capped poly(hydroxyether of bisphenol A) telechelics.* [J]. Journal of Colloid and Interface Science, 2011. **363**(1): p. 250-260.
76. Ritzenthaler, S., et al., *ABC triblock copolymers/epoxy-diamine blends. 1. Keys to achieve nanostructured thermosets.* [J]. Macromolecules, 2002. **35**(16): p. 6245-6254.
77. Ritzenthaler, S., et al., *ABC triblock copolymers/epoxy-diamine blends. 2. Parameters controlling the morphologies and properties.* [J]. Macromolecules, 2003. **36**(1): p. 118-126.
78. Verchere, D., et al., *Miscibility of epoxy Monomers with Carboxyl-Terminated Butadiene Acrylonitril Random Copolymer.* [J]. Polymer, 1989. **30**(1): p. 107-115.
79. Hansen, C.M., *Hansen solubility parameters.* [M]. CRC Press: London, 2007. **2nd edition**.
80. Jaffrennou, B., et al., *Nanostructured poly(urethane)s and poly(urethane-urea)s from reactive solutions of poly styrene-b-butadiene-b-(methyl methacrylate) -triblock copolymers.* [J]. European Polymer Journal, 2008. **44**(11): p. 3439-3455.
81. Misra, R., et al., *Molecular miscibility and chain dynamics in POSS/polystyrene blends: Control of POSS preferential dispersion states.* [J]. Polymer, 2009. **50**(13): p. 2906-2918.
82. Lim, S.K., et al., *Polyhedral oligomeric silsesquioxane and polyethylene nanocomposites and their physical characteristics.* [J]. Journal of Industrial and Engineering Chemistry, 2010. **16**(2): p. 189-192.
83. Ruiz-Perez, L., et al., *Toughening by nanostructure.* [J]. Polymer, 2008. **49**(21): p. 4475-4488.
84. Friedrich, K., S. Fakirov, and Z. Zhang, *Polymer composites: from nano-to-macro-scale.* [M]. New York, Springer, 2005.
85. Bugnicourt, E., et al., *Effect of sub-micron silica fillers on the mechanical performances of epoxy-based composites.* [J]. Polymer, 2007. **48**(6): p. 1596-1605.
86. Camino, G., A. Fina, D. Tabuani, *POSS as Fire Retardants.* [C]. MoDeSt-Workshop 08 on Nano-filled Fire Retardant Polymers and Polymeric Composites Beijing (China), 2008. **16-17**.
87. Chigwada, G., et al., *Fire retardancy of vinyl ester nanocomposites: Synergy with phosphorus-based fire retardants.* [J]. Polymer Degradation and Stability, 2005. **89**(1): p. 85-100.
88. Zhang, Z.P., et al., *Thermo-oxygen degradation mechanisms of POSS/epoxy nanocomposites.* [J]. Polymer Degradation and Stability, 2007. **92**(11): p. 1986-1993.
89. Glodek, T.E., et al., *Properties and performance of fire resistant eco-composites using polyhedral oligomeric silsesquioxane (POSS) fire retardants.* [J]. Composites Science and Technology, 2008. **68**(14): p. 2994-3001.
90. Lu, S.Y. and I. Hamerton, *Recent developments in the chemistry of halogen-free flame retardant polymers.* [J]. Progress in Polymer Science, 2002. **27**(8): p. 1661-1712.

Chapter5 Summary

5.1 Retrospect

The RAFT polymerization of several POSS monomers with different vertex groups was investigated. It was found that the controllability was weakened when a limitation of DP_n reached. Vertex group dependence was found in terms of limitation of DP_n, i.e. ~18 for MACyPOSS and ~30 for MAiBuPOSS by comparing the change of SEC curves. The effects of bulky side group on RAFT polymerization also manifested in the following chain extension. The CTE was obviously decreased when MMA and BuA were used for chain extension as manifested in slowly consumption of macro CTA. With the addition of small amount (up to 10mol%) of St, the efficiency was increased. POSS based BCP with different topology such as AB diblock，BAB tri-block and $(BA)_3$ tri-arm were synthesized using CTA with different functionality.

The thermal, mechanical properties of POSS based polymer were studied and the effects of POSS vertex group and aggregation state on the properties were investigated. It was found that the POSS block played a totally different role from POSS random incorporated in polymer chain. PMAiBuPOSS block will abnormally increase the T_g of PMMA block even its own low transition temperature, meanwhile, PMACyPOSS BCP showed behaviors similar with thermosets as the POSS block played a role of cross linking phase. Results on thermal degradation showed slight difference between BCP and statistic copolymer. Morphology study on char residual of BCP showed that meso-porous silica obtained after pyrolysis in air.

Self-assembly behavior of POSS based block in selective solvent was studied. Self-assembled nano-aggregates with various morphologies were prepared via dispersion RAFT polymerization in apolar solvent using PMAiBuPOSS macro CTA. By simply varying the dosage, polymerization time or temperature, continuous micelle transition was observed. It was found that increase the chain length of macro CTA will turn the pathway to vesicle from mechanism Ⅰ (through cylindrical micelle) to mechanism Ⅱ (through Ostwald ripening). This discovery will be helpful in extensive synthesis of nanomaterials, particularly cylindrical

micelles as well as theoretical studies on self-assembly of BCP.

Nano-construction of O/I hybrid epoxy materials based on POSS based copolymers. The effect of functional group content on miscibility of POSS based statistic copolymer and epoxy was investigated. It was found that the incorporation of GMA improved the miscibility of modifier and matrix as well as complicacy of properties. A novel method to nanostructure epoxy hybrid from self-assembly of POSS based BCPs possessing high POSS weight ratio synthesized via RAFT polymerization in epoxy precursors was presented. Thanks to the presence of the miscible PMMA block, the BCP is capable to self-organize on a nanometer scale in epoxy precursors solutions, forming micelles owning inorganic-rich POSS core and PMMA corona. The results showed that the nano phase formed by POSS was homogeneously dispersed in matrix, thus the transparency preserved. The measurements indicated that the thermo-mechanical, fracture and char formation properties of resulted POSS based O/I hybrids were well improved and the thermal stability was slightly affected.

5.2 Innovation

(1) It was the first time to systematically investigated the RAFT polymerization of POSS macromers and found the effect of bulky side group on controllability of RAFT polymerization.

(2) The effect of rigid POSS block with strong interaction on thermo-mechanical properties was firstly studied and found that physical cross-linked linear polymer showed the behavior similar with thermosets.

(3) Nano-aggregates of POSS BCP with various morphologies were successfully prepared. Continuous micelle transition was observed by simply varying the dosage, polymerization time or temperature. The effect of the chain length of macro CTA on vesicle formation pathway selection was experimentally confirmed.

(4) A novel method to nanostructure epoxy hybrid from self-assembly of POSS based BCPs was presented. Different from traditional coil BCP, the presence of PMACyPOSS rigid block formed inorganic-rich core like inorganic NPs. The properties of epoxy were improved by “nano-reinforcement” of NPs even with PMMA crona. The hybrid system from this

method possesses high homogeneity and well size/morphology control when compared with that from traditional sol-gel process.

5.3 Prospective

(1) Even the controllability of RAFT polymerization of POSS macromers were improved when compared with other CRP system, the steric hindrance still dramatically affect the system.

(2) Lack of further study on properties and application of self-assemblies of POSS based BCPs.

(3) Systematical study on hybrid epoxy properties particularly the mechanical properties are required to quantitatively evaluate the "nano-reinforcement"

FOLIO ADMINISTRATIF

THESE SOUTENUE DEVANT L'INSTITUT NATIONAL DES SCIENCES APPLIQUEES DE LYON

NOM :DENG

DATE de SOUTENANCE : 2012

Prénoms :Yuanming

TITRE :
ÉTUDE SUR LA POLYMERIZATION RAFT ET NANO-STRUCTURES SYSTEME HYBRIDE DE MACROMERES POSS

NATURE : Doctorat

Numéro d'ordre : 2012-ISAL-

Ecole doctorale : Matériaux de Lyon

Spécialité : Matériaux Polymères et Composites

Cote B.I.U. - Lyon : T 50/210/19 / et bis

CLASSE :

RESUME :. Ce travail est généralement destiné à synthétiser BCPs à base d'POSS par polymérisation RAFT, à étudier leurs comportements d'auto-assemblage, à la recherche sur l'effet de POSS auto-assemblage structure sur les propriétés en vrac et à préparer nanostructuré époxy hybride par auto-assemblage de la copolymère base d'POSS. Dans le Chapitre1, Nous avons étudié la polymérisation RAFT de macromères POSS et capables de synthétiser bien définis BCPs à base d'POSS avec la fraction POSS élevé et une topologie différente tels que AB, BAB et $(BA)_3$. Le groupe de vertex et l'effet sur la morphologie propriétés thermo-mécaniques de BCPs à base d'POSS et la relation structure-propriété ont été investigated.Polymérisation RAFT dispersion dans solvant apolaire a été appliquée pour obtenir divers agrégats ayant une morphologie différente dans Chapitre2. Refroidissement de transition induite morphologie réversible a été trouvé et la sélection dans la formation des vésicules voie a été étudiée. Nano-construction de matériaux O/I époxy hybrides à base de copolymères à base d'POSS a été étudiée dans Chapitre 4. L'effet de la teneur en groupe fonctionnel sur la miscibilité de copolymère statistique base d'POSS et de l'époxy a été étudiée. Une nouvelle méthode à la technologie hybride époxy nanostructure impliquant l'auto-assemblage de BCPs à base d'POSS en résine époxy a été présenté. Homogénéité élevée et bien la taille/morphologie de contrôle de coeur-corona structure contenant coeur POSS rigide et soluble dans les réseaux corona PMMA ont été obtenus.

Mots-Clés : nanocomposites; POSS; O/ I hybrides; copolymère à bloc; auto-assemblage.

Laboratoire (s) de recherche : Ingenierie des Matériaux Polymères (IMP)
UMR 5223 INSA de Lyon

Directeurs de thèse: Prof. Jean-François GERARD, Prof. Lizong DAI

Président de jury :

Composition du jury :

Prof. LU	Canzhong	Fujian Institute of Structure of Matter, CAS	– Rapporteur
Prof. CHEN	Xudong	Sun Yat-sen University	– Rapporteur
Prof.GERARD	Jean-François	INSA Lyon	– Directrice de thèse
Prof.DAI	Lizong	Xiamen University	– Directrice de thèse
Prof.Wu	Huihuang	Xiamen University	– Examinateur
Dr.XU	Yiting	Xiamen University	– Examinateur